IOWA STATE UNIVERSITY
Digital Repository

2010

Use of steady-state and time-resolved fluorescence spectroscopy as a tool to investigate photophysics of biologically and environmentally relevant systems

Sayantan Bose
Iowa State University

Follow this and additional works at: https://lib.dr.iastate.edu/etd

Part of the Chemistry Commons

Recommended Citation

www.manaraa.com

Use of steady-state and time-resolved fluorescence spectroscopy as a tool to investigate photophysics of biologically and environmentally relevant systems

by

Sayantan Bose

A dissertation submitted to the graduate faculty

in partial fulfillment of the requirements for the degree of

DOCTOR OF PHILOSOPHY

Major: Physical Chemistry

Program of Study Committee:
Jacob W. Petrich, Major Professor
Mark S. Gordon
Mark S. Hargrove
Xueyu Song
Theresa Windus

Iowa State University

Ames, Iowa

2010

Dedicated to my parents

TABLE OF CONTENTS

ACKNOWLEDGEMENT

First and foremost, I am heartily thankful to my research advisor, Prof. Jacob W. Petrich, whose encouragement, guidance and support from the initial to the final level enabled me to develop an understanding of the subject. With his undaunted enthusiasm, his inspiration, and his great efforts to explain concepts clearly, he helped to make my research work fun for me. This thesis would not have been possible without his kind support, trenchant critiques, probing questions, and remarkable patience. I could not have imagined having a better advisor and mentor for my Ph.D study.

Besides my advisor, I like to thank the rest of my Program of Study (POS) committee members: Prof. Mark S. Gordon, Prof. Mark S. Hargrove, Prof. Xueyu Song and Prof. Theresa Windus for their time and support.

Prof. Gordon has always been a source of inspiration and fun for me through all the various interactions we had in the last five years inside and outside lecture rooms. I am privileged to have him as a lecturer in couple of the chemistry courses that I took during my graduate studies. Prof. Hargrove besides being a member of my POS is also our collaborator and I have spent a significant amount of time in his research laboratory, purifying and making proteins. The suggestions and contributions from Mark during my work in his laboratory are worth mentioning. He has also generously supplied us with different wild-type and mutant proteins which formed an integral part of my thesis work. Besides Mark, Prof. Song has a very important contribution to my thesis. We indulge in very successful collaboration with him regarding the theoretical aspects of solvation dynamics. We always tend to compare our experimental data with those obtained from the MD simulations from

him. This collaborative effort from Mark, Song and us led to publish our research in prestigious ACS journals. It has also been a pleasure to contribute and work with Jake, Song and Mark on grants proposals that they submit together to different funding organizations. Prof. Windus has been a source of encouragement all through. I am grateful to her for the opportunities I got to interact with various researchers thourgh Chem 660 and providing me exposure to their diverse research areas. I also enjoyed discussing my research with her recently when she agreed to be in my POS. I was highly benefited by the Chem 667 course that she taught, along with other professors like Song, Hoffman, and Gordon. Since the curriculum of this course was very relevant to my research it helped me a lot in understanding the fundamental theoretical concepts.

I like to express my gratitude to our other collaborators: Dr. Daniel W. Armstrong for synthesizing and purifying room temperature ionic liquids, Dr. George Kraus for synthesizing chromophores, Dr. Tom Casey and Mark Rasmussen from NADC for supplying different murine tissues, Dr. Sumit Choudhudry, Victor Lin, Zhiqun Lin and Malika Jeffries-EL for the polymer photophysics work. I gratefully thank Prof. Klaus Schmidt-Rohr, Hans Stauffer, David Hoffman, Amy Andreotti and Yeon-Kyun Shin for their invaluable lectures in all the CHEM and BBMB courses which immensely contributed to my learning and understanding of various subject matters.

I thank my fellow labmates, Ram Adhikary, Charles Barnes and Philip Carlson. Our group has always been a source of friendships as well as good advice and collaboration. I can never forget the great fun times we had together in and outside lab. I am indebted especially to Ram, who is not only my labmate but also my room-mate for last seven years since my days at IIT Bombay, India where I was pursuing my Masters. Ram's contribution

towards the completion my Ph.D work is indispensable. He helped me to learn a lot about how to use, maintain and troubleshoot different instruments in our laboratory. His fun loving nature and stupid but hilarious jokes, always kept me refreshed even during the stressful times. I am also grateful to the previous labmates like Dr.s Prasun Mukherjee, Mintu Halder and Lindsay Headley who have helped me learn during my initial research work. I enjoyed working with the undergraduates like Alyse, Frank, Alexandria and Rachel. I thank Hargrove group members such as Jordan Witmer, Smita Kakar, Puspita Halder, Ryan Strums and Cynthia Salas for all their help at various stages of my work. I like to thank my friends Debu, Shibu, Rajarshi, Supratim, Sumohan and all my undergraduate students.

I am grateful to all my professors in Indian Institute of Technology, Bombay, India. Of many, I owe my deepest gratitude to Dr. Anindya Datta who encouraged me to join Jake's group. My sincere thanks to Dr. Samita Basu, (Saha Institute of Nuclear Physics, Kolkata, India), for offering me the summer internship opportunities. I have always been fortunate to be blessed with some greatest teachers since my childhood, of which I would like to specially mention Sudip Chattopadhya, Rathin Mukherjee, Dhrubajyoti Roy Choudhury.

Last, but not the least, I would like to express my heartfelt gratitude to my parents, for their unconditional love, constant support and immense faith and encouragement. I am running short of words to acknowledge their contribution in every aspect of my life. I thereby dedicate this thesis to my parents. I cannot miss thanking my fiancée Piya (to whom I will be married next year) for her love, support and endurance. I also thank my other family members, relatives and friends for their love and support. My sincere apologies to those whom I could not mention due lack of space, but thank them equally.

CHAPTER I: INTRODUCTION

Steady-state and time-resolved fluorescence spectroscopy are among the most widespread and powerful tools in the study of physical, chemical and biological systems. In this thesis, we discuss the use of these technologies to study range of important processes occurring on timescales from femtoseconds (10^{-15} s) to nanoseconds (10^{-9} s). In particular, we employ the techniques of time-correlated single photon counting and fluorescence upconversion, which are described in detail in subsequent chapter. The physical problems that we address with these technologies are: solvation dynamics in various systems, especially proteins; the use of ionic liquids for the hydrolysis of cellulose; and stereoselective photophysics in chiral ionic liquids.

Solvation Dynamics

In solvation dynamics, we suppose that a charge distribution of the solute, initially in equilibrium with the surrounding polar solvent molecules, is instantaneously changed. This sudden alteration of charge disturbs the solvent equilibrium, and the system will relax to a new state of equilibrium in accordance with new charge distribution. The main point of interest here is how much time does the system takes to relax to the new equilibrium and what features control this relaxation.[1] These features are highly relevant to reaction rates involving charge transfer because such transfer can be retarded by the inability of the solvent to reorganize instantaneously as the reaction proceeds. In other words if the solvent molecules fail to adapt to the new charge distribution as the reactants pass through the transition state, the evolving products may recross the free-energy barrier.[2]

Solvation energies relevant to these modifications can be studied experimentally by spectroscopic methods, and theoretically by statistical mechanics.[3]
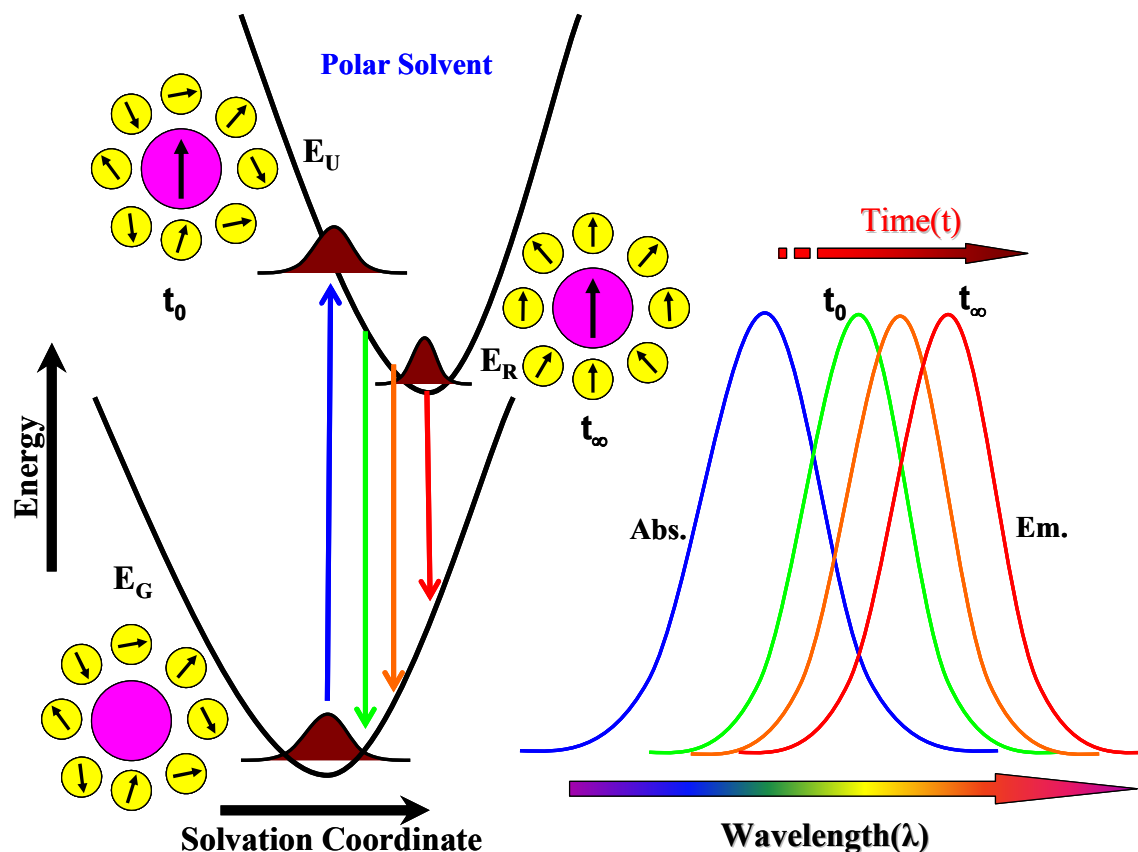
Figure I.1. Description of solvation dynamics process, showing the relaxation from t=0 to t=∞, with the stabilization of the energy with time.

Figure I.1 shows a simple description of the process of solvation of a solute molecule (purple sphere) surrounded by polar solvent molecules (yellow spheres) with the arrows representing the dipole moments. E_G is the energy of the solute in equilibrium with the solvent dipoles before undergoing any change in dipole moment. E_U is the energy at the very instant of the instantaneous change in dipole moment (unrelaxed state). E_R is the energy of completely solvated (relaxed state). The difference in energy between E_U and E_R is defined as the solvent reorganization energy, and the time taken by the system to relax from E_U to E_R

is the solvation time. Use of ultrafast spectroscopic techniques is immensely helpful for monitoring solvation process occurring on the order of 10^{-15}s (femtoseconds) to 10^{-9}s (nanoseconds) depending on the nature of the solvent used in the study. Water is known to exhibit the fastest solvation compared to other polar solvents,[2] whereas proteins exhibit both sub-picosecond and longer relaxation times.[4,5] On the other hand, viscous solvents like ionic liquids show slower response times, on the pico- to nanosecond time scales.[6-10]

It is possible to develop a method for studying solvation energies and solvation times theoretically by invoking linear response theory and making use of the time correlation functions.

Linear Response Theory

As no such general theory exists for non-equilibrium systems, equilibrium statistical mechanics can be extended to describe small deviations from equilibrium in a way that preserves its general nature by exploiting linear response theory. The latter is basically a statistical mechanical expansion about equilibrium, in which a system in thermal equilibrium is perturbed to a slight extent by an externally applied (constant or time-dependent) field. The response due to this perturbation is assumed to be linear. This forms the basis of linear response theory. It is used to compute the solvation free energies of molecules from molecular dynamics simulations.[11]

Let us consider a system in equilibrium, described by an unperturbed Hamiltonian $\hat{H}_0$. The Hamiltonian is changed to $\hat{H}$ when an external force F is acting on the system.

$$\hat{H}_0 \rightarrow \hat{H} = \hat{H}_0 + \hat{H}_1 \tag{I.1}$$

where $\hat{H}_1 = -\hat{A}F$ and $\hat{A}$ is an operator that represents a dynamical variable $A(r^N, p^N)$ that couples to the force F. If we consider another dynamical variable B, represented by an

operator $\hat{B}$, which will show a linear response to the perturbation on A, the response in B will be represented by the ensemble average $\langle \Delta B \rangle$. If we consider a constant external force, i.e., dealing with the equilibrium case, the $\langle B \rangle_0$ and $\langle B \rangle$ can be represented as,

$$\langle B \rangle_0 = \frac{\int dr^N \int dp^N B e^{-\beta H_0}}{\int dr^N \int dp^N e^{-\beta H_0}}$$

$$\langle B \rangle = \frac{\int dr^N \int dp^N B e^{-\beta(H_0+H_1)}}{\int dr^N \int dp^N e^{-\beta(H_0+H_1)}}$$

(I.2)

where $\langle B \rangle_0$ is the equilibrium value of B, $\langle B \rangle$ in the value displaced from the equilibrium, and $\beta = \frac{1}{k_B T}$. Therefore the induced deviation of B from the original equilibrium value is

$$\begin{aligned}
\Delta\langle B \rangle = \langle B \rangle - \langle B \rangle_0 &= -\beta(\langle H_1 B \rangle_0 - \langle H_1 \rangle_0 \langle B \rangle_0 \\
&= \beta F(\langle AB \rangle_0 - \langle A \rangle_0 \langle B \rangle_0), \text{ since } \hat{H_1} = -\hat{A}F \\
&= \beta \langle \delta A \delta B \rangle_0 F \\
&= \chi_{BA} F
\end{aligned}$$

(I.3)

where $\langle \delta A \delta B \rangle$ is the correlation between equilibrium fluctuations in A and B, and χ_{BA} is the response function coefficient of the linear relationship between F and $\langle \Delta B \rangle$, which is also referred to as susceptibility. Proceeding in the same way as in the static case, under linear response theory, the time evolution we obtain is,

$$\Delta\langle B(t) \rangle = \langle B(t) \rangle - \langle B \rangle_0 = -\beta(\langle H_1(0)B(t) \rangle_0 - \langle H_1 \rangle_0 \langle B \rangle_0)$$

$$= \beta F \langle \delta A(0) \delta B(t) \rangle_0$$

(I.4)

with $A(0) - \langle A \rangle_0$ and $B(t) - \langle B \rangle_0$ are the fluctuations from the average equilibrium values. If we consider the case when the external force is oscillating with a certain frequency, the system will reach a state of dynamic equilibrium with time, where the system will be oscillating with the same frequency, and the amplitude of oscillation will characterize the response. Assuming that the force is small, and that there is linear relationship between the response $\langle \Delta B(t) \rangle$ and the force, we can write

$$\langle \Delta B(t) \rangle = \int_{-\infty}^{t} dt' \chi_{BA}(t-t') F(t') \tag{I.5}$$

where $F(t)=F$(t<0); =0(t≥0), with

$$\int_{-\infty}^{0} dt' \chi_{BA}(t-t') = \frac{1}{k_B T} \langle \delta A(0) \delta B(t) \rangle_0 \text{ for t>0} \tag{I.6}$$

Taking the time derivative gives,

$$\chi_{BA}(t) = -\frac{\xi(t)}{k_B T} \langle \delta A(0) \delta \dot{B}(t) \rangle_0 \tag{I.7}$$

This equation relates the pulse response function to a correlation function of the system involving one of the variables A and the time derivative $\dot{B}(t)$ of the other, B. The $\langle \rangle_0$ denotes an ensemble average calculated with $\hat{H} = \hat{H}_0$.

The nature of A and F may vary. In solvation dynamics, the response changes in the first three multipole moments of a solute's charge distribution.[13] Commonly the relaxation of solvation energy is computed after the step function change in either point charge (q), dipole (μ) or axial quadrupole (Q) located at the center of the solute. In the linear response regime, the solvation energies are linearly proportional to $q\langle \Phi \rangle$, $\mu.\langle \nabla\Phi \rangle$ and $Q.\langle \nabla\nabla\Phi \rangle$, where Φ is

the electrostatic potential. So the electrostatic free energy of solvation of such point multipoles can be written as

$$E_{solv}(t) = \frac{1}{2}q\langle\Phi\rangle \tag{I.8}$$

$$= \frac{1}{2}\mu\langle\nabla\Phi\rangle \tag{I.9}$$

$$= \frac{1}{2}Q\langle\nabla\nabla\Phi\rangle \tag{I.10}$$

Substituting $B = \Phi, A = -\Phi, F = -q$, we get

$$\Delta\langle\Phi(t)\rangle = \langle\Phi(t)\rangle - \langle\Phi(\infty)\rangle_0 \tag{I.11}$$

$$= \frac{q}{k_B T}(\langle\delta\Phi(0)\delta\Phi(t)\rangle_0) \tag{I.12}$$

Thus the expression for solvation under linear response can be written as

$$S(t) \equiv \frac{E_{solv}(t) - E_{solv}(\infty)}{E_{solv}(0) - E_{solv}(\infty)} \tag{I.13}$$

Considering linear response again, the above equation becomes,

$$S(t) = \frac{\langle\Phi(t)\rangle - \langle\Phi(\infty)\rangle}{\langle\Phi(0)\rangle - \langle\Phi(\infty)\rangle} \tag{I.14}$$

$$S(t) = C(t) \equiv \frac{\langle\delta\Phi(0)\delta\Phi(t)\rangle}{\langle\delta\Phi^2\rangle} \tag{I.15}$$

Experiment

Recent developments in ultrafast spectroscopic techniques have made it possible to compare the experimental data and theory and simulations. Fluorescence upconversion[12] and photon-echo[4,13] techniques provide time resolution in the range from tens to hundreds of

femtoseconds. The evolution of solvation free energy can be achieved by monitoring the time-dependent shift in the emission spectrum of a probe molecule in a polar solvent.

Figure I.1, describes the method in which solvation is monitored experimentally using fluorescence Stokes shift measurements.[12] For studying solvation, a good solvatochromic probe molecule is chosen,[14,15] which undergoes a large dipole moment change upon excitation and shows a significant fluorescence red shift with increasing solvent polarity. Initially the probe, which is in equilibrium with respect to the polar solvent molecules, is excited with an ultrafast pulse of light, producing an instantaneous change in the dipole moment. On the time-scale of this electronic polarization, the solvent dipoles cannot reorganize themselves to this change in the dipole moment, in accord with the Born–Oppenheimer principle. But with time, the solvent dipoles start to reorganize around the excited dipole and the excited electronic state becomes stabilized, until it reaches an equilibrium condition where the probe has undergone complete solvent reorganization. If emission from these transient excited states is monitored with respect to time, then we can observe a time-dependent red shift of the emission spectrum relative to the t=0 spectrum, as shown in Figure I.1. Solvation function is given by,

$$S(t) = \frac{\nu(t) - \nu(\infty)}{\nu(0) - \nu(\infty)} \qquad (I.16)$$

following equation I.13, where $\nu(0)$ is the frequency of the maximum of the emission spectrum at t=0, and $\nu(\infty)$ is the one taken when equilibrium is reached, which is usually obtained from the steady-state spectrum. $\nu(t)$ s are corresponding peak maxima of the time-resolved emission spectra at different times.

If the excitation induces a small perturbation, then under linear response theory we can write,

$$S(t) = \frac{\nu(t) - \nu(\infty)}{\nu(0) - \nu(\infty)} \propto C(t) \equiv \frac{\langle \delta \Delta E(0) \delta \Delta E(t) \rangle}{\langle \delta \Delta E^2 \rangle} \equiv \frac{\langle \delta \nu(0) \delta \nu(t) \rangle}{\langle \delta \nu^2 \rangle} \qquad (I.17)$$

in which $\delta \Delta E(t) = \Delta E(t) - \langle \Delta E(t) \rangle$ and $\Delta E(t)$ is the interaction energy difference between the probe in its excited and ground state with surrounding solvent molecules at time t. Thus $S(t)$ and $C(t)$ are obtained from experiment and MD simulations respectively, and under the assumption of linear response theory the non-equilibrium ($S(t)$) and equilibrium response ($C(t)$) is considered to be equal, as explained in the above section.

Dielectric Response

Dielectric materials are non-conductors but can be polarized in the presence of external perturbations such as electric or magnetic fields. The electric properties of dielectric substances are defined by a quantity called the dielectric constant, which is generally independent of the applied field but depends on frequency for alternating fields. Usually dielectric materials are divided into two categories: polar and non-polar. A polar dielectric is one in which the individual molecules has a dipole moment even in the absence of any applied field. A non-polar dielectric is one whose molecules do not have any intrinsic dipole moment unless they are placed in an external electric field. In the latter case the field induces a perturbation of the electron cloud resulting in the shift in the center of positive and negative charges. If a system initially at equilibrium is perturbed by an external field (E), it takes a finite time for the electric charges to *relax* to their natural random positions and orientations. Thus if E is suddenly removed, the polarization (P) would show a gradual decrease or decay

asymptotically to zero. The time scale and the exact shape of the decay profile with time depend on the structure of the material and the mechanism causing the polarization.

There are two distinct types of time dependence which occur in nature.[16] First, there are regular oscillations of a system at a definite frequency, which will absorb energy from a suitable input signal over a narrow range of frequencies close to the resonant frequency. The second type is the general and random fluctuations caused by the thermal energy ($1/2k_BT$), associated with each degree of freedom of a system. These random fluctuations absorb energy in significant amounts if the frequency of the input signal is sufficiently high. The study of the resonant type of time dependence comes under the heading of "spectroscopy," whereas the relaxation type in the electrical case is known as dielectric relaxation. In practice the relaxation is not measured directly, but by finding the relative permittivity of the system at different frequencies of an applied sinusoidal field. At low frequencies, the polarization at a given time, P(t) can be obtained by,

$$P(t) = (\varepsilon_S - 1)\varepsilon_0 E(t) \tag{I.18}$$

But if the frequency of the applied field is increased to a such a point, where the polarization of the system is no longer able to follow the rapid changes in electric field, then ε_S becomes a complex quantity,

$$\varepsilon_S = \varepsilon_1 + i\varepsilon_2, \tag{I.19}$$

where ε_1 and ε_2 are the real and imaginary parts of the complex permittivity. The frequency dependence of the complex dielectric constant $\varepsilon(\omega)$ proposed by Debye is

$$\varepsilon(\omega) = \varepsilon_\infty + \frac{\varepsilon_S - \varepsilon_\infty}{1 - i\omega\tau_D} \tag{I.20}$$

where ε_S and ε_∞ are the static and infinite frequency dielectric constants respectively and τ_D is the Debye relaxation time.

The first theoretical models applied to solvation dynamics in polar media[17-19] assumed the solvent as a homogeneous continuum characterized by $\varepsilon(\omega)$ and solute ε_C as a spherical cavity with a centered point charge or dipole. Dynamical predictions of such homogeneous continuum models can be described by equation I.13. Since the continuum model predicts a single exponential relaxation time ($S_n(t) = e^{-t/\tau_L}$), the Debye equation can be split into real and imaginary parts as[20]

$$\varepsilon_1(\omega) = \varepsilon_\infty + \frac{\varepsilon_S - \varepsilon_\infty}{1 + i\omega^2\tau_D^2} \tag{I.21}$$

$$\varepsilon_2(\omega) = \frac{(\varepsilon_S - \varepsilon_\infty)\omega\tau_D}{1 + i\omega^2\tau_D^2} \tag{I.22}$$

The relaxation time τ_L can be related to Debye relaxation time τ_D as

$$\tau_L = \left(\frac{2\varepsilon_\infty + \varepsilon_C}{2\varepsilon_0 + \varepsilon_C}\right)\tau_D \tag{I.23}$$

The measured solvation times (τ) are independent of the probe molecule employed in the solvation studies,[15,21] and they are generally greater than the predicted τ_L, and usually lie between τ_D and τ_L. Deviation of τ from τ_L bears a linear correlation with $\varepsilon_0/\varepsilon_\infty$[22] suggesting that the assumption of the solvent as homogeneous continuum fails to consider the inhomogeneity in the solvent environment, which arises from the molecular details of the solvent. The observed decay of solvation response function S(t) deviates from single exponential behavior, which is contrary to the predictions from simple continuum theory. This is because in continuum theory the solvent molecules relax with a characteristic time τ_L

(longitudinal relaxation time), which is not a single molecule property but rather a collective response of many solvent molecules. The assumption in continuum theory, that the contribution of solvent molecules in proximity to the solute and in the bulk (far from solute) are equal is also unreasonable.[15,22] These inadequacies in capturing the true solvation behavior in polar solvents led to the advent of inhomogeneous dielectric continuum models, which considered molecular aspects of solvation, where the dielectric constant varies continuously as function of distance from the solute. In this case, the solvent molecules far from the solute are considered to behave like a continuum and the contribution of the solvent molecules in the proximity of a solute is much higher compared to those in the bulk. This dielectric inhomogeneity also accounted for multiple solvent relaxation times, which were not observed in the simple continuum theory.[1]

Dielectric properties of heterogeneous systems like proteins, micelles, etc. are far more complicated than those of simple bulk polar solvents, which have been very well studied. The work presented in this thesis mainly focuses on dielectric relaxation in protein environments. Dielectric properties of proteins play important roles in their structural and functional characteristics. Evaluation of electrostatic energies in proteins includes dielectric constants that represent the effect of the protein environment. There are several electrostatic models that have been used to evaluate electrostatic energies in proteins because these effects play a major role in enzyme catalysis,[4,8] electron transfer,[9,10] proton transport,[4,11,12] ion channels,[13,14] ligand binding,[15,16] macromolecular assembly,[1,17] and signal transduction.[18] The conceptual problems associated with the proper evaluation of electrostatic energies and the nature of the dielectric constant are far from trivial. A simple approach is to approximate the protein interior by a dielectric continuum represented by a single dielectric constant,

embedded in a cavity surrounded by another dielectric continuum representing the solvent.[4,23-25] In this approach the inhomogeneous nature of the protein interior is ignored.[26] On the other hand, detailed molecular dynamics simulations using atomistic models[27,28] considering atomic point charges[29,30] inside the cavity is computationally costly when applied in simulations of large proteins.

Considering the difficulties in obtaining the dielectric response in proteins reliably Song has developed a well-defined middle ground between the dielectric continuum approach and detailed atomistic simulations where a protein molecule in solution is represented by a set of polarizable dipoles embedded in a dielectric medium of solvent molecules.[35] The positions of the dipoles are assigned based on the native structure of the protein provided by the x-ray crystal structure. An intrinsic set of polarizabilities obtained for each naturally occurring amino acid residues is assumed to be universal and can be used for predicting dielectric properties of any large proteins and can successfully capture the salient features of proteins' inhomogeneity. This model has been reported to be easily generalized to the dynamical case where the evaluation of frequency dependent intrinsic polarizabilities can predict the time-dependent dielectric response of systems in which chromophores are bound to the interior of large proteins.[4,5,36-39]

To validate the model proposed by Song it is very important to have a model system which can be exploited to study the dielectric response in protein environment by experiments and simulations. Numerous systems have been used so far to study solvation phenomenon in proteins. Early studies by Marohn, Boxer, and coworkers have used ANS-DMA and DANCA, respectively, to show that relaxation in myoglobin occurs on nanosecond time scales, unlike that in polar solvents.[40,41] The former probe molecule afforded a single

exponential response of 9.1 ns while the latter, a more complicated response with both shorter and longer response times. Recently, Boxer and coworkers [42,43] have incorporated a synthetic fluorescent amino acid, Aladan (synthesized with PRODAN and alanine residue), into seven different sites of the B1 domain of the 56-amino acid protein, streptococcal protein G, GB1, to measure the time-dependent Stokes shifts from the femtosecond to nanosecond time scales. These probes are substantially flexible, and are likely to undergo excited-state charge transfer reactions, which could seriously complicate the interpretation of solvation dynamics. This class of chromophores is notable for its dual emission from locally-excited and charge-transfer states.[12,44] Fleming and coworkers probed eosin in the hydrophobic pocket of lysozyme to study its relaxation in the pocket environments using photon-echo peak shift experiments and have reported that almost 70% of the relaxation is completed within < 20 fs.[4]

The Biological Water Model

On the contrary Zhong, Zewail and coworkers used the intrinsic single tryptophan of various proteins[45-51] as a probe to study solvation dynamics and have reported slow relaxation, from which they inferred the presence of "biological water": water molecules in the immediate vicinity of a surface believed to have different properties from those of bulk water [52-56]. For example, they report that the dynamics are significantly slower for the surface tryptophan residues in Subtilisin Carlsberg [47] and in monellin [48] than for that of tryptophan in bulk water, and they argue that the slow relaxation arises from the water molecules constrained on the protein surface.[45]

This "biological water" comprises two components: one is "free water" and the other is attached to the biomolecule by a strong hydrogen bond and rotates only in a coupled

fashion with the slowly rotating biomolecule. The latter species is termed "bound water". Beyond this solvation shell the water molecules behave as ordinary water, and are termed "bulk water". Thus, the model consists of three parts. First, it is assumed that the "free water" molecules are free to rotate and to contribute to the dielectric relaxation process. The bound waters are at least doubly hydrogen bonded, so they can rotate only in concert with the biomolecule. Second, the dynamic exchange between the free and bound water species exists at all times: $[H_2O]_{freewater} \Leftrightarrow [H_2O]_{boundwater}$. Third, the effect of the rotation of the biomolecule is included in the theoretical scheme.[57]

These differences in the interpretations of various experiments are in no small part due to the lack of a reliable dielectric response function for the studied proteins from either experiments or computer simulations. The discrepancies between the results for these different probe molecules led us to search for other probes. Earlier studies by Stryer showed that ANS non-covalently and stoichiometrically binds with apomyoglobin and apohemoglobin, using fluorescence excitation, emission and polarization measurements.[58] Later Cocco and Lecomte have characterized the ANS–apomyoglobin complex using nuclear magnetic resonance spectroscopy, and proved that ANS resides in the distal side of the heme pocket.[59] We thus initially considered probe molecules like ANS[59] and biliverdin,[60] for both of which there are structures of their complexes with apomyoglobin. However, neither of these chromophores is ideal because their absorption spectra are complicated by overlapping electronic states. Even if internal conversion from higher-lying states to the lower fluorescent state is faster than solvation dynamics, as has been suggested to be the case in tryptophan,[45,47,48,61] an accurate determination of the reorganization energy[4,8] based on the steady-state spectra becomes very difficult. Although chromophores like PRODAN,

DANCA,[62] ANS[58,59] and ANSDMA[40] are reported to bind to the heme-pocket of apomyoglobin, they are not apt for studying solvation dynamics in protein environments because of the possibility of emission from different excited states. Thus we have proposed an alternative and robust system: coumarin 153 inside the heme pockets of monomeric heme proteins, such as myoglobin and leghemoglobin, as discussed below.

Heme Proteins

A heme protein is a metalloprotein containing a prosthetic group (heme) bound with the rest of the protein (globin). Heme is constituted of a tetrapyrrole moiety called porphyrin with iron located in its center. Heme containing proteins have attracted the attention of the scientific community since the beginning of modern enzymology. With their colored prosthetic groups, varied oxidation states, and diverse biological functions, they have provided a rich and fertile terrain for the elucidation by chemists, biophysicists, and biologists of protein structure–function relationships.[63] Much of the earliest work on heme proteins centered on the readily available globins (hemoglobin, myoglobin), peroxidases, and electron transfer proteins (the cytochromes). Heme proteins have diverse biological functions including oxygen transport, catalysis, active membrane transport, electron transfer and other sensory and defence functions. The heme group in myoglobin and hemoglobin gives the ability to bind oxygen because of the presence of iron atom. It also contributes to the red color found in muscles and blood. Each heme group contains an iron atom that is able to bind to one oxygen (O_2) molecule.
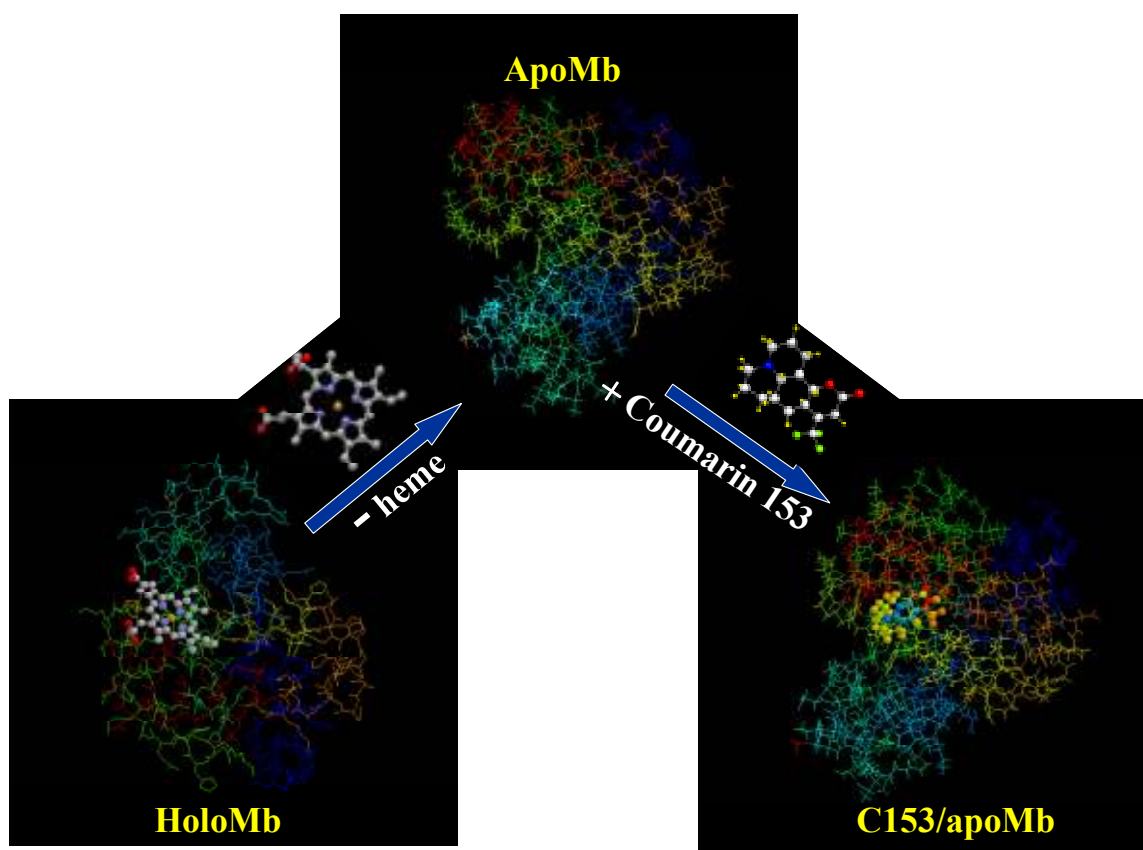
Figure I.2. System studied: Myoglobin with the prosthetic heme group is the holo-form, and that without the heme is the apo-form. Fluorescent dye coumarin 153 is inserted in the vacant heme pocket of the apomyoglobin.

Our work has been focused on relatively smaller globular heme proteins such as myoglobins and leghemoglobins. Myoglobin is the monomeric hemoglobin consisting of 153 amino acid residues found in muscle fibers of most mammals. Leghemoglobins are also monomeric heme proteins and are found in root nodules of leguminous plants. Comparisons between them are interesting because myoglobin and leghemoglobin share a common globin fold, but they have differences in their hemepockets.[64,65] For example, the F-helix is oriented in such a way that in myoglobin HisF8 (His93) eclipses the pyrrole nitrogens of the porphyrin but in leghemoglobin it is staggered with respect to them.   In the myoglobin

proximal hemepocket, SerF7 facilitates a hydrogen bonding network that drives HisF8 into a conformation that destabilizes ligand affinity. The opposite is true in leghemoglobin, which lacks SerF7 and contains a proximal hemepocket that destabilizes ligand binding. The two proteins exhibit differences on the distal sides of their heme pockets as well. The leghemoglobin distal pocket is larger and more flexible than those of most other hemoglobins and contains a combination of HisE7 (His64) and TyrB10 not found naturally in any other hemoglobin.

Figure I.3. Structure of solvatochromic probe coumarin 153 (C153)

There are four main considerations for our choice of this system. First, coumarin 153 (C153) is a well characterized and widely used chromophore for solvation dynamics studies [14,15,66-75] because it is exquisitely inert, structurally rigid and also associated with a large change of dipole moment upon optical excitation. Also the excited-state solvation has been demonstrated not to involve any contributions other than those from S_1.[66] Second, binding studies and molecular dynamics simulations indicate that coumarin indeed is in the hemepocket. [36,37] We have experimentally obtained a binding constant of ~ 6 μM for coumarin 153 and apomyoglobin and have characterized the complex[36,37] using Job's plot, capillary electrophoresis, fluorescence anisotropy, and circular dicroism experiments.

Having characterized the C153/apomyoglobin complex (Figure I.2) as a model system to study solvation dynamics in protein environments,[5,38] we have performed

fluorescence upconversion experiments to construct the solvation correlation function, C(t) and have compared the experimentally determined functions with those obtained from molecular dynamic simulations. [39] We discuss these in chapters III, IV and V in details.

Room Temperature Ionic Liquids

Room temperature ionic liquids, most commonly comprised of organic cations and inorganic anions, are receiving an increasing amount of attention because of their utility as environmentally friendly, "green" solvents and because of a host of practical applications to which they are amenable. [76-79] The term "ionic liquids" was selected with care, because it was believed that the more commonly used phrase 'molten salts' invoked a flawed image of these solvents as being high temperature, corrosive viscous media (for example, molten cryolite). In reality, room temperature ionic liquids can be liquid at temperatures as low as –96°C, are colorless, and easily handled. In the recent academic and patent literature, ionic liquids are normally taken as being liquids entirely made of ions that are fluid at temperatures around 100°C or below. There is nothing sacred about the temperature of 100°C. It is merely a convenient, arbitrary marker.[76]

The importance of ionic liquids has consequently stimulated considerable interest in their dynamic solvation properties. [6,8,31,80-107] Major questions regarding dynamic solvation by ionic liquids deal with whether the organic cation or the inorganic anion solvate preferentially on different time scales, the role of the correlated motion of the ion pairs and their lifetime, and the importance of translational motion of the ions relative to dipolar relaxation. [8,31,97]

Chiral recognition is a very important phenomenon in biochemical systems as well as in technological applications, enabling specific design of pharmaceuticals, chiral sensors and

molecular devices.[108]   In asymmetric organic photochemistry, chiral recognition in the excited state is vital to achieve enantio-selectivity during photosensitization and quenching processes.   As a result, investigations of stereoselective photochemical processes have become an attractive area in recent years,[109,110] and chiral ionic liquids provide a fascinating medium to study stereoselective processes. Only a few examples of chiral ionic liquids have been reported so far. [111-116]

Armstrong and co-workers have used a variety of methods to synthesize chiral ionic liquids either from chiral starting materials or using asymmetric synthesis.[117] They have provided the first application of chiral ionic liquids as stationary phases in chromatography using chiral ionic liquids as stationary phases in gas chromatography. Several compounds have been separated using these ionic-liquid-based chiral selectors. A large number of compounds, including alcohols, amines, sulfoxides, and epoxides were injected into the chiral-ionic-liquid based columns. These experiments demonstrate the first successful application of chiral ionic liquids as stationary phases in gas chromatography.[118],[119]

Chiral discrimination in excited-state processes has been studied by several groups in the past few years. The groups of Miranda[120-131] and Tolbert[132] have made considerable advances in this domain. Electron transfer induced by photoexcitation plays a vital role in numerous chemical and biological processes[23,133,134]. The rate of electron transfer is said to depend on the viscosity and the polarity of the solvent, especially in the case of intermolecular processes.

We have studied the interaction of a chiral naproxen dyad molecule in menthyl-based NTf_2 ionic liquids and bis(tertrabutylphosphonium) tartrate ionic liquids. We found that unlike in the menthyl pair, the amount of quenching is different in the bis(TBP) tartrate

isomeric liquids; and the tartrate enantiomers have a different temperature dependence on the nonradiative rate of the dyad. This chiral discrimination most likely arises from the steric effects of the different conformations of the chiral molecules. We have shown that viscosity and polarity of the solvents can influence the rate of electron transfer. On the other hand, such electron transfer was frustrated in the menthyl-based NTf$_2$ solvents. It is noteworthy that we have observed chiral discrimination by ionic liquids on both radiative and nonradiative processes.[135,136]

Cellulose and Cellulase enzymes

The efficient conversion of biomass into fuels is becoming increasingly important owing to diminishing resources of fossil fuels, as well as to global warming issues. Cellulose is the most abundant biorenewable material on the planet and is one of the main constituents of biomass. Consequently, during the past two decades, considerable effort has been devoted to the hydrolysis of cellulose in order to convert it into fuel. [137-143] There are, however, limitations to this process that are imposed mainly by the limited solubility of cellulose in water or other organic solvents. That is, cellulose is a linear polysaccharide chain (Figure I.4) consisting of hundreds to thousands of D-anhydroglucopyranose linked together by β (1→4)–glycosidic bonds.[139] In order to make the entire process of enzyme-catalyzed hydrolysis of cellulose green, the use of ionic liquids as solvents or co-solvents has received growing attention.

Of the several steps involved in the production of ethanol from cellulose, the most crucial and difficult is the cellulolysis, which is the hydrolysis of the cellulose polymer chain into glucose units.[139,141,143] Different catalysts have been used for this reaction, such as metal

chlorides,[140,142] acids, or enzymes.[137,144,145] The most common and widely used enzyme for this saccharification of cellulose is cellulase.
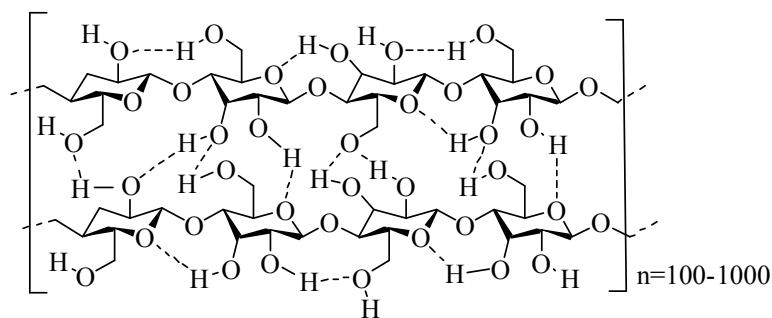
Figure I.4. Structure of linear polymer chain of cellulose, showing inter chain hydrogen bonding interactions.

Cellulase refers to a class of enzymes produced chiefly by fungi, bacteria, and protozoa that catalyze the cellulolysis (or hydrolysis) of cellulose. However, there are also cellulases produced by other types of organisms such as plants and animals. Several different kinds of cellulases are known, which differ structurally and mechanistically. Cellulases from fungal origin are known to be most powerful in cellulose hydrolysis.[146] The most common fungi from which cellulase has been prepared are *Tricoderma reesei*,[147,148] *Tricoderma viride*,[149] *Tricoderma koningii*,[150] *Aspergillus niger*,[151] *Sporotrichum pulverulentum*.[152] These fungi produce multicomponent enzyme system consisting of 1,4-β-*D*-glucanohydrolase (endoglucanse; EC 3.2.1.4), 1,4-β-*D*-glucan cellobiohydrolase (exoglucanase; EC 3.2.1.91) and β-*D*-glucoside glucohydrolase (β-glycosidase; EC 3.2.1.21) etc. Endoglucanase and exoglucanase work synergistically [153] in the hydrolysis of cellulose polymers, whereas β-glycosidase functions in removal of cellobiose, which is a strong inhibitor of endo- and exoglucanases (Figure I.5).[154,155]
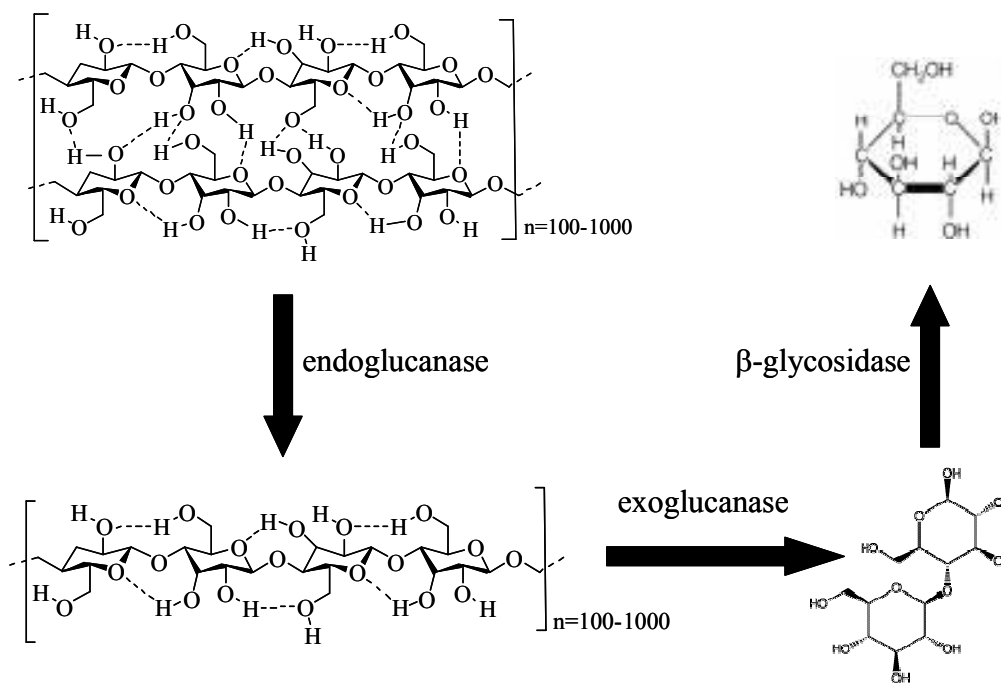
Figure I.5. Role of individual cellulase components in the hydrolysis of cellulose to glucose.

During the last decades, much attention has been paid in the field of biocatalysis in ionic liquids [144,156-159] by both academia and industry, because ionic liquids satisfy the green principles[76] that they should be environmentally benign, less hazardous, and provide improvements to industrial processes. Although numerous exploratory studies have been performed recently, the relationship between the structure of the ionic liquid and the activity or stability of the enzyme is not clearly understood. The most thoroughly studied enzyme in ionic liquids so far is *Candida antarctica* lipase B, used to catalyze transesterification reactions. [144,156,160] The work presented in this thesis is mainly devoted to cellulase in ionic liquids and its effect on the stability and activity of cellulase, since studies of cellulase-induced catalysis in ionic liquids is limited. [141,161-164]

The physical and chemical properties of ionic liquids vary considerably depending on their cation–anion pair. Several attempts have been made to explore the activity of enzymes in ionic liquids, and there are various issues concerning the stability of these biomacromolecules in ionic liquids. Most of them are ineffective for biocatalyis. It has been suggested that ionic liquids containing the anions Cl^-, Br^-, NO_3^-, $CF_3SO_3^-$ denature enzymes owing to their higher basicity and, hence, higher affinity for hydrogen bonds.[77,165] There are diverse opinions concerning the effect of fluorinated anions, such as BF_4^- and PF_6^-, on the enzyme's lifetime. Some reports suggest that since charge can be distributed over several fluorine atoms, the hydrogen bond affinity is minimized between the solvent and the enzyme and that, consequently, there is no interference with the internal hydrogen bonding network of the enzyme, maintaining its secondary structure.[144]

Biocatalysis in ionic liquids requires careful attention to the issue of the purity of ionic liquids.[144] Several groups have disagreed on whether or not an enzyme is active in a particular ionic liquid.   For example, Schöfer et al. [166] reported that *Candida antarctica* lipase B had no activity in bmim BF_4 or bmim PF_6, but other groups reported good activity for transesterification or ammoniolysis in the same ionic liquids. [167-169] Impurities may cause these inconsistencies.

One must also consider the compromise between viscosity and solubility. High viscosity is probably inherent to ionic liquids due to strong intermolecular forces between solvent ions.[144,170,171] The inherent high viscosity of the ionic liquids is a retarding factor for the rate of enzymatic hydrolysis, since it slows the diffusion of the enzyme to its target. Viscosity increases with the length of the alkyl chain. Although the highly viscous bmim Cl (11000 cP at 20°C[171]) slows down the rate of cellulase induced hydrolysis of cellulose,[161] it

can dissolve a substantial amount of cellulose.[172] As opposed to bmim Cl, cellulose has very limited solubility in bmim PF_6 (317 cP at 20°C[171]) and bmim BF_4 (233 cP at 20°C[173]), whereas the latter keeps the enzyme active. Thus it is very challenging to find the right combination for the cation–anion pair that can form a compromise between the opposing factors of dissolving cellulose, retaining the activity of the enzymes, and having a low viscosity.

The work presented in chapter VI and VII explores the activity of cellulase in a wide variety of ionic liquids with a judicious choice of different cations and anions and compare them with each other. We employed steady-state optical absorbance and fluorescence measurements as well as differential scanning calorimetry and thermal and microwave heating techniques to understand the stability of cellulase and its activity in different ionic liquids. We found that certain ionic liquids [174] stabilize the cellulases at temperatures as high as 115 ˚C whereas the enzymes are irreversibly denatured at 50 ˚C in aqueous buffer. Hydrolysis in ionic liquids is slower than that in buffer, which is attributed to the higher viscosity of the ionic liquids. Furthermore, while quenching of the fluorescence of the intrinsic amino acids of cellulases has been interpreted as a signal of protein denaturation (attributed to chloride ions), we demonstrate that such quenching is not necessarily associated with denaturation. When it does occur, for example, in the presence of ionic liquids formed from imidazolium cations and chloride anions, it arises from the imidazolium rather than the chloride.

Having established that in HEMA the cellulase is stable and thermally resistant even at temperatures close to 100°C, we extended our studies to aqueous mixtures of HEMA at different temperatures.[175] We have studied a pure component of cellulase, endo-1,4-β-D-

glucanase from fungus *Aspergillus niger* and found that the pure endoglucanase denatures at ~55˚C and the cellulose hydrolysis reaction ceases after two hours in buffer but the reaction progresses monotonically in the ionic liquid. Furthermore, HEMA imparts substantial stability to the enzyme, permitting the activity to peak at 75˚C. As a result HEMA proves to be a novel, green medium for performing cellulose hydrolysis reactions to convert biomass into biofuels. Because of the thermal stability it imparts to enzymes, it provides an ideal starting point for the design of ionic liquids, not only for the hydrolysis of biomass, but for use with a wide spectrum of enzymatic reactions.

Thesis Organization

Following this general introduction based on the various systems studied and their background and significance presented in the current chapter, the succeeding chapters are organized as follows.

Chapter II. Experimental techniques, fundamental concepts underlying them, and methods of data analysis.

Chapter III. Solvation dynamics in two monomeric heme proteins: myoglobin and leghemoglobin. Comparison of fluorescence upconversion measurements with molecular dynamics simulations.

Chapter IV. Several considerations for the construction of the solvation correlation function and its implications for the interpretation of dielectric relaxation in proteins are presented in detail.

Chapter V. Comparison of the dielectric response obtained from fluorescence upconversion measurements and molecular dynamics simulations for coumarin 153 bound to the heme

pocket of wild type apomyoglobin and its mutants. The agreement and disagreement between experiment and theory is explained based on the structure of the dye-protein complex used in the simulation studies. Extensive characterization studies have been performed using NMR and fluorescence methods.

Chapter VI. Enzyme catalyzed hydrolysis of cellulose in several ionic liquids. Out of the many liquids studied only two were found to be effective in balancing the condition of cellulose hydrolysis and enzyme stability. This work presented is a green approach towards the production of biofuels.

Chapter VII. Extension of the work presented in chapter VI. Cellulose hydrolysis was studied using a pure enzyme *Aspergillus niger* in different aqueous mixtures of ionic liquid, tris-(2-hydroxyethyl)-methylammonium methylsulfate (HEMA) at different temperatures.

Chapter VIII. Influence of chiral ionic liquids on stereoselective fluorescence quenching by photoinduced electron transfer in a naproxen dyad.

Chapter IX. General conclusions drawn from the work presented in this entire thesis.

References

(1)   Maroncelli, M. *J. Mol. Liq.* **1993**, *57*, 1.

(2)   Jimenez, R.; Fleming, G. R.; Kumar, P. V.; Maroncelli, M. *Nature* **1994**, *369*, 471.

(3)   McQuarrie, D. A. *Statistical Mechanics*; University Science Books, 2000.

(4)   Jordanides, X. J.; Lang, M. J.; Song, X.; Fleming, G. R. *J. Phys. Chem. B* **1999**, *103*, 7995.

(5)   Halder, M.; Mukherjee, P.; Bose, S.; Hargrove, M. S.; Song, X.; Petrich, J. W. *J. Chem. Phys.* **2007**, *127*, 055101/1.

(6)   Ingram, J. A.; Moog, R. S.; Ito, N.; Biswas, R.; Maroncelli, M. *J. Phys. Chem. B* **2003**, *107*, 5926.

(7)   Arzhantsev, S.; Jin, H.; Baker, G. A.; Maroncelli, M. *J. Phys. Chem. B* **2007**, *111*, 4978.

(8)   Chowdhury, P. K.; Halder, M.; Sanders, L.; Calhoun, T.; Anderson, J. L.; Armstrong, D. W.; Song, X.; Petrich, J. W. *J. Phys. Chem. B* **2004**, *108*, 10245.

(9)   Mukherjee, P.; Crank, J. A.; Halder, M.; Armstrong, D. W.; Petrich, J. W. *J. Phys. Chem. A* **2006**, *110*, 10725.

(10)   Mukherjee, P.; Crank, J. A.; Sharma, P. S.; Wijeratne, A. B.; Adhikary, R.; Bose, S.; Armstrong, D. W.; Petrich, J. W. *J. Phys. Chem. B* **2008**, *112*, 3390.

(11)   Nitzan, A. *Chemical Dynamics in Condensed Phases*, 1st ed.; Oxford University Press, 2007.

(12)   Lakowicz, J. R. *Principles of fluorescence spectroscopy*, 3rd ed.; Springer: New York, 2004.

(13)   Lang, M. J.; Jordanides, X. J.; Song, X.; Fleming, G. R. *J. Chem. Phys.* **1999**, *110*, 5884.

(14)   Horng, M. L.; Gardecki, J. A.; Papazyan, A.; Maroncelli, M. *J. Phys. Chem.* **1995**, *99*, 17311.

(15)   Maroncelli, M.; Fleming, G. R. *J. Chem. Phys.* **1987**, *86*, 6221.

(16)   Fröhlich, H. *Theory of Dielectrics*, 2nd ed.; Oxford University Press: New York, 1986.

(17)   Simon, J. D. *Acc. Chem. Res.* **1988**, *21*, 128.

(18)   Bagchi, B.; Oxtoby, D. W.; Fleming, G. R. *Chemical Physics* **1984**, *86*, 257.

(19)   Loring, R. F.; Yan, Y. Y.; Mukamel, S. *Chem. Phys. Lett.* **1987**, *135*, 23.

(20)   Böttcher, C. J. F. *Theory of Electric Polarization*, Second ed.; Elsevier: Amsterdam, 1973; Vol. 2.

(21)   Kahlow, M. A.; Kang, T. J.; Barbara, P. F. *J. Chem. Phys.* **1988**, *88*, 2372.

(22)   Castner, E. W.; Fleming, G. R.; Bagchi, B.; Maroncelli, M. *J. Chem. Phys.* **1988**, *89*, 3519.

(23)   Marcus, R. A.; Sutin, N. *Biochim. Biophys. Acta* **1985**, *811*, 265.

(24)   King, G.; Warshel, A. *J. Chem. Phys.* **1989**, *91*, 3647.

(25)   Bader, J. S.; Kuharski, R. A.; Chandler, D. *J. Chem. Phys.* **1990**, *93*, 230.

(26)   Simonson, T. *Curr. Opin. Struc. Biol.* **2001**, *11*, 243.

(27)   Zheng, C.; Wong, C. F.; McCammon, J. A.; Wolynes, P. G. *Chem. Scripta* **1989**, *29A*, 171.

(28)   Simonson, T. *Proc. Natl. Acad. Sci. USA* **2002**, *99*, 6544.

(29)   Sharp, K. A.; Honig, B. *Ann. Rev. Biophys. Chem.* **1990**, *19*, 301.

(30)   Simonson, T.; Perahia, D.; Brünger, A. T. *Biophys. J.* **1991**, *59*, 670.

(31)   Halder, M.; Headley, L. S.; Mukherjee, P.; Song, X.; Petrich, J. W. *J. Phys. Chem. A* **2006**, *110*, 8623.

(32)   Hsu, C. P.; Song, X. Y.; Marcus, R. A. *J. Phys. Chem. B* **1997**, *101*, 2546.

(33)   Song, X.; Chandler, D. *J. Chem. Phys.* **1998**, *108*, 2594.

(34)   Bader, J. S.; Kuharski, R. A.; Chandler, D. *Abstr. Paper Am. Chem. Soc.* **1990**, *199*, 65.

(35)   Song, X. *J. Chem. Phys.* **2002**, *116*, 9359.

(36)   Chowdhury, P. K.; Halder, M.; Sanders, L.; Arnold, R. A.; Liu, Y.; Armstrong, D. W.; Kundu, S.; Hargrove, M. S.; Song, X.; Petrich, J. W. *Photochem. Photobiol.* **2004**, *79*, 440.

(37)   Mukherjee, P.; Halder, M.; Hargrove, M.; Petrich, J. W. *Photochem. Photobiol.* **2006**, *82*, 1586.

(38)   Bose, S.; Adhikary, R.; Mukherjee, P.; Song, X.; Petrich, J. W. *J. Phys. Chem. B* **2009**, *113*, 11061.

(39)   Bose, S.; Adhikary, R.; Barnes, C. A.; Fulton, D. B.; Hargrove, M. S.; Song, X.; Petrich, J. W. *J. Phys. Chem. A* **2010**, in press.

(40)   Bashkin, J. S.; Mclendon, G.; Mukamel, S.; Marohn, J. *J. Phys. Chem.* **1990**, *94*, 4757.

(41)   Pierce, D. W.; Boxer, S. G. *J. Phys. Chem.* **1992**, *96*, 5560.

(42)   Abbyad, P.; Shi, X.; Childs, W.; McAnaney, T. B.; Cohen, B. E.; Boxer, S. G. *J. Phys. Chem. B* **2007**, *111*, 8269.

(43)   Cohen, B. E.; McAnaney, T. B.; Park, E. S.; Jan, Y. N.; Boxer, S. G.; Jan, L. Y. *Science* **2002**, *296*, 1700.

(44)   Adhikary, R.; Barnes, C. A.; Petrich, J. W. *J. Phys. Chem. B* **2009**, *113*, 11999.

(45)   Pal, S. K.; Peon, J.; Bagchi, B.; Zewail, A. H. *J. Phys. Chem. B* **2002**, *106*, 12376.

(46)   Zhong, D. P.; Pal, S. K.; Zhang, D. Q.; Chan, S. I.; Zewail, A. H. *Proc. Natl. Acad. Sci. USA* **2002**, *99*, 13.

(47)   Pal, S. K.; Peon, J.; Zewail, A. H. *Proc. Natl. Acad. Sci. USA* **2002**, *99*, 1763.

(48)   Peon, J.; Pal, S. K.; Zewail, A. H. *Proc. Natl. Acad. Sci. USA* **2002**, *99*, 10964.

(49)   Lu, W.; Kim, J.; Qiu, W.; Zhong, D. *Chem. Phys. Lett.* **2004**, *388*, 120.

(50)   Qiu, W.; Kao, Y.-T.; Zhang, L.; Yang, Y.; Wang, L.; Stites, W. E.; Zhong, D.; Zewail, A. H. *Proc. Natl. Acad. Sci. USA* **2006**, *103*, 13979.

(51)   Qiu, W.; Zhang, L.; Okobiah, O.; Yang, Y.; Wang, L.; Zhong, D.; Zewail, A. H. *J. Phys. Chem. B.* **2006**, *110*, 10540.

(52)   Nandi, N.; Bhattacharyya, K.; Bagchi, B. *Chem. Rev.* **2000**, *100*, 2013.

(53)   Bhattacharyya, K.; Bagchi, B. *J. Phys. Chem. A* **2000**, *104*, 10603.

(54)   Pal, S. K.; Mandal, D.; Sukul, D.; Sen, S.; Bhattacharyya, K. *J. Phys. Chem. B* **2001**, *105*, 1438.

(55)   Guha, S.; Sahu, K.; Roy, D.; Mondal, S. K.; Roy, S.; Bhattacharyya, K. *Biochemistry* **2005**, *44*, 8940.

(56)   Sahu, K.; Mondal, S. K.; Ghosh, S.; Roy, D.; Sen, P.; Bhattacharyya, K. *J. Phys. Chem. B* **2006**, *110*, 1056.

(57)   Nandi, N.; Bagchi, B. *J. Phys. chem. B* **1997**, *101*, 10954.

(58)   Stryer, L. *J. Mol. Biol.* **1965**, *13*, 482.

(59)   Cocco, M. J.; Lecomte, J. T. J. *Protein Sci.* **1994**, *3*, 267.

(60)   Wagner, U. G.; Muller, N.; Schmitzberger, W.; Falk, H.; Kratky, C. *J. Mol. Biol.* **1995**, *247*, 326.

(61)   Shen, X.; Knutson, J. R. *J. Phys. Chem. B* **2001**, *105*, 6260.

(62)   Macgregor, R. B.; Weber, G. *Nature* **1986**, *316*, 70.

(63)   Raven, E.; Montellano, P. R. O. d. *Nat. Prod. Rep.* **2007**, *24*, 499.

(64) Kundu, S.; Snyder, B.; Das, K.; Chowdhury, P.; Park, J.; Petrich, J. W.; Hargrove, M. S. *Proteins: Struct. Funct. Genet.* **2002**, *46*, 268.

(65) Kundu, S.; Hargrove, M. S. *Proteins: Struct. Funct. Genet.* **2003**, *50*, 239.

(66) Lewis, J. E.; Maroncelli, M. *Chem. Phys. Lett.* **1998**, *282*, 197.

(67) Kovalenko, S. A.; Ruthmann, J.; Ernsting, N. P. *Chem. Phys. Lett.* **1997**, *271*, 40.

(68) Muhlpfordt, A.; Schanz, R.; Ernsting, N. P.; Farztdinov, V.; Grimme, S. *Phys. Chem. Chem. Phys.* **1999**, *1*, 3209.

(69) Changenet-Barret, P.; Choma, C. T.; Gooding, E. F.; DeGrado, W. F.; Hochstrasser, R. M. *J. Phys. Chem. B* **2000**, *104*, 9322.

(70) Jiang, Y.; McCarthy, P. K.; Blanchard, D. J. *Chem. Phys.* **1994**, *183*, 249.

(71) Flory, W. C.; Blanchard, D. J. *Appl. Spectrosc.* **1998**, *52*, 82.

(72) Palmer, P. M.; Chen, Y.; Topp, M. R. *Chem. Phys. Lett.* **2000**, *318*, 440.

(73) Chen, Y.; Palmer, P. M.; Topp, M. R. *Int. J. Mass Spectrom* **2002**, *220*, 231.

(74) Agmon, N. *J. Phys. Chem.* **1990**, *94*, 2959.

(75) Maroncelli, M.; Fee, R. S.; Chapman, C. F.; Fleming, G. R. *J. Phys. Chem.* **1991**, *95*, 1012.

(76) Seddon, K. R. *Nature (Materials)* **2003**, *2*, 363.

(77) Anderson, J. L.; Ding, J.; Welton, T.; Armstrong, D. W. *J. Am. Chem. Soc* **2002**, *124*, 14247.

(78) Anderson, J. L.; Armstrong, D. W.; Wei, G.-T. *Anal. Chem.* **2006**, *78*, 2893.

(79) Pandey, S. *Analytica Chimica Acta* **2006**, *556*, 38.

(80) Karmakar, R.; Samanta, A. *J. Phys. Chem. A* **2002**, *106*, 6670.

(81)   Karmakar, R.; Samanta, A. *J. Phys. Chem. A* **2002**, *106*, 4447.

(82)   Karmakar, R.; Samanta, A. *J. Phys. Chem. A* **2003**, *107*, 7340.

(83)   Ito, N.; Arzhantsev, S.; Maroncelli, M. *Chem. Phys. Lett.* **2004**, *396*, 83.

(84)   Ito, N.; Arzhantsev, S.; Heitz, M.; Maroncelli, M. *J. Phys. Chem. B* **2004**, *108*, 5771.

(85)   Arzhantsev, S.; Ito, N.; Heitz, M.; Maroncelli, M. *Chem. Phys. Lett.* **2003**, *381*, 278.

(86)   Arzhantsev, S.; Hui, J.; Baker, G. A.; Naoki, I.; Maroncelli, M. "Solvation dynamics in ionic liquids, results from ps and fs emission spectroscopy." Femtochemistry VII, 2005.

(87)   Arzhantsev, S.; Hui, J.; Naoki, I.; Maroncelli, M. *Chem. Phys. Lett.* **2006**, *417*, 524.

(88)   Hyun, B.-R.; Dzyuba, S. V.; Bartsch, R. A.; Quitevis, E. L. *J. Phys. Chem. A* **2002**, *106*, 7579.

(89)   Giraud, G.; Gordon, C. M.; Dunkin, I. R.; Wynne, K. *J. Chem. Phys.* **2003**, *119*, 464.

(90)   Cang, H.; Li, J.; Fayer, M. D. *J. Chem. Phys.* **2003**, *119*, 13017.

(91)   Shirota, H.; Funston, A. M.; Wishart, J. F.; Castner, E. W., Jr. *J. Chem. Phys.* **2005**, *122*, 184512.

(92)   Rajian, J. R.; Li, S.; Bartsch, R. A.; Quitevis, E. L. *Chem. Phys. Lett.* **2004**, *393*, 372.

(93)   Shirota, H.; Castner, E. W., Jr. *J. Phys. Chem. A* **2005**, *109*, 9388.

(94)   Weingärtner, H.; Knocks, A.; Schrader, W.; Kaatze, U. *J. Phys. chem. A* **2001**, *105*, 8646.

(95)   Wakai, C.; Oleinikova, A.; Ott, M.; Weingärtner, H. *J. Phys. Chem. B* **2005**, *109*, 17028.

(96)   Ito, N.; Huang, W.; Richert, R. *J. Phys. Chem. B* **2006**, *110*, 4371.

(97)   Headley, L. S.; Mukherjee, P.; Anderson, J. L.; Ding, R.; Halder, M.; Armstrong, D. W.; Song, X.; Petrich, J. W. *J. Phys. Chem. A* **2006**, *110*, 9549.

(98)   Margulis, C. J.; Stern, H. A.; Berne, B. J. *J. Phys. Chem. B* **2002**, *106*, 12017.

(99)   Shim, Y.; Duan, J.; Choi, M. Y.; Kim, H. J. *J. Chem. Phys.* **2003**, *119*, 6411.

(100)   Znamenskiy, V.; Kobrak, M. N. *J. Phys. Chem. B* **2004**, *108*, 1072.

(101)   Kobrak, M. N.; Znamenskiy, V. *Chem. Phys. Lett.* **2004**, *395*, 127.

(102)   Del Popolo, M. G.; Voth, G. A. *J. Phys. Chem. B* **2004**, *108*, 1744.

(103)   Morrow, T. I.; Maginn, E. J. *Journal of Physical Chemistry B* **2002**, *106*, 12807.

(104)   Hu, Z.; Margulis, C. J. *Proc. Natl. Acad. Sci. U.S.A.* **2006**, *103*, 831.

(105)   Lang, B.; Angulo, G.; Vauthey, E. *J. Phys. Chem. A* **2006**, *110*, 7028.

(106)   Samanta, A. *J. Phys. Chem. B* **2006**, *110*, 13704.

(107)   *Journal of Physical Chemistry B* **2007**, *111*, 4639.

(108)   Beddell, C. R. *The Design of Drugs to Macaromolecular Targets*; Wiley, Chichester, 1992.

(109)   Inoue. *Chem. Rev.* **1992**, *92*, 741.

(110)   Griesbeck, A. G.; Meierhenrich, U. J. *Angew. Chem.* **2002**, *41*, 3147.

(111)   Howarth, J.; Hanlon, K.; Fayne, D.; McCormac, P. B. *Tetrahedon Lett.* **1997**, *38*, 3097.

(112)   Earle, M. J.; McCormac, P. B.; Seddon, K. R. *Green Chem.* **1999**, *1*, 23.

(113)   Wasserscheid, P.; Bösmann, A.; Bolm, C. *Chem. Commun.* **2002**, *2002*, 200.

(114)   Bao, W.; Wang, Z.; Li, Y. H. *J. Org. Chem.* **2003**, *68*, 591.

(115)   Bwambok, D. K.; Marwani, H. M.; Fernand, V. E.; Fakayode, S. O.; Lowry, M.; Negulescu, I.; Strongin, R. M.; Warner, I. M. *Chirality* **2008**, *20*, 151.

(116)   Yu, S.; Lindeman, S.; Tran, C. D. *J. Org. Chem.* **2008**, *73*, 2576.

(117)   Ding, J.; Armstrong, D. W. *Chirality* **2005**, *17*, 281.

(118)   Ding, J.; Welton, T.; Armstrong, D. W. *Anal. Chem.* **2004**, *76*, 6819.

(119)   Ding, J.; Desikan, V.; Han, X.; Xiao, T. L.; Ding, R.; Jenks, W. S.; Armstrong, D. W. *Org. Lett.* **2005**, *7*, 335.

(120)   Abad, S.; Pischel, U.; Miranda, M. A. *J. Phys. Chem. A* **2005**, *109*, 2711.

(121)   Pischel, U.; Abad, S.; Miranda, M. A. *Chem. Commun.* **2003**, 1088.

(122)   Boscá, F.; Andreu, I.; Morera, I. M.; Samadi, A.; Miranda, M. A. *Chem. Commun.* **2003**, 1592.

(123)   Miranda, M. A.; Lahoz, A.; Martinez-Mañez, R.; Boscá, F.; Castell, J. V.; Pérez-Prieto, J. *J. Am. Chem. Soc* **1999**, *121*, 11569.

(124)   Pischel, U.; Abad, S.; Domingo, L. R.; Boscá, F.; Miranda, M. A. *Angew. Chem. Int. Ed.* **2003**, *42*, 2531.

(125)   Miranda, M. A.; Lahoz, A.; Boscá, F.; Metni, M. R.; Abdelouahab, F. B.; Castell, J. V.; Pérez-Prieto, J. *Chem. Commun.* **2000**, 2257.

(126) Boscá, F.; Marin, M. L.; Miranda, M. A. *Photochem. Photobiol.* **2001**, *74*, 6
37.

(127) Boscá, F.; Canudas, N.; Marin, M. L.; Miranda, M. A. *Photochem. Photobiol.*
2000, *71*, 173.

(128) Vayá, I.; Jiménez, M. C.; Miranda, M. A. *Tetrahedron: Asymm.* **2005**, *16*,
2167.

(129) Jiménez, M. C.; Stiriba, S.-E.; Tormos, R.; Pérez-Prieto, J.; Miranda, M. A.
Photochem. Photobiol. Sci. **2004**, *3*,

36.

(130) Encinas, S.; Climent, M. J.; Belmadoui, N.; Miranda, M. A. *Chem. Commun.*
2005, 2572.

(131) Abad, S.; Pischel, U.; Miranda, M. A. *Photochem. Photobiol. Sci.* **2005**, *4*,
69.

(132) Solntsev, K. M.; Tolbert, L. M.; Cohen, B.; Huppert, D.; Hayashi, Y.;
Feldman, Y. *J. Am. Chem. Soc.* **2002**, *124*, 9046.

(133) Wang, Z. Y.; Pearlstein, R. M.; Jia, Y. W.; Fleming, G. R.; Norris, J. R.
Chemical Physics **1993**, *176*, 421.

(134) Jimenez, R.; Fleming, G. R. *Adv. Photosynth.* **1996**, *3*, 63.

(135) Adhikary, R.; Bose, S.; Mukherjee, P.; Thite, A.; Kraus, G. A.; Wijeratne, A.
B.; Sharma, P.; Armstrong, D. W.; Petrich, J. W. *J. Phys. Chem. B* **2008**, *112*, 7555.

(136) Bose, S.; Wijeratne, A. B.; Thite, A.; Kraus, G. A.; Armstrong, D. W.;
Petrich, J., W. *J. Phys. Chem. B* **2009**, *113*, 10825.

(137) Ladisch, M. R.; Ladisch, C. M.; Tsao, G. T. *Science* **1978**, *201*, 743.

(138)   Lynd, L. R.; Cushman, J. H.; Nichols, R. J.; Wyman, C. E. *Science* **1991**, *251*, 1318.

(139)   Zhang, Y.-H. P.; Lynd, L. R. *Biotechnol. Bioeng.* **2004**, *88*, 797.

(140)   Su, Y.; Brown, H. M.; Huang, X.; Zhou, X.-d.; Amonette, J. E.; Zhang, Z. C. *Appl. Catalysis A* **2009**, *361*, 117.

(141)   Dadi, A. P.; Varanasi, S.; Schall, C. A. *Biotechnol. Bioeng.* **2006**, *95*, 904.

(142)   Zhao, H.; Holladay, J. E.; Brown, H.; Zhang, Z. C. *Science* **2007**, *316*, 1597.

(143)   Xiang, Q.; Lee, Y. Y.; Pettersson, P. O.; Torget, R. W. *Appl. Biochem. Biotechnol.* **2003**, *107*, 505.

(144)   Park, S.; Kazlauskas, R. J. *Curr. Opin. Biotechnol.* **2003**, *14*, 432.

(145)   Lu, Y.; Zhang, Y.-H. P.; Lynd, L. R. *Proc. Natl. Acad. Sci.* **2006**, *103*, 16165.

(146)   Beldman, G.; Searle-van Leeuwen, M.; Rombouts, F. M.; Voragen, F. G. J. *Eur. J. Biochem.* **1985**, *146*, 301.

(147)   Mandels, M.; Meideiros, J. E.; Andreotti, R. E.; Bisset, F. H. *Biotechnol. Bioeng.* **1981**, *23*, 2009.

(148)   Tangu, S. K.; Blanch, H. W.; Wilke, C. R. *Biotechnol. Bioeng.* **1981**, *23*, 1837.

(149)   Shin, S. B.; Kitakawa, Y.; Suga, K. I.; Ichikawa, K. *J. Ferment. Technol.* **1978**, *56*, 396.

(150)   Woods, T. M. *Biochem. J.* **1968**, *109*, 217.

(151)   Hurst, P. L.; Nielsen, J.; Sullivan, P. A.; Shepherd, M. G. *Biochem. J.* **1977**, *165*, 33.

(152)   Eriksson, K. E.; Pettersson, B. *Eur. J. Biochem.* **1975**, *51*, 193.

(153) Kleman-Leyer, K. M.; Siika-Aho, M.; Teeri, T. T.; Kirk, T. K. *Appl. Environ. Microbiol.* **1996**, *62*, 2883.

(154) Woodward, J.; Wiseman, A. *Enzyme Microbial Technol.* **1982**, *4*, 73.

(155) van Tilbeurgh, H.; Loontiens, F. G.; Engelborgs, Y.; Claeyssens, M. *Eur. J. Biochem.* **1989**, *184*, 553.

(156) Sheldon, R. A.; Lau, R. M.; Sorgedrager, M. J.; Rantwijk, F. v.; Seddon, K. R. *Green Chem.* **2002**, *4*, 147.

(157) Rantwijk, F. v.; Sheldon, R. A. *Chem. Rev.* **2007**, *107*, 2757.

(158) Yang, Z.; Pan, W. *Enzyme Microbial Technol.* **2005**, *37*, 19.

(159) Cantone, S.; Hanefeld, U.; Basso, A. *Green Chem.* **2007**, *9*, 954.

(160) Lau, R. M.; Rantwijk, F. v.; Seddon, K. R.; Sheldon, R. A. *Org. Lett.* **2000**, *2*, 4189.

(161) Turner, M. B.; Spear, S. K.; Huddleston, J. G.; Holbrey, J. D.; Rogers, R. D. *Green Chem.* **2003**, *5*, 443.

(162) Kamiya, N.; Matsushita, Y.; Hanaki, M.; Nakashima, K.; Narita, M.; Goto, M.; Takahashi, H. *Biotechnol. Lett.* **2008**, *30*, 1037.

(163) Liying, L.; Hongzhang, C. *Chinese Science Bulletin* **2006**, *51*, 2432.

(164) Jones, P. O.; Vasudevan, P. T. *Biotechnol. Lett.* **2010**, *32*, 103.

(165) Kaar, J. L.; Jesionowski, A. M.; Berberich, J. A.; Moulton, R.; Russell, A. J. *J. Am. Chem. Soc.* **2003**, *125*, 4125.

(166) Schofer, S. H.; Kaftzik, N.; Wasserscheid, P.; Kragl, U. *Chem. Commun.* **2001**, 425.

(167) Kim, K.-W.; Song, B.; Choi, M.-Y.; Kim, M.-J. *Org. Lett.* **2001**, *3*, 1507.

(168)   Itoh, T.; Akasaki, E.; Kudo, K.; Shirakami, S. *Chem. Lett.* **2001**, *30*, 262.

(169)   Lau, R. M.; Rantwijk, F. v.; Seddon, K. R.; Sheldon, R. A. *Org. Lett.* **2000**, *2*, 4189.

(170)   Welton, T. *Chem. Rev.* **1999**, *99*, 2071.

(171)   Seddon, K. R.; Stark, A.; Torres, M.-J. Viscosity and density of 1-alkyl-3-methylimidazolium ionic liquids. In *Clean Solvents: Alternative Media for Chemical Reactions and Processing.*; ACS Symposium Series, 2002; Vol. 819; pp 34.

(172)   Swatloski, R. P.; Spear, S. K.; Holbrey, J. D.; Rogers, R. D. *J. Am. Chem. Soc.* **2002**, *124*, 4974.

(173)   Carda-Broch, S.; Berthod, A.; Armstrong, D. W. *Anal. Bioanal. Chem.* **2003**, *375*, 191.

(174)   Bose, S.; Armstrong, D. W.; Petrich, J. W. *J. Phys. Chem. B* **2010**, *114*, 8221.

(175)   Bose, S.; Petrich, J. W. *Green. Chem.* **2010**, submitted.

CHAPTER II: EXPERIMENTAL TECHNIQUES AND DATA ANALYSIS

Fluorescence spectroscopy measurements can be broadly classified into two categories, namely, steady-state and time-resolved.[1] Steady-state measurements involve constant illumination of the sample with a continuous beam of light while the emission spectrum is recorded by scanning the emission monochromator and corrected for detector response.[2] Steady-state spectra generally report on equilibrium conditions when all the vibrational and solvent induced relaxation of the excited species are completed and the rate of excitation and emission under constant illumination are equal. On the other hand, time-resolved measurements are performed with a pulsed light source; and the decay of the fluorescence intensity is monitored as a function of time with fast detection systems. A steady-state observation is the average of the time-resolved phenomena over the intensity decay of the sample. For a fluorophore that exhibits exponential fluorescence decay, the intensity profile is given by,

$$I(t) = I_0 \exp(-t/\tau) \qquad (\text{II.1})$$

where I_0 and τ are the intensity at t=0 and the mono-exponential decay time, respectively. The fluorescence quantum yield is the ratio of the number of photons emitted to the number absorbed. It is expressed as,

$$\Phi = \frac{k_r}{k_r + k_{nr}} \qquad (\text{II.2})$$

where k is the rate of depopulation of the excited state through radiative (r) and non-radiative (nr) processes. The fluorescence lifetime (τ) is related to the quantum yield as

$$\tau = \Phi/k_r. \qquad (\text{II.3})$$

Another simple way of relating the steady-state to the time-resolved measurement is,

$$I_{SS} = \int_0^\infty I_0 \exp(-t/\tau)dt = I_0\tau \qquad (II.\ 4)$$

which is in accordance with equation 2 and 3, where I_{SS} is the steady-state fluorescence intensity.

This chapter solely focuses on the time-resolved measurements and associated concepts of different time-resolved techniques used in the latter chapters of the thesis. As mentioned above, all time-domain experiments need a pulsed light source, which in our laboratory is the pulsed laser. The chapter begins with the description of the principle excitation source obtained from the titanium-sapphire oscillator, whose output is frequency doubled or tripled to produce blue and ultra-violet source for exciting different fluorophores. The two principle ultrafast time-resolved techniques, namely time-correlated single photon counting and fluorescence upconversion, have been described in detail. In the next section of data analysis, the two most important parameters of solvation dynamics, the reorganization energy and solvation correlation function, are discussed in detail. Other photophysical processes, such as fluorescence resonance energy transfer and fluorescence anisotropy decay are also discussed.

Ti:Sapphire Oscillators

Titanium:sapphire lasers were introduced in 1986,[3] and thereafter they quickly replaced most dye lasers, which had previously served as the major research tool in ultrafast spectroscopy. Ti:sapphire lasers are very convenient because they can easily be tuned to the required pump wavelength and allow one to work with very high pump brightness due to their good beam quality and high output power of typically several watts.
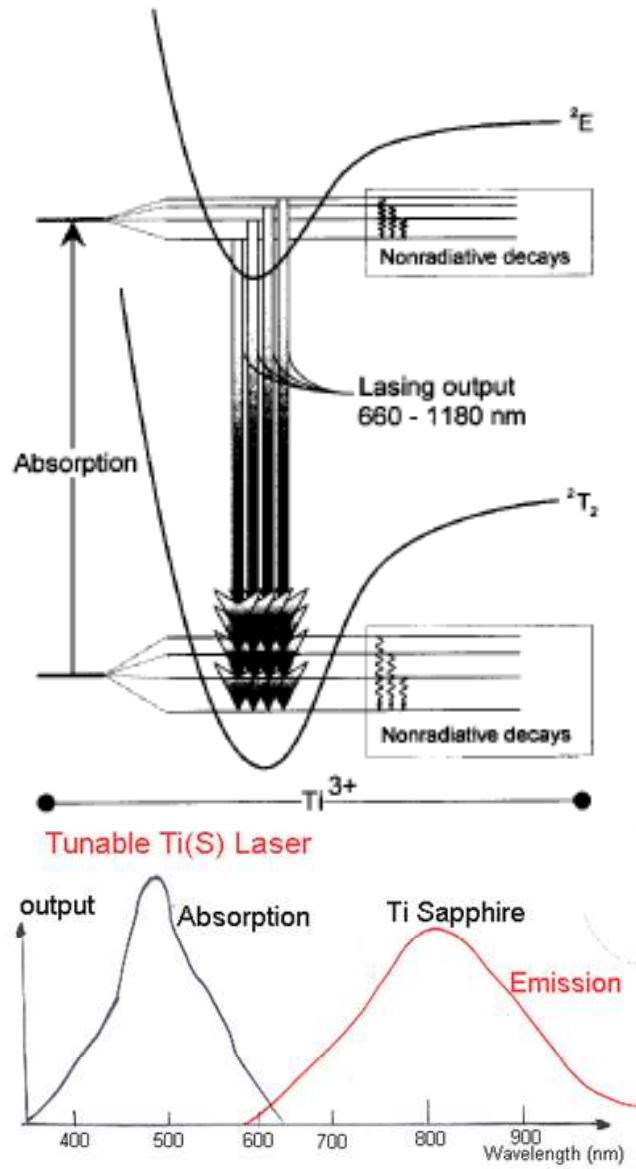
Figure II.1. Ti-Sapphire energy level diagram and its absorption and emission range. [4]
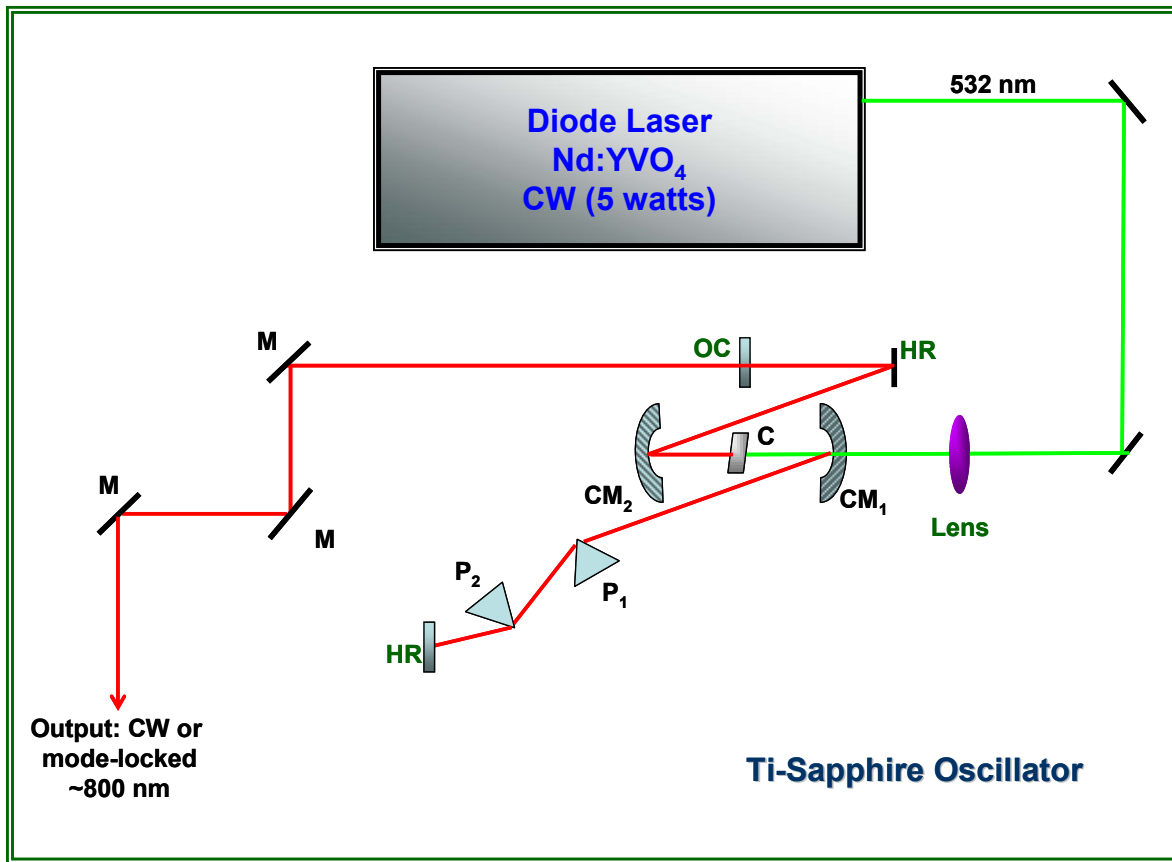
Figure II.2. Schematic diagram of the Ti-Sapphire oscillator build in our laboratory based on Kapteyn-Murnane cavity design.[5]

The gain medium of the oscillator is the Ti-sapphire crystal, which consists of 0.1% titanium added to sapphire (Al_2O_3) to replace aluminum in the crystal lattice. The titanium atom interacts strongly with the host crystal to make the range of transition energies exceptionally broad. The Ti^{3+} ion has a very large gain bandwidth (much larger than that of rare-earth-doped gain media), allowing the generation of very short pulses[6-8] and also wide wavelength tunability. The maximum gain and laser efficiency are at ~ 800 nm. The possible tuning range is ~660 nm to 1180 nm.[9] The Ti-Sapphire oscillator is conveniently pumped with a 5W Spectra Physics Millenia V Nd:YVO_4 (532 nm) laser. A favorable feature of the Ti:sapphire lasers is that they are self-mode locking[5,10] and simple tapping on the appropriate

mirror can convert it from continuous mode to mode-locked operation by locking the phases of laser modes to yield an ultrafast pulse. The phenomenon of self mode locking is termed Kerr lens mode locking.

Kerr lens mode locking is caused by the self-focusing effect that is produced by the nonlinear refractive-index change of the laser rod or an additional nonlinear medium such as a crystal.[11,12] When an additional intracavity aperture is introduced,[13] the operation of mode locking can be understood as an effect of the intensity-dependent loss produced by the combined action of self-focusing and the aperture. The operation of mode locking therefore is similar to passive mode-locking in solid-state lasers with a fast saturable absorber.
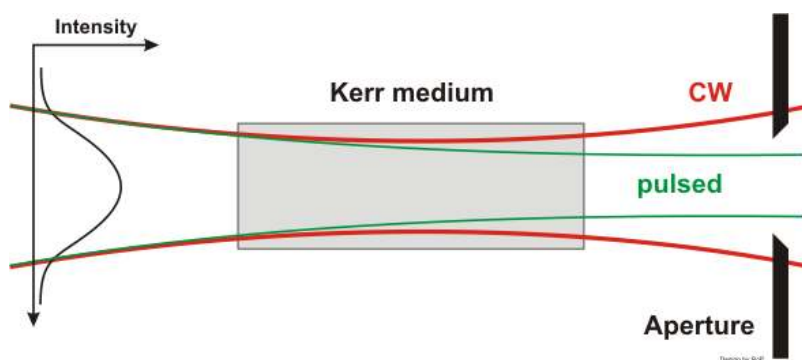
Figure II.3. Basic principle of Kerr lens mode locking.

For highly intense incident light, the refractive index (n) of the passing medium depends on the intensity as

$$n(I) = n_0 + n_2(I) \qquad\qquad (II.5)$$

where n_2 is the non-linear refractive index. This intensity-dependent change of refractive index is caused by the non-linear polarization of the electron shell induced by the electric field of the optical wave and is called the Optical Kerr Effect (OKE).[14,15] The

electromagnetic field inside the laser cavity has a Gaussian distribution of intensity, which creates a similar distribution of the refractive index. The high-intensity beam is self-focused by the photoinduced lens. This is a consequence of nonlinear response in which the refractive index of the material is larger in the center of the beam than at its periphery. Thus the medium behaves like a positive lens tending the incident laser beam to be focused. If the medium length is short enough, the focus will occur outside the material, on other hand catastrophic damage will occur if the focusing takes place inside the nonlinear medium where its length is sufficiently long.[16] On chopping the leading and trailing edges, the transmitted pulse becomes shorter than the incident pulse[17-19] as shown in Figure II.3.

Second and Third Harmonic Generation

Nonlinear optics is the study of phenomena that occurs as a consequence of the alteration of optical properties of a medium by the presence of light. At high optical intensities the material response is nonlinear in the input power and new optical frequencies can be generated by various intriguing nonlinear optical processes [16,20]. The basis for most theories in nonlinear optics is a Taylor expansion of the material polarization $P(t)$ in powers of the electric field $E(t)$ as

$$P(t) = \chi^{(1)}E(t) + \chi^{(2)}E^2(t) + \chi^{(3)}E^3(t) + ... \qquad (II.6)$$

$\chi^{(1)}$ is the linear susceptibility. In linear optics involving weak to moderate optical intensities, the polarization depends linearly with the applied electric field, but it deviates from linearity with high optical intensities; and the second and third order dependence arises as shown in equation II.6, with $\chi^{(2)}$ and $\chi^{(3)}$ being the second- and third-order non-linear optical susceptibilities. An important symmetry aspect of the above Taylor expansion is that all even-order coefficients must disappear for media with inversion symmetry. The

explanation is simple: the operation $\vec{r} \rightarrow -\vec{r}$ leaves the inversion-symmetric media unaffected, but does add minus signs to both $\vec{P} \rightarrow -\vec{P}$ and $\vec{E} \rightarrow -\vec{E}$. This is only possible when $\chi^{(n)} = 0$ for even n. The phenomena of second and third harmonic generation are most common examples of non-linear optical interaction where the second and third order term in equation II.6 is associated with the second and third harmonic generation, respectively.

The process of second-harmonic generation proceeds in two steps. In the first step, the incident field E_1 at frequency ω_1 excites a weak nonlinear polarization at the double frequency $P_2 \propto E_1^2$. In the second step this induced nonlinear polarization P_2 radiates and emits an optical field E_2 at optical frequency 2ω. This emission is only efficient when the induced dipoles radiate in-phase, which occurs when the refractive indices at ω and 2ω are identical, i.e., when $n(\omega) \approx n(2\omega)$. This so-called index matching or phase matching is of crucial importance for the efficiency of second-harmonic generation, and it can only be conveniently reached in birefringent (or double refracting) materials.[21,22] In birefringent crystals the refractive index depends not only on wavelength, but also on the polarization direction of the electric field vector E with respect to the crystal as illustrated in Figure II.4.[23] In uniaxial crystals, one axis (the so-called optic axis) is different from the other two identical axes. Electric field components perpendicular to the optic axis propagate according to the *ordinary refractive index* $n_o(\lambda)$, whereas the orthogonal field components propagate according to the so-called *extra-ordinary index* $n_e(\theta,\lambda)$ and it depends on θ as

$$\frac{1}{n_e^2(\theta,\lambda)} = \frac{\sin^2\theta}{n_e^2(\lambda)} + \frac{\cos^2\theta}{n_O^2(\lambda)} \tag{II.7}$$
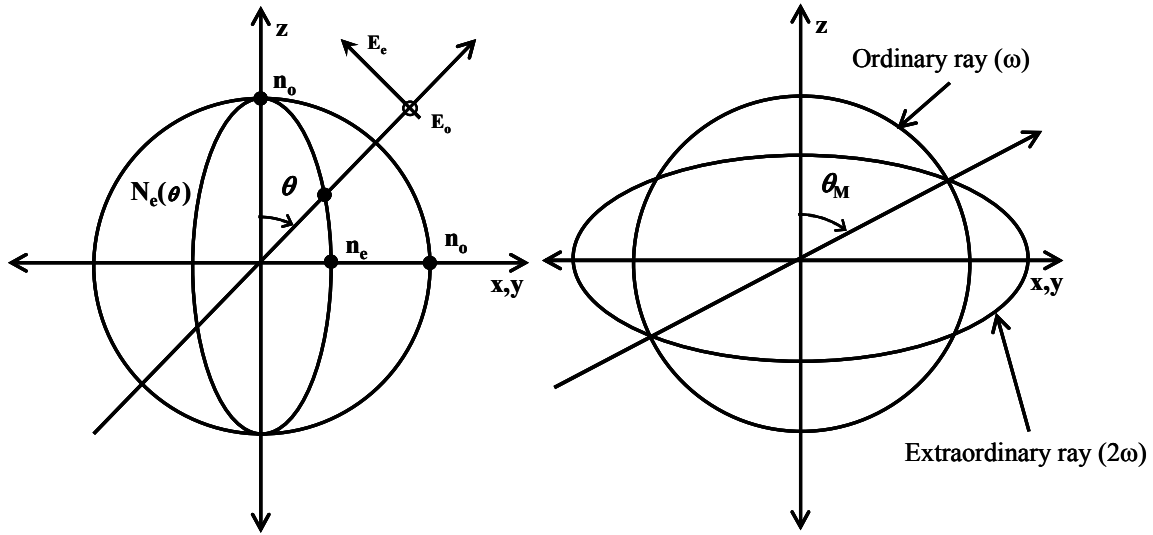
Figure II.4. (Left) Refractive index ellipsoid for a uniaxial crystal, with optic axis along z-direction and n_O and n_e are the ordinary and extraordinary refractive indices and θ is the angle between the direction of the electric field (*E*) and the z-axis. (Right) Possibility of index matching at angle θ_M for an ordinary ray (ω) and extraordinary ray (2ω).[24]

From Figure II.4, in the case of a uniaxial crystal, the ordinary refactive index is independent of the angle (θ) between the propagation vector of the electric field and the optic axis, whereas extraordinary refractive index varies with θ. The amount of birefringence, which is the difference between n_O and n_e is minimum when the *E* vector is parallel to the z-axis ($\theta = 0°$), i.e., $n_e = n_O$. When the *E* vector propagates in the xy-plane ($\theta = 90°$), birefringence is maximized. The index matching condition is achieved for an ordinary ray with frequency ω and an extraordinary ray with 2ω, when the ellipse of $n_e^{2\omega}$ intersects the circle of n_O^{ω} at an angle θ_M, which can be derived from equation II.7 and is given by

$$\sin^2 \theta_M = \frac{(n_O^{\omega})^{-2} - (n_O^{2\omega})^{-2}}{(n_e^{2\omega})^{-2} - (n_O^{2\omega})^{-2}} \tag{II.8}$$

The third order term $\chi^{(3)}E^3(t)$ in equation II.6 is responsible for the third harmonic generation. If the electric field $E(t) = E_0 \cos(\omega t)$, then the third order non-linear polarization can be written as[16]

$$P^{(3)}(t) = \frac{1}{4}\chi^{(3)}E_0^3 \cos 3\omega t + \frac{3}{4}\chi^{(3)}E_0^3 \cos \omega t \qquad (II.9)$$

The first term in the above equation describes a response at frequency 3ω which is due to an applied field of frequency ω, resulting in the generation of third harmonic beam.

In our experimental apparatus we use a frequency tripler from U-Oplaz technologies, which is equipped with a second harmonic LBO crystal (type I) and a third harmonic BBO crystal (type I). The ~800 nm fundamental (ω) output from the Ti-sapphire oscillator is frequency doubled (2ω) to generate 400 nm beam which was the main excitation source for our experiments involving coumarin. For the naproxen samples, the third harmonic (3ω), ~266 nm light, is generated using both ω and 2ω beams.[25]

Time Correlated Single-Photon Counting

Time correlated single photon counting (TCSPC) is the most popular technique for almost all-time domain measurements. The single-photon counting measurement relies on the existence of a probability distribution for the emission of a single photon following an excitation event, which yields the actual intensity against time distribution of all the emitted photons subsequent to excitation. The experiment begins with an excitation pulse, which excites the sample and starts the time measurement clock. In an ideal time-correlation experiment each photon emitted by the sample as a result of excitation is to be timed and recorded. The response time of the detector and the mode of operation of the time-to-amplitude converter (TAC) requires only the timing of the first photon in a given time

interval after occurrence of the excitation event. Before the signal reaches the TAC, it passes through a constant function discriminator (CFD), whose function is to measure the arrival time of the photoelectron pulse with the highest possible time resolution. This goal is compromised because the pulses due to single photoelectrons have a distribution of amplitudes. If one measures the arrival of the pulses by the time when the signal exceeds a threshold, there is a spread, Δt, in the measured times due to pulse height variations. While this effect may seem minor, it can be the dominant factor in an instrument response function.

The heart of the TCSPC technique is the time-to-amplitude converter (TAC) which is analogous to a fast stopwatch. The role of the TAC is to measure the time gap between the START pulse generated by the excitation pulse and that of STOP pulse, which is the first photon arriving from the fluorescence of the sample. The START signal produced by the excitation pulses from the laser is used to trigger the voltage ramp of the TAC. This ramp is stopped when the first fluorescence photon hits the detector, and a pulse is generated whose amplitude is proportional to the charge of the capacitor and hence the time gap between the start and stop pulses. The output from the TAC is fed into an analog-to-digital converter (ADC) where it gains a numerical value and is then stored in a data storage device in an address corresponding to that number. Excitation and data storage are repeated in this manner until the histogram of number of counts in a particular time channel represents the decay curve of the sample to a desired precision. The detector used in our system is the multi-channel plate (MCP) photomultiplier tube (PMT). MCP-PMT provides a tenfold shorter pulse width than any other PMT, and displays lower intensity after-pulses. The design of an MCP is completely different from that of a conventional photomultiplier because it does not have dynodes. Instead, the photoelectrons are amplified along narrow

channels lined with the dynode material. Because these channels are very narrow, typically 4 to 12 microns in diameter, all the electrons travel the same path and hence have the same transit time in principle. Smaller channels result in less transit time spread. In the MCP-PMT the channels are angled relative to each other, which prevents feedback between the channels and broadening of the time response.[26,27] Also, the first MCP surface is typically covered with aluminum, which prevents secondary electrons emitted from the top of the MCP from entering adjacent channels. The other most important advantage of MCP-PMTs over normal PMTs and avalanche photodiodes (APDs) is the lower transit time distribution of the former, which improves the time-resolution of the detector.

The TAC is the rate-limiting component in data collection, and it takes microseconds to discharge the capacitor and rest the TAC, which works perfectly for lower repetition rate sources like flash lamps (~50kHz), but becomes overloaded with high repetition rate lasers producing MHz pulses.   This problem is cleverly obviated by making the TAC operate in reverse mode.[28-30] In this mode of operation the first photon detected from the *sample* serves as the start pulse, and the signal from the excitation pulse is the stop signal. In this way the TAC is only activated if the emitted photon is detected.

Laboratory Set-up for TCSPC

The laser source for our time-correlated single-photon counting measurements is a homemade mode-locked Ti-sapphire laser,[31] (Figure II.5) with a repetition rate of 82 MHz. The fundamental from the Ti-sapphire oscillator is modulated by a Pockels cell (Model 350-160, Conoptics Inc) to reduce the repetition rate to about 8.8 MHz and is subsequently frequency doubled by focusing tightly into a 0.4-mm BBO crystal.
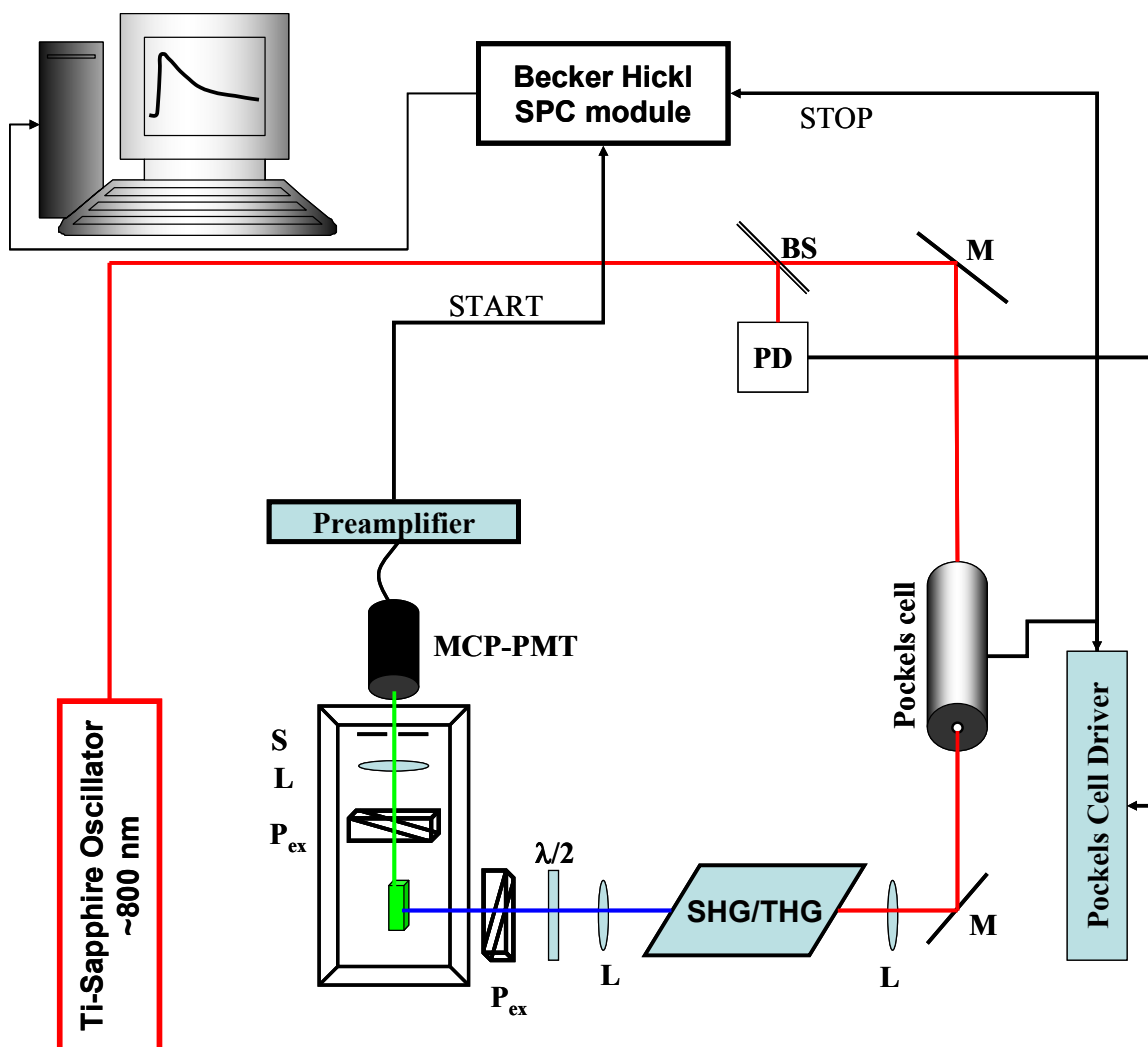
Figure II.5. Schematic diagram of home-made TCSPC set-up in our laboratory. L: lens, M: mirror, P_{ex}: excitation polarizer, P_{em}: emission polarizer, SHG/THG: second or third harmonic crystal, BS: beam splitter, PD: photo-diode, S: shutter, $\lambda/2$: half waveplate, MCP-PMT: multichannel plate photomultiplier tube, SPC: single photon counting.

The resulting blue light, which has a central wavelength of 407 nm, provides the excitation source. The fluorescence decays are collected at the magic angle (polarization of 54.7° with respect to the vertical) to nullify anisotropic effects. Emission is collected through a single monochromator (ISA H10) fitted with a slit having an 8-nm band pass. A half-wave plate before a vertical polarizer ensures that polarization of the excitation light.

Recent modifications[32] in the TCSPC experimental system include the replacement of NIM-style electronics by Becker & Hickl photon counting module Model SPC-630. In the CFD channel our previous ORTEC pre-amplifier has also been replaced by Becker & Hickl HFAC pre-amplifier. The instrument-response function of the apparatus has a full-width-at-half-maximum (fwhm) of ~45 ps, instead of ~100 ps which we had obtained with the NIM system.

Fluorescence Upconversion

The challenge for the ultrafast spectroscopist is to develop techniques that can take full advantage of the ultrashort pulse widths of the femtosecond lasers [33,34] to study the dynamics of various systems. Using a time-correlated single photon counting technique in conjunction with fast photomultipliers, it is possible to improve the time resolution at most to approximately tens of picoseconds.[35] One of the best way for achieving time resolution comparable to the laser pulse width itself is based on techniques that use nonlinearity induced by the laser pulse as a gate for luminescence.[36] Mahr and Hirsh first used one such frequency mixing technique in which the luminescence excited by an ultrafast laser is mixed with the laser in a nonlinear crystal to generate sum or difference frequency radiation.[37] Since the mixing process takes place only during the presence of the laser pulse, this provides time resolution comparable to the laser pulse width, provided certain conditions are satisfied. The technique of sum frequency generation is also known as upconversion, which provides sub-piocsecond time.[38-48]
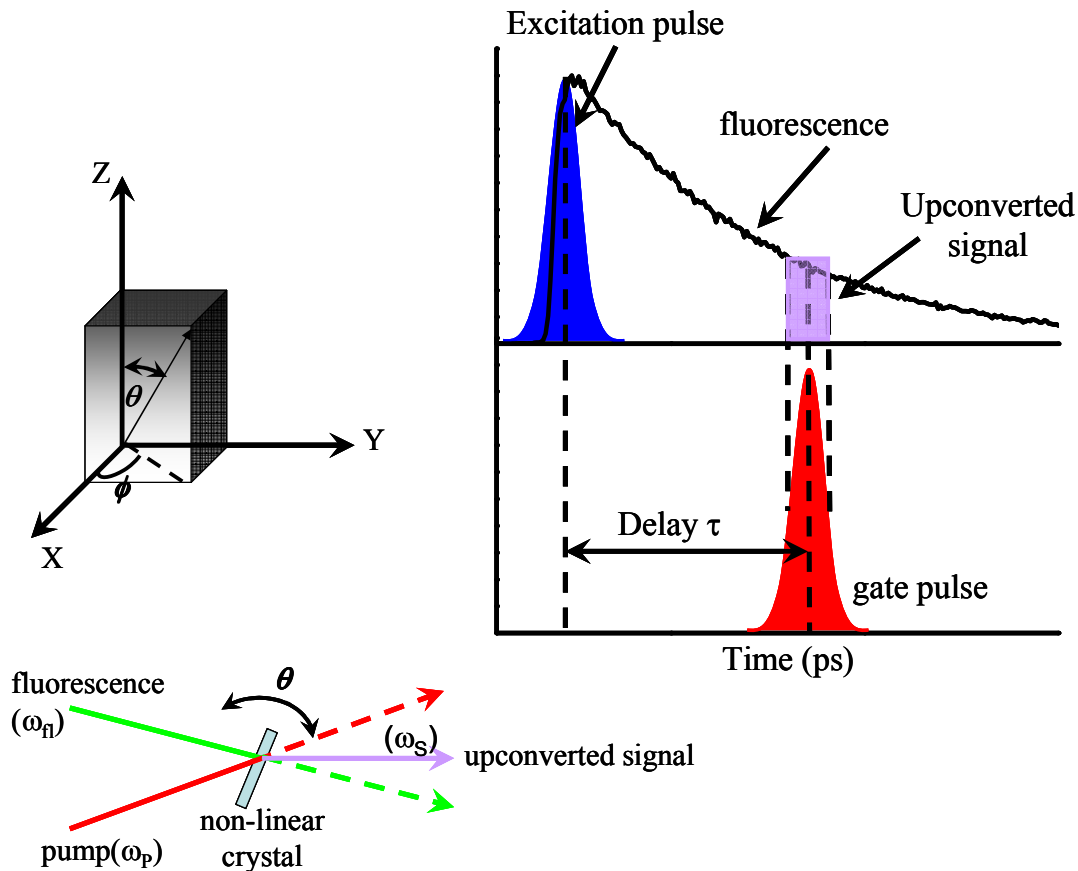
Figure II.6. Schematic diagram of upconversion technique. Sum frequency radiation is generated in a nonlinear crystal only during the time that a delayed laser pulse is present. The angles θ and φ are defined.

The basic principle of obtaining time resolution using frequency mixing techniques is demonstrated in Figure II.6. The visible fluorescence photon energy ($h\nu_{fl}$) excited by an ultrafast laser and a pump laser ($h\nu_P$) are focused on a nonlinear crystal, which is oriented at an appropriate angle with respect to the fluorescence and pump beams. Sum or difference frequency photons are generated only during the time that the pump pulse is present at the crystal. Thus, frequency mixing acts as a light gate and provides time resolution comparable to the laser pulse width. The time evolution of fluorescence may be obtained by varying the

delay of the laser at the nonlinear crystal. Of the two mixing beams, one is set at fixed time delay and delay for the other is varied using a translation stage with a retro-reflector, as shown in the Figure II.7.
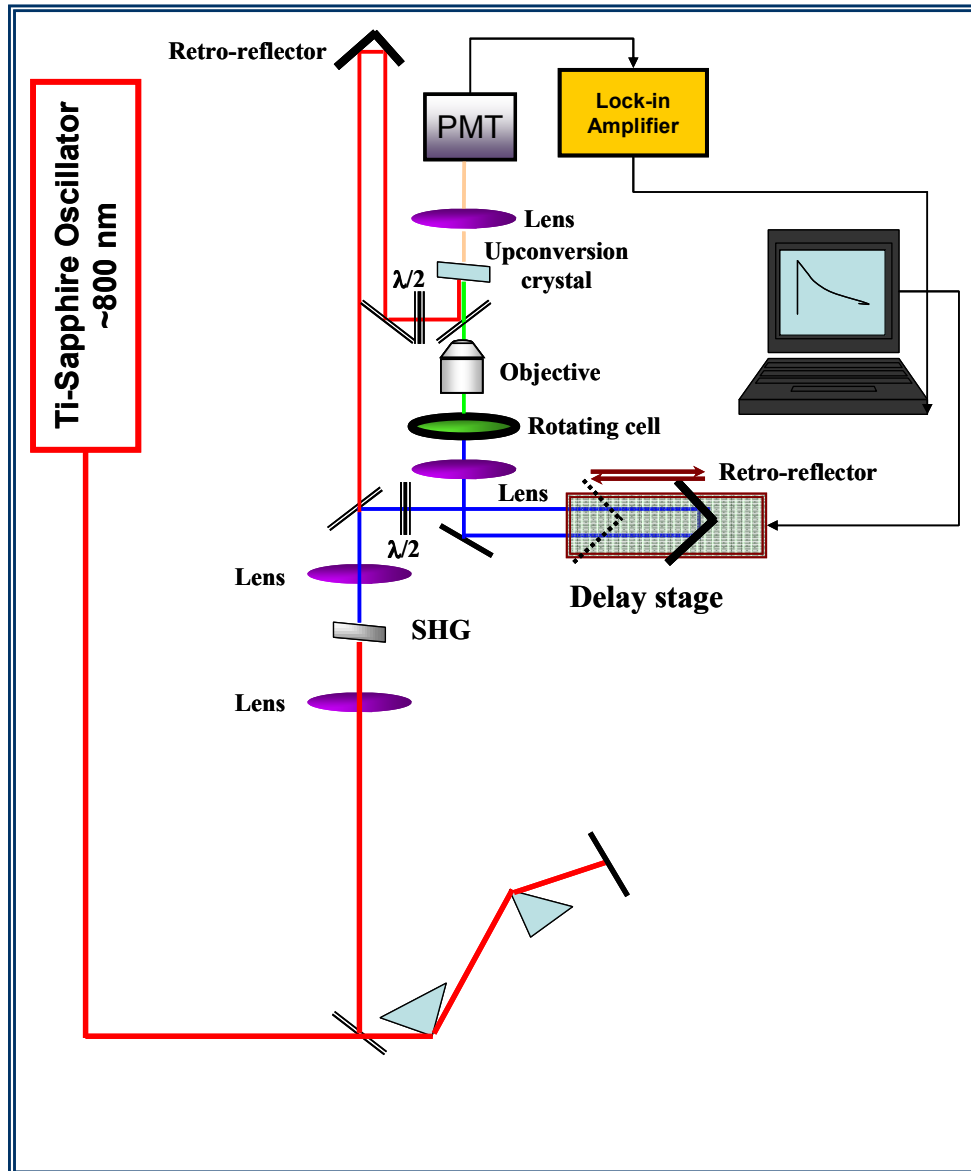
Figure II.7. Schematic diagram of home-made upconversion set-up in our laboratory.

The efficiency of frequency mixing maximizes if the phase matching condition are satisfied, [20,49] such as,

$$\nu_{fl} + \nu_P = \nu_S \qquad \text{(II.10)}$$

$$\vec{k}_{fl} + \vec{k}_P = \vec{k}_S \qquad \text{(II.11)}$$

where $h\nu$ and $\vec{k}$ are the photon energies and wave vectors of fluorescence, pump and sum frequency or upconverted beams represented by subscripts fl, P and S respectively. In the case of collinear phase matching, equation II.11 reduces to

$$\left(\frac{n}{\lambda}\right)_{fl} + \left(\frac{n}{\lambda}\right)_P = \left(\frac{n}{\lambda}\right)_S \qquad \text{(II.12)}$$

where n is the refractive index at appropriate wavelength (λ). In the case of an anisotropic crystal, the refractive index depends on the direction of propagation along X, Y and Z as shown in Figure II.6; and they are designated as n_X, n_Y, and n_Z, respectively. Crystals are often uniaxial, where the optic axis is along the z-direction and under such condition $n_X = n_X = n_O$ (ordinary index) and $n_Z = n_e$ (extra-ordinary index). Thus propagation along $\vec{k}$ can be written as

$$\frac{\sin^2\theta}{(1/n_i^2) - (1/n_{O,i}^2)} + \frac{\cos^2\theta}{(1/n_i^2) - (1/n_{e,i}^2)} = 0 \qquad \text{(II.13)}$$

In general, the phase matching conditions (equations II.10 and II.12) cannot be satisfied if all three (fl, P, and S) waves propagate as ordinary (O) rays in the crystal. However, if one or more of the rays propagate as extraordinary (E) rays, phasematching conditions may be satisfied by varying the angle between the wave normals and the optic axis. If fl and P are polarized parallel to each other (both O or both E), the interaction is termed *type I*; if they are

polarized orthogonal, it is *type II*. The phase matching condition is also dependent on the central wavelength of the incident beams, and thus the phase matching angle (θ_M) for type I (BBO-crystal), with the interaction O+O $\rightarrow$ E is given by,

$$\sin^2 \theta_M = \frac{(1/n_S^2(\theta_M)) - (1/n_{O,S}^2)}{(1/n_{e,S}^2) - (1/n_{O,S}^2)}.$$ (II.14)

A precise determination of the zero time delay is essential in all ultrafast measurements. The best means of determining the zero in a fluorescence upconversion system is by obtaining a cross-correlation trace between the scattered laser light from the sample under investigation and a delayed laser beam at the nonlinear crystal used for frequency upconversion. Such a trace provides not only an accurate zero but also an accurate measure of the system response time.[36]

Although the fluorescence upconversion technique provides much superior time resolution of a few hundreds of femtoseconds, the alignment of the set-up is very critical, because of the spatial and temporal overlap of the two beams. On the other hand the upconverted signal is very weak; and an optical chopper and lock-in electronics are required to eliminate the background noise.

Laboratory Set-up for Fluorescence Upconversion

The laser source for fluorescence upconvesrion is a home-made Ti-sapphire laser. The fundamental output from the amplifier (814 nm) is doubled by a type-I LBO crystal (2 mm). The frequency-doubled blue pulses (407 nm) are separated from the fundamental by a dielectric mirror coated for 400 nm and are focused onto a rotating cell containing the sample using a 5-cm convex lens. The remaining fundamental is used as the gate to upconvert emission. Fluorescence is collected by an LMH-10x microscopic objective (OFR Precision

Optical Products) coated for near UV transmission. The gate and the emission are focused by a quartz lens (12 cm) onto a type-I 0.4-mm BBO crystal (MgF2 coated, cut at 31°, and mounted by Quantum Technology, Inc). The polarization of both the gate and excitation source is controlled with a set of zero-order half-wave plates for 800 and 400 nm, respectively. The upconverted signal is then directed into an H10 (8 nm/mm) monochromator (Jobin Yvon/Spex Instruments S. A. Group) with a 5-cm convex lens coupled to a Hamamatsu R 980 PMT equipped with a UG11 UV-pass filter and operated at maximum sensitivity. The PMT output is amplified in two stages (total by a factor of 25, 5 for each stage) by a Stanford research Systems SR-445 DC-300 MHz amplifier with input terminated at 500 Ω and is carefully calibrated after a long (1-2 h) warm-up. Photon arrival events are registered with SR-400 gated photon counter operated in CW mode with a threshold level of -100 mV. This signal is fed into a boxcar averager. A part of the blue pulse train is used to normalize pump-beam fluctuations. A translation stage (Compumotor) with a resolution of 0.06 mm/step is used to delay the exciting pulses and a computer with an interfacing card from Keithley Metrabyte (DAS 800) is used for driving the motor. The instrument-response function is obtained by collecting the cross-correlation function of the blue and red pulses; the resulting third harmonic intensity is plotted against delay time. The cross-correlation functions typically have a fwhm of ~300 fs. All curves are fit and deconvoluted from the instrument function using an iterative convolute and compare least-squares algorithm.

Reorganization Energy

Steady-state excitation and emission spectra were recorded with a SPEX Fluoromax with a 4-nm band pass and were corrected for detector response. A 1-cm path length quartz

cuvette was used for the measurements. The steady-state spectra can be used to compute the reorganization energy, λ, by means of[50]

$$\lambda = \hbar \frac{\int\limits_{0}^{\infty} d\nu \left[\sigma_a(\nu) - \sigma_f(\nu)\right]\nu}{\int\limits_{0}^{\infty} d\nu \left[\sigma_a(\nu) + \sigma_f(\nu)\right]} \qquad (II.15)$$

The σ_a and σ_f are the absorption (or excitation) and emission spectral line-shapes, respectively, on a wavenumber scale. The reorganization energy is widely used as a measure of the strength of interactions between a chromophore and its surrounding dielectric media in solvation dynamics studies. It is usually taken as half of the Stokes shift. This estimation is accurate if the excitation and emission spectra are Gaussian, but it becomes unreliable if they are not. The actual computation of λ is accomplished by first manipulating the emission and excitation spectra to permit their addition and subtraction. This requires normalized spectra consisting of equally spaced points. These spectra are then converted to corresponding line-shapes. This conversion is done by plotting the spectra in wavenumber scale and dividing the absorption and emission spectra by ν and ν^3 respectively. We interpolate and renormalize them so as to obtain spectra having 20 cm^{-1} spacing between each point and then shift the crossing point of the two curves so that it lies at 0 cm^{-1}. The spectral baselines are then corrected by subtracting the lowest intensity and renormalizing. This manipulation is motivated by the low-intensity emission near 800 nm and questions concerning the utility of the correction factors of our fluorometer in this region. In any case, baseline subtraction is minor and changes the final result by approximately 1%. An appropriate number of zeros is added to the high-energy end of the emission spectrum and to the low-energy end of the

excitation spectrum so that the curves can be added and subtracted along their entire breadths. λ may now be calculated according to equation II.15. In practice, however, the integration is more conveniently performed from negative infinity to zero instead of from zero to positive infinity to avoid interference from transitions to higher-lying excited states. Taking these limits of integration is permitted as long as there is mirror image symmetry between the emission and excitation spectra. All data manipulations were performed with Microcal Origin 7.0.
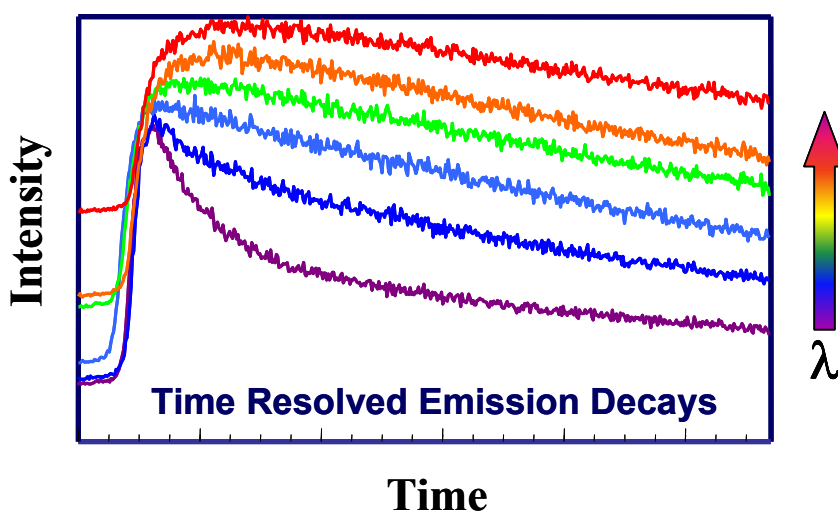
Figure II.8. Representative wavelength resolved fluorescence transients.

Measurement of Time resolved Emission Spectra and Construction of Solvation Correlation Function

Prior to the invention of the time-correlated single-photon counting technique (TCSPC), time-resolved emission spectra (TRES) were measured directly using pulse-sampling or time-gated detection methods in which the intensity decay was repetitively sampled during pulsed excitation. The detection gate was placed across the intensity decay

until the entire decay was measured. But this technique is limited to the measurement of nanosecond lifetimes.[51-53]   Direct recording of TRES does not provide for deconvolution using an instrument response function and thus the TRES contained distortions owing to the instrument response function.
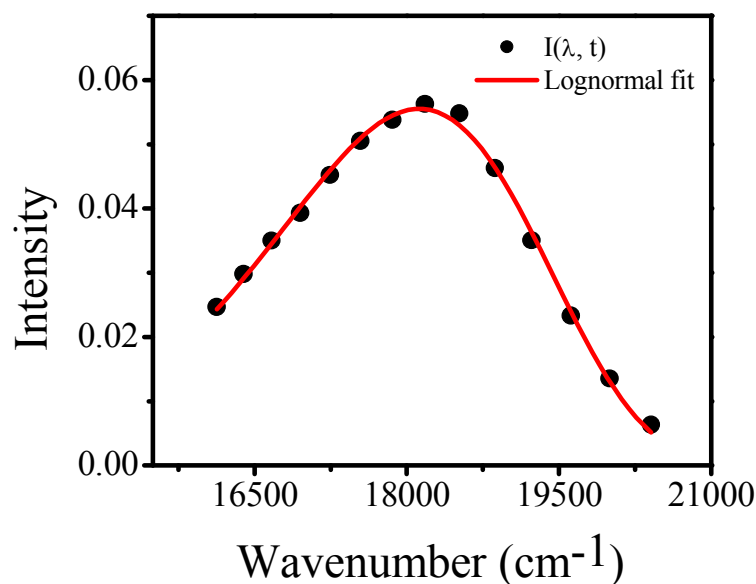
Figure II.9.   Representative time resolved emission spectrum fitted with a lognormal function to obtain the peak maxima, $\nu(t)$.

Currently, time-resolved emission spectra are reconstructed after deconvoluting the time resolved intensity decays with the corresponding instrument response function. First a series of time resolved fluorescence intensity decays $I_\lambda(t)$ are collected at different wavelengths spanning the entire wavelength range of the steady-state emission spectrum (Figure II.8). These traces at each wavelength are fitted to sums of exponentials as

$$I_\lambda(t) = \sum_i a_i \exp(-t/\tau_i) \tag{II.16}$$

where a_i are the pre-exponential factors, sum of which equals 1, τ_i is the decay time constant. The decays at the blue end are faster whereas those collected at the red edge show significant rise times due to the increase in population of the relaxed state. This trend of traces is indicative of the solvation process. Time resolved emission spectra $I(\lambda,t)$ are constructed by normalizing the traces obtained from equation II.16 so that the time integrated intensity at each wavelength is equal to the steady-state intensity at that wavelength.

Thus $I(\lambda,t)$ can be expressed as,

$$I(\lambda,t) = I_\lambda^{SS} \frac{I_\lambda(t)}{\int_0^\infty I_\lambda(t)} \qquad (II.17)$$

where I_λ^{SS} is the steady-state emission intensity at a given wavelength. $\int_0^\infty I_\lambda(t)$ is the average lifetime at each different wavelengths. The time resolved emission spectrum is finally obtained (Figure II.9) by fitting the data points $I(\lambda,t)$ obtained at each given time to a lognormal function[48,54]

$$I(\nu;t) = h\left\{\exp\left[-\ln 2\left\{\ln(1+\alpha)/\gamma\right\}^2\right]\right\} \qquad (II.18)$$

where, $\alpha \equiv \dfrac{2\gamma(\nu - \nu_P)}{\Delta}$. Four of these parameters namely h = height of the peak, ν_P = peak frequency, γ = asymmetry parameter and Δ = width parameter, are adjusted in a non-linear least square fitting procedure for each time point. As shown in Figure II.8, these lognormal fits provide a very good representation of the time-resolved emission spectra in polar solvents. Using these fitting procedures, the peak frequency maxima $(\nu(t))$ is obtained as a function of time.

Followed by the pulsed excitation, the solvent dipoles start to reorganize themselves around the excited dipole of the chromophore, leading to the stabilization of the excited state with time. If the time resolved emission spectra are constructed as a function of time, they will progressively shift to longer wavelengths (lower energy) with time.
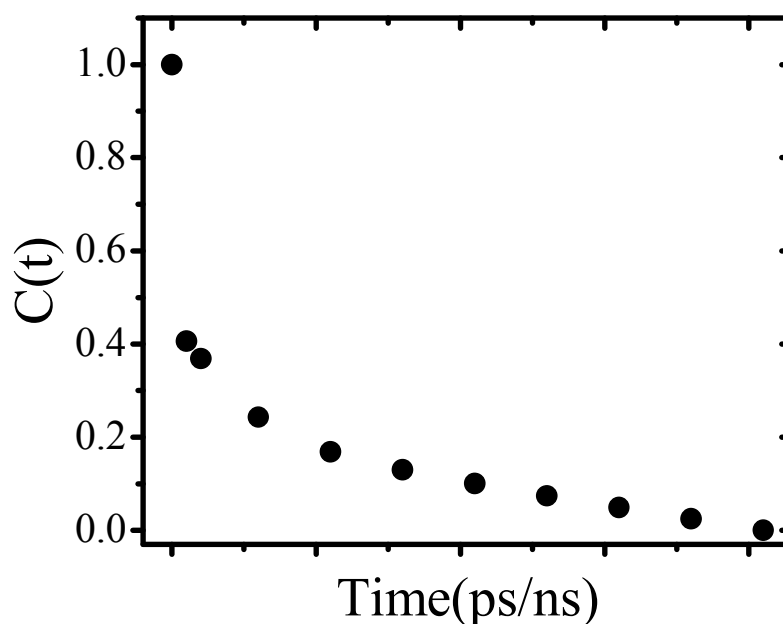
Figure II.10. Representative solvation correlation function plotted against time.

Solvation dynamics is best described by the following normalized correlation function:

$$C(t) = \frac{v(t) - v(\infty)}{v("0") - v(\infty)} \tag{II.19}$$

where $v("0")$ and $v(\infty)$ are the peak maxima at time t=0 and infinity. The decay of $C(t)$ with time (Figure II.10) is fitted with a sum of two or three exponentials to obtain the average

solvation time (τ_S). Because $C(t)$ is a normalized function, the accurate determination of $C(t)$ depends upon accurate values for $\nu("0")$ and $\nu(\infty)$.

$\nu(\infty)$ is (usually[55,56]) the frequency at infinite time, obtained from the maximum of the steady state spectrum. $\nu(\infty)$ is usually given by the equilibrium spectrum.[32,57-59] (This is not, however, true in the case of very slowly relaxing solvents, as has been demonstrated in the case of certain ionic liquids [55,56,60]: here the emission spectrum at ~3 times the fluorescence lifetime of the probe is *red-shifted* to that of the equilibrium spectrum.) The $\nu(t)$ are determined from the maxima of the log-normal fits of the TRES. In most of the cases, however, the spectra are broad, so there is some uncertainty in the exact position of the emission maxima. Thus, we have considered the range of the raw data points in the neighborhood of the maximum to estimate an error for the maximum obtained from the lognormal fit. Depending on the width of the spectrum (i.e. "zero-time", steady-state, or time-resolved emission spectrum), we have determined the typical uncertainties as follows: "zero-time" ~ steady-state (~ $\pm$ 100 cm^{-1}) < time-resolved emission (~ $\pm$ 200 cm^{-1}). We use these uncertainties to compute error bars for the $C(t)$. Finally, in generating the $C(t)$, the first point was obtained from the "zero time" spectrum. The second point was taken at the maximum of the instrument response function.

Calculation of zero-time emission spectrum

Since the time scale for electronic excitation is much faster than for nuclear motion, the excitation instantaneously changes the charge distribution of the probe but the position and orientation of the neighboring solvent molecules remain unaltered. $\nu("0")$ is the maximum of the estimated "zero-time" spectrum of the fluorescent probe after it has undergone intramolecular events contributing to its relaxation and before it has been altered

by interactions with the solvent. The appropriate value for $\nu(0)$ is not obtained from the emission spectrum obtained immediately upon optical excitation with infinite time resolution, even if such an experiment were possible. The construction of the "zero-time" spectrum, which thus assumes such a time-scale separation of events, has been described by a robust, model independent, and simple procedure by Fee and Maroncelli.[61]
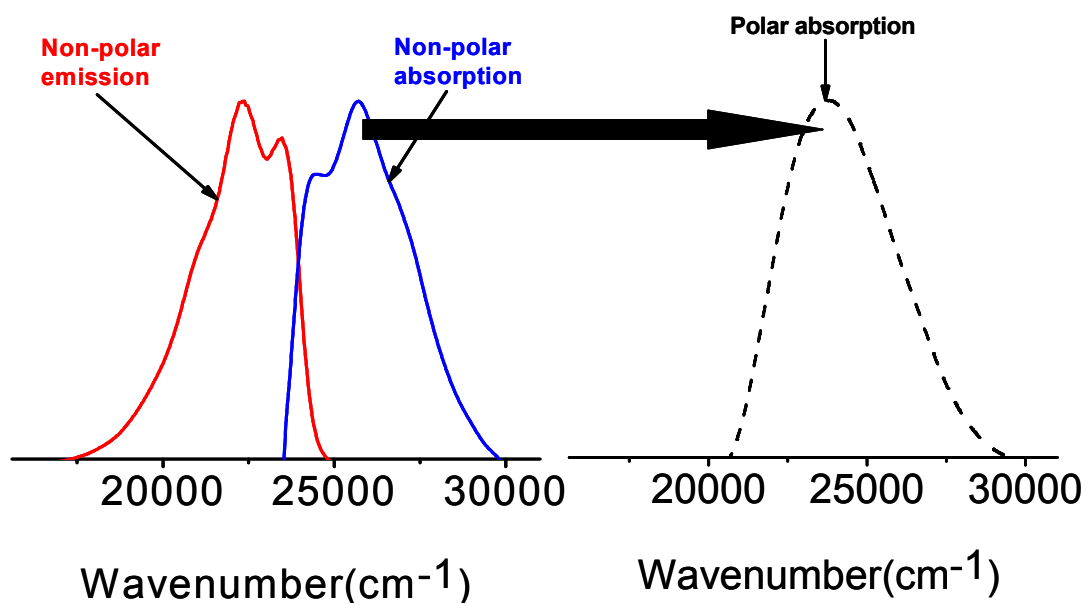
Figure II.11. Representative absorption and emission spectra of coumarin 153 in a non-polar solvent (hexane) and its absorption spectrum in a polar solvent (methanol). These spectra are the basic requirements for computing the zero-time spectrum. The arrow shows how non-polar absorption spectrum is to be superimposed on to the polar absorption spectrum to obtain a reasonable zero-time spectrum in the polar solvent, which will be provided by the non-polar emission spectrum.

The calculation of the zero-time spectrum requires the absorption spectrum of the probe in the solvent of interest (polar medium), and absorption and emission spectra of the probe in a non-polar solvent of reference, which usually is chosen to be hexane. In a non-polar solvent no solvent induced shift is expected to occur between the absorption and

emission so this pair can be considered to relate to the two spectra of equal origin state. Now if the frequencies of non-polar spectral pair are shifted in such a way such the non-polar absorption spectrum is superimposed on to the absorption spectrum recorded in the polar solvent as shown in Figure II.11, then the non-polar emission spectrum provides a reasonable zero-time spectrum in the polar solvent.[48]

Calculation of the time-zero spectrum relies on interpreting the absorption and emission spectrum of the probe in any particular solvent as resulting from the action of an inhomogeneous distribution of solvent environments (differing only by an overall spectral shift, δ) on an intrinsic vibronic lineshape, which is assumed to be solvent independent. The absorption spectrum can be assumed to be described by the same lineshape function $g(v)$ and thus the corresponding spectrum in a non-polar solvent ($A_{nP}(v)$) is given by

$$A_{nP}(v) \propto vg(v) \tag{II.20}$$

and that in polar solvent ($A_P(v)$) is represented by

$$A_P(v) \propto v\int g(v-\delta)p(\delta)d\delta \tag{II.21}$$

where $p(\delta)$ describes the Gaussian distribution of solutes over different solvent environments as

$$p(\delta) = \frac{1}{\sqrt{2\pi\sigma^2}}\exp\left\{-\frac{(\delta-\delta_0)^2}{2\sigma^2}\right\} \tag{II.22}$$

where δ_0 is the average shift induced by the polar solvent and σ is the variance of the distribution. Parameters like δ_0 and σ are determined by iterative fitting of polar absorption spectrum to equation II.21. The emission spectrum in non-polar solvent ($F_{nP}(v)$) can be expressed in terms of emission lineshape function as

$$F_{nP}(\nu) \propto \nu^3 f(\nu) \tag{II.23}$$

Considering all these line-shape functions, the emission spectrum observed immediately after monochromatic excitation with frequency ν_{ex}, which is the desired zero-time spectrum is given by,

$$F_P(t=0) \propto \nu^3 \nu_{ex} \times \int g(\nu_{ex} - \delta)p(\delta)f(\nu - \delta)k_{rad}(\delta)d\delta \tag{II.24}$$

where k_{rad} is the radiative rate-constant, which is calculated as

$$k_{rad}(\delta) \propto \frac{\int f(\nu - \delta)\nu^3 d\nu}{\int f(\nu - \delta)d\nu} \tag{II.25}$$

The zero-time spectrum obtained from equation II.24 is the fluorescence spectrum observed before any solvent motion occurs, but after all the intramolecular equilibration is complete. It is given by the convolution of the is solvent distribution initially transferred to the excited state, $g(\nu_{ex} - \delta)p(\delta)$ immediately after optical excitation and the fluorescence intensity function $f(\nu - \delta)k_{rad}(\delta)$. This method of computing zero-time spectrum provides a critical check on whether all of the spectral relaxation has actually been observed in a time-resolved experiment. It also accounts for the missing component of the solvent relaxation that occurs within the finite time resolution of a given experimental set-up.

Fee and Maroncelli have tested the validity of the above model using three different probes such as coumarin 153, coumarin 102 and 4-aminophthalimide dissolved in frozen solvents, where no spectral relaxation due solvent motion is expected.[61] Thus the emission spectrum obtained under these conditions directly yielded the zero-time spectrum which is in very good agreement (<10% of the total dynamic stokes shift) with those computed using the above described method. In our previous work we have discussed a means of computing the

reorganization energy of coumarin 153 due to intramolecular vibrations. The value obtained, 2068 cm^{-1}, is commensurate with that obtained from computing the reorganization energy from the zero-time spectra, 1870±185 cm^{-1}, which speaks to the appropriateness of our method as well as to the robustness of the zero-time method described above.[62] The importance of using calculated zero-time spectrum in constructing the solvation correlation function $C(t)$ has been elaborated in chapter IV, where we have shown that underestimating the position of the "zero-time" spectrum can exaggerate the amplitudes of slower solvation phenomenon leading incorrect interpretations of solvent relaxation.[32,63-69]

Fee and Maroncelli also provided a simpler equation for approximating the maximum of the zero-time spectrum:

$$\nu_P^{em}(t=0) = \nu_P^{abs} - (\nu_{nP}^{abs} - \nu_{nP}^{em}) \qquad (II.26)$$

where P and nP refer to the position of the emission or absorption spectra in polar or nonpolar solvents, respectively. In our experience, this approximation usually deviates from that obtained by the full method by at least a few hundred wavenumbers. Some workers[70-76] use equation II.26 as a quick way of estimating the position of the zero-time spectrum, but we propose that it is no substitute for using the full method—especially when quantitative interpretations of $C(t)$ are required.

Fluorescence Resonance Energy transfer

Fluorescence resonance energy transfer (FRET) is unique in its capacity to supply accurate spatial measurements and to detect molecular complexes over distances from 10 A to 100 Å, enabling the definition and detection of a variety of biological organizations.[77] FRET is the physical process by which energy is transferred non-radiatively from an excited molecular chromophore (the donor, D) to another chromophore (the acceptor, A) by means

of intermolecular long-range dipole-dipole coupling. The energy transfer being non-radiative the donor does not actually emit a photon and acceptor does not absorb a photon, which justifies the term resonance energy transfer.
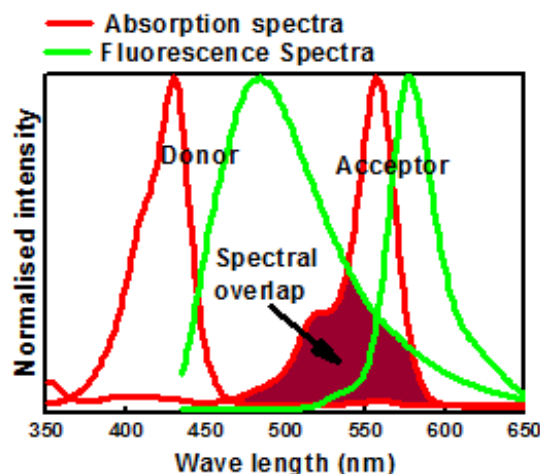
Figure II.12. Representative absorption and emission spectra of an ideal donor-acceptor pair. Filled region is the spectral overlap between the fluorescence spectrum of donor and absorption spectrum of acceptor.

The essential requirements for effective transfer over distances from 10 to 100 Å are that the emission spectrum of D and the absorbance spectrum of A overlap adequately (Figure II.12), and that both the quantum yield of D (ϕ_D) and the absorption coefficient of A (ε_A) are sufficiently high. In addition, for the dipole-dipole vectorial interaction to occur, either the transition dipoles of D and A must be oriented favorably relative to each other, or one (or both) must have a certain degree of rapid rotational freedom so that this latter condition is usually satisfied for chromophores attached to biomolecules in solution.[78]

The rate of Förster dipole – dipole energy transfer is given by

$$k_T(r) = \frac{1}{\tau_D}\left(\frac{R_0}{R}\right)^6 \qquad (II.27)$$

where τ_D is the average fluorescence lifetime of the donor, R is the distance between donor and acceptor and R_0 is the critical distance at which the rate of energy transfer is inverse of fluorescence lifetime of donor. The rate constant of non-radiative energy transfer from the donor (D) excited state (ψ_D^e) to the acceptor (A) whose excited and ground states are defined by the wavefunctions ψ_A^e and ψ_A^g is given by the matrix[79]

$$k_T(r) \propto \left| \left\langle \psi_D^g \psi_A^e \left| V \right| \psi_D^e \psi_A^g \right\rangle \right|^2 . \tag{II.28}$$

Since $V \propto \vec{\mu}_A . \vec{E}_D$, $\vec{E}_D \propto -\nabla \dfrac{\mu x}{\vec{R}^3}$ and therefore

$$V \propto \kappa \frac{\mu_A \mu_D}{\vec{R}^3} . \tag{II.29}$$

Substituting the equation II.29 into equation II.28 we get,

$$k_T(r) \propto \left| \left\langle \psi_D^g \psi_A^e \left| \kappa \frac{\mu_A \mu_D}{\vec{R}^3} \right| \psi_D^e \psi_A^g \right\rangle \right|^2 . \tag{II.30}$$

This result implies that the rate of energy transfer varies inversely to the sixth power of the internuclear distance (R) between the donor and the acceptor. Thus, the expression for $k_T(r)$ expression can be split into donor emission and acceptor absorption matrices respectively as follows

$$k_T(r) \propto \frac{\kappa^2}{\vec{R}^3} \left| \left\langle \psi_D^g \psi_A^e \left| \mu_D \right| \psi_D^e \psi_A^g \right\rangle \right|^2 \left| \left\langle \psi_D^g \psi_A^e \left| \mu_A \right| \psi_D^e \psi_A^g \right\rangle \right|^2 . \tag{II.31}$$

The emission matrix can be related to the rate of spontaneous emission (ν^{-3}/τ_{rad}) and in the case of monochromatic absorption the second matrix can be represented as $\varepsilon_A \nu^{-1}$, with ε_A being the molar absorption coefficient. Equation II.31 can be rewritten using $1/\tau_{rad} = \phi_D/\tau_D$ as

$$k_T(r) \propto \frac{\kappa^2}{R^6}\frac{\phi_D}{\tau_D}\varepsilon_A v^{-4} \tag{II.32}$$

$F_D(v)$ is the corrected fluorescence intensity of the donor in the frequency range v to $v+dv$ with the total intensity (area under the curve) normalized to unity, and integrating over the entire range of frequency we get,

$$k_T(r) \propto \frac{\kappa^2}{R^6}\frac{\phi_D}{\tau_D}\int \varepsilon_A(v)F_D(v)v^{-4}dv \tag{II.33}$$

Quantitative structural details can be gleaned from the energy transfer data by computing the critical distance, R_0:

$$R_0^6 = \frac{9000(\ln 10)\Phi_D}{128\pi^5 n^4 N}\kappa^2 \left(\frac{\int_0^\infty F_D(\bar{v})\varepsilon_A \bar{v}^{-4}d\bar{v}}{\int_0^\infty F_D(\bar{v})d\bar{v}} \right) \tag{II.34}$$

where κ^2 is the orientation factor, n is the refractive index of the medium (considered as 1.33), N is Avogadro's number, Φ_D is the fluorescence quantum yield of the donor. In order to calculate the D – A distance it is necessary to know R_0, which in turn depends on factors such as κ^2, Φ_D, n and the spectral overlap integral. κ^2 is dependent on the relative orientation of the donor and acceptor moieties and their degrees of freedom. We have determined the distance between the fluorescent dye (coumarin 153 – acceptor) embedded inside the heme pockets of apomyoglobins from the two tryptophans (donor) using steady-state and time-resolved fluorescence studies by selectively exciting the donor and acceptor individually to characterize the structure of the dye-protein complexes.[80] Details of the calculations have been presented in chapter V.

Fluorescence Anisotropy

Upon excitation with polarized light, the emission from many samples is also polarized. The extent of polarization of the emission is described in terms of the anisotropy (*r*). Samples exhibiting non-zero anisotropies are said to display polarized emission. The origin of anisotropy is the existence of transition dipole moments for absorption and emission that lie along specific directions within the fluorophore structure. In homogeneous solution the ground-state fluorophores are all randomly oriented. When excited by polarized light, those fluorophores that have their absorption transition dipole moments oriented along the electric vector of the incident light are preferentially excited. Hence the excited-state population is partially oriented. A significant fraction of the excited molecules have their transition moments oriented along the electric vector of the polarized exciting light. The emission can become depolarized by a number of processes. All chromophores have transition moments that lie along a specific direction in the molecule. Rotational diffusion changes the direction of the transition moments and is one common cause of depolarization.[78] Anisotropy measurements reveal the average angular displacement of the fluorophore that occurs between absorption and subsequent emission of a photon.[81] This angular displacement is dependent upon the rate and extent of rotational diffusion during the lifetime of the excited state. The rate of rotational diffusion depends on the viscosity of the solvent and the size and shape of the rotating molecule.[56,60,82-84]

The measurement of fluorescence anisotropy is illustrated in Figure II.13. For most experiments, the sample is excited with vertically polarized light through a polarizer placed in front of the sample cell. The electric vector of the excitation light is oriented parallel to the vertical or *z*-axis. The intensity of the emission is measured through another polarizer

placed after the sample cell. When the emission polarizer is oriented parallel (‖) to the direction of the polarized excitation the observed intensity is called $I_{\parallel}$. Similarly, when the polarizer is perpendicular ($\perp$) to the excitation the intensity is called $I_{\perp}$. These intensity values are used to calculate the anisotropy[85]

$$r(t) = \frac{I_{\parallel}(t) - I_{\perp}(t)}{I_{\parallel}(t) + 2I_{\perp}(t)} \tag{II.35}$$
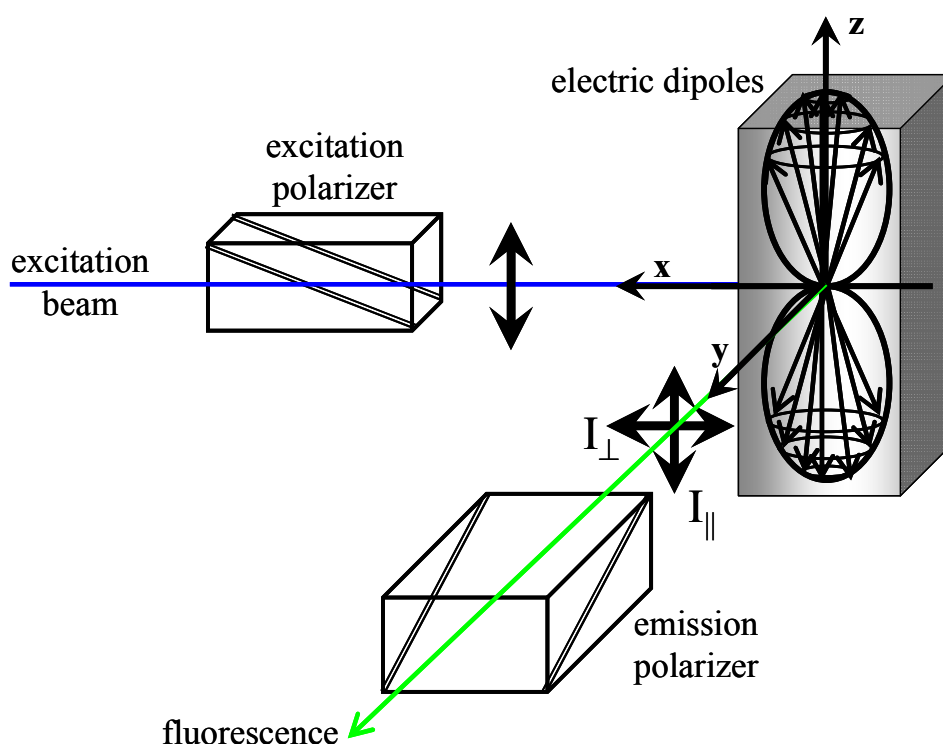
Figure II.13. Schematic diagram of measurement of fluorescence anisotropy. The arrows inside the cube, represents excited state distribution of electric dipole aligned around z-axis after polarized excitation.

The anisotropy often decays as $r(t) = r_0 \exp(-t/\tau_{rot})$, with r_0 being the limiting anisotropy at t=0. τ_{rot} is the depolarization time of the fluorophore. For molecules with z-axis symmetry, the angular dependence of anisotropy (r_0) can be written as $r_0 = 0.4 \times (3 < \cos^2 \beta - 1)/2$ where β is the angle between the absorption and emission dipole. In the case of collinear geometry between the absorption and emission dipoles r_0 equals 0.4, which is the maximum possible value. The value of the anisotropy becomes zero when β= 54.7°(the magic angle), and becomes negative at angles greater than the magic angle. It is important to note that normal lifetime decays are collected with the emission polarizer set at 54.7° with respect to the polarization of the excitation source to eliminate anisotropy effects.

Fitting of anisotropy data is very important to obtain accurate results. One common way of analyzing anisotropy results is to fit the parallel and perpendicular decays separately and then applying the results into equation II.35. We follow the method described by Cross and Fleming[86] in which parallel- and perpendicular-polarized fluorescence curves were fit simultaneously. This method takes full advantage of the statistical properties of the measured curves; and, in some cases, it is shown to be more sensitive than other methods to systematic errors present in the data.

Time-resolved fluorescence anisotropy has been used to characterize the rigidity or flexibility of probes bound to a macromolecule. For spherical molecules anisotropy decay is expected to single exponential. In bulk solvents, the decay is very fast (<100 ps) due to rapid and free rotational diffusion of a spherical probe molecule of radius ~4.0 Å.[87] Deviation from single exponential behavior is observed for chromophores bound on the surface and is characterized by a fast response (due to its individual local motions) followed by a slower

decay time due to the rotation of the entire macromolecule.[88,89] Single exponential decays for bound chromophores are a signature of rigid binding in a buried site and is characterized by a very slow rotational time characteristic of those of the entire macromolecule.[80,87]

Viscosity Measurements

Viscosity is one of the most important properties of fluid. Viscosity is the tendency of the fluid to resist motion. Essentially it is a measure of the frictional force between adjacent layers of fluid as they slide past each other. Viscosity in general depends strongly on temperature. It increases with temperature in the case of gases owing to molecular interchange between adjacent moving layers, whereas it decreases for case of liquids owing to the weakening of intermolecular cohesive forces. Viscosity has a dominant effect on phenomenon like solvent mediated processes[55,56,90-92] like electron/proton transfer,[93] charge transfer[94] or other diffusive processes like catalysis.[95] In this thesis we have studied various processes like solvation dynamics,[32,60] electron transfer[84,96] and enzyme catalysis[97,98] in highly viscous solvents[99] called room temperature ionic liquids.

We measure viscosities of different solvents at different temperatures using a ViscoLab 4000 piston style viscometer from Cambridge Applied Systems. It measures the viscosity by determining the amount of magnetic force needed to move a piston of certain weight and thickness vertically up and down through the liquid.

References

(1)   Geddes, C. D.; Lakowicz, J. R.; Rosenfeld, M. Y. *J. Fluo.* **2002**, *12*, 119.

(2)   Gardecki, J. A.; Maroncelli, M. *Appl. Spectrosc.* **1998**, *52*, 1179.

(3)   Moulton, P. F. *J. Opt. Soc. Am. B* **1986**, *3*, 125.

(4)   Kim, H., http://www.mpifr-bonn.mpg.de/div/submmtech/heterodyne/photonic_laser/dualmodeTiSa.html.

(5)   Asaki, M. T.; Huang, C. P.; Garvey, D.; Zhou, J.; Kapteyn, H. C.; Murnane, M. M. *Opt. Lett.* **1993**, *18*, 977.

(6)   Lamb, K.; Spence, D. E.; Hong, J.; Yelland, C.; Sibbett, W. *Opt. Lett.* **1994**, *19*, 1864.

(7)   Spence, D. E.; Sibbett, W. *J. Opt. Soc. Am. B: Opt. Phys.* **1991**, *8*, 2053.

(8)   Spence, D. E.; Kean, P. N.; Sibbett, W. *Opt. Lett.* **1991**, *16*, 42.

(9)   Hecht, J. *Understanding Lasers: An Entry-Level Guide*, 2nd ed.; IEEE Press Understanding Science & Technology Series.

(10)   Asaki, M. T.; Backus, S.; Baldwin, C.; Shi, C.; Murnane, M. M.; Kapteyn, H. C. *Springer Ser. Chem. Phys.* **1994**, *60*, 213.

(11)   Herrmann, J. *J. Opt. Soc. Am. B* **1994**, *11*, 498.

(12)   Slobodchikov, E.; Ma, J.; Kamalov, V.; Tominaga, K.; Yoshihara, K. *Optics Letters* **1996**, *21*, 354.

(13)   Slobodchikov, E.; Sakabe, S.; Kuge, T.; Kawato, S.; Hashida, M.; Izawa, Y. *Opt. Rev.* **1999**, *6*, 149.

(14)   Castner, E. W., Jr.; Maroncelli, M. *J. Mol. Liq.* **1998**, *77*, 1.

(15)   Smith, N. A.; Lin, S. J.; Meech, S. R.; Shirota, H.; Yoshihara, K. *Journal of Physical Chemistry A* **1997**, *101*, 9578.

(16)   Boyd, R. W. *Nonlinear Optics*; Academic Press, Inc.: Boston, 1992.

(17)   Huang, C. P.; Asaki, M. T.; Backus, S.; Murnane, M. M.; Kapteyn, H. C. *Opt. Lett.* **1992**, *17*, 1289.

(18)   Huang, C. P.; Asaki, M. T.; Backus, S.; Nathel, H.; Kapteyn, H. C.; Murnane, M. M. *Springer Ser. Chem. Phys.* **1993**, *55*, 160.

(19)   Zhou, J.; Garvey, D.; Huang, C. P.; Asaki, M. T.; Nathel, H.; Kapteyn, H. C.; Murnane, M. M. *Proc. SPIE-Int. Soc. Opt. Eng.* **1993**, *1860*, 2.

(20)   Shen, Y. R. *The Principles of Nonlinear Optics*; Wiley: New York, 1984.

(21)   Boyd, G. D.; Ashkin, A.; Dziedzic, J. M.; Kleinman, D. A. *Phys. Rev.* **1965**, *137*, 1305.

(22)   Sapaev, U. K.; Kulagin, I. A.; Usmanov, T. *J. Opt. B. Quantum Semiclass Opt.* **2003**, *5*, 355.

(23)   Dmitriev, V. G.; Gurzadyan, G. G.; Nikogosyan, D. N. *Handbook of nonlinear optical crystals*, 3rd ed.; Springer: Berlin, 1991.

(24)   Hawkes, J.; Latimer, I. Laser Oscillation. In *Lasers*; Prentice Hall: London, 1995; pp 302.

(25)   Liu, H.; Yao, J.; Puri, A. *Opt. Commun.* **1994**, *109*, 139.

(26)   Timothy, J. G.; Bybee, R. L. *Rev. Sci. Instrum.* **1977**, *48*, 292.

(27)   Lo, C. C.; Leskovar, B. *IEEE Trans. Nucl. Sci.* **1981**, *28*, 698.

(28)   Haugen, G. R.; Wallin, B. W.; Lytle, F. E. *Rev. Sci. Instrum.* **1979**, *50*, 64.

(29)   Bowman, L. E.; Berglund, K. A.; Nocera, D. G. *Rev. Sci. Instrum.* **1993**, *64*, 338.

(30)   Baumier, W.; X., S. A.; Göβl, G.; Penzkofer, A. *Meas. Sci. Technol.* **1992**, *3*, 384.

(31)   Chowdhury, P. K.; Halder, M.; Sanders, L.; Calhoun, T.; Anderson, J. L.; Armstrong, D. W.; Song, X.; Petrich, J. W. *J. Phys. Chem. B* **2004**, *108*, 10245.

(32)   Bose, S.; Adhikary, R.; Mukherjee, P.; Song, X.; Petrich, J. W. *J. Phys. Chem. B* **2009**, *113*, 11061.

(33)   Maroncelli, M.; Castner, E. W., Jr.; Webb, S. P.; Fleming, G. R. *Springer Ser. Chem. Phys.* **1986**, *46*, 303.

(34)   Fleming, G. R. *Chemical Applications of Ultrafast Spectroscopy*; Oxford University Press: London, 1986.

(35)   Murao, T.; Yamazaki, I.; Yoshihara, K. *Appl. Opt.* **1982**, *21*, 2297.

(36)   Shah, J. *IEEE J. Quant. Electron.* **1988**, *24*, 276.

(37)   Mahr, H.; Hirch, M. D. *Opt. Commun.* **1975**, *13*, 96.

(38)   Doust, T.; Beddard, G. S. "Picosecond fluorescence measurements using frequency upconversion"; Quantum Electron. Electro-Opt., Proc. Natl. Quantum Electron. Conf., 5th, 1983.

(39)   Jarzeba, W.; Kahlow, M.; Barbara, P. F. "Ultrafast fluorescence measurements in chemistry"; SPSE Proc. - Photochem. Imaging, Summer Symp., 1988.

(40)   Kahlow, M. A.; Jarzeba, W.; DuBruil, T. P.; Barbara, P. F. *Rev. Sci. Instrum.* **1988**, *59*, 1098.

(41)   Mokhtari, A.; Chesnoy, J.; Laubereau, A. *Springer Ser. Chem. Phys.* **1988**, *48*, 470.

(42)   Biblarz, O. *J. Appl. Phys.* **1989**, *66*, 5685.

(43)   Eads, D. D.; Todd, D.; Ruggiero, A.; Fleming, G. R. *Abstr. Paper Am. Chem. Soc.* **1989**, *198*, 19.

(44)   Jarzeba, W.; Kahlow, M.; Barbara, P. F. *J. Imaging Sci.* **1989**, *33*, 53.

(45)   Mokhtari, A.; Chebira, A.; Chesnoy, J. *J. Opt. Soc. Am. B: Opt. Phys.* **1990**, *7*, 1551.

(46)   Gardecki, J.; Horng, M. L.; Papazyan, A.; Maroncelli, M. *J. Mol. Liq.* **1995**, *65/66*, 49.

(47)   Kishimoto, S.; Hirao, K. *Optronics* **1997**, *184*, 136.

(48)   Horng, M. L.; Gardecki, J. A.; Papazyan, A.; Maroncelli, M. *J. Phys. Chem.* **1995**, *99*, 17311.

(49)   Zernike, F.; Midwinter, J. E. *Applied nonlinear optics*; Wiley: New York, 1973.

(50)   Jordanides, X. J.; Lang, M. J.; Song, X.; Fleming, G. R. *J. Phys. Chem. B* **1999**, *103*, 7995.

(51)   Ware, W. R.; Chow, P. P.; Lee, S. K. *Chem. Phys. Lett.* **1968**, *2*, 356.

(52)   Ware, W. R.; Lee, S. K.; Brant, G. J.; Chow, P. P. *J. Chem. Phys.* **1970**, *54*, 4729.

(53)   Chakraborty, S. K.; Ware, W. R. *J. Chem. Phys.* **1971**, *55*, 5494.

(54)   Maroncelli, M.; Fleming, G. R. *J. Chem. Phys.* **1987**, *86*, 6221.

(55)   Arzhantsev, S.; Ito, N.; Heitz, M.; Maroncelli, M. *Chem. Phys. Lett.* **2003**, *381*, 278.

(56)   Ito, N.; Arzhantsev, S.; Heitz, M.; Maroncelli, M. *J. Phys. Chem. B* **2004**, *108*, 5771.

(57)   Halder, M.; Headley, L. S.; Mukherjee, P.; Song, X.; Petrich, J. W. *J. Phys. Chem. A* **2006**, *110*, 8623.

(58)   Mukherjee, P.; Crank, J. A.; Halder, M.; Armstrong, D. W.; Petrich, J. W. *J. Phys. Chem. A* **2006**, *110*, 10725.

(59)   Halder, M.; Mukherjee, P.; Bose, S.; Hargrove, M. S.; Song, X.; Petrich, J. W. *J. Chem. Phys.* **2007**, *127*, 055101/1.

(60)   Mukherjee, P.; Crank, J. A.; Sharma, P. S.; Wijeratne, A. B.; Adhikary, R.; Bose, S.; Armstrong, D. W.; Petrich, J. W. *J. Phys. Chem. B* **2008**, *112*, 3390.

(61)   Fee, R. S.; Maroncelli, M. *Chem. Phys.* **1994**, *183*, 235.

(62)   Headley, L. S.; Mukherjee, P.; Anderson, J. L.; Ding, R.; Halder, M.; Armstrong, D. W.; Song, X.; Petrich, J. W. *J. Phys. Chem. A* **2006**, *110*, 9549.

(63)   Pal, S. K.; Peon, J.; Bagchi, B.; Zewail, A. H. *J. Phys. Chem. B* **2002**, *106*, 12376.

(64)   Zhong, D. P.; Pal, S. K.; Zhang, D. Q.; Chan, S. I.; Zewail, A. H. *Proc. Natl. Acad. Sci. USA* **2002**, *99*, 13.

(65)   Pal, S. K.; Peon, J.; Zewail, A. H. *Proc. Natl. Acad. Sci. USA* **2002**, *99*, 1763.

(66)   Peon, J.; Pal, S. K.; Zewail, A. H. *Proc. Natl. Acad. Sci. USA* **2002**, *99*, 10964.

(67)   Lu, W.; Kim, J.; Qiu, W.; Zhong, D. *Chem. Phys. Lett.* **2004**, *388*, 120.

(68)   Qiu, W.; Kao, Y.-T.; Zhang, L.; Yang, Y.; Wang, L.; Stites, W. E.; Zhong, D.; Zewail, A. H. *Proc. Natl. Acad. Sci. USA* **2006**, *103*, 13979.

(69)   Qiu, W.; Zhang, L.; Okobiah, O.; Yang, Y.; Wang, L.; Zhong, D.; Zewail, A. H. *J. Phys. Chem. B.* **2006**, *110*, 10540.

(70)   Bhattacharyya, K. *Accounts of Chemical Research* **2003**, *36*, 95.

(71)   Mandal, U.; Ghosh, S.; Mitra, G.; Adhikari, A.; Dey, S.; Bhattacharyya, K. *Chem. Asian Journal* **2008**, *3*, 1430.

(72)   Seth, D.; Chakraborty, A.; Setua, P.; Sarkar, N. *J. Phys. Chem. B* **2007**, *111*, 4781.

(73)   Chakraborty, A.; Seth, D.; Chakrabarty, D.; Setua, P.; Sarkar, N. *J. Phys. Chem. A* **2005**, *109*, 11110.

(74)   Chakraborty, A.; Seth, D.; Chakrabarty, D.; Setua, P.; Sarkar, N. *J. Phys. Chem. A* **2005**, *109*, 11110.

(75)   Adhikari, A.; Sahu, K.; Dey, S.; Ghosh, S.; Mandal, U.; Bhattacharyya, K. *J. Phys. Chem. B* **2007**, *111*, 12809.

(76)   Sahu, K.; Mondal, S. K.; Ghosh, S.; Roy, D.; Sen, P.; Bhattacharyya, K. *J. Phys. Chem. B* **2006**, *110*, 1056.

(77)   Clegg, R. M. *Curr. Opin. Biotechnol.* **1995**, *6*, 103.

(78)   Lakowicz, J. R. *Principles of fluorescence spectroscopy*, 3rd ed.; Springer: New York, 2004.

(79)   Clegg, R. M. *Fluorescence resonance energy transfer*; John Wiley and sons: New York, 1996.

(80)   Bose, S.; Adhikary, R.; Barnes, C. A.; Fulton, D. B.; Hargrove, M. S.; Song, X.; Petrich, J. W. *J. Phys. Chem. A* **2010**, in press.

(81)   Chapman, C. F.; Fee, R. S.; Maroncelli, M. *J. Phys. Chem.* **1990**, *94*, 4929.

(82)   Ingram, J. A.; Moog, R. S.; Ito, N.; Biswas, R.; Maroncelli, M. *J. Phys. Chem. B* **2003**, *107*, 5926.

(83)   Ito, N.; Arzhantsev, S.; Maroncelli, M. *Chem. Phys. Lett.* **2004**, *396*, 83.

(84)   Adhikary, R.; Bose, S.; Mukherjee, P.; Thite, A.; Kraus, G. A.; Wijeratne, A. B.; Sharma, P.; Armstrong, D. W.; Petrich, J. W. *J. Phys. Chem. B* **2008**, *112*, 7555.

(85)   Jablonski, A. *Bull. l'Acad. Pol. Sci. Ser. A.* **1960**, *8*, 259.

(86)   Cross, A. J.; Fleming, G. R. *Biophys. J.* **1984**, *46*, 45.

(87)   Chowdhury, P. K.; Halder, M.; Sanders, L.; Arnold, R. A.; Liu, Y.; Armstrong, D. W.; Kundu, S.; Hargrove, M. S.; Song, X.; Petrich, J. W. *Photochem. Photobiol.* **2004**, *79*, 440.

(88)   Petrich, J. W.; Martin, J. L.; Breton, J. *Springer Ser. Chem. Phys.* **1988**, *48*, 576.

(89)   Das, K.; Smirnov, A. V.; Wen, J.; Miskovsky, P.; Petrich, J. W. *Photochem. Photobiol.* **1999**, *69*, 633.

(90)   Arzhantsev, S.; Hui, J.; Naoki, I.; Maroncelli, M. *Chem. Phys. Lett.* **2006**, *417*, 524.

(91)   Arzhantsev, S.; Jin, H.; Baker, G. A.; Maroncelli, M. *J. Phys. Chem. B* **2007**, *111*, 4978.

(92)   Jin, H.; Li., X.; Maroncelli, M. *J. Phys. chem. B* **2007**, *111*, 13473.

(93)   Swallen, S. F.; Weidemaier, K.; Tavernier, H. L.; Fayer, M. D. *J. Phys. Chem.* **1996**, *100*, 8106.

(94)   Changenet, P.; Plaza, P.; Martin, M. M.; Meyer, Y. H. *J. Phys. Chem. A* **1997**, *101*, 8186.

(95)   Hay, S.; Pudney, C. R.; Sutcliffe, M. J.; Scrutton, N. S. *Angew. Chem.* **2008**, *47*, 537.

(96)   Bose, S.; Wijeratne, A. B.; Thite, A.; Kraus, G. A.; Armstrong, D. W.; Petrich, J., W. *J. Phys. Chem. B* **2009**, *113*, 10825.

(97)   Bose, S.; Armstrong, D. W.; Petrich, J. W. *J. Phys. Chem. B* **2010**, *114*, 8221.

(98)   Bose, S.; Petrich, J. W. *Green. Chem.* **2010**, submitted.

(99)   Krossing, I.; Slattery, J. M.; Daguenet, C.; Dyson, P. J.; Oleinikova, A.;

Weingartner, H. *J. Am. Chem. Soc.* **2006**, *128*, 13427.

CHAPTER III. SOLVATION DYNAMICS IN PROTEIN ENVIRONMENTS: COMPARISON OF FLUORESCENCE UPCONVERSION MEASUREMENTS OF COUMARIN 153 IN MONOMERIC HEMEPROTEINS WITH MOLECULAR DYNAMICS SIMULATIONS

A paper published in the *Journal of Chemical Physics*

Mintu Halder[1], Prasun Mukherjee[1], Sayantan Bose[1], Mark S. Hargrove[2],

Xueyu Song*[,1], and Jacob W. Petrich*[,1]

Abstract

The complexes of the fluorescence probe coumarin 153 with apomyoglobin and apoleghemoglobin are used as model systems to study solvation dynamics in proteins. Time-resolved Stokes shift experiments are compared with molecular dynamics simulations, and very good agreement is obtained. Solvation of the coumarin probe is very rapid with approximately 60% occurring within 300 fs and is attributed to interactions with water (or possibly to the protein itself). Differences in the solvation relaxation (or correlation) function, $C(t)$, for the two proteins are attributed to differences in their heme pockets.

Introduction

It has been well established by numerous experimental and theoretical studies that solvation dynamics in polar solvents can be described by linear response theory.[1-13] In general, the full frequency dependent dielectric function of the polar solvent (and, perhaps, even of ionic solvents [14]) gives a good description of the solvation dynamics from the ultra-fast regime to that of diffusive relaxation. Some direct and successful comparisons between theory and experiments have been established. [1,12-15] Such success is achieved largely because the dielectric fluctuations of polar solvents can be described accurately by simple linear response models, such as the dielectric continuum model. [16-18] On the other hand, the structure and function of a protein are determined by a delicate balance of different interactions, mainly of noncovalent nature. Among these, the correct description of electrostatic interactions is critical in the understanding of protein properties. To date, much effort has been put to the investigation of their static role in the structure and function of a protein, and considerable progress has been made with this approach for the analysis of structural stability, molecular recognition and drug design, the efficiency of enzyme catalysis, and other properties. [19-22] For many elementary processes occurring in a protein its dynamical dielectric response is also important. A prime example is that electron and energy transfers in photosynthesis are modulated by the dielectric medium of a protein complex. [16] Studies of these dynamical responses have been a very active field, both theoretically and experimentally; [23-34] but in spite of considerable efforts towards the understanding of the dielectric relaxation processes in proteins, [2,35,36] up to now a reliable estimate for the dielectric response function of proteins is still lacking.

For example, a range of experiments has been performed to study dielectric relaxation in proteins; but the results have been very disparate. Early studies suggested that slow relaxation, on the nanosecond time scale, exists in myoglobin, [23,24] in contrast to polar solvents. This may not be unexpected owing to structural constraints, but the role of a protein's interior motions in its dielectric relaxation is presently unclear from various experimental studies. [25,26,29] Homoelle et al. have suggested that the dynamical fluctuations observed in phycobiliproteins involve the interior motions of the protein substantially. [25] Fraga and Loppnow [37] have shown that the resonance Raman spectra are affected by the different residue compositions of the blue copper proteins from different species. On the other hand, experimental and theoretical studies of lysozyme suggest that significant contributions of the observed dynamical fluctuations come from the surrounding water solvent and the water molecules attached on the protein surface. [26] As another example, Zewail and coworkers used tryptophan as a probe to study solvation dynamics in proteins [29-34,38] and have reported slow relaxation from which they inferred the presence of "biological water": water molecules in the immediate vicinity of a surface believed to have different properties from those of bulk water. [2,39-42] For example, they report that the dynamics are significantly slower for the surface tryptophan residues in Subtilisin Carlsberg [31] and in monellin [32] than for that of tryptophan in bulk water, and they argue that the slow relaxation arises from the water molecules constrained on the protein surface. [29] The changes in fluorescence emission maxima that they report for Subtilisin and monellin are, however 1,440 cm^{-1} and 960 cm^{-1}, respectively. Given this difference of 480 cm^{-1} for the two surface tryptophans, it would seem that there is also a considerable relaxation arising from the different amino acids neighboring them.

These differences in the interpretations of various experiments are in no small part due to the lack of a reliable dielectric response function for the studied proteins from either experiments or computer simulations. Studies of the solvation dynamics in proteins, nevertheless, offer the best means of investigating the dielectric response. In this work, we discuss the solvation dynamics of the complexes of coumarin 153 (C153, Figure III.1) with the monomeric hemeproteins, apomyoglobin and apoleghemoglobin, in water. There are four main considerations for the choice of this system.
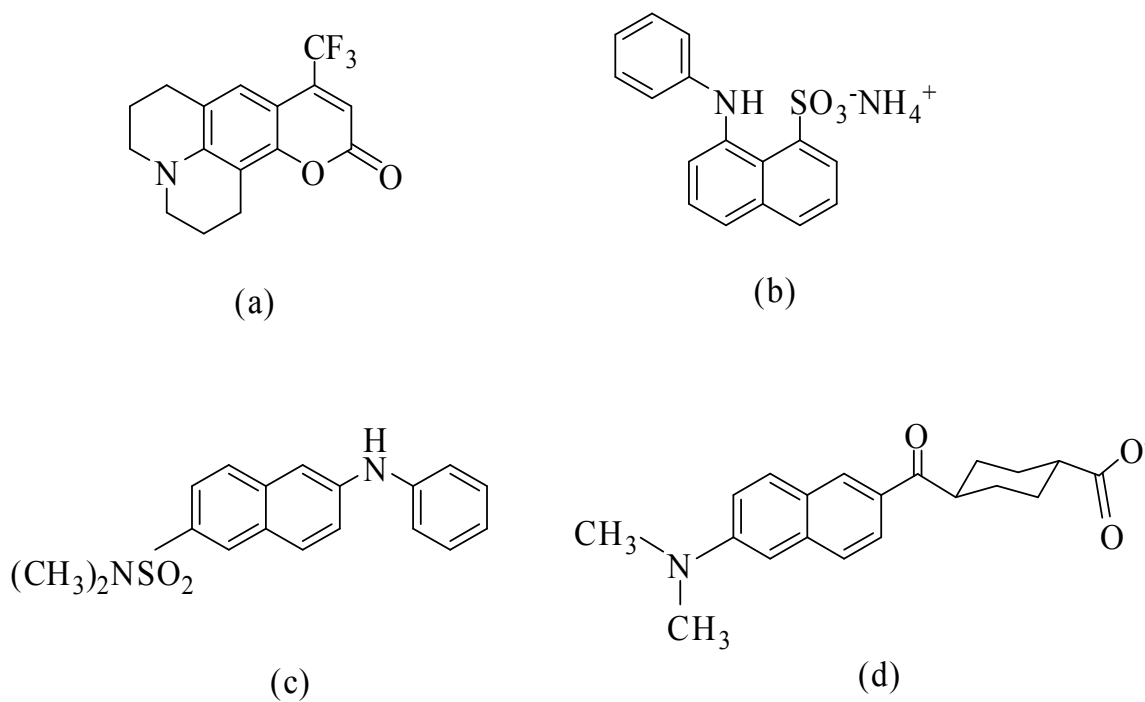
Figure III.1. Structures of the fluorescent probe molecules: (a) coumarin 153 (C153), (b) the ammonium salt of 8-anilino-1-naphthalenesulfonic acid (1,8-ANS), (c) anilino-2-aminonaphthalene-6-dimethylsulfonamide (2,6-ANSDMA) and (d) 2′-(N,N-dimethylamino)-6-naphthoyl-4-*trans*-cyclohexanoic acid (DANCA). The structures for ANSDMA and DANCA were incorrectly transmitted in reference. [43]

First, coumarin 153 (C153) is a well characterized and widely used chromophore for solvation dynamics studies. [44-55]

Second, we have experimentally obtained a binding constant of ~ 6 μM for coumarin 153 and apomyoglobin and have characterized the complex. [43,56] In fact, one of our motivations for using coumarin to probe the hemepocket was the existence of an NMR structure of the dye ANS, a molecule similar to coumarin (Figure III.1), in the hemepocket of apomyoglobin. [57] Binding studies based upon a Job's plot analysis, circular dichroism, fluorescence depolarization, capillary electrophoresis, and molecular dynamics simulations indicate that coumarin indeed is in the hemepocket (Figure III.2). Furthermore, the coumarin's rotation in the hemepocket is very slow compared to the relaxation time scale of interest (see Figure III.2 of ref. [43]). Finally, for the H64Y/V68F double mutant of myoglobin the reorganization energy increases by 5 cm^{-1} and for the H64W mutant it decreases by 90 cm^{-1}, on the other hand, a surface mutant D112N, has, within experimental error, the same reorganization energy as the wild type. This confirms the presence of coumarin in the hemepocket as opposed to the surface.

Third, while myoglobin and leghemoglobin share a common globin fold, they have differences in their hemepockets, [58,59] the region to be probed by the coumarin. For example, the F-helix is oriented in such a way that in myoglobin HisF8 (His93) eclipses the pyrrole nitrogens of the porphyrin but in leghemoglobin it is staggered with respect to them. In the myoglobin proximal hemepocket, SerF7 facilitates a hydrogen bonding network that drives HisF8 into a conformation that destabilizes ligand affinity. The opposite is true in leghemoglobin, which lacks SerF7 and contains a proximal hemepocket that destabilizes ligand binding. The two proteins exhibit differences on the distal sides of their heme pockets as well. The leghemoglobin distal pocket is larger and more flexible than those of most other

hemoglobins and contains a combination of HisE7 (His64) and TyrB10 not found naturally in any other hemoglobin.

Fourth, we can produce a broad range of mutant proteins in which one or several amino acids are strategically replaced, so as to test how specific substitutions can affect solvation dynamics.
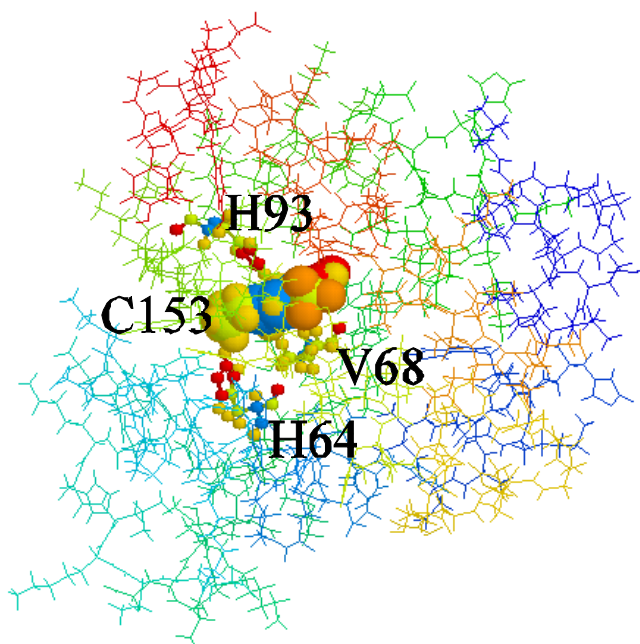
Figure III.2. A snapshot of equilibrated C153-apomyoglobin in water from 3-ns molecular dynamics simulations using CHARMM22 force field. The C153 is shown in a space-filling model, and two histidine residues in the hemepocket are also shown with stick and ball models. His93 is the proximal histidine belonging to the F helix and is also referred to as HisF8. His64 is the distal histidine, also referred to as HisE7.

Materials and Methods

C153 was purchased from Exciton Inc. (Dayton, OH) and used without further purification. Horse heart myoglobin (Mb) was purchased from Sigma. Apoproteins were

prepared using a method described elsewhere. [60] C153 has very low solubility in water. A stock solution of C153 was prepared by adding a microliter amount of a concentrated solution of C153 in methanol to water. That is, concentrated C153/MeOH was added to water, keeping the organic content < 0.3 % (v/v) in the final solution. To prepare a 5×10^{-5} M solution of C153/water, 5 µL of 20×10^{-3} M C153/MeOH solution was added to 2 ml of water. The resulting solution was sonicated. For fluorescence upconversion experiments a stock solution of C153/MeOH was added to 1.2 ml of ~ 1.2×10^{-3} M apoprotein solution keeping the organic content < 3 % (v/v) in the final solution with 1:1 protein to C153 ratio. All samples were equilibrated for about 2 hours before taking the steady state and time resolved measurements. For soybean leghemoglobin (Lba), ammonium sulfate was added to 30% saturation and centrifuged at 14000 rpm for 10 min. The protein in the supernatant was then precipitated by slowly adding ammonium sulfate (to avoid local denaturation) to 90% saturation followed by centrifugation at 14000 rpm for 10 min. The pellets were resuspended in 20mM Tris buffer, pH 8.0 and then loaded onto a Phenyl Sepharose (Sigma) column which was pre-equilibrated with 2 M ammonium sulfate in 20 mM Tris buffer, pH 8.0. The protein was eluted with 0.4 M ammonium sulfate. The eluted protein was dialysed into 20 mM Tris buffer, pH 8.0. The dialysed protein was loaded onto a DEAE (Phramacia column) and eluted with 75 mM NaCl in 20 mM Tris buffer, pH 8.0. The eluted protein was concentrated to ~1 mL and then it was run through a size exclusion column and washed with 10 mM phosphate buffer, pH 7.0.

Steady-state measurements. Steady-state absorbance spectra were obtained on a Hewlett-Packard 8453 UV-visible spectrophotometer with 1-nm resolution. All samples were prepared in 10 mM phosphate buffer solution. The concentrations of apoproteins were

determined spectrophotometrically using the extinction coefficient 15.2 mM^{-1}cm^{-1} at 280 nm [43]. Steady-state fluorescence spectra were obtained on a Spex Fluoromax-2 with a 4-nm bandpass and corrected for lamp spectral intensity and detector response. For both fluorescence and absorption measurements, a 3-mm path-length quartz cuvette was used. The adequacy of the correction factors and the calibration of our fluorometer were checked against the tabulations of Gardecki and Maroncelli. [61]

Time-resolved measurements. The apparatus for fluorescence upconversion measurements is described elsewhere. [62] The instrument response function had a full-width–at-half-maximum (FWHM) of 300 fs. A rotating sample cell was used. To construct the time-resolved spectra from upconversion measurements, a series of decays were collected typically from 480 nm to 560 nm at 10-nm intervals. Transients were fit to sums of exponentials, and time-dependent spectra were reconstructed from these fits by normalizing to the steady-state spectra:

$$S(\lambda, t) = D(\lambda, t) \frac{S_0(\lambda)}{\int_0^\infty D(\lambda, t) dt} \tag{III.1}$$

$D(\lambda,t)$ is the wavelength-resolved fluorescence decay, and $S_0(\lambda)$ is the steady-state emission intensity at a given wavelength. We have employed the traditional approach of fitting the time-resolved spectra to a log-normal function, [44,62] from which we extract the peak frequency, $\nu(t)$, as a function of time.

The solvation dynamics were described by the normalized correlation function:

$$C(t) = \frac{\nu(t) - \nu(\infty)}{\nu("t = 0") - \nu(\infty)} \tag{III.2}$$

ν("t = 0") is the frequency at "zero time." [14,63,64] $\nu(\infty)$ is (usually [65,66]) the frequency at "infinite time," the maximum of the steady-state fluorescence spectrum. $\nu(t)$ is determined

by taking the maxima from the lognormal fits as the emission maximum. In most of the cases, however, the spectra are broad, so there is some uncertainty in the exact position of the emission maxima. Thus, we have considered the range of the raw data points in the neighborhood of the maximum to estimate an error for the maximum obtained from the lognormal fit. Depending on the width of the spectrum (i.e. "zero-time", steady-state, or time-resolved emission spectrum), we have determined the typical uncertainties as follows: "zero-time" ~ steady-state (~ $\pm$ 100 cm^{-1}) < time-resolved emission (~ $\pm$ 200 cm^{-1}). We use these uncertainties to compute error bars for the C(t). Finally, in generating the C(t), the first point was obtained from the "zero time" spectrum. The second point was taken at the maximum of the instrument response function. Fractional solvation at 300 fs is given by f (t = 300 fs) = 1 – C (t = 300 fs).

Molecular dynamics simulations. The starting configurations of horse heart myoglobin (HHMB) and leghemoglobin (LEGMB) are from the protein DATA BANK (PDB id 1WLA and 1BIN) with TIP3P water models. To have a reasonable starting point for the C153-protein complex the heme is replaced by C153 and then energy minimization is used to obtain the starting configuration of the C153-protein complex. Standard constant pressure-temperature MD was performed using the ORAC package [67] with the Amber force field. [68] In all simulations, short-range non-bonded interactions were calculated up to a 10 Å cutoff, whereas long-range electrostatic interactions were treated by the SPME method using a very fine grid, 128 points per axis, with periodic boundary conditions, and Ewald convergence parameter of 0.43 Å^{-1}. Three different Nosé-Hoover thermostats were coupled to solute, solvent, and total center of mass. An external pressure of 0.1 MPa was applied all along the trajectory. A five time-step rRESPA [69] algorithm with times of 0.5-1.0-2.0-4.0-12.0 fs was

used with bond constraints on hydrogen covalent bonds handled by a Shake-Rattle-like algorithm. The final system was first equilibrated with velocity rescaling for 60 ps at 50 K and 80 ps at 300 K. Following this initial equilibration, we ran the system for one additional nanosecond at constant temperature (T = 300 K) and pressure (P = 0.1 MPa). To achieve full relaxation, the simulation box was entirely flexible for the first 300 ps, whereas for the remainder of the run, only isotropic changes of the box were allowed. [67] Finally, the system was simulated for an additional 10 ns. As we have demonstrated in our previous work, [43] an equilibrium configuration for C153 in the heme-pocket of the protein can be found and experimental measurements seem to support our interpretation. Using the equilibrated configuration, additional 12-ns trajectories are generated and are used for the calculation of solvation correlations functions.

Using the charges of C153 in the ground and excited states, [13] the solvation correlation function can be obtained within the linear response theory [70] as

$$C(t) = \frac{<\delta\Delta E(t)\delta\Delta E(0)>}{<\delta\Delta E(0)\delta\Delta E(0)>}, \tag{III.3}$$

where $\delta\Delta E(t) = \Delta E(t) - <\Delta E(t)>$, and $\Delta E(t)$ is the interaction energy difference between C153 in its excited state and ground state with surrounding protein and water molecules at time t. The symbol $< \cdots >$ denotes the ensemble average in the simulation.
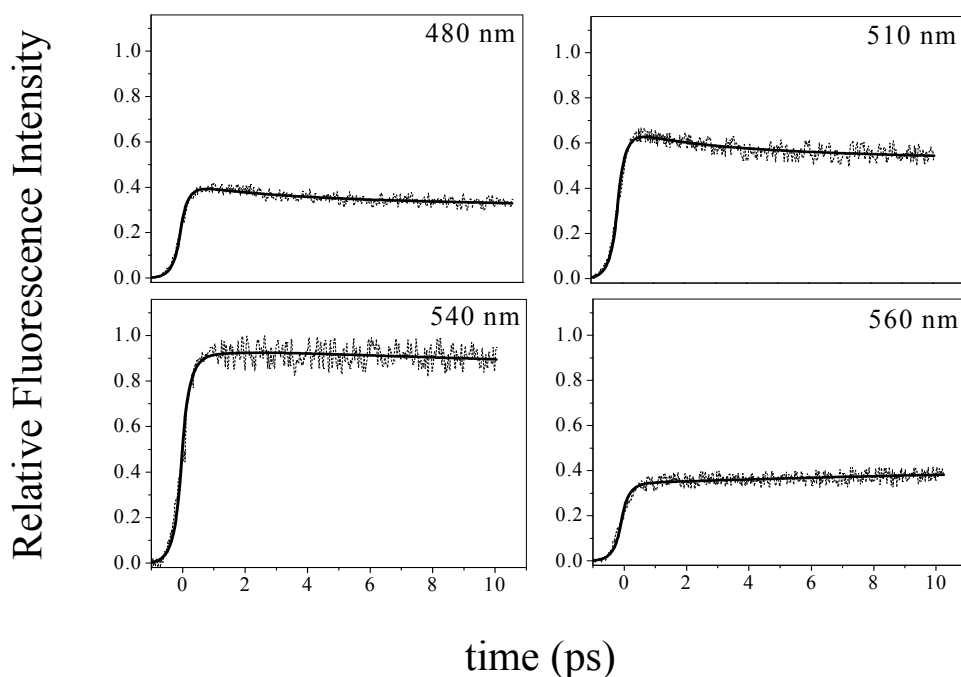
Figure III.3. Fluorescence upconversion traces obtained for C153 in apoMb at the indicated wavelengths. The maximum intensity of the traces are give relative to the most intense, i.e., that at 540 nm. The decays used to construct the time-resolved emission spectra were typically collected over a range of wavelengths from 480 to 560 nm at 10 nm intervals, a total of eight or nine decays was used to generate the time-resolved emission spectra, from which the C(t) were calculated.

Results

Representative wavelength resolved traces obtained on an ~10-ps time scale by means of fluorescence upconversion are shown in Figure III.3. Figure III.4 provides the time-resolved emission spectra at 300 fs and 10.3 ps along with the steady-state and "zero-time" spectra. Figure III.5 presents the solvation correlation functions, C(t). The C(t) obtained from molecular dynamics simulations are also compared with the experimental data in Figure III.5. Relevant fitting parameters are summarized in Table III.I. The salient results are:

1.   Almost 60 % of the solvation is complete in both apoMb and apoLba within the time resolution of our instrument (300 fs).

2.   The initial faster solvation is followed by a slower response, which is slower in apoLba than in apoMb by about a factor of 4 (Table III.I).

3.   There is excellent agreement between the C(t) from fluorescence upconversion experiments and those obtained from molecular dynamics simulations.

TABLE III.1. Solvation parameters of C153 in two monomeric heme proteins (20°C)[a]

System	f_{300fs}	$a_1{}^b$	τ_1	τ_2	a_1 calc	$\tau_1{}^{calc.}$	$\tau_2{}^{calc.}$	$<\tau>$	$<\tau>$ calc	$\nu("0")^c$	$\lambda("0")^d$	$\lambda(\infty)^d$
apoMb	0.64	0.59	0.02	3.4	0.73	0.14	9.3	1.4	2.6	20,260	1,850	2,450
apoLba	0.59	0.60	0.09	13	0.60	0.19	13	5.3	5.3	20,660	1,840	2,590

[a] Unless otherwise indicated, the parameter refers to that experimentally obtained. The time constants are in picoseconds and the frequencies and reorganization energies are given in wavenumbers.

[b] The solvation relaxation functions, C(t), are in both cases fit to a sum of two decaying exponentials, $C(t) = a_1 \exp(-t/\tau_1) + a_2 \exp(-t/\tau_2)$, where $a_1 + a_2 = 1$. C(t) is fit from its value at unity, i.e., starting at "t = 0"; consequently the early part of its decay is determined by only two points. The τ_1 we report are thus upper limits for the early portion of the relaxation. The average solvation time was calculated according to equation: $<\tau> = \sum_i a_i\tau_i$.

[c] For apoMb/C153, $\nu("0") - \nu(\infty) = 1530$ cm^{-1}; for apoLba/C153, $\nu("0") - \nu(\infty) = 1600$ cm^{-1}. The "zero-time" spectra were calculated according to the method described elsewhere.[5,32,33] We use the "zero-time" *spectrum* in our analysis (Figure III.4), and not any approximation for obtaining its maximum. We use hexane as the nonpolar solvent for the "zero-time" calculation.

[d] The reorganization energy, discussed elsewhere,[12,31,33] at "t = 0" and at steady state.

Discussion

The rapidity of the solvation in both the proteins studied here suggests that water is playing a dominant role, which is consistent with the report by Fleming and coworkers[26] that

solvation in the lysozyme/eosin system is dominated by water. (Solvation in bulk water is characterized largely by an ~30-fs component and is complete in ~15 ps. [15,71]) The remainder of the solvation can be attributed to motions of the protein matrix or coupled protein-water [72] motions. The protein's contribution to solvation should not be neglected. For example, Nilsson and Halle have simulated the Stokes shift in the protein monellin [73] and have discussed how to separate the relative contributions of protein and water. They find a significant protein component, at least 25%. Li et al. [72] find that the relative protein and water contributions can vary substantially with the conformational substate of myoglobin: sometimes the protein contribution can even be larger than water. Both Nilsson and Halle [73] and Li et al. [72] find that the protein contribution also has an ultrafast component. Li et al. also found that, in disagreement with the "biological water" picture, protein motion (or protein-water motion) was essential for the slow (~50-100-ps) time-scale Stokes shifts. This feature was independent of the dynamics apparent from the protein and water Stokes shift contributions.

Our results are, however, at odds with those of previous attempts to exploit the myoglobin system to study the solvation response of proteins. These studies [23,24] used the fluorescent probes, 2,6-ANSDMA and DANCA (Figure III.1). The former probe molecule afforded a single exponential response of 9.1 ns; the latter, a more complicated response with both shorter and longer response times. The discrepancy between the results for these two probe molecules as well as the predominance of the long-lived response time caused us to search for other probes. We consequently opted for coumarin 153, which not only has been studied in a very wide range of solvents and in the gas phase, but whose excited-state

solvation has been demonstrated not to involve any contributions other than those from S_1.[44-55]
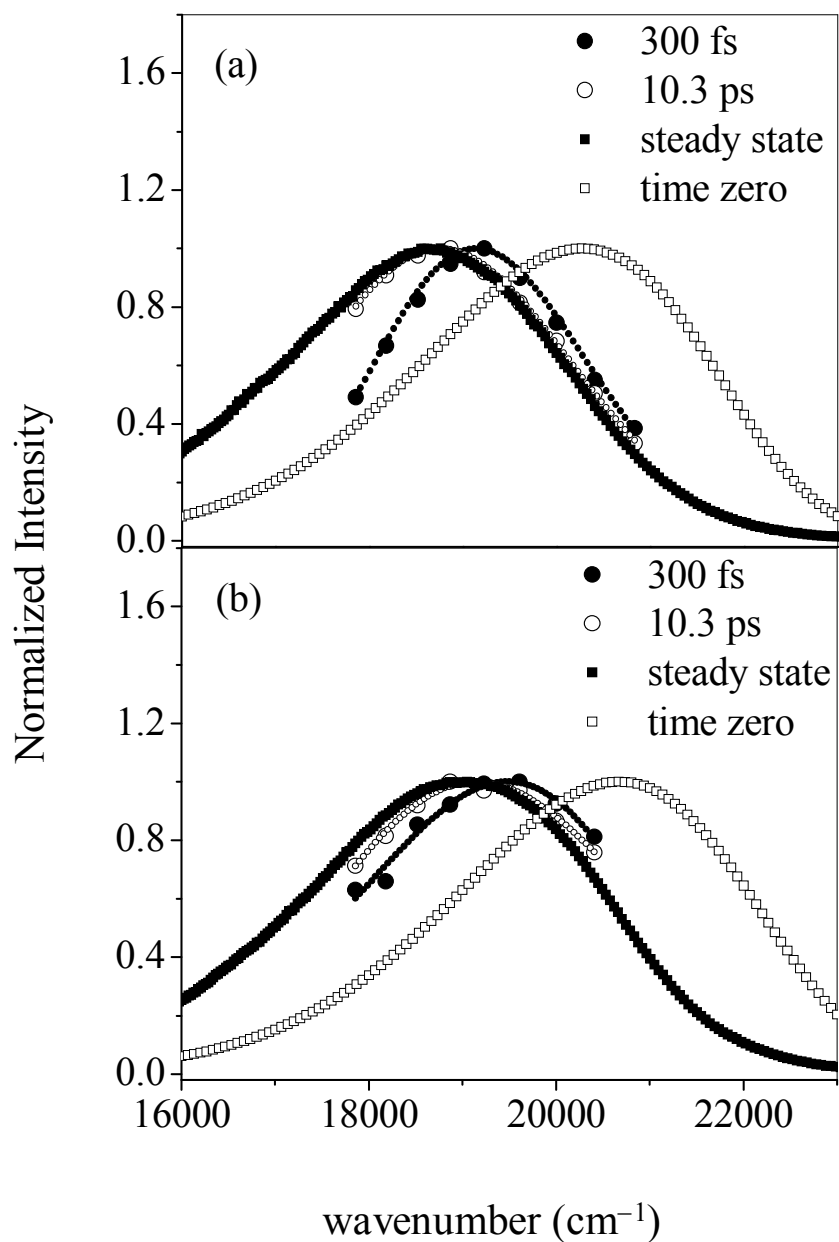
Figure III.4. Normalized time resolved emission spectra for C153 in (a) apoMb and (b) apoLba at 300 fs and 10.3 ps. Corresponding steady-state and "zero-time" spectra are included. Almost 60 % of the solvation is complete in both systems within the time resolution of our instrument (300 fs).
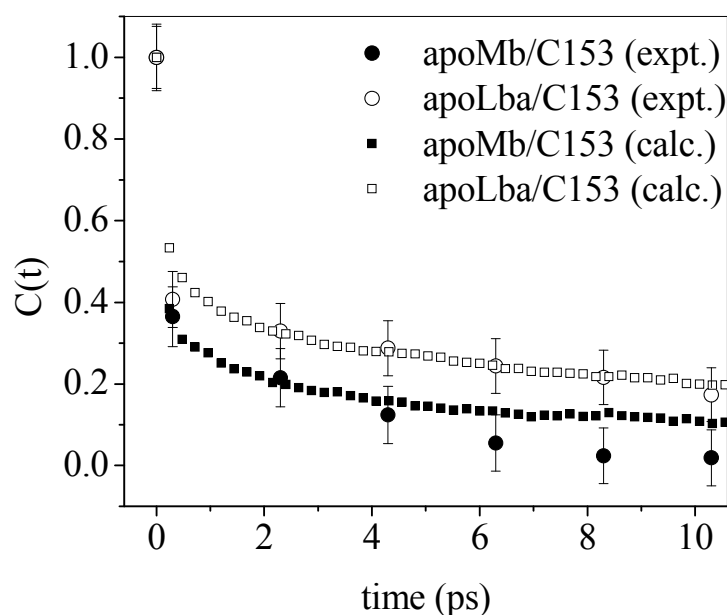
Figure III.5. Comparison of C(t) for C153 in apoMb and apoLba obtained from fluorescence upconversion experiments with those obtained from molecular dynamics simulations. In both proteins, the initial fast component occurs within the time resolution of our instrument.

Our results are also at odds with those of other studies, [31,33,34] from which it is suggested that aqueous solvation in proteins is much slower than that in bulk water. This slow solvation is attributed to "biological water": [2,39-42] in restricted environments, water is proposed to solvate on a much slower time scale, tens to hundreds of picoseconds, as opposed to ~1 ps. [2] We note, however, that an accurate determination of C(t) depends upon appropriate values for $v(0)$ and $v(\infty)$. The latter is usually given by the equilibrium spectrum. This is not, however, true in the case of very slowly relaxing solvents, as has been demonstrated in the case of certain ionic liquids: [65,66] for example, here the emission spectrum at ~3 times the fluorescence lifetime of the probe is *red-shifted* to that of the equilibrium spectrum. The appropriate value for $v(0)$ is not obtained from the emission spectrum obtained immediately upon optical excitation with infinite time resolution, even if

such an experiment were possible, but that arising from the spectrum of a vibrationally relaxed excited state that has been fully solvated by its internal motions but that has not yet responded to the surrounding solvent. Fee and Maroncelli [63] have described a robust, model independent, and simple procedure for generating this "zero-time" *spectrum* (ν("0")); and we have checked its validity using a different method for estimating the "zero-time" reorganization energy. [64] Finally, Li et al. [72] have compared experiments and simulations for protein solvation and note a significant discrepancy between theory and experiment: namely, a very rapid early relaxation is obtained in the simulations but is absent in the experiments. We suggest, based on our results and others to which we refer, that these authors are in fact simulating the solvation appropriately and are, rather, missing the rapid dynamics in their experiment and its analysis.

Conclusions

The results presented here attest to the utility of coumarin 153 as a probe of protein dynamics, as we suggested in earlier work. [43,56] Since the late 1980s, coumarin 153 has proved to be the most useful and reliable probe of solvation dynamics, has been exhaustively studied, and has successfully withstood numerous challenges to this title. [44-55] Its priority in this arena can be attributed to its large Stokes shift (crucial for acquiring an accurate estimate of C(t)), relative rigidity, nonreactivity in the excited state, and that its spectral features arise from only one electronic state. The solvation relaxation functions, C(t), obtained from complexes of coumarin 153 with apomyoglobin and apoleghemoglobin by means of fluorescence upconversion experiments and molecular dynamics simulations are in excellent agreement. Solvation of the coumarin probe is very rapid with approximately 60% occurring within 300 fs and is attributed to interactions with water and possibly the protein. The

hemepockets of myoglobin and leghemoglobin differ considerably [58,59] as we note in the Introduction, and this manifests itself in both the experimental results and the molecular dynamics simulations.

The literature concerning protein dielectric relaxation contains conflicting reports and conclusions. Our results are in good agreement with those obtained by Fleming and coworkers, [26] who find that the initial solvation dynamics of the lysozyme/eosin complex are identical to those of eosin in bulk water. Our results are, however, rather different from those obtained in other studies. Notably, the dynamics we observe are much more rapid than those reported in other work involving monomeric hemeproteins. [23,24] We suggest that the probes used, ANSDMA and DANCA (Figure III.2), are not ideal probes of solvation. They are much more flexible than coumarin, and they are likely to undergo excited-state charge transfer reactions, which could seriously complicate the interpretation of solvation dynamics. This class of chromophores is notable for its dual emission from locally-excited and charge-transfer states. [74]

We suggest that owing to their methods of analyzing the Stokes shift data, other workers have exaggerated the amount of the slowly relaxing component of solvation that they attribute to "biological water." [2,31,33,34,39-42] While it is possible that water molecules may be tightly bound to the protein surface and in this way contribute to slower solvation events, we propose that there is no cogent evidence for excluding ultrafast solvation from bulk water.

Finally, we stress the importance of accurately obtaining the "zero-time" spectrum. Its knowledge is fundamental to an accurate construction of the solvation relaxation function.

Acknowledgements

References

(1)   Song, X. *AIP Conf. Proc.* **1999**, *492*, 417.

(2)   Nandi, N.; Bhattacharyya, K.; Bagchi, B. *Chem. Rev.* **2000**, *100*, 2013.

(3)   Simon, J. D. *Acc. Chem. Res.* **1988**, *21*, 128.

(4)   Fleming, G. R.; Wolynes, P. G. *Phys. Today* **1990**, *43*, 36.

(5)   Barbara, P. F.; Jarzeba, W. Ultrafast Photochemical Intramolecular Charge Transfer and Excited State Solvation. In *Advances in Photochemistry*; Volman, D. H., Hammond, G. S., Gollnick, K., Eds.; John Wiley & Sons, 1990.

(6)   Maroncelli, M. *J. Mol. Liq.* **1993**, *57*, 1.

(7)   Hynes, J. T. Charge Transfer Reactions and Solvation Dynamics. In *Ultrafast Dynamics of Chemical Systems*, 1994; Vol. 7; pp 345.

(8)   Fleming, G. R.; Cho, M. H. *Annu. Rev. Phys. Chem.* **1996**, *47*, 109.

(9)   Stratt, R. M.; Maroncelli, M. *J. Phys. Chem.* **1996**, *100*, 12981.

(10)   Castner, E. W., Jr.; Maroncelli, M. *J. Mol. Liq.* **1998**, *77*, 1.

(11)   Mukamel, S. *Principles of Nonlinear Optical Spectroscopy*, First Edition ed.; Oxford University Press: New York, 1995.

(12)   Hsu, C. P.; Song, X. Y.; Marcus, R. A. *J. Phys. Chem. B* **1997**, *101*, 2546.

(13)   Song, X.; Chandler, D. *J. Chem. Phys.* **1998**, *108*, 2594.

(14)   Halder, M.; Headley, L. S.; Mukherjee, P.; Song, X.; Petrich, J. W. *J. Phys. Chem. A* **2006**, *110*, 8623.

(15)   Lang, M. J.; Jordanides, X. J.; Song, X.; Fleming, G. R. *J. Chem. Phys.* **1999**, *110*, 5884.

(16)   Marcus, R. A.; Sutin, N. *Biochim. Biophys. Acta* **1985**, *811*, 265.

(17)   King, G.; Warshel, A. *J. Chem. Phys.* **1989**, *91*, 3647.

(18)   Bader, J. S.; Kuharski, R. A.; Chandler, D. *Abstr. Paper Am. Chem. Soc.* **1990**, *199*, 65.

(19)   Perutz, M. F. *Science* **1978**, *210*, 1187.

(20)   Warshel, A.; Russel, S. T. *Q. Rev. Biol.* **1984**, *17*, 283.

(21)   Sharp, K. A.; Honig, B. *Ann. Rev. Biophys. Chem.* **1990**, *19*, 301.

(22)   Nakamura, H. *Q. Rev. Biophys.* **1996**, *29*, 1.

(23)   Pierce, D. W.; Boxer, S. G. *J. Phys. Chem.* **1992**, *96*, 5560.

(24)   Bashkin, J. S.; Mclendon, G.; Mukamel, S.; Marohn, J. *J. Phys. Chem.* **1990**, *94*, 4757.

(25)   Homoelle, B. J.; Edington, M. D.; Diffey, W. M.; Beck, W. F. *J. Phys. Chem. B* **1998**, *102*, 3044.

(26)   Jordanides, X. J.; Lang, M. J.; Song, X.; Fleming, G. R. *J. Phys. Chem. B* **1999**, *103*, 7995.

(27)   Brooks, C. L.; Karplus, M.; Pettitt, B. M. *Proteins: A Theoretical Perspective of Dynamics, Structure, and Thermodynamics*; Wiley, 1987; Vol. 71.

(28)   Marchi, M.; Gehlen, J. N.; Chandler, D.; Newton, M. *J. Am. Chem. Soc.* **1993**, *115*, 4178.

(29)   Pal, S. K.; Peon, J.; Bagchi, B.; Zewail, A. H. *J. Phys. Chem. B* **2002**, *106*, 12376.

(30)   Zhong, D. P.; Pal, S. K.; Zhang, D. Q.; Chan, S. I.; Zewail, A. H. *Proc. Natl. Acad. Sci. USA* **2002**, *99*, 13.

(31)   Pal, S. K.; Peon, J.; Zewail, A. H. *Proc. Natl. Acad. Sci. USA* **2002**, *99*, 1763.

(32)   Peon, J.; Pal, S. K.; Zewail, A. H. *Proc. Natl. Acad. Sci. USA* **2002**, *99*, 10964.

(33)   Qiu, W.; Kao, Y.-T.; Zhang, L.; Yang, Y.; Wang, L.; Stites, W. E.; Zhong, D.; Zewail, A. H. *Proc. Natl. Acad. Sci. USA* **2006**, *103*, 13979.

(34)   Qiu, W.; Zhang, L.; Okobiah, O.; Yang, Y.; Wang, L.; Zhong, D.; Zewail, A. H. *J. Phys. Chem. B.* **2006**, *110*, 10540.

(35)   Sheppard, R. J.; Grant, E. H.; South, G. P. *Dielectric Behavior of Biological Molecules, first edition*; Oxford University Press: Clarendon, 1978.

(36)   Pethig, R. *Ann. Rev. Phys. Chem.* **1992**, *43*, 177.

(37)   Fraga, E.; Loppnow, G. R. *J. Phys. Chem. B* **1998**, *102*, 7659.

(38)   Lu, W.; Kim, J.; Qiu, W.; Zhong, D. *Chem. Phys. Lett.* **2004**, *388*, 120.

(39)   Bhattacharyya, K.; Bagchi, B. *J. Phys. Chem. A* **2000**, *104*, 10603.

(40)   Sahu, K.; Mondal, S. K.; Ghosh, S.; Roy, D.; Sen, P.; Bhattacharyya, K. *J. Phys. Chem. B* **2006**, *110*, 1056.

(41)   Pal, S. K.; Mandal, D.; Sukul, D.; Sen, S.; Bhattacharyya, K. *J. Phys. Chem. B* **2001**, *105*, 1438.

(42)   Guha, S.; Sahu, K.; Roy, D.; Mondal, S. K.; Roy, S.; Bhattacharyya, K. *Biochemistry* **2005**, *44*, 8940.

(43)   Chowdhury, P. K.; Halder, M.; Sanders, L.; Arnold, R. A.; Liu, Y.; Armstrong, D. W.; Kundu, S.; Hargrove, M. S.; Song, X.; Petrich, J. W. *Photochem. Photobiol.* **2004**, *79*, 440.

(44)   Maroncelli, M.; Fleming, G. R. *J. Chem. Phys.* **1987**, *86*, 6221.

(45)   Horng, M. L.; Gardecki, J. A.; Papazyan, A.; Maroncelli, M. *J. Phys. Chem.* **1995**, *99*, 17311.

(46)   Lewis, J. E.; Maroncelli, M. *Chem. Phys. Lett.* **1998**, *282*, 197.

(47)   Kovalenko, S. A.; Ruthmann, J.; Ernsting, N. P. *Chem. Phys. Lett.* **1997**, *271*, 40.

(48)   Muhlpfordt, A.; Schanz, R.; Ernsting, N. P.; Farztdinov, V.; Grimme, S. *Phys. Chem. Chem. Phys.* **1999**, *1*, 3209.

(49)   Changenet-Barret, P.; Choma, C. T.; Gooding, E. F.; DeGrado, W. F.; Hochstrasser, R. M. *J. Phys. Chem. B* **2000**, *104*, 9322.

(50)   Jiang, Y.; McCarthy, P. K.; Blanchard, D. J. *Chem. Phys.* **1994**, *183*, 249.

(51)   Flory, W. C.; Blanchard, D. J. *Appl. Spectrosc.* **1998**, *52*, 82.

(52)   Palmer, P. M.; Chen, Y.; Topp, M. R. *Chem. Phys. Lett.* **2000**, *318*, 440.

(53)   Chen, Y.; Palmer, P. M.; Topp, M. R. *Int. J. Mass Spectrom* **2002**, *220*, 231.

(54)   Agmon, N. *J. Phys. Chem.* **1990**, *94*, 2959.

(55)   Maroncelli, M.; Fee, R. S.; Chapman, C. F.; Fleming, G. R. *J. Phys. Chem.* **1991**, *95*, 1012.

(56)   Mukherjee, P.; Halder, M.; Hargrove, M.; Petrich, J. W. *Photochem. Photobiol.* **2006**, *82*, 1586.

(57)   Cocco, M. J.; Lecomte, J. T. J. *Protein Sci.* **1994**, *3*, 267.

(58)   Kundu, S.; Snyder, B.; Das, K.; Chowdhury, P.; Park, J.; Petrich, J. W.; Hargrove, M. S. *Proteins: Struct. Funct. Genet.* **2002**, *46*, 268.

(59)   Kundu, S.; Hargrove, M. S. *Proteins: Struct. Funct. Genet.* **2003**, *50*, 239.

(60)   Hargrove, M. S.; Singleton, E. W.; Quillin, M. L.; Ortiz, L. A.; Phillips, G. N.; Olson, J. S.; Mathews, A. J. *J. Biol. Chem.* **1994**, *269*, 4207.

(61)   Gardecki, J. A.; Maroncelli, M. *Appl. Spectrosc.* **1998**, *52*, 1179.

(62)   Chowdhury, P. K.; Halder, M.; Sanders, L.; Calhoun, T.; Anderson, J. L.; Armstrong, D. W.; Song, X.; Petrich, J. W. *J. Phys. Chem. B* **2004**, *108*, 10245.

(63)   Fee, R. S.; Maroncelli, M. *Chem. Phys.* **1994**, *183*, 235.

(64)   Headley, L. S.; Mukherjee, P.; Anderson, J. L.; Ding, R.; Halder, M.; Armstrong, D. W.; Song, X.; Petrich, J. W. *J. Phys. Chem. A* **2006**, *110*, 9549.

(65)   Arzhantsev, S.; Ito, N.; Heitz, M.; Maroncelli, M. *Chem. Phys. Lett.* **2003**, *381*, 278.

(66)   Ito, N.; Arzhantsev, S.; Heitz, M.; Maroncelli, M. *J. Phys. Chem. B* **2004**, *108*, 5771.

(67)   Marchi, M.; Procacci, P. *J. Chem. Phys.* **1998**, *109*, 5194.

(68)   Pearlman, D. A.; Case, D. A.; Caldwell, J. W.; Ross, W. S.; Cheatham, T. E., III; DeBolt, S.; Ferguson, D.; Seibel, S.; Kollman, P. *Comp. Phys. Commun.* **1995**, *91*, 1.

(69)   Tuckerman, M. E.; Berne, B.; Martyna, G. *J. Chem. Phys.* **1990**, *97*, 1992.

(70)   Maroncelli, M.; Fleming, G. R. *J. Chem. Phys.* **1988**, *89*, 5044.

(71)   Jimenez, R.; Fleming, G. R.; Kumar, P. V.; Maroncelli, M. *Nature* **1994**, *369*, 471.

(72)   Li, T.; Hassanali, A. A.; Kao, Y.-T.; Zhong, D.; Singer, S. J. *J. Am. Chem. Soc.* **2007**, *129*, 3376.

(73)   Nilsson, L.; Halle, B. *Proc. Natl. Acad. Sci. U. S. A.* **2005**, *102*, 13867.

(74)   Lakowicz, J. R. *Principles of fluorescence spectroscopy*, 3rd ed.; Springer: New York, 2004.

CHAPTER IV. CONSIDERATIONS FOR THE CONSTRUCTION OF THE SOLVATION CORRELATION FUNCTION AND IMPLICATION OF DIELECTRIC RELAXATION IN PROTEINS

A paper published in the *Journal of Physical Chemistry B*

Sayantan Bose, Ramkrishna Adhikary, Prasun Mukherjee, Xueyu Song,

and Jacob W. Petrich[*]

Abstract

The dielectric response of proteins is conveniently measured by monitoring the time-dependent Stokes shift of an associated chromophore. The interpretation of these experiments depends critically upon the construction of the solvation correlation function, *C(t)*, which describes the time-dependence of the Stokes shift--and hence the dielectric response of the medium to a change in charge distribution. We provide an analysis of various methods of constructing this function and review selected examples from the literature. The naturally occurring amino acid, tryptophan, has been frequently used as a probe of solvation dynamics in proteins. Its nonexponential fluorescence decay has stimulated the generation of an alternative method of constructing *C(t)*. In order to evaluate

_____

Departments of Chemistry Iowa State University; Ames, Iowa 50011, USA.
*Author to whom all correspondence should be addressed.

this method, we have studied a system mimicking tryptophan. The system is comprised of two coumarins (C153 and C152) having different fluorescence lifetimes but similar solvation times. The coumarins are combined in different proportions in methanol to make binary probe mixtures. We use fluorescence upconversion spectroscopy to obtain wavelength-resolved kinetics of the individual coumarins in methanol as well as the binary mixtures of 75:25, 50:50, and 25:75 of C153:C152. The solvation correlation functions are constructed for these systems using different methods and are compared.

Introduction

It has been well established by numerous experimental and theoretical studies that solvation dynamics in polar solvents can be described by linear response theory [1-13]. In general, the full frequency dependent dielectric function of the polar solvent (and, perhaps, even of ionic solvents[14]) gives a good description of the solvation dynamics from the ultrafast regime to that of diffusive relaxation. Some direct and successful comparisons between theory and experiments have been established [11,12,14,15]. The reason for such success is largely because the dielectric fluctuations of polar solvents can be described accurately by simple linear response models, such as the dielectric continuum model [16-18]. On the other hand, the dielectric response in proteins is more complicated. There exist many length scales due to the structural constraints created by the carbon back bone. Some studies indicate that a linear response model may be valid from atomistic simulations [19,20]. A simple dielectric continuum description is clearly insufficient, even though such a description has been widely used to correlate experimental data [21-24].

Studies of the solvation dynamics in proteins offer the best means of investigating the dielectric response and making a comparison with theory. A range of theoretical and

experimental work has been performed to study dielectric responses in proteins; but the results have been very disparate. Early studies suggested that slow relaxation, on the nanosecond time scale, exists in myoglobin [25,26] in contrast to polar solvents. This may not be unexpected owing to structural constraints, but the role of a protein's interior motions in its dielectric relaxation is presently unclear from various experimental studies [27-30]. Recently, Boxer and coworkers [31,32] have incorporated a synthetic fluorescent amino acid, Aladan, into seven different sites of the B1 domain of the 56-amino acid protein, streptococcal protein G, GB1, to measure the time-dependent Stokes shifts from the femtosecond to nanosecond time scales. The seven sites range from buried within the protein core to fully solvent-exposed on the protein surface. Their results clearly offer another demonstration that the protein dielectric response is highly inhomogeneous, which is also demonstrated from Golosov and Karplus' molecular dynamics simulations for the same system [33]. Experimental and theoretical studies of lysozyme suggest that significant contributions of the observed dynamical fluctuations come from the surrounding water solvent and the water molecules attached on the protein surface [28].

As another example, Zewail and coworkers used the intrinsic single tryptophan as a probe to study solvation dynamics in proteins [29,34-39] and have reported slow relaxation from which they inferred the presence of "biological water": water molecules in the immediate vicinity of a surface believed to have different properties from those of bulk water [1,40-43]. For example, they report that the dynamics are significantly slower for the surface tryptophan residues in Subtilisin Carlsberg [35] and in monellin [36] than for that of tryptophan in bulk water, and they argue that the slow relaxation arises from the water molecules constrained on the protein surface [29].

We have previously discussed the solvation dynamics of the complexes of coumarin 153 (C153, Figure IV.1) with the monomeric hemeproteins, apomyoglobin and apoleghemoglobin, in water [44]. There are four main considerations for our choice of this system. First, coumarin 153 (C153) is a well characterized and widely used chromophore for solvation dynamics studies [45-56]. Second, binding studies and molecular dynamics simulations indicate that coumarin indeed is in the hemepocket [57,58]. We have experimentally obtained a binding constant of ~ 6 μM for coumarin 153 and apomyoglobin and have characterized the complex [57,58]. In fact, one of our motivations for using coumarin to probe the hemepocket was the existence of an NMR structure of the dye ANS in the hemepocket of apomyoglobin [59]. Third, while myoglobin and leghemoglobin share a common globin fold, they have differences in their hemepockets [60,61], the region to be probed by the coumarin. Fourth, we can produce a broad range of mutant proteins in which one or several amino acids are strategically replaced, so as to test how specific substitutions can affect solvation dynamics.

Figure IV.1. Structures of the fluorescent probe molecules that are used in this study: (a) coumarin 153 and (b) coumarin 152.
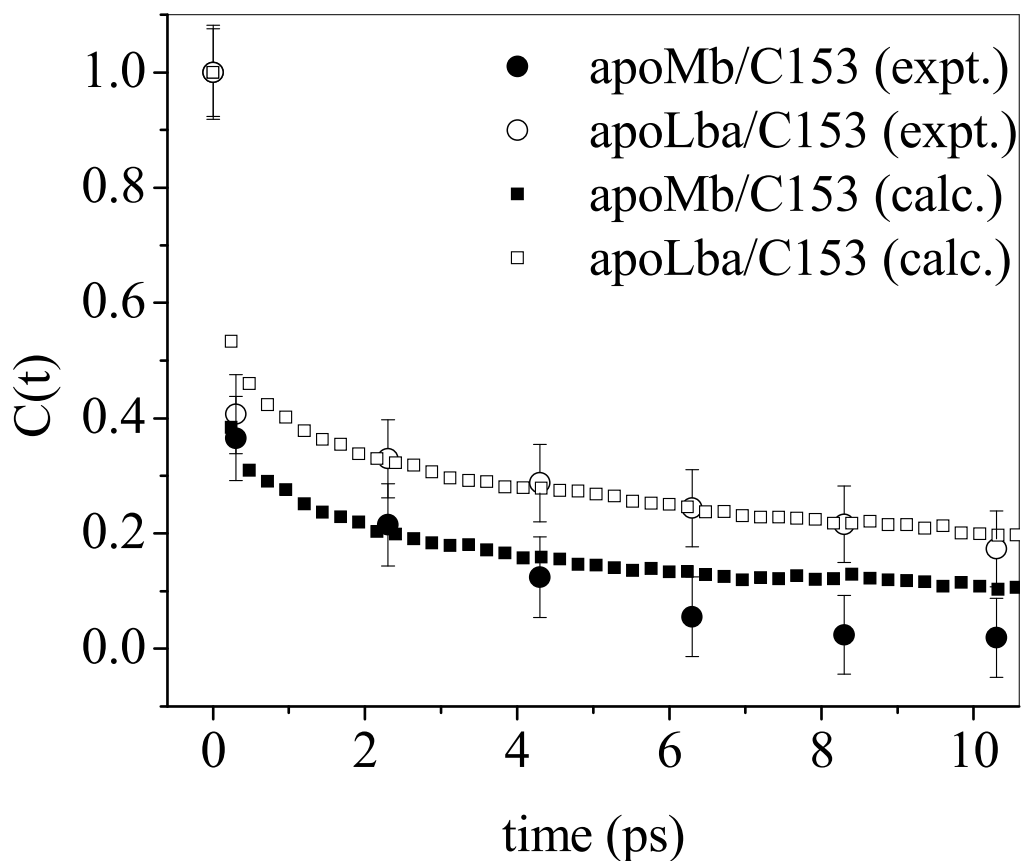
Figure IV.2. Comparison of *C(t)* for C153 in apoMb and apoLba obtained from fluorescence upconversion experiments with those obtained from molecular dynamics simulations. In both proteins, the initial fast component occurs within the time resolution of our instrument and experiment and simulations show excellent agreement with each other. [44]

We found that:

1.   Almost 60 % of the solvation is complete in both apoMb and apoLba within the time resolution of our instrument (300 fs).

2.   The initial faster solvation is followed by a slower response, which is slower in apoLba than in apoMb by about a factor of 4 (Figure IV.2).

3.   There is excellent agreement between the *C(t)* from fluorescence upconversion experiments and those obtained from molecular dynamics simulations.

The rapidity of the solvation in both the proteins studied here suggests that water plays a dominant role, which is consistent with the report by Fleming and coworkers [28] who studied solvation in the lysozyme/eosin system. (Solvation in bulk water is characterized largely by an ~30-fs component and is complete in ~15 ps [15,62].) The remainder of the solvation can be attributed to motions of the protein matrix or coupled protein-water [63] motions. Of course, the protein's contribution to solvation should not be neglected. For example, Nilsson and Halle have simulated the Stokes shift in the protein monellin [64] and have discussed how to separate the relative contributions of protein and water. They found a significant protein component, at least 25%. Li *et al.* [63] found that the relative protein and water contributions can vary substantially with the conformational substate of myoglobin: sometimes the protein contribution can even be larger than water. Both Nilsson and Halle [64] and Li *et al.* [63] found that the protein contribution also has an ultrafast component. Li *et al.* also found that, in disagreement with the "biological water" picture, protein motion (or protein-water motion) was essential for the slow (~50–100 ps) time-scale Stokes shifts. This feature was independent of the dynamics apparent from the protein and water Stokes shift contributions.

Our results are at odds with those of Zewail, Zhong, and coworkers [35,38,39,65,66], and we suggest that the origins of the discrepancies lie in the methods used to compute *C(t)*. More recently, Zhong and coworkers have studied the solvation of different mutants of apomyoglobin [66]. All of the solvation correlation functions they report decay much more slowly than those presented in Figure IV.2. (We note, however, that the simulations of Singer and coworkers [63] are consistent with the dynamics reported in Figure IV.2.) Here, we evaluate various methods of constructing *C(t)*, present new data on the solvation dynamics of

systems containing two different solvation probes in varying ratios, and comment on the consequences of using the *C(t)*s thus generated.

Materials and Methods

Coumarin 153 (C153) and Coumarin 152 (152) (Exciton Inc., Dayton, OH) were used as received. Methanol (HPLC grade) from Aldrich was used without further purification. Five sets of solutions in methanol were made with C153:C152 mole fraction ratios of: 1:0; 0.75:0.25; 0.50:0.50; 0.25:0.75; 0:1. The total concentration of the probe was fixed at 8×10^{-6} M for all the mixtures for both steady-state and lifetime experiments. Stock solutions of 1×10^{-5} M were prepared for both C153 and C152 and then diluted in methanol to maintain the required mole-fractions of the probes in mixtures.

Preparation of micellar solutions. N-acetyl-L-tryptophanamide (NATA) (Figure IV.1) and the surfactant, TX-100 (reduced), were obtained from Sigma. For experiments in micelles, the NATA concentration was kept at $\sim 5 \times 10^{-6}$ M in $\sim 25 \times 10^{-3}$ M TX-100 (reduced) (~100 times CMC). Under these conditions there is one NATA molecule for every 50 micelles (assuming an aggregation number of 100), to minimize aggregation.

Steady-state experiments. Steady-state absorption spectra were obtained on a Hewlett-Packard 8453 UV-visible spectrophotometer with 1-nm resolution. Steady-state fluorescence spectra were obtained on a Spex Fluoromax-4 with a 3-nm bandpass and corrected for lamp spectral intensity and detector response. For absorption and fluorescence measurements, a 1-cm path-length quartz cuvette was used. Coumarin and NATA samples were excited at 407 and 295 nm, respectively.

Lifetime experiments. The lifetime measurements were acquired using the time-correlated single-photon counting (TCSPC) method, which has been described in detail elsewhere [67].

Recent modifications in the TCSPC experimental set-up include the replacement of NIM-style electronics by the Becker & Hickl photon counting module Model SPC-630. In the CFD channel our previous ORTEC pre-amplifier has also been replaced by Becker & Hickl HFAC pre-amplifier. The data were acquired in 1024 channels with a time window of 12 ns. The instrument response function had a full width at half-maximum (FWHM) of ~50 ps. A 1-cm path length quartz cuvette was used for all the time-resolved measurements. Fluorescence decays were collected at the magic angle (polarization of 54.7°) with respect to the vertical excitation light at 407 nm, with 65,000 counts at the peak channel.

Upconversion experiments. The apparatus for fluorescence upconversion measurements is described elsewhere[67]. The instrument response function had a full width at half-maximum (FWHM) of 300 fs. A rotating sample cell was used. To construct the time-resolved spectra from upconversion measurements, a series of decays were collected typically from 480 nm to 570 nm at 10-nm intervals in a time window of 10 ps. Experiments were also done on a 100-ps time scale to ensure that complete solvent relaxation was observed.

Methods of Constructing the Solvation Correlation Function, C(t). Two methods of constructing the solvation correlation function will be discussed in detail. In the first method, wavelength-resolved fluorescence transients were fit to sums of exponentials (typically 2 or 3, as necessary to fit the data) and time-dependent spectra were reconstructed from these fits by normalizing to the steady-state spectra:

$$I(\lambda,t) = \frac{I_\lambda^{SS} I_\lambda(t)}{\sum_i a_i \tau_i} \qquad (IV.1)$$

$I_\lambda(t)$ is the wavelength-resolved fluorescence decay, expressed as $\sum_i a_i \exp(-t/\tau_i)$, and

I_λ^{SS} is the steady-state emission intensity at a given wavelength. We have employed the

traditional approach of fitting the time-resolved emission spectra (TRES) to a log-normal

function [45,67,68], from which we extract the peak frequency $\nu(t)$ as a function of time.

We describe the solvation dynamics by the following normalized correlation function:

$$C(t) = \frac{\nu(t) - \nu(\infty)}{\nu("0") - \nu(\infty)} \quad . \tag{IV.2}$$

Because *C(t)* is a *normalized* function, the accurate determination of *C(t)* depends upon

accurate values for ν("0") and ν(∞). ν("0") is the frequency at zero-time, estimated using the

method of Fee and Maroncelli [69]. The appropriate value for ν(0) is not obtained from the

emission spectrum obtained immediately upon optical excitation with infinite time

resolution, even if such an experiment were possible, but that arising from the spectrum of a

vibrationally relaxed excited state that has been fully solvated by its internal motions but that

has not yet responded to the surrounding solvent, thus the use of the notation "0." Fee and

Maroncelli [69] have described a robust, model independent, and simple procedure for

generating this "zero-time" spectrum, ν("0"); and we have checked its validity using a

different method for estimating the "zero-time" reorganization energy[70].

ν(∞) is (usually[71,72]) the frequency at infinite time, obtained from the maximum of the

steady state spectrum. ν(∞) is usually given by the equilibrium spectrum. (This is not,

however, true in the case of very slowly relaxing solvents, as has been demonstrated in the

case of certain ionic liquids [71,72]: here the emission spectrum at ~3 times the fluorescence

lifetime of the probe is *red-shifted* to that of the equilibrium spectrum.) The ν(t) are

determined from the maxima of the log-normal fits of the TRES. In most of the cases, however, the spectra are broad, so there is some uncertainty in the exact position of the emission maxima. Thus, we have considered the range of the raw data points in the neighborhood of the maximum to estimate an error for the maximum obtained from the lognormal fit. Depending on the width of the spectrum (i.e. "zero-time", steady-state, or time-resolved emission spectrum), we have determined the typical uncertainties as follows: "zero-time" ~ steady-state (~ ± 100 cm^{-1}) < time-resolved emission (~ ± 200 cm^{-1}). We use these uncertainties to compute error bars for the $C(t)$. Finally, in generating the $C(t)$, the first point was obtained from the "zero time" spectrum. The second point was taken at the maximum of the instrument response function.

As noted in the Introduction, Zewail, Zhong, and coworkers use a different approach to calculate $C(t)$ [37-39,66]. They fit the fluorescence intensity transients, $I_\lambda(t)$, to a sum of 4 exponentials, keeping two of the longer components fixed when the solvation probes have biexponential lifetimes (such as tryptophan). Thus, the $I_\lambda(t)$ term is separated into two parts, one for solvation relaxation and the other for population relaxation; and $I_\lambda(t)$ is expressed as:

$$I_\lambda(t) = I_\lambda^{solv}(t) + I_\lambda^{popul}(t) = \sum_i a_i e^{-t/\tau_i} + \sum_j b_j e^{-t/\tau_j} \tag{IV.3}$$

This permits the overall TRES to be written as,

$$I(\lambda,t) = \frac{I_\lambda^{SS} I_\lambda(t)}{\sum_i a_i \tau_i + \sum_j b_j \tau_j}, \tag{IV.4}$$

where the lifetime-associated emission spectra are,

$$I^{popul}(\lambda,t) = \frac{I_\lambda^{SS} I_\lambda^{popul}(t)}{\sum_i a_i \tau_i + \sum_j b_j \tau_j}. \tag{IV.5}$$

The function, $\nu_s(t)$, containing contributions from solvation and population relaxation is obtained from the maxima of log-normal fits to the TRES obtained from Equation IV.4. $\nu_l(t)$ is similarly obtained from Equation IV.5, and provides the contributions solely from population relaxation. $\nu_s(0)$ and $\nu_l(0)$ are *extrapolated zero-time points* obtained by setting t = 0 in Equations IV.4 and IV.5. The emission maximum $\nu_s(t)$ becomes almost equal to $\nu_l(t)$ at a time, t_{sc}, where the solvation is assumed to be complete, and is defined as ν_{sc} (the subscript "sc" denoting "solvation complete"). Note that this time is not equivalent to that at which the spectrum attains its steady-state value. Here, the solvation correlation function, *C(t)*, is:

$$C(t) = \frac{\nu_s(t) - \nu_{sc}}{\nu_s(0) - \nu_{sc}}, \qquad (IV.6)$$

Finally, by subtracting the contributions from population relaxation, $\nu_l(t)$, from $\nu_s(t)$, the expression for *C(t)* used by Zewail, Zhong, and coworkers is obtained:

$$C(t) = \frac{\nu_S(t) - \nu_l(t)}{\nu_S(0) - \nu_l(0)}. \qquad (IV.7)$$

Results and Discussion

Accounting for Experimentally Unresolvable Solvation in Constructing *C(t)*

While obtaining the time-resolved emission profiles is crucial to a determination of the time-dependent Stokes shift and an understanding of the dielectric response of the medium, equally crucial is the construction of the solvation correlation function. Because *C(t)* is a normalized function, its computation and interpretation depend critically on the values used in its denominator for the "zero-time" and "steady-state" spectra (Equation IV.2).

Failure to provide accurate values for these terms can overemphasize slow events and ignore fast events in solvation.
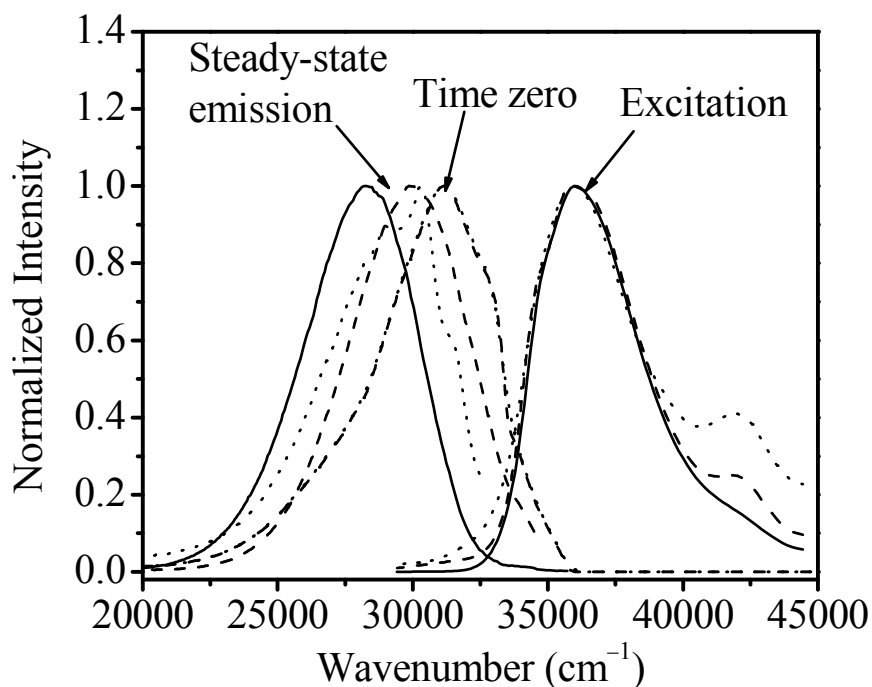
Figure IV.3. Normalized excitation and emission spectra of NATA in 10mM potassium phosphate buffer of pH 7 (solid line), acetonitrile (dashed line) and TX-100 micelle (dotted line). Corresponding time zero spectra in acetonitrile and TX-100 micelle are also included. The construction of the "zero-time" spectrum is discussed elsewhere [14,69,70]. The overlap of excitation spectra in these systems indicates that their "zero-time" spectra are identical. It is known that the tryptophyl absorption spectrum is relatively insensitive to environment [82], and this is borne out in the Figure, where the excitation spectra of NATA in water, acetonitrile, and micelles are essentially superimposable.

The expressions for $C(t)$ given by Equations IV.3-7 were obtained because it was concluded, based on earlier work such as that for subtilisin Carlsberg [35] and monellin [36], that aqueous solvation of tryptophan in proteins could be significantly slower than (or comparable to the time scales of) population relaxation. In particular, because rapid solvation could be resolved for tryptophan in water, it was proposed that *all* the solvation in water was resolved,

not only for tryptophan but also for its analogs and proteins containing it [35,36]. This is a crucial assumption that can severely affect the interpretation of the computed *C(t)* if indeed all the solvation dynamics have not been resolved or accounted for.
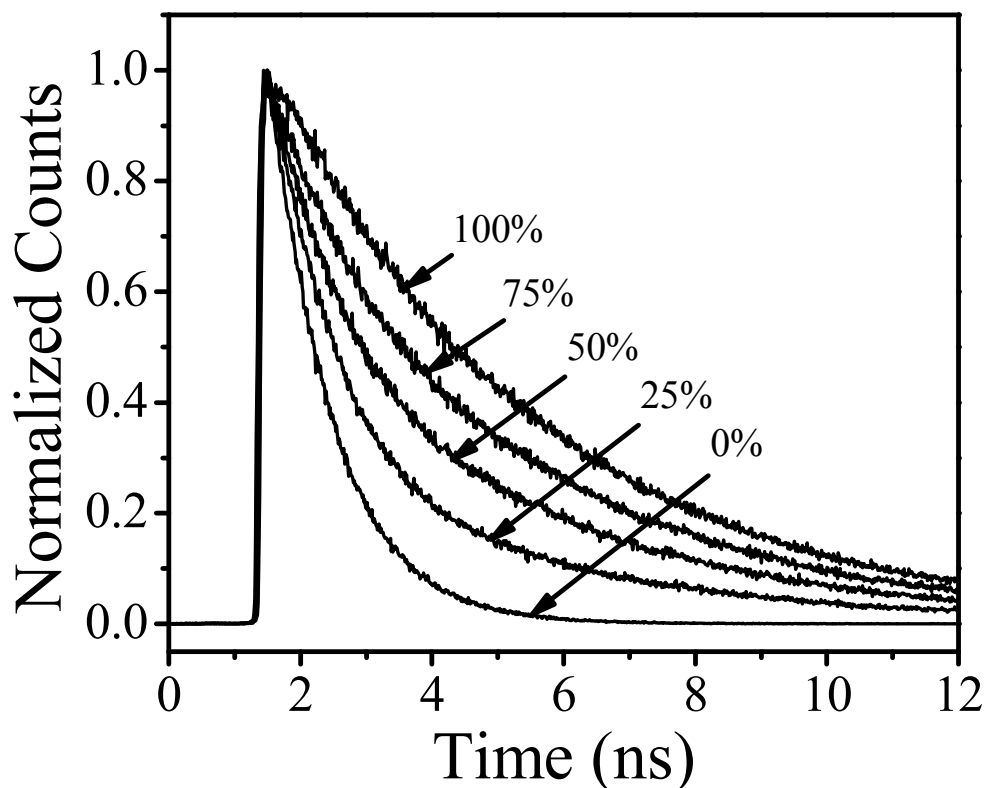
Figure IV.4. Lifetime decay traces (λ_{ex} = 407 nm, $\lambda_{em} \geq$ 425 nm) of five different mixtures of C153 and C152 in methanol. The five traces shown are with 100:0, 75:25, 50:50, 25:75 and 0:100 % C153:C152 mixtures. The labels given in the Figure are the percentages of C153 in the mixtures. The lifetime decreased consistently from 4 ns to 0.9 ns with increasing percentage of C152. The components of the individual lifetimes reflected the corresponding percentages of the coumarins in the excited state. Because the optical densities of the pure coumarins at 407 nm differ only slightly, the excited state percentages for C153 were found to be 79.5, 53.0, and 26.5, nearly the same as the corresponding molar percentages of 75, 50, and 25 in the ground state.

In order to assess how much solvation may have been missed in such an experiment, we provide spectral parameters in Table IV.1 and spectra in Figure IV.3 for N-acetyl-L-

tryptophanamide (NATA). As Table IV.1 indicates, the "zero-time" spectrum obtained for NATA/TX-100 by Zewail and coworkers is red-shifted with respect to that obtained using the Fee and Maroncelli method, resulting in a total spectral shift that is about 20% smaller. We suggest that this 20% comprises solvation events that were unresolvable with their experimental apparatus. Similarly, based upon the assumption that NATA provides a good model for tryptophan in proteins, we suggest that the zero-time spectrum they propose for subtilisin Carlsberg (30,710 cm^{-1} rather than 31,160 cm^{-1} obtained from the Fee and Maroncelli method) is indicative of unresolved solvation events. Subsequent work by Zewail, Zhong, and coworkers, predicated, it would seem, on the evidence that these results provide for slow solvation, devoted considerable effort to the construction of the solvation correlation function [37-39,66] and led to the form of *C(t)* given by Equation IV.7.

Testing *C(t)* Constructions with a Model Tryptophan System

Equations IV.3-7 were conceived in order to address the peculiarities of tryptophan fluorescence. Petrich et al.[73,74] and Szabo and Rayner [75] have shown that the fluorescence decay of tryptophan is well described by a biexponential with two components of ~600 ps and ~3 ns, each corresponding to different spectra whose maxima are at ~335 and ~350 nm, respectively.

In order to compare Equations IV.2 and IV.7 quantitatively, we exploit a model system that mimics tryptophan by using two coumarins having different fluorescence lifetimes, but similar solvation times. The model consists of coumarin 153 and coumarin 152 (Figure IV.1), which are mixed together in different proportions in methanol. We use fluorescence upconversion spectroscopy to study the solvation dynamics, using the

individual coumarins in methanol as well as the binary mixtures of 75:25, 50:50 and 25:75 of C153:C152.

Fluorescence lifetime measurements of five sets of C153:C152 mixtures in methanol are shown in Figure IV.4. Pure C153 and C152 have single exponential lifetimes of 4.0 and 0.9 ns respectively, whereas the mixtures have biexponential decays with the same time constants, whose amplitudes were proportional to their ground state population ratios, as indicated in Table IV.2. The representative wavelength-resolved traces obtained on a 10-ps time scale from 480 to 570 nm at 10-nm intervals are presented in Figure IV.5.

Using the approach leading to Equation IV.2 and the Fee and Maroncelli [69] method for obtaining ν("0"), $C(t)$ was computed. The spectral positions are compiled in Table IV.3. The average solvation times obtained for pure C153 and C152 in methanol were 4.35 and 5.00 ps, respectively. That is, as expected for similar solvation probes, the solvation times are nearly identical within experimental error. Furthermore, as expected, despite the difference in the fluorescence lifetimes of the two probes, the average solvation times of the probe mixtures are within the range of solvation times of the pure probes (Table IV.2).

The data for coumarin mixtures were also subjected to the approach leading to Equation IV.7. Figures IV.6a-c provide a comparison of the $C(t)$s obtained from Equations IV.2 and 7 for three coumarin mixtures. In each case, Equation IV.7 suggests that the amplitude of slow solvation is significantly greater than that provided by Equation IV.2. This discrepancy is clearly a result of the difference in the values of "zero-time" (Table IV.3) used in the respective equations. In fact, if the Fee and Maroncelli "zero-time" is inserted into Equation IV.7, much better agreement of the correlation functions is obtained.

As a control experiment, our *C(t)* for C153 in methanol obtained using Equation IV.2 is compared with that obtained by Maroncelli and coworkers [46] in Figure IV.6d. The agreement is very good, even though the time resolution of the systems used is different. Ours is ~ 300 fs while theirs is ~ 110 fs. The *C(t)* for solvation in methanol has been well documented. Gustavsson et al.[76] and Jarzeba et al.[77] have obtained similar results. Equation IV.7 clearly exaggerates the slow component of solvation in methanol.

TABLE IV.1. Spectral Parameters for Solvation in Various Systems [a]

System	v_{exc} [b]	v("0") [c]	v(∞) [c]	Δv [c]	λ("0") [d]	$\lambda(\infty)$ [d]
NATA/hexane	37,450		32,260			3,820
NATA/H$_2$O	35,970	31,160	28,250	2,910	4,220	5,300
NATA/CH$_3$CN	35,840	31,160	29,850	1,310	4,140	4,280
NATA/TX-100	35,970	31,160 30,420[35]	30,310 29,750[35]	850 670[35]	4,010	4,600
C153/hexane	25,770		22,370			2,100
C153/CH$_3$CN	23,980	21,010	19,160	1,850	2,040	2,850
apoMb/C153	22,940	20,260	18,730	1,530	1,850	2,450
apoLba/C153	23,200	20,660	19,060	1,600	1,840	2,590
Subtilisin Carlsberg[35]		30,710	29,270	1,440		
Monellin[36]				960		

[a] All values are given in wavenumbers (cm^{-1}).
[b] The maximum of the fluorescence excitation spectrum (exc), which is equivalent to the absorption spectrum.
[c] The maximum of the "zero-time" spectrum, which is discussed in the text and whose computation is discussed in detail elsewhere [69,70]. The Δv were calculated as (v("0") - v(∞)), unless otherwise indicated. For monellin [36], Subtilisin Carlsberg and NATA/TX-100 [35], v(120 ps), v(200 ps), and v(250 ps), respectively, are used instead of v(∞).
[d] The reorganization energy, which is a more quantitative measure of solvation and whose computation is discussed elsewhere [28]. The reorganization energies cited in reference [57] were mistakenly obtained using spectra instead of lineshapes, and are consequently incorrect. Also, in this earlier cited work, a 40:1 protein to C153 ratio was used.

TABLE IV.2. Solvation and Lifetime parameters for different C153/C152 Mixtures in Methanol

System		Lifetime Parameters					Solvation Parameters						
C153 (%)	C152 (%)	a_1	τ_1 (ns)	a_2	τ_2 (ns)	$<\tau_f>^a$ (ns)	a_1	τ_1 (ps)	a_2	τ_2 (ps)	a_3	τ_3 (ps)	$<\tau_s>^b$ (ps)
100	0			1.0	4.0	4.0	0.54	0.14	0.23	3.4	0.23	15.2	4.35
75	25	0.25	0.9	0.75	4.0	3.2	0.50	0.02	0.25	3.0	0.25	13.0	4.00
50	50	0.48	0.9	0.52	4.0	2.5	0.49	0.03	0.25	1.0	0.26	17.0	4.70
25	75	0.72	0.9	0.28	4.0	1.8	0.51	0.02	0.19	1.1	0.30	14.9	4.70
0	100	1.0	0.9			0.9	0.48	0.02	0.22	1.0	0.30	16.0	5.00

[a] The average lifetimes, $<\tau_f>$ are associated with an error bar of $\pm$ 0.2 ns based on the average of three measurements.

[b] Solvation time $<\tau_s>$ was calculated using the traditional method of $C(t)$ calculation according to Equation IV.2, using the zero-time peak maxima from Fee-Maroncelli's method [69].

TABLE IV.3. **Comparison of Zero-Time Spectral Positions (cm^{-1}) Using Different Methods**

System		$\nu_s(0)^a$	Time Zero				Difference of mid-pt^f	Difference of Peak-max^f
			Full Method^b		Approx Method^c			
C153 (%)	C152 (%)		Mid-point^d	Peak maxima^e	Mid-point^d	Peak maxima^e		
100	0		20520	20770	20410	20230	110	540
75	25	20000	21360	21450	21000	21530	360	-80
50	50	20120	21690	21710	21870	21160	-180	550
25	75	20200	21500	21730	21550	21510	-50	220
0	100		21480	21760	21670	21790	-190	-30

^{a} $\nu_s(0)$, obtained from Equation IV.7, is the extrapolated zero-time point obtained by setting t = 0 in Equation IV.4 [37-39,66].

^{b} Calculated using full Fee and Maroncelli's method [69], where the entire zero-time spectrum is constructed.

^{c} Approximation using $\nu_{em}^{polar}(0) = \nu_{abs}^{polar} - (\nu_{abs}^{non-polar} - \nu_{em}^{non-polar})$ [69].

^{d} Mid point frequencies are calculated as $\nu_{mid} = (\nu_+ + \nu_-)/2$, where ν_+ and ν_- are the midpoint frequencies at the blue and red edges of the spectrum, respectively.

^{e} Peak maxima of the zero-time spectrum obtained from log-normal fitting using the full Fee and Maroncelli procedure and are used in Equation IV.2, for the construction of *C(t)*.

^{f} Differences are calculated as: (full method)-(approx. method).

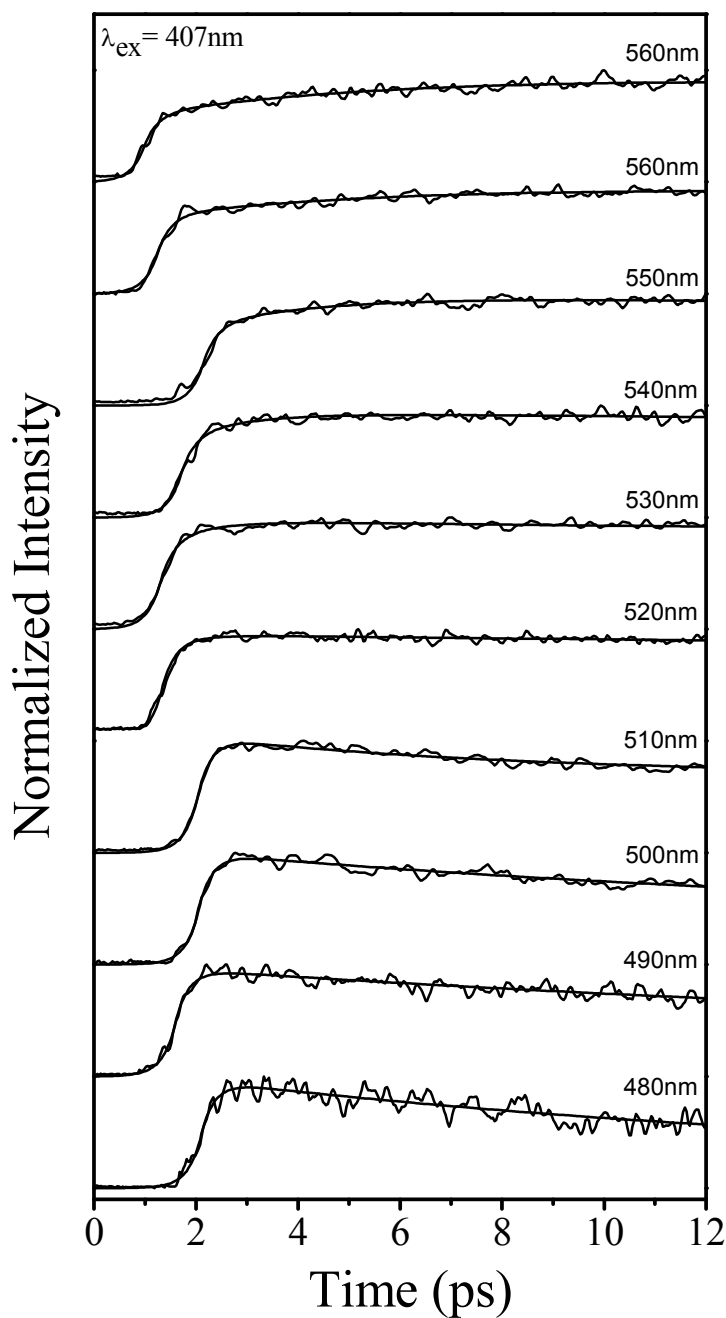**Figure IV.5**. Representative normalized upconversion traces for the 75:25-C153:C152 mixture obtained at wavelengths from 480 to 570 nm at 10-nm intervals. These traces were fit in two ways, one with a sum of 2-3 exponentials, and also with four exponentials, using $\sum_i a_i \exp(-t/\tau_i) + \sum_j b_j \exp(-t/\tau_j)$, keeping two of the longer components, τ_j, fixed at the two lifetimes of the coumarins in binary mixtures.
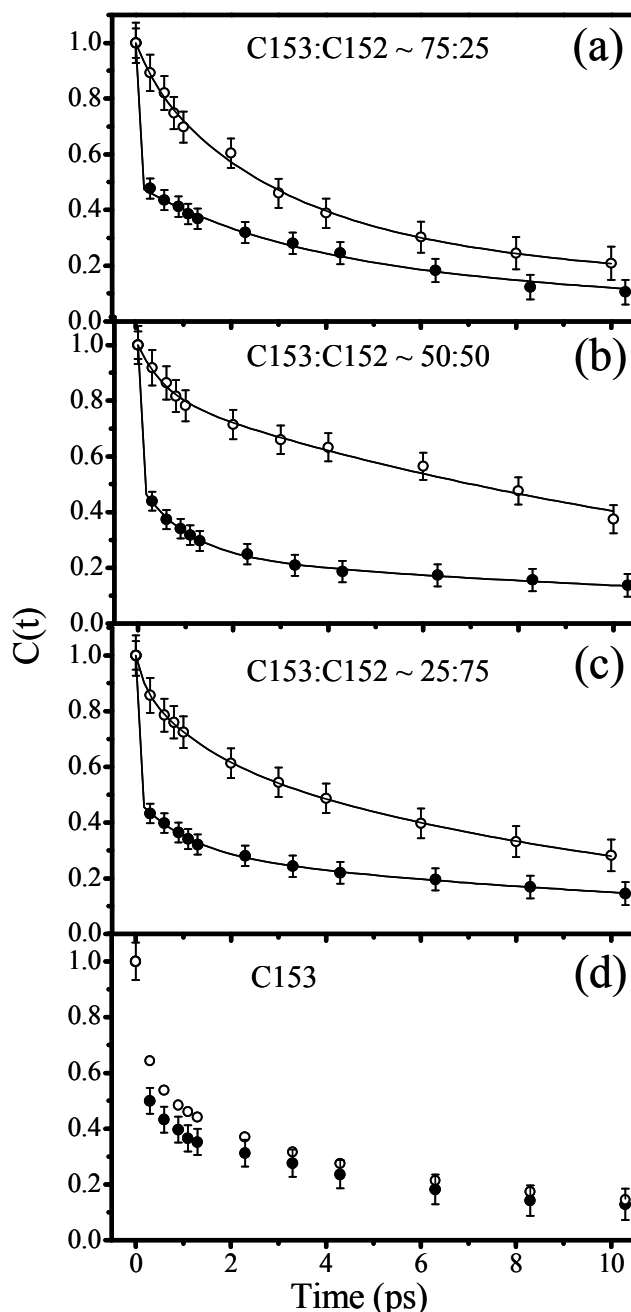
Figure IV.6. Solvation correlation functions, *C(t)*, of (a) 75:25, (b) 50:50, (c) 25:75 (from top to bottom) of C153:C152 mixtures in methanol, calculated using Equation IV.2 (●), and using Equation IV.7 (○). The bottom most panel (d) shows the *C(t)* of pure C153 in methanol using Equation IV.2 (●) and that obtained by Maroncelli and coworkers (○). All *C(t)* decays are fit with a sum of three exponentials and fitting parameters obtained from Equation IV.2 are listed in Table IV.2. From panel a-c, it can be seen that the solvation is considerably slower using Equation IV.7 as opposed to the approach given by Equation IV.2. Panel d presents a control experiment showing good agreement of our *C(t)* with that of Maroncelli for pure C153 in methanol.

Approximate Methods

Based upon the comparison above and work we have presented elsewhere [44,70,78], we suggest that the method of Fee and Maroncelli for obtaining the zero-time spectrum is the soundest available. Its details are clearly described in their paper [69], briefly alluded to above, and provide the basis for the construction of an *entire* emission spectrum. In this paper, Fee and Maroncelli also provide a simple equation for approximating the maximum of the zero-time spectrum:

$$v^P_{em}(0) = v^P_{abs} - (v^{nP}_{abs} - v^{nP}_{em}),$$ (IV.10)

where P and nP refer to the position of the emission or absorption spectra in polar or nonpolar solvents, respectively. In our experience, this approximation usually deviates from that obtained by the full method by at least a few hundred wavenumbers. Comparisons are provided in Table IV.3. Bhattacharya and coworkers use Equation IV.10 as a quick way of estimating the position of the zero-time spectrum [43,79], but we propose that it is no substitute for using the full method—especially when quantitative interpretations of *C(t)* are required.

Conclusions

As a result of the comparisons provided above, especially in the Tables and in Figure IV.6, we conclude that it is unnecessary to make additional corrections for multiple lifetimes of the solvation probe (or probes). Lifetime effects are automatically accounted for in the construction of the time-resolved spectra by means of Equation IV.1. The only instance where lifetime effects are important is when the solvation time is considerably longer than the excited-state lifetime, that is, in circumstances where there are no photons available to probe the continually evolving process. This situation occurs in highly viscous systems, such as glasses and ionic liquids [71,72,78,80,81]. It might also be expected to occur in very slow

processes in proteins, such as large amplitude conformational changes and folding and unfolding processes, which, however, the experiments discussed here are not designed to investigate.

While Equation IV.7 adequately reproduces the form of the solvation dynamics at longer times, it significantly overemphasizes its amplitude. This is a consequence of underestimating the position of the "zero-time" spectrum by more than 1000 cm^{-1} (Table IV.3). Consequently, it is possible to exaggerate the amplitudes of slower solvation phenomenon that may be attributed to "biological water", water-protein interactions, or the protein itself.

We stress that $C(t)$ is a normalized function whose form and interpretation depend critically upon the terms in its denominator, namely the positions of the "zero-time" and "steady-state" spectra, the former of which we argue is most accurately provided by the full method of Fee and Maroncelli [69]. Finally, we note the excellent agreement between experiment and theory that is emerging in the study of solvation dynamics of proteins, for example, our earlier study of monomeric hemeproteins, and recent work by Boxer and coworkers [31] and Golosov and Karplus [33].

Acknowledgements

References

(1)   Nandi, N.; Bhattacharyya, K.; Bagchi, B. *Chem. Rev.* **2000**, *100*, 2013.

(2)   Simon, J. D. *Acc. Chem. Res.* **1988**, *21*, 128.

(3)   Fleming, G. R.; Wolynes, P. G. *Physics Today* **1990**, *43*, 36.

(4) Barbara, P. F.; Jarzeba, W. Ultrafast Photochemical Intramolecular Charge Transfer and Excited State Solvation. In *Advances in Photochemistry*; Volman, D. H., Hammond, G. S., Gollnick, K., Eds.; John Wiley & Sons, 1990.

(5) Maroncelli, M. *J. Mol. Liq.* **1993**, *57*, 1.

(6) Hynes, J. T. Charge Transfer Reactions and Solvation Dynamics. In *Ultrafast Dynamics of Chemical Systems*, 1994; Vol. 7; pp 345.

(7) Fleming, G. R.; Cho, M. H. *Annu. Rev. Phys. Chem.* **1996**, *47*, 109.

(8) Stratt, R. M.; Maroncelli, M. *J. Phys. Chem.* **1996**, *100*, 12981.

(9) Castner, E. W., Jr.; Maroncelli, M. *J. Mol. Liq.* **1998**, *77*, 1.

(10) Mukamel, S. *Principles of Nonlinear Optical Spectroscopy*, First Edition ed.; Oxford University Press: New York, 1995.

(11) Hsu, C. P.; Song, X. Y.; Marcus, R. A. *J. Phys. Chem. B* **1997**, *101*, 2546.

(12) Song, X.; Chandler, D. *J. Chem. Phys.* **1998**, *108*, 2594.

(13) Nitzan, A. *Chemical Dynamics in Condensed Phases*, 1st ed.; Oxford University Press, 2007.

(14) Halder, M.; Headley, L. S.; Mukherjee, P.; Song, X.; Petrich, J. W. *J. Phys. Chem. A* **2006**, *110*, 8623.

(15) Lang, M. J.; Jordanides, X. J.; Song, X.; Fleming, G. R. *J. Chem. Phys.* **1999**, *110*, 5884.

(16) Marcus, R. A.; Sutin, N. *Biochim. Biophys. Acta* **1985**, *811*, 265.

(17) King, G.; Warshel, A. *J. Chem. Phys.* **1989**, *91*, 3647.

(18) Bader, J. S.; Kuharski, R. A.; Chandler, D. *Abstracts of Papers of the American Chemical Society* **1990**, *199*, 65.

(19)   Zheng, C.; Wong, C. F.; McCammon, J. A.; Wolynes, P. G. *Chem. Scripta* **1989**, *29A*, 171.

(20)   Simonson, T. *Proc. Natl. Acad. Sci. USA* **2002**, *99*, 6544.

(21)   Warshel, A.; Russel, S. T. *Q. Rev. Biol.* **1984**, *17*, 283.

(22)   Sharp, K. A.; Honig, B. *Ann. Rev. Biophys. Chem.* **1990**, *19*, 301.

(23)   Schutz, C. N.; Warshel, A. *Proteins: Struc. Func. Gen.* **2001**, *44*, 400.

(24)   Simonson, T. *Curr. Opin. Struc. Biol.* **2001**, *11*, 243.

(25)   Pierce, D. W.; Boxer, S. G. *J. Phys. Chem.* **1992**, *96*, 5560.

(26)   Bashkin, J. S.; Mclendon, G.; Mukamel, S.; Marohn, J. *J. Phys. Chem.* **1990**, *94*, 4757.

(27)   Homoelle, B. J.; Edington, M. D.; Diffey, W. M.; Beck, W. F. *J. Phys. Chem. B* **1998**, *102*, 3044.

(28)   Jordanides, X. J.; Lang, M. J.; Song, X.; Fleming, G. R. *J. Phys. Chem. B* **1999**, *103*, 7995.

(29)   Pal, S. K.; Peon, J.; Bagchi, B.; Zewail, A. H. *J. Phys. Chem. B* **2002**, *106*, 12376.

(30)   Fraga, E.; Loppnow, G. R. *J. Phys. Chem. B* **1998**, *102*, 7659.

(31)   Abbyad, P.; Shi, X.; Childs, W.; McAnaney, T. B.; Cohen, B. E.; Boxer, S. G. *J. Phys. Chem. B* **2007**, *111*, 8269.

(32)   Cohen, B. E.; McAnaney, T. B.; Park, E. S.; Jan, Y. N.; Boxer, S. G.; Jan, L. Y. *Science* **2002**, *296*, 1700.

(33)   Golosov, A. A.; Karplus, M. *J. Phys. Chem. B* **2007**, *111*, 1482.

(34)   Zhong, D. P.; Pal, S. K.; Zhang, D. Q.; Chan, S. I.; Zewail, A. H. *Proc. Natl. Acad. Sci. USA* **2002**, *99*, 13.

(35)   Pal, S. K.; Peon, J.; Zewail, A. H. *Proc. Natl. Acad. Sci. USA* **2002**, *99*, 1763.

(36)   Peon, J.; Pal, S. K.; Zewail, A. H. *Proc. Natl. Acad. Sci. USA* **2002**, *99*, 10964.

(37)   Lu, W.; Kim, J.; Qiu, W.; Zhong, D. *Chem. Phys. Lett.* **2004**, *388*, 120.

(38)   Qiu, W.; Kao, Y.-T.; Zhang, L.; Yang, Y.; Wang, L.; Stites, W. E.; Zhong, D.; Zewail, A. H. *Proc. Natl. Acad. Sci. USA* **2006**, *103*, 13979.

(39)   Qiu, W.; Zhang, L.; Okobiah, O.; Yang, Y.; Wang, L.; Zhong, D.; Zewail, A. H. *J. Phys. Chem. B.* **2006**, *110*, 10540.

(40)   Bhattacharyya, K.; Bagchi, B. *J. Phys. Chem. A* **2000**, *104*, 10603.

(41)   Pal, S. K.; Mandal, D.; Sukul, D.; Sen, S.; Bhattacharyya, K. *J. Phys. Chem. B* **2001**, *105*, 1438.

(42)   Guha, S.; Sahu, K.; Roy, D.; Mondal, S. K.; Roy, S.; Bhattacharyya, K. *Biochemistry* **2005**, *44*, 8940.

(43)   Sahu, K.; Mondal, S. K.; Ghosh, S.; Roy, D.; Sen, P.; Bhattacharyya, K. *J. Phys. Chem. B* **2006**, *110*, 1056.

(44)   Halder, M.; Mukherjee, P.; Bose, S.; Hargrove, M. S.; Song, X.; Petrich, J. W. *J. Chem. Phys.* **2007**, *127*, 055101/1.

(45)   Maroncelli, M.; Fleming, G. R. *J. Chem. Phys.* **1987**, *86*, 6221.

(46)   Horng, M. L.; Gardecki, J. A.; Papazyan, A.; Maroncelli, M. *J. Phys. Chem.* **1995**, *99*, 17311.

(47)   Lewis, J. E.; Maroncelli, M. *Chem. Phys. Lett.* **1998**, *282*, 197.

(48)   Kovalenko, S. A.; Ruthmann, J.; Ernsting, N. P. *Chem. Phys. Lett.* **1997**, *271*, 40.

(49)   Muhlpfordt, A.; Schanz, R.; Ernsting, N. P.; Farztdinov, V.; Grimme, S. *Phys. Chem. Chem. Phys.* **1999**, *1*, 3209.

(50)   Changenet-Barret, P.; Choma, C. T.; Gooding, E. F.; DeGrado, W. F.; Hochstrasser, R. M. *J. Phys. Chem. B* **2000**, *104*, 9322.

(51)   Jiang, Y.; McCarthy, P. K.; Blanchard, D. J. *Chem. Phys.* **1994**, *183*, 249.

(52)   Flory, W. C.; Blanchard, D. J. *Appl. Spectrosc.* **1998**, *52*, 82.

(53)   Palmer, P. M.; Chen, Y.; Topp, M. R. *Chem. Phys. Lett.* **2000**, *318*, 440.

(54)   Chen, Y.; Palmer, P. M.; Topp, M. R. *Int. J. Mass Spectrom* **2002**, *220*, 231.

(55)   Agmon, N. *J. Phys. Chem.* **1990**, *94*, 2959.

(56)   Maroncelli, M.; Fee, R. S.; Chapman, C. F.; Fleming, G. R. *J. Phys. Chem.* **1991**, *95*, 1012.

(57)   Chowdhury, P. K.; Halder, M.; Sanders, L.; Arnold, R. A.; Liu, Y.; Armstrong, D. W.; Kundu, S.; Hargrove, M. S.; Song, X.; Petrich, J. W. *Photochem. Photobiol.* **2004**, *79*, 440.

(58)   Mukherjee, P.; Halder, M.; Hargrove, M.; Petrich, J. W. *Photochem. Photobiol.* **2006**, *82*, 1586.

(59)   Cocco, M. J.; Lecomte, J. T. J. *Protein Sci.* **1994**, *3*, 267.

(60)   Kundu, S.; Snyder, B.; Das, K.; Chowdhury, P.; Park, J.; Petrich, J. W.; Hargrove, M. S. *Proteins: Struct. Funct. Genet.* **2002**, *46*, 268.

(61)   Kundu, S.; Hargrove, M. S. *Proteins: Struct. Funct. Genet.* **2003**, *50*, 239.

(62)   Jimenez, R.; Fleming, G. R.; Kumar, P. V.; Maroncelli, M. *Nature* **1994**, *369*, 471.

(63)   Li, T.; Hassanali, A. A.; Kao, Y.-T.; Zhong, D.; Singer, S. J. *J. Am. Chem. Soc.* **2007**, *129*, 3376.

(64)   Nilsson, L.; Halle, B. *Proc. Natl. Acad. Sci. U. S. A.* **2005**, *102*, 13867.

(65)   Hassanali, A. A.; Li, T.; Zhong, D.; Singer, S. J. *J. Phys. Chem. B* **2006**, *110*, 10497.

(66)   Zhang, L.; Wang, L.; Kao, Y.; Qiu, W.; Yang, Y.; Okobiah, O.; Zhong, D. *Proc. Natl. Acad. Sci. USA* **2007**, *104*, 18461.

(67)   Chowdhury, P. K.; Halder, M.; Sanders, L.; Calhoun, T.; Anderson, J. L.; Armstrong, D. W.; Song, X.; Petrich, J. W. *J. Phys. Chem. B* **2004**, *108*, 10245.

(68)   Mukherjee, P.; Crank, J. A.; Halder, M.; Armstrong, D. W.; Petrich, J. W. *J. Phys. Chem. A* **2006**, *110*, 10725.

(69)   Fee, R. S.; Maroncelli, M. *Chem. Phys.* **1994**, *183*, 235.

(70)   Headley, L. S.; Mukherjee, P.; Anderson, J. L.; Ding, R.; Halder, M.; Armstrong, D. W.; Song, X.; Petrich, J. W. *J. Phys. Chem. A* **2006**, *110*, 9549.

(71)   Arzhantsev, S.; Ito, N.; Heitz, M.; Maroncelli, M. *Chem. Phys. Lett.* **2003**, *381*, 278.

(72)   Ito, N.; Arzhantsev, S.; Heitz, M.; Maroncelli, M. *J. Phys. Chem. B* **2004**, *108*, 5771.

(73)   Petrich, J. W.; Chang, M. C.; McDonald, D. B.; Fleming, G. R. *J. Am. Chem. Soc.* **1983**, *105*, 3824.

(74)   Petrich, J. W.; Chang, M. C.; Fleming, G. R. *NATO ASI Ser., Ser. A* **1985**, *85*, 77.

(75)   Szabo, A. G.; Rayner, D. M. *J. Am. Chem. Soc.* **1980**, *102*, 554.

(76)   Gustavsson, T.; Cassara, L.; Gulbinas, V.; Gurzadyan, G.; Mialocq, J.-C.; Pommeret, S.; Sorgius, M.; van der Meulen, P. *J. Phys. Chem. A* **1998**, *102*, 4229.

(77)   Jarzeba, W.; Walker, G. C.; Johnson, A. E.; Barbara, P. F. *Chem. Phys.* **1991**, *152*, 57.

(78)   Mukherjee, P.; Crank, J. A.; Sharma, P. S.; Wijeratne, A. B.; Adhikary, R.; Bose, S.; Armstrong, D. W.; Petrich, J. W. *J. Phys. Chem. B* **2008**, *112*, 3390.

(79)   Adhikari, A.; Sahu, K.; Dey, S.; Ghosh, S.; Mandal, U.; Bhattacharyya, K. *J. Phys. Chem. B* **2007**, *111*, 12809.

(80)   Ito, N.; Huang, W.; Richert, R. *J. Phys. Chem. B* **2006**, *110*, 4371.

(81)   Arzhantsev, S.; Jin, H.; Baker, G. A.; Maroncelli, M. *J. Phys. Chem. B* **2007**, *111*, 4978.

(82)   Lakowicz, J. R. *Principles of fluorescence spectroscopy*, 2nd ed.; Springer: New York, 2004.

CHAPTER V. COMPARISON OF DIELECTRIC RESPONSE OBTAINED FROM FLUORESCENCE UPCONVERSION MEASUREMENTS AND MOLECULAR DYNAMICS SIMULATIONS FOR COUMARIN 153 – APOMYOGLOBIN COMPLEXES AND STRUCTURAL ANALYSIS OF THE COMPLEXES BY NMR AND FLUORESCNCE METHODS

A paper published in the *Journal of Physical Chemistry B*

Sayantan Bose[1], Ramkrishna Adhikary[1], Charles A. Barnes[1], D. Bruce Fulton[2],

Mark S. Hargrove[2], Xueyu Song[1], and Jacob W. Petrich [1,]*

Abstract

We present a comparison of the dielectric response obtained from fluorescence upconversion experiments and from molecular dynamics simulations of the complexes of coumarin 153 with five apomyoglobins (apoMbs): wild-type horse heart (HH-WT) and those of wild-type sperm whale (SW-WT); its two triple mutants, L29F/H64Q/V68F and H64L/V68F/P88A; and its double mutant, L29F/V68L. Comparisons between experimental and simulated solvation relaxation functions, $C(t)$s, for the wild-type proteins range from very good to excellent. For the three mutants we investigated, however, agreement between

experiment and simulation was considerably inferior. Thus, an NMR study of the complex of the HH-WT complex apoMb; and fluorescence energy transfer and anisotropy studies of the five complexes were performed to investigate the structures upon which the simulations were based. The NMR measurements confirm our earlier conclusions that the C153 lies in the heme pocket of the HH-WT apoMb. For the wild-type complexes, fluorescence energy transfer measurements provide two rise times, suggesting a definite spatial relationship between the two Trp donors and the C153 acceptor. These results confirm the structural integrity of the wild-type complexes and validate the initial structures used for the molecular dynamics simulations. On the other hand, the three mutants provided single exponential rise times for energy transfer, suggesting that the position of the C153 used in the simulations may have been in error or that the C153 is mobile on the time scale of the energy transfer experiment. Fluorescence anisotropy studies also suggest that the double mutant was not structurally intact. Furthermore, examination of these systems demonstrates the sensitivity of C153 to its environment and permits the observation of differences in the heme pockets. These results point to the importance of structural characterization of modified proteins used in studies of the dielectric response and suggest strategies for performing molecular dynamics simulations of modified proteins.

Introduction

The study of solvation dynamics is a powerful tool for understanding the dielectric relaxation of solvating media. For homogeneous dielectric fluids, solvation dynamics can be described by linear response theory. [1-12] A simple dielectric continuum theory[13-15] adequately describes their dielectric response, which led to several successful comparisons between theory and experiments. [11,12,16,17] However, for inhomogeneous dielectric materials, such as

proteins, dielectric fluctuations are severely restricted due to the inherent constraints of the materials. The delicate balance in the electrostatic interactions play important role to control structure, function and dynamics in proteins.[18-22] The nature of the interactions is heterogeneous because the charged and polar groups in protein can interact over long distances with each other and surrounding solvent molecules. A large protein can have its dielectric response vary from place to place. [23-29] A sudden change in the charge distribution for many elementary processes such as electron and energy transfer in a protein causes dielectric relaxation due to the adjustment of its structure in response to the new charge distribution. Traditional dielectric continuum theory assumes that there is only one intrinsic microscopic length scale. Hence, such theory is questionable when applied to inhomogeneous dielectric materials. As a result understanding the dielectric response in proteins is very challenging due to the existence of different length scales of relaxation.

In a series of papers, [30-33] we have discussed the extensive literature on this topic and have suggested the utility of using the fluorescent probe, coumarin 153 (C153), to study the dielectric response of monomeric hemoglobins, such as myoglobin. The choice of C153 was in large part inspired by the work of Cocco and Lecomte who characterized the complex of the fluorescent dye ANS (Figure V.1a) with apomyoglobin (apoMb) using nuclear magnetic resonance (NMR) spectroscopy and proved that ANS resides in the distal side of the heme pocket.[34] Using 2D- DQF-COSY and NOESY experiments, they showed that the H_a and H_b protons of ANS have cross peaks with heme pocket residues such as His64, Val67, Val68, and Ala71.
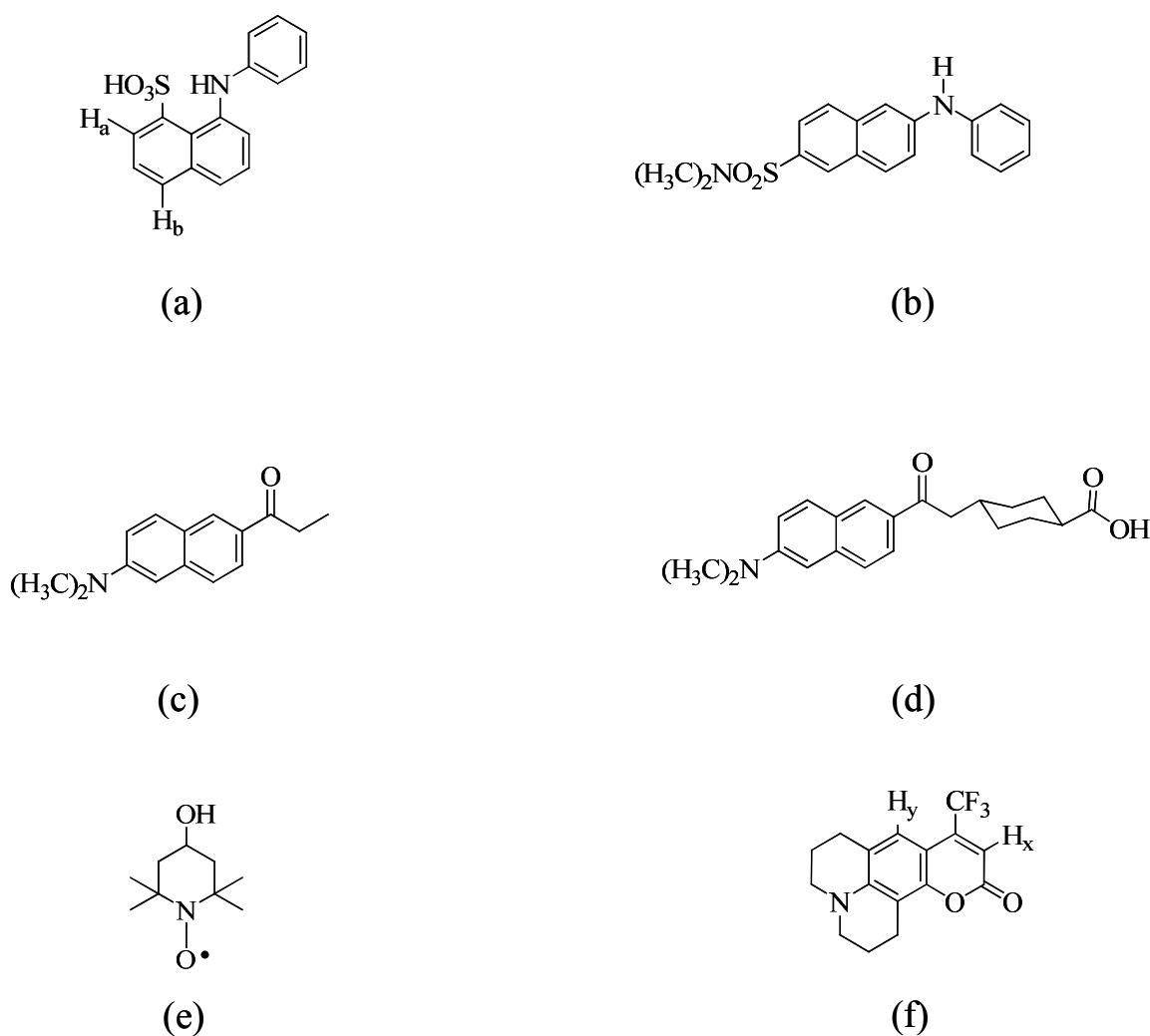
Figure V.1. Structures of different probes discussed here. (a) 8-anilino-1-naphthalenesulfonic acid (ANS), (b) 2-anilino-6-N,N-dimethylnaphthalenesulfonamide (ANSDMA), (c) 6-Propionyl-2-(N,N-dimethylamino)naphthalene (PRODAN), (d) 2′-(N,N-dimethylamino)-6-naphthoyl-4-trans-cyclohexanoic acid (DANCA), (e) 4-hydroxy-2,2,6,6-tetramethylpiperidine 1-oxy (TEMPOL) and (f) Coumarin 153 (C153).

We, thus, initially, considered the probe ANS, [34] for which there is a structure of its complex with apoMb. This probe is not, however, ideal because its absorption spectrum is complicated by overlapping electronic states.[35] Even if internal conversion from higher-lying states to the lower fluorescent state is faster than solvation dynamics, as has been suggested

to be the case in Trp,[36-39] an accurate determination of the reorganization energy[40,41] based on the steady-state spectra becomes very difficult. In addition, while ANS[34,42] as well as other chromophores such as PRODAN[43], DANCA,[44] and ANSDMA[45] (Figure V.1b-d) may bind to the heme pocket of apoMb, they are also capable of charge transfer in the excited state, which could complicate the interpretation of the fluorescence upconversion results. [46]

On the other hand, C153 is exquisitely inert, structurally rigid, and is also associated with a large change of dipole moment upon optical excitation. This is why it is has been so extensively employed as a probe of solvation dynamics.[30-33,47-59] We consequently opted for C153 as a probe for studying the dielectric response of proteins. Elsewhere, we have shown using Job's plot experiments that C153 binds to apoMb with a 1:1 stoichiometry with $K_D \cong$ 6×10^{-6} M.[30,31] The ANS-apoMb complex is reported to have $K_D \cong 3 \times 10^{-6}$ M.[42] The anisotropy decay time (τ_{rot}) of C153 when bound to apoMb is 9.2 ns,[30] which is consistent with the slow rotational correlation time of apoMb,[60] whereas free C153 exhibits a very fast depolarization time of ~100 ps in bulk solvent.[30] More significantly, the anisotropy decay of bound C153 was single-exponential, which supports rigid binding of coumarin in the heme pocket; because single-exponential decay would not be expected for a surface bound chromophore.[61,62]

These findings, suggesting that a 1:1, well-defined complex of C153 and apoMb could be formed, authorized us to perform a comparison of the solvation correlation functions (dielectric responses) obtained from fluorescence upconversion experiments and molecular dynamics simulations[32] of C153 with wild-type horse heart (HH-WT) apoMb and with apoleghemoglobin (apoLba). This comparison provided excellent agreement between experiment and theory and emboldened us to perform the similar set of comparisons

presented here for the complexes of C153 with four apoMbs: those of wild-type sperm whale (SW-WT); its two triple mutants, L29F/H64Q/V68F and H64L/V68F/P88A; and its double mutant, L29F/V68L. All of these mutant proteins do bind heme and fold to form stable holoproteins. Mutations at each position have various effects on the oxygen binding properties of the holoprotein, and have various effects on the stability of the apoprotein. For example, mutations of HisE7 to an apolar side chain lower oxygen affinity in the holoprotein, and increase stability to denaturation. The effects of mutations at other positions are generally milder. In general, when a polar side chain is introduced into the heme pocket, the resulting mutant apoprotein is less stable.

The intent of this comparison is to initiate a detailed study of the effects of individual amino acids on the dielectric response with the ultimate goal of developing a new type of model for the response.[63] The basic philosophy behind such a model is to account for the dielectric inhomogeneity of a protein without full atomistic details. Our previous results have indicated that a model based on the polarizabilities at the residue level can offer a universal description for proteins' dielectric response.

Despite the encouraging, initial success on this path obtained with the horse heart system, the results for the sperm whale system revealed themselves to be more complicated. Although the agreement between experiment and theory was excellent for the SW-WT, the agreement varied for the mutants. Our previous work suggests no reason to attribute such disagreement to the force fields used in the simulation but rather to question the structure of the complex used as the starting point for the simulation. Thus, *un esprit critique* requires that painstaking attention be paid to structural details when comparisons are being made

between theory and experiment for different proteins and, in particular, the same proteins with slight modifications.

Our work presents, in outline:

1. a comparison of the dielectric response obtained from fluorescence upconversion experiments and from molecular dynamics simulations of the complexes of coumarin 153 with five apoMbs (apoMbs): wild-type horse heart (HH-WT) and those of wild-type sperm whale (SW-WT); its two triple mutants, L29F/H64Q/V68F and H64L/V68F/P88A; and its double mutant, L29F/V68L;

2. an NMR study of the complex of C153 with HH-WT apoMb (we have used equine myoglobin, because it contains more resolved lines (especially from histidines) compared to the SW-WT [64]);

3. fluorescence energy transfer and anisotropy studies of the five complexes to complement the NMR studies.

We believe that this is the most thorough structural characterization to date of any system, whether it be based on nonnatural fluorescence probes or mutants, employed for the investigation of the dielectric response of proteins.

Materials and Methods

Coumarin 153 (C153) was purchased from Exciton Inc. (Dayton, OH) and used without further purification. 4-hydroxy-2,2,6,6- tetramethylpiperidinyl-1-oxy (TEMPOL) (Figure V.1e), deuterated water (D_2O), dimethylsulfoxide (DMSO-d_6) and methanol (HPLC grade) from Aldrich was used without further purification. Equine myoglobin (Mb) was purchased from Sigma. Recombinant sperm whale myoglobins and its mutants were constructed, expressed, and purified as described elsewhere.[65,66]

Sample Preparation for NMR experiments   Apoproteins were prepared using a method described elsewhere.[32,67]   Protein concentrations were kept between ~ 1.5–2.0 mM for the NMR experiments. Because C153 is sparingly soluble in water, a stock solution of 40 mM was prepared in DMSO-d_6 and then added to the apoMb, keeping the stoichiometry 1:1. The solution was shaken for an hour and then dialyzed against 5 L pH 7.0 buffer overnight at 4°C. The solution was then centrifuged and concentrated using Centricon-3 (Amicon) to 0.5 mL, and the process was repeated four times by adding D_2O for deuterium exchange. The protein samples were stored at –20°C without lyophilization. A 0.05 M TEMPOL solution was prepared in D_2O and the appropriate microliter volume was added to a 500 μL protein solution and was equilibrated overnight at 4°C before doing the NMR experiments.

Sample preparation for Fluorescence Measurements. Concentrations of 1:1 C153/apoMb complexes were maintained from 5.0×10^{-6} to 80×10^{-6} M by adding microliter amounts of 20×10^{-3} M C153/MeOH to pH 7.0 buffer, keeping the organic content < 0.3 % (v/v) in the final sample for all the steady-state and lifetime measurements. The resulting solution was sonicated. For fluorescence upconversion experiments a stock solution of C153/MeOH was added to 1.2 ml of ~ 1.0×10^{-3} M apoprotein solution, keeping the organic content < 3 % (v/v) in the final solution with 1:1 protein to C153 ratio. The concentrations of the apoproteins were determined spectrophotometrically using an extinction coefficient of 15.2 mM^{-1}cm^{-1} at 280 nm.[30] All samples were equilibrated overnight at 4°C before making the steady-state or time-resolved measurements.

NMR Experiments.   NMR spectra were recorded at a sample temperature of 25 °C using a Bruker Avance 700 spectrometer operating at a ^{1}H frequency of 700.13 MHz and equipped

with a 5-mm H/C/N cryoprobe. Experiments were done in pure deuterated solvents in standard 5 mm NMR tubes (Wilmad). 1D ^{1}H and 2D ^{1}H-^{1}H NOESY spectra were acquired using standard experimental protocols. Very weak solvent saturation (B_1 power of 5 Hz) was used during recycling delays and the NOESY mixing time to suppress the residual HOD signal. For 1D spectra, 8 scans were accumulated with a sweep width of 25252 Hz (36 ppm). For NOESY spectra 400 time increments each consisting of 80 scans were acquired with a sweep width in both dimensions of 9803 Hz (14 ppm). The NOESY mixing time was 150 ms.

Steady-state Measurements. Steady-state absorption spectra were obtained on a Hewlett-Packard 8453 UV-visible spectrophotometer with 1-nm resolution. Steady-state fluorescence spectra were obtained on a Spex Fluoromax-4 with a 2-nm bandpass and corrected for lamp spectral intensity and detector response. For absorption and fluorescence measurements, a 3-mm path-length quartz cuvette was used. The steady-state spectra can be used to compute the reorganization energy, λ[68]

$$\lambda = \hbar \frac{\int_0^\infty d\nu [\sigma_a(\nu) - \sigma_f(\nu)]\nu}{\int_0^\infty d\nu [\sigma_a(\nu) + \sigma_f(\nu)]} \tag{V.1}$$

The $\sigma_{a,f}$ are the absorption (or excitation) and emission spectral line-shapes, respectively. $\lambda(\infty)$ represents the total stokes-shift, which is calculated using the steady-state excitation, ν_{ex}, and emission, $\nu(\infty)$, spectra. On the other hand, $\lambda("0")$, which is the measure of intramolecular contribution and not solvent relaxation, is computed using steady-state excitation (ν_{ex}) and calculated "zero-time" spectra, $\nu("0")$. These values are collated in Table V.3.

Time-resolved Measurements. Lifetime measurements were made using the time-correlated single-photon counting (TCSPC) apparatus described elsewhere.[33,41] The data were acquired in 1024 channels with a time window of 3.33 ns. The instrument response function had a full width at half-maximum (FWHM) of ~40 ps. A 3-mm path-length quartz cuvette was used for all the time-resolved measurements. Fluorescence decays were collected at the magic angle (polarization of 54.7°) with respect to the vertical excitation light at 266 nm, with ~ 40000 counts in the peak channel. To obtain the rotational dynamics of C153, samples were excited at 407 nm and emission was collected parallel and perpendicular to the polarization of the excitation light. Anisotropy data were aquired in 1024 channels with a time window of 22 ns collecting 65530 counts in the peak channel. The fluorescence upconversion measurements were done with the apparatus described elsewhere. [41] The instrument response function had a full width at half-maximum (FWHM) of 300 fs. A rotating sample cell was used. To construct the time-resolved spectra from upconversion measurements, a series of decays were collected, typically from 480 nm to 560 nm at 10-nm intervals, in a time window of 10 ps. The wavelength-resolved fluorescence transients were fit to sums of exponentials (typically 2 or 3, as necessary to fit the data), and time-resolved emission spectra (TRES) were reconstructed as described elsewhere. [33,41]

We have employed the traditional approach of fitting the time-resolved emission spectra to a log-normal function [41,47,69], from which we extract the peak frequency $\nu(t)$ as a function of time. We describe the solvation dynamics by the following normalized correlation function:

$$C(t) = \frac{v(t) - v(\infty)}{v("0") - v(\infty)} \quad . \tag{V.2}$$

Because *C(t)* is a *normalized* function, the accurate determination of *C(t)* depends upon accurate values for $v("0")$ and $v(\infty)$. $v("0")$ is the frequency at zero-time, estimated using the method of Fee and Maroncelli [70], who have described a robust, model independent, and simple procedure for generating this "zero-time" spectrum, $v("0")$. We have checked its validity using a different method for estimating the "zero-time" reorganization energy[68]. $v(\infty)$ is (usually[71,72]) the frequency at infinite time, obtained from the maximum of the steady state spectrum. (This is not, however, true in the case of very slowly relaxing solvents, as has been demonstrated in the case of certain ionic liquids [71-73]: where the emission spectrum at ~3 times the fluorescence lifetime of the probe is *red-shifted* to that of the equilibrium spectrum.) The $v(t)$s are determined from the maxima of the log-normal fits of the TRES. In most of cases, however, the spectra are broad, so there is some uncertainty in the exact position of the emission maxima. Thus, we have considered the range of the raw data points in the neighborhood of the maximum to estimate an error for the maximum obtained from the log-normal fit. Depending on the width of the spectrum (i.e., "zero-time", steady-state, or time-resolved emission spectrum), we have determined the typical uncertainties as follows: "zero-time" ~ steady-state (~ $\pm$ 100 cm^{-1}) < time-resolved emission (~ $\pm$ 200 cm^{-1}). We use these uncertainties to compute error bars for the *C(t)*. Finally, in generating the *C(t)*, the first point was obtained from the "zero-time" spectrum. The second point was taken at the maximum of the instrument response function. Fractional solvation at 300 fs is given by f_{300fs} = 1 − *C (t = 300 fs)*.

Recently, we provided an analysis [33] of various methods of constructing $C(t)$ and reviewed selected examples from the literature.[36-38,74-79] We demonstrated that it is possible to exaggerate the amplitudes of slower solvation phenomenon that may be attributed to "biological water", water-protein interactions, or the protein itself.

Molecular Dynamics Simulations. The starting configurations of sperm whale myoglobin (SW-WT) are from the protein DATA BANK (PDB id 1VXD) and with TIP3P water models. To have a reasonable starting point for the C153-protein complex the heme is replaced by C153 and then energy minimization is used to obtain the starting configuration of the C153/apoMb complex. Standard constant pressure-temperature MD was performed using the ORAC package[80] with the Amber force field. [81] In all simulations, short-range non-bonded interactions were calculated up to a 10 Å cutoff, whereas long-range electrostatic interactions were treated by the SPME method using a very fine grid, 128 points per axis, with periodic boundary conditions, and Ewald convergence parameter of 0.43 Å^{-1}. Three different Nosé-Hoover thermostats were coupled to solute, solvent, and total center of mass. An external pressure of 0.1 MPa was applied all along the trajectory. A five time-step rRESPA [37] algorithm with times of 0.5-1.0-2.0-4.0-12.0 fs was used with bond constraints on hydrogen covalent bonds handled by a Shake-Rattle-like algorithm. The final system was first equilibrated with velocity rescaling for 60 ps at 50 K and 80 ps at 300 K. Following this initial equilibration, we ran the system for one additional nanosecond at constant temperature (T = 300 K) and pressure (P = 0.1 MPa). To achieve full relaxation, the simulation box was entirely flexible for the first 300 ps, whereas for the remainder of the run, only isotropic changes of the box were allowed. [35] Finally, the system was simulated for an additional 10 ns. As we have demonstrated in our previous work, [30] an equilibrium configuration for C153 in

the heme pocket of the protein can be found and experimental measurements seem to support our interpretation. Using the equilibrated configuration, additional 12-ns trajectories are generated and are used for the calculation of solvation correlations functions for horse heart apoMb complexes; and 30-ns trajectories are used for the corresponding calculations for the sperm whale apoMb complexes.
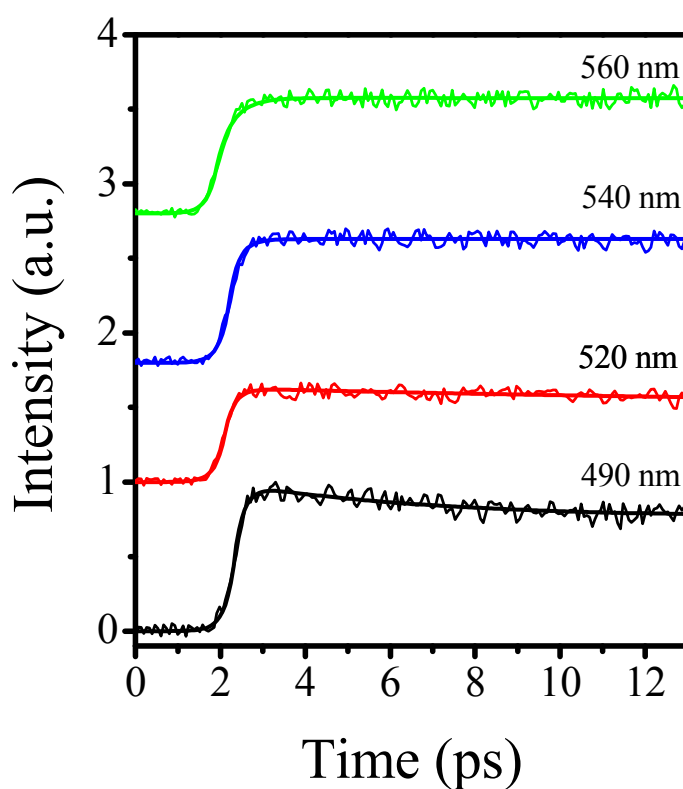

Figure V.2. Representative fluorescence upconversion traces obtained for C153 in H64L/V68F/P88A apoMb mutant at the indicated wavelengths. The decay at blue end of the spectrum decays faster than that of at the red end of the spectrum. The decay at the red end of the spectrum shows a growing component. The decays used to construct the time-resolved emission spectra were typically collected over a range of wavelengths from 480 to 560 nm at 10-nm intervals, a total of nine decays were used to generate the time-resolved emission spectra, from which the $C(t)$ values were calculated.

Using the charges of C153 in the ground and excited states,[12] the solvation correlation function can be obtained within the linear response theory[82] as

$$C(t) = \frac{<\delta\Delta E(t)\delta\Delta E(0)>}{<\delta\Delta E(0)\delta\Delta E(0)>} \tag{V.3}$$

where $\delta\Delta E(t) = \Delta E(t) - <\Delta E(t)>$ and $\Delta E(t)$ is the interaction energy difference between C153 in its excited state and ground state with surrounding protein and water molecules at time t. The symbol $<\cdots>$ denotes the ensemble average in the simulation. The reorganization energy λ is calculated using $\lambda = <(\delta\Delta E)^2>/2k_B T$. For the simulations of the mutants, the residues of the equilibrated WT-apoMb/C153 complex are mutated to the desired amino acids starting from the equilibrated wild type and C153 complex structure. Then, an energy minimization and 1-ns equilibration run is performed. Using the equilibrated configuration, additional 30-ns trajectories are generated and are used for the calculation of solvation correlations functions and the reorganization energies.

Results and Discussions

Dielectric Relaxation of the ApoMb Complexes

Representative wavelength-resolved decay traces of C153/apoMb complexes are presented in Figure V.2. The solvation correlation function, *C*(*t*), obtained from spectral reconstruction from fluorescence unpconversion traces and from molecular dynamics simulations for C153 in HH-WT and SW-WT apoMbs and its mutants using eq 2 and 3 are given in Figure V.3 and V.4. There is remarkable agreement between the *C*(*t*)s from fluorescence upconversion experiments and those obtained from molecular dynamics simulations in the SW-WT apoMb, but deviations were observed in the mutants. The time constants for the dielectric relaxation in all the systems are collated in Table V.1. For all the

apoMb complexes studied here, the experimentally obtained solvation response was best fit to two decaying exponentials, with a significant (~60%) (Table V.1) response being completed within the time resolution of our experimental apparatus (~300fs) succeeded by a slower response, which is also consistent with the MD results. This ultrafast relaxation suggests that water is playing a dominant role, which is consistent with the report by Fleming and coworkers [40] that solvation in the lysozyme/eosin system is dominated by water. (Solvation in bulk water is characterized largely by an ~30-fs component and is complete in ~15 ps. [17,83]) The remainder of the solvation can be attributed to motions of the protein matrix or coupled protein-water [84] motions. The protein's contribution to solvation should not be neglected. For example, Nilsson and Halle have simulated the Stokes shift in the protein monellin [85] and have discussed how to separate the relative contributions of protein and water. They find a significant protein component, at least 25%. Li et al. [84] find that the relative protein and water contributions can vary substantially with the conformational substate of myoglobin: sometimes the protein contribution can even be larger than water. Both Nilsson and Halle [85] and Li et al. [84] find that the protein contribution also has an ultrafast component.   In general, there will always be some slow relaxation due to the conformational motions of proteins. In our case, the structures of C153/wild type complexes obtained from NMR and FRET measurements are consistent with those obtained from simulations. For the mutants, the structures of the C153 complexes used in the simulations are not that certain, as indicated by the comparison with the experimental evidence. This may be the reason for less satisfactory agreements between the $C(t)$s.

TABLE V.1. C(t) parameters obtained from upconversion experiments and MD simulations [a]

System		f_{300fs}	a_1	τ_1 (ps)	a_2	τ_2 (ps)	a_3	τ_3 (ps)	$<\tau_{solv}>$ (ps)
HH-WT	Expt.	0.64	0.59	0.02	0.41	3.4			1.4
	Simul.		0.73	0.14	0.27	9.3			2.6
SW-WT	Expt.	0.61	0.69	0.14	0.31	15.2			4.8
	Simul.		0.53	0.07	0.18	1.16	0.29	15.0	4.7
L29F/H64Q/V68F	Expt.	0.56	0.61	0.12	0.39	15.4			6.1
	Simul.		0.47	0.07	0.17	1.6	0.34	28.0	10.3
H64L/V68F/P88A	Expt.	0.64	0.68	0.12	0.32	5.5			1.8
	Simul.		0.43	0.06	0.18	1.0	0.39	40.0	15.8
L29F/V68L	Expt.	0.60	0.60	0.10	0.40	3.8			1.6
	Simul.		0.38	0.06	0.16	1.1	0.46	52.0	23.2

[a] Results from experiments and simulations are fit to a sum of exponentials. That three exponentials are used to fit the results from simulations and only two, those from experiments, is a consequence of the error bars for the experimental results being larger than those for the data points resulting from the simulations.

Another example of agreement between experiment and theory that has emerged in the study of solvation dynamics of proteins is the recent work by Boxer and coworkers [86] and by Golosov and Karplus .[87] In our previous reports[32] on solvation dynamics in HH-WT apoMb and apoLba (where the heme pockets differs significantly[88,89]), we have also found excellent agreement between the C(t) obtained from both experiments and molecular

dynamics simulations. It is significant that the only difference between the heme pockets of the two WT Mbs is that Val67 in HH is replaced by Thr in SW. A close comparison of the $C(t)$s for these two systems indicates small but significant differences that must arise from this single amino acid substitution (Figure V.3).
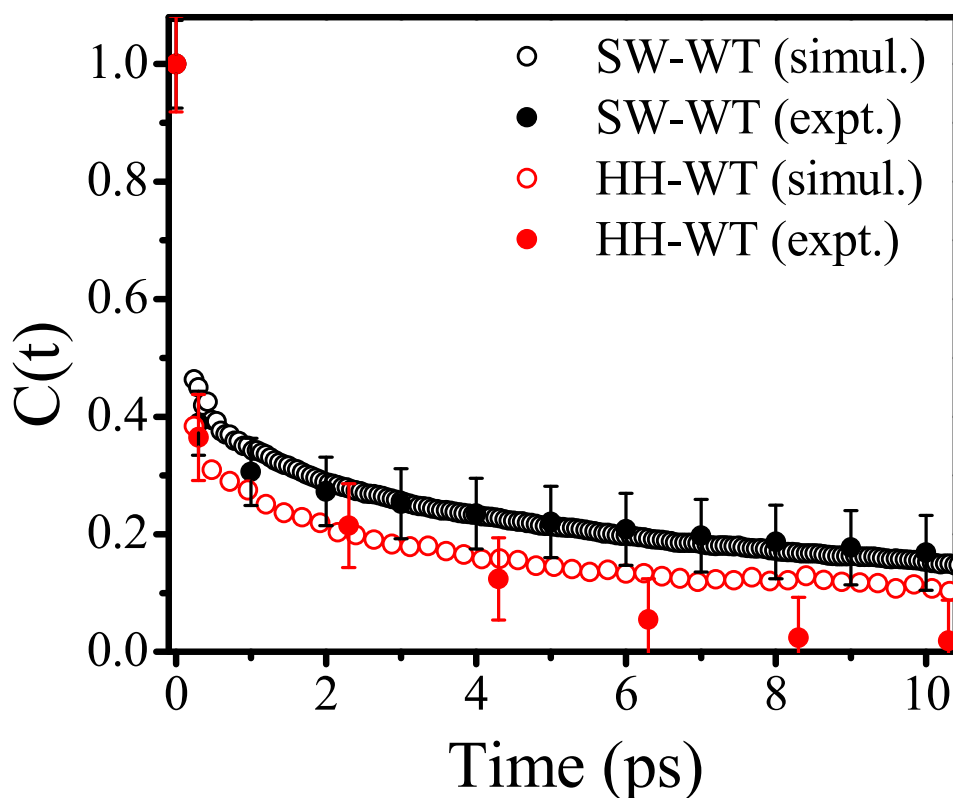

Figure V. 3. Comparison of $C(t)$ for C153 in wild type sperm whale and horse heart apoMb obtained from fluorescence upconversion experiments with those from molecular dynamics simulations. In both proteins, the initial fast component occurs within the time resolution of our instrument. There is a remarkable agreement between experiment and theory for both the wild type apoproteins. There is only one change between the heme pockets of the horse heart and sperm whale myoglobins: Val67 in HH is replaced by Thr in SW.
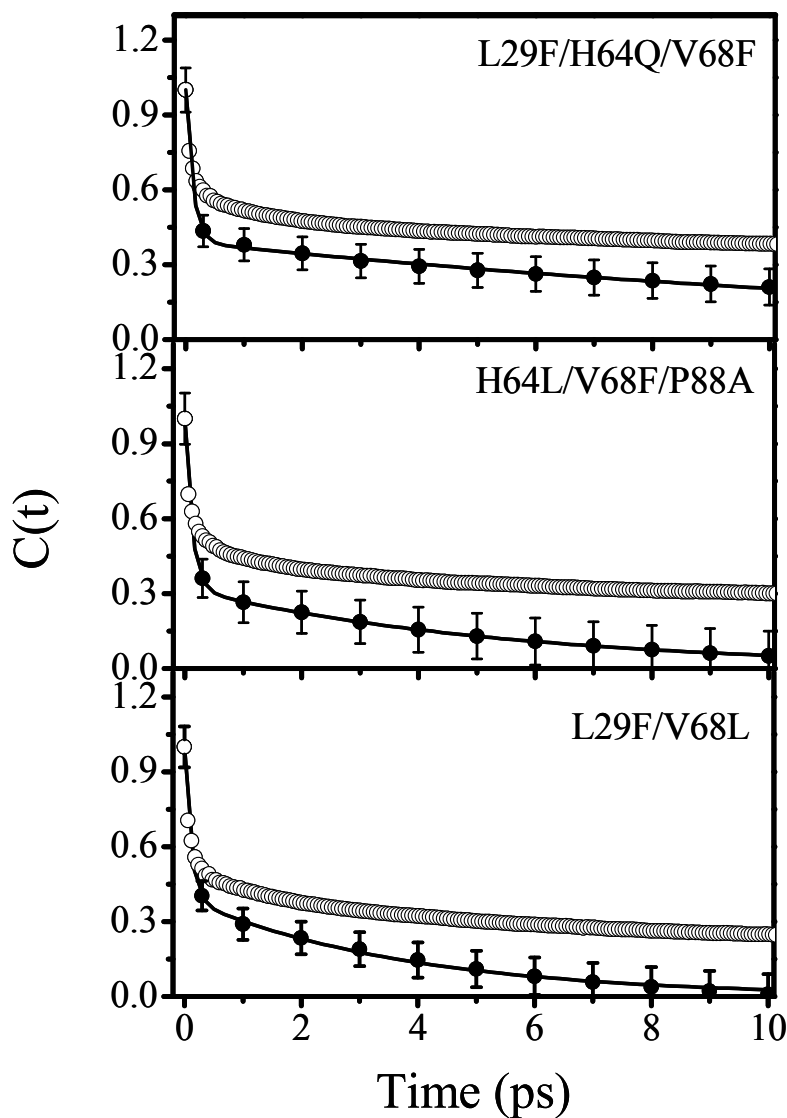
Figure V.4. Comparison of solvation correlation functions, *C*(*t*) for C153 in sperm whale apoMb mutants obtained from fluorescence upconversion experiments (closed circles) with those obtained from molecular dynamics simulations (open circles). *C*(*t*)s from experiments and simulations were calculated using eqs 2 and 3 respectively, and were fitted with a sum of two and three exponentials respectively.

The sensitivity of C153 to its local environment is also reflected by the reorganization

energies for each of the C153/apoMb complexes. The reorganization energies differed not

only between the WT and its mutants, but also between the two WT apoMbs (sperm whale and horse heart, Table V.3). The solvation response is thus critically dependent on the environment that the probe (C153) experiences inside the heme pocket.

While there is very good agreement between experiment and simulation for the wild-types proteins, the agreement for the mutant proteins is much less satisfactory. The origin of this discrepancy for the mutants may be found by means of the structural studies of the complexes that we now discuss.
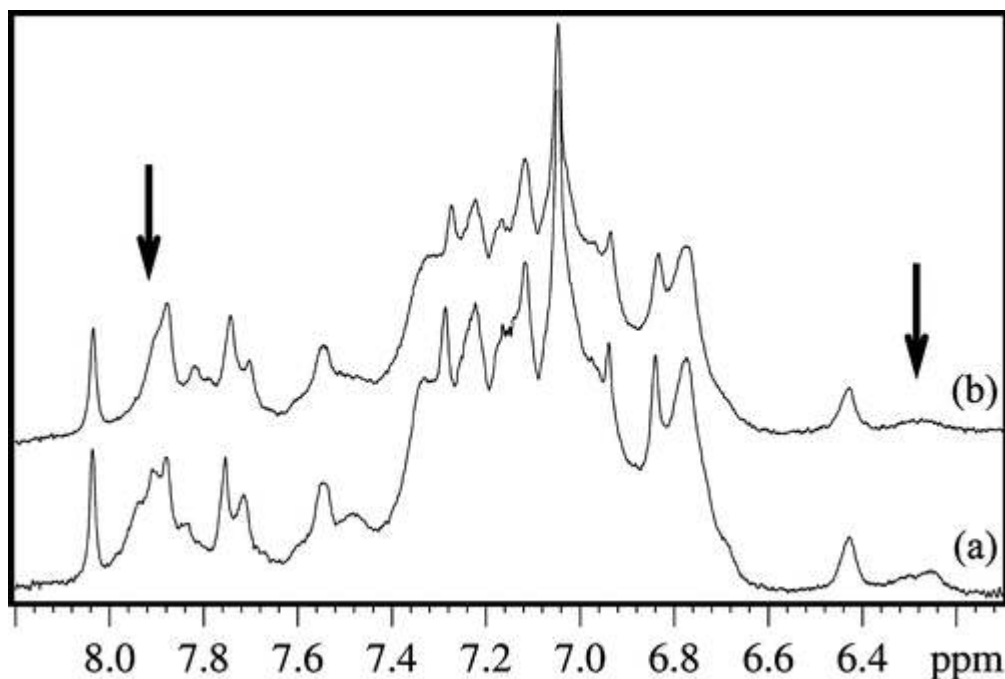

Figure V.5. Representative 1D, ^{1}H-NMR spectra of (a) equine apoMb and (b) its complex with 2 equivalents of TEMPOL in D$_2$O at 298 K and pH 7.0. Addition of TEMPOL selectively broadens signals (indicated by arrows) from C$^\varepsilon$ H of His64 and C$^\zeta$ H of Phe33 in the heme pocket, which confirms that the paramagnetic dye binds to the distal side of the pocket
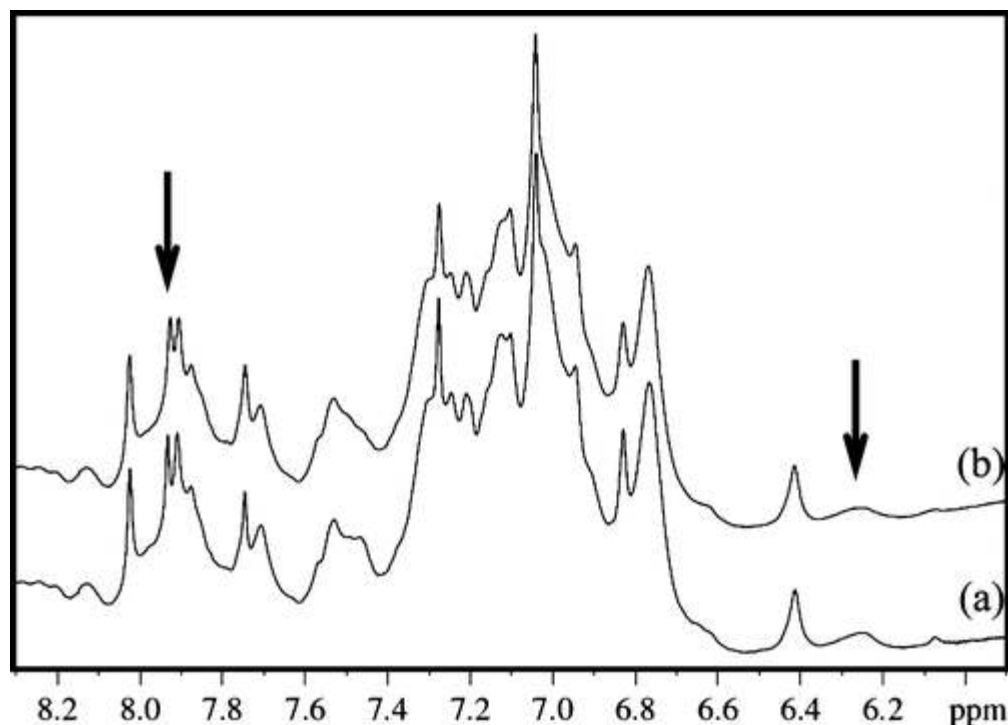
Figure V.6. Representative 1D ^{1}H-NMR spectra of (a) the 1:1 complex of C153/equine apoMb. A new peak at 6.04 ppm arises due to the proton (H_x, Figure V.1f) adjacent to the carbonyl carbon in C153; (b) the complex of C153/equine apoMb with two equivalents of TEMPOL in D$_2$O at 298 K and pH 7.0. There is no perturbation in either the His64 or the Phe33 signals (indicated by arrows) as was seen in Figure V.5. The two spectra 'a' and 'b' are almost identical, which indicates that coumarin occupies the heme pocket and prohibits the entry of TEMPOL.

Structural Characterization of the Complex of C153 and HH – WT ApoMb by NMR

One-dimensional ^{1}H-NMR spectra of HH-WT apoMb and of the complex of two equivalents of the paramagnetic dye, TEMPOL (Figure V.1e), with one equivalent of apoMb in D$_2$O are shown in Figure V.5. Although the overall spectral characteristics remain similar, specific signals are perturbed upon addition of TEMPOL. In particular, the peak at 7.91 ppm arising from C$^\varepsilon$H of His64 in the E7-helix is broadened upon insertion of TEMPOL. Also the peak due to C$^\zeta$H of Phe33 is broadened, which is consistent with the reports of Cocco

and Lecomte.[34]   Excess addition of TEMPOL, beyond two equivalents, was avoided to prevent attenuation of other signals by through-space relaxation.
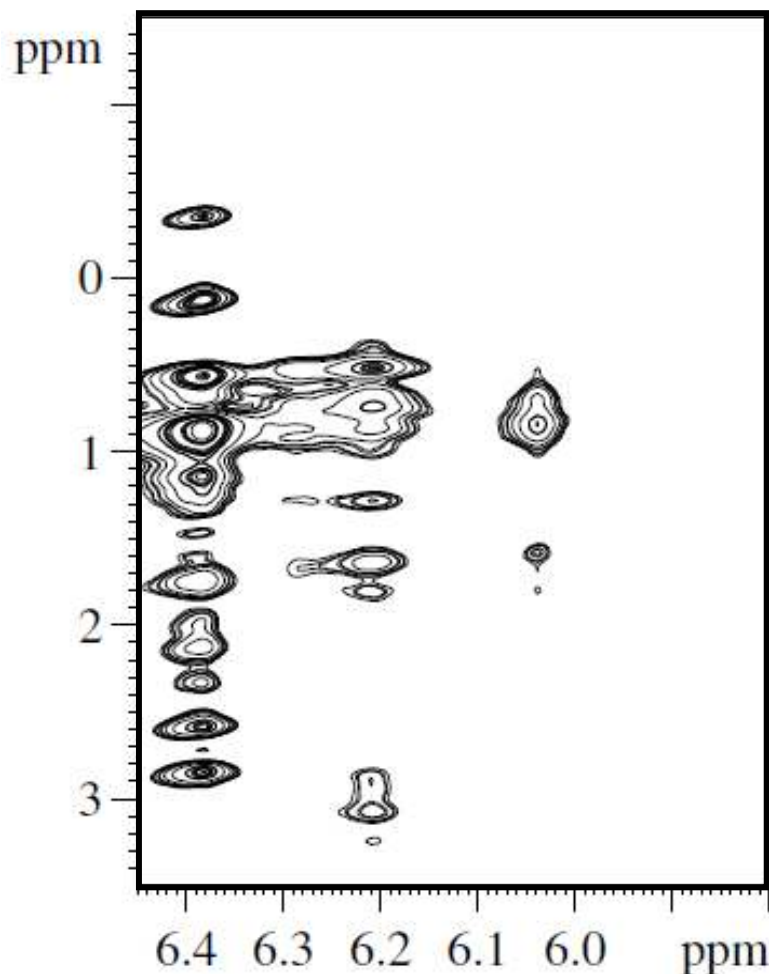
Figure V.7. NOESY spectrum of C153/apoMb complex in D_2O at 298 K and pH 7.0. The resonance at 6.04 ppm arises from H_x C153, and the cross peaks arise from Val67 and Ala 71. Other weaker cross peaks are unidentified. The assigned cross peaks show that C153 is in the distal side of the heme pocket, constituted by Leu29, His64, Val67, Val68, and Ala71.

When, however, C153 is added to apoMb, several signals are seen to have sharpened and shifted as seen in Figure V.6a, which indicates a decreased rate of backbone amide exchange and a change in the population of various conformers. A new peak at 6.04 ppm arises in the C153-apoMb spectrum due to the proton (H_x, Figure V.1f) adjacent to the

carbonyl carbon in C153. Other signals from coumarin could not be resolved due to their overlap with other signals from the apoprotein residues.

When TEMPOL was added to the C153/apoMb complex, no changes in the signals from pocket residues, such as His64 and Phe33 were observed as was the case when adding TEMPOL to apoMb (Figure V.6b). The peak at 7.45 ppm is considerably broadened on addition of TEMPOL in both cases (with and without C153) showing that it arises from a solvent exposed residue. These observations collectively suggest that C153 provides certain rigidity to the flexible structure of the apoprotein and thus prevents TEMPOL from diffusing inside the heme pocket. This is consistent with our circular dichroism results reported elsewhere[30] which showed that addition of C153 helps to regain some of the secondary structure present in the native holo form of myoglobin.

Based on the assignments of Lecomte[34,64,90-95] and coworkers, we have assigned selected NOEs from the heme pocket residues in the 2D NMR spectra. Comparing the spectra of apoMb with that of the C153/apoMb complex, new cross peaks can be interpreted as follows (Figure V.7). The resonance at 6.04 ppm arises from the proton (H_x, Figure V.1f) adjacent to the carbonyl carbon in C153, which has cross peaks with methyl protons of Val67 and also with those of Ala71. The peak at 7.93 ppm from C^ε H of His64 is sharpened and slightly shifted downfield on addition of C153. His64 shows strong NOEs with methyl protons of Val67 and Leu29 at 0.89 and 1.70 ppm, respectively. C153 selectively perturbed the residues on the distal side of the heme pocket. A complete characterization of the apoMb structure is very difficult owing to its large size, partial unfolding, and exchange among different conformations. Chemical shifts, internuclear distances, NOEs, and dihedral angles are inadequate to provide correlation between various motions and interchanging

conformations, because although the global unfolding of the apoprotein is cooperative, the local motions, like folding-unfolding processes occurs independently.[64,94,95] Moreover chemical shift degeneracy of various protons hinder the assignments of peaks in the NMR spectra.
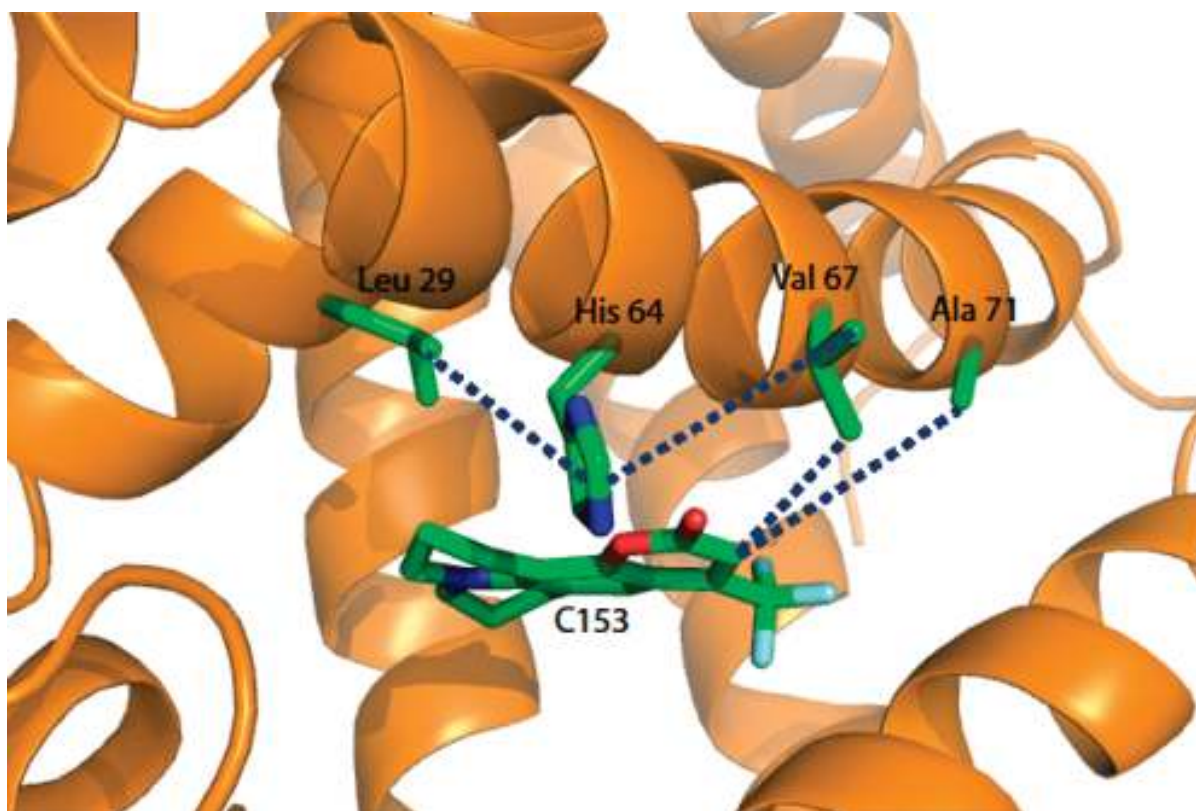
Figure V.8. Representative diagram of apoMb, constructed by the removal of the heme from wild-type equine holo myoglobin (1WLA.pdb), showing the interactions of C153 proton with Val67 and Ala71, along with other selective interactions among the distal residues such as His64–Leu29 and His64–Val67 as obtained from NMR studies.

Based on the above 1D- and 2D-NMR results, a tentative location of C153 can be obtained. Considering the NOEs of coumarin with the pocket residues and inter-residue interactions, it can be confirmed that the fluorescent dye (C153) occupies the distal side of the heme pocket, similar to the case of ANS, as shown in Figure V.8, which illustrates the approximate distances and location of C153 with respect to the distal heme pocket residues.

The H_x proton of C153 is < 5 Å from the methyl residues of Val67 and Ala71. Accurate determination of inter-proton distances using the NOE cross peak intensity is unreliable[95] because of the rapid to intermediate time scales of exchange among the related conformations within the apoprotein.

TABLE V.2. Summary of Results for C153/apoMbs[a]

System	Anisotropy[b]		Lifetime[c,d]					
	r(0)	τ_{rot} (ns)	a_1	τ_1 (ns)	a_2	τ_2 (ns)	a_3	τ_3 (ns)
HH WT	0.29	9.2	1.0	5.1	-0.13	0.2	-0.23	0.5
SW WT	0.32	10.5	1.0	5.0	-0.18	0.42	-0.22	0.1
L29F/H64Q/V68F	0.32	10.2	1.0	5.0	-0.18	0.25		
H64L/V68F/P88A	0.28	10.0	1.0	7.3	-0.33	0.17		
L29F/V68L	0.18	>20.0	0.84	5.5	0.16	0.84	-0.27	0.25

[a] All experiments were repeated at least three times.

[b] Error bars for r(0) and τ_{rot} are within 3-5%. The fluorescence anisotropy is measured by probing the C153: λ_{ex} = 407 nm; $\lambda_{em} \geq$ 500 nm.

[c] Lifetime experiments were done at λ_{ex} = 266 nm, $\lambda_{em} \geq$ 500 nm and components varied within a range of 10%.

[d] Components with negative amplitude refer to the growth in the fluorescence decay traces of C153 observed at 266 nm excitation in all the apoMb complexes, which was completely absent using 407 nm excitation. The rise time can originate only from the acceptor (C153) emission and indicates energy transfer from Trp to C153. The decay time constants are associated with positive amplitudes.
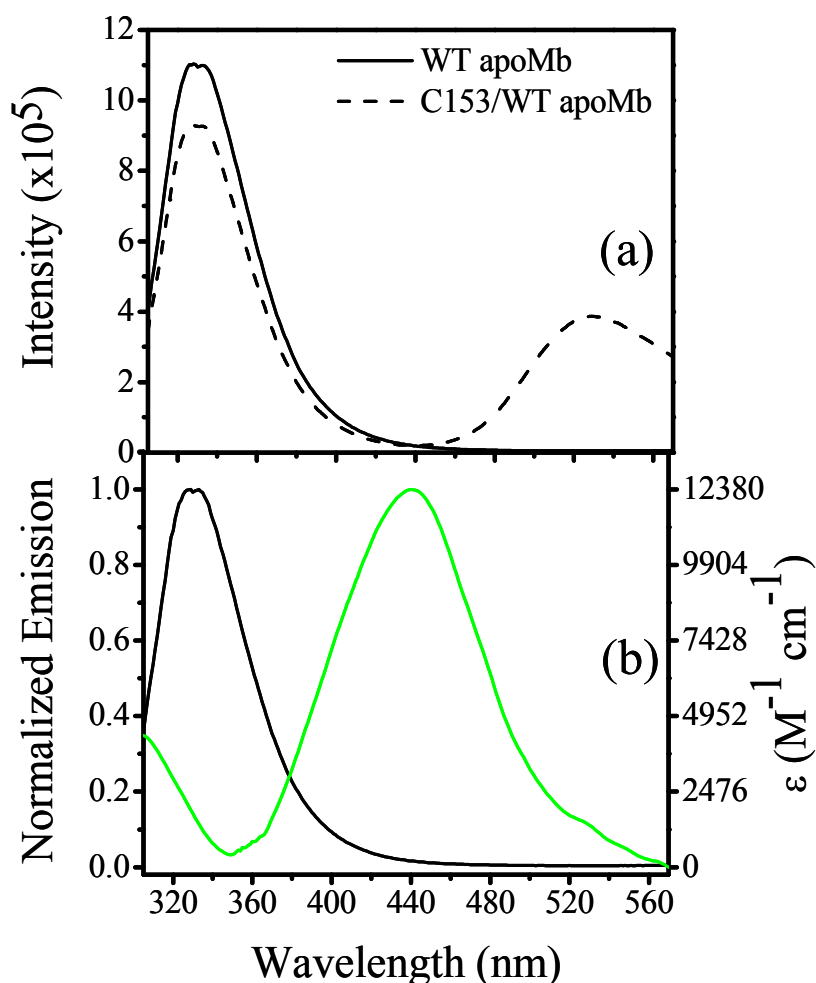
Figure V.9. (a) Steady-state fluorescence spectra (λ_{ex} = 266 nm) of WT horse–heart apoMb with (- - -) and without C153 (——). The peak maxima at 330 and 530 nm are due to Trps and C153. Addition of C153 into the heme pocket quenches the Trp fluorescence in apoMb, indicating energy transfer from Trp to C153. (b) Spectral overlap of C153 molar extinction coeffient (ε) (green) and tryptophan emission (black) in the 1:1 WT equine apoMb/C153 complex. The calculated R_0 is 25.5 and 27 Å for Trp14 and Trp7. The distances, R, between Trp14 and Trp7 from C153 are 17.3 and 20.1 Å, respectively.

Characterization of the Complexes of C153 and ApoMbs by Fluorescence Energy Transfer and Fluorescence Anisotropy

Fluorescence Energy Transfer. In order to characterize the C153/apoMb complexes further, we performed steady-state and time-resolved fluorescence energy transfer experiments.

Figure V.9a presents quenching of the donor (D), Trp, fluorescence from apoMb ($\Phi_{Trp}^{ApoMb} = 0.11$) after insertion of the acceptor (A), C153, into the heme pocket ($\Phi_{Trp}^{C153/ApoMb} = 0.09$). The fluorescence quantum yield of Trp (Φ_{Trp}) in apoMb was calculated using Trp in buffer (pH 7.0) as a standard. [62,96,97] There is significant overlap of the Trp emission and C153 absorption spectra (Figure V.9b), which is a critical factor in energy transfer between D and A. When excited at 266 nm, a shortening of the Trp lifetime was observed in all the C153/apoMb complexes (τ = 2.0 ns), compared to the lifetime in the free apoproteins (τ = 2.3 ns). The fluorescence lifetime of C153 in the apoMb complexes was also monitored exciting at λ_{ex} = 266 and 407 nm and $\lambda_{em} \geq$ 505 nm. Excitation at 407 nm only excites the acceptor (see Figure V.9) resulting in its prompt fluorescence since no energy transfer can occur. Figure V.10 presents the time-resolved fluorescence decays of C153/apoMb complexes when Trp and C153 are selectively excited. The sets of decays are clearly different when excited at 266 and 407 nm. Upon exciting at 266 nm, significant growth in the fluorescence decay traces of C153 was observed in all the apoMb complexes, which was absent completely at 407 nm excitation. The rise time can thus, originate only from the acceptor (C153) emission and indicates energy transfer from Trp to C153.

A crucial result in helping us to characterize the C153/apoMb complexes is that for the wild-type complexes *two exponentials were required to fit the rise times adequately* (Table V.2 and Figure V.10). It is reasonable to observe two rise times for the energy transfer since the apoMbs have two Trps (Trp7 and Trp14) and energy transfer from two Trps at different distances from C153 can lead to two different rise times (Table V.2). But more importantly for purposes of the structural characterization, this result also implies that
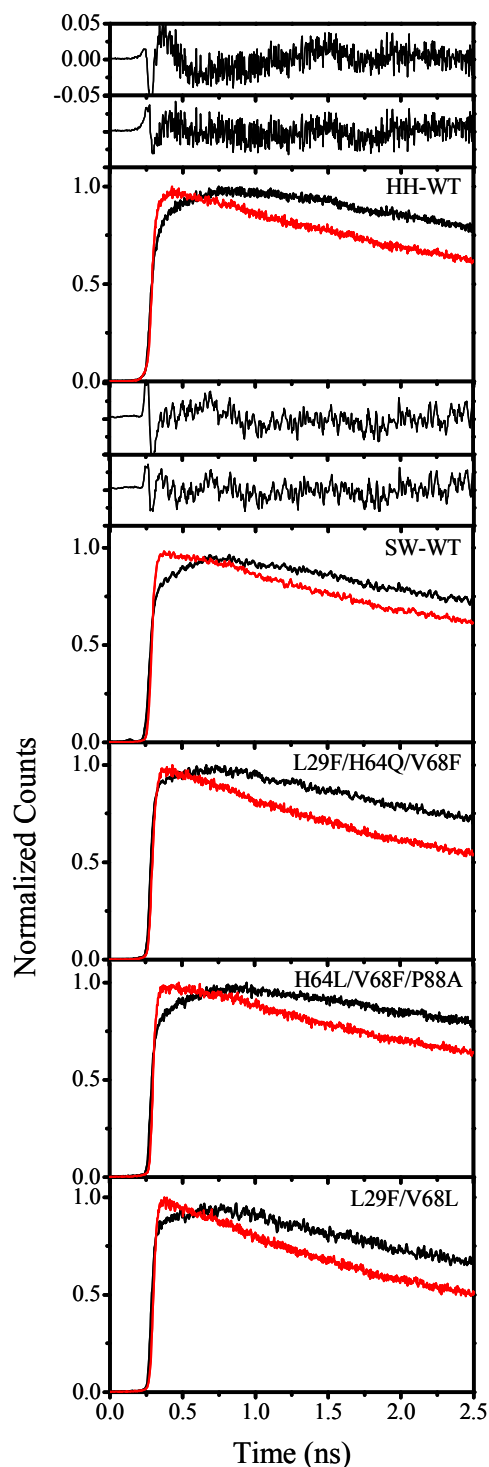
Figure V.10. Fluorescence decay traces of complexes of C153 with HH-WT and SW-WT apoMbs, and the mutants of the latter. λ_{ex} = 266 nm (black) or λ_{ex} = 407 nm (red). $\lambda_{em} \geq$ 500 nm. Upon exciting at 266 nm, a rise in the fluorescence decay traces of C153 was

observed in all of the apoMb complexes. This rise was absent for λ_{ex} = 407 nm. All the measurements were repeated three times. Data for the HH samples were acquired in 4096 channels, whereas the rest were taken in 1024 channels. The residuals from the fits for wild type HH and SW are shown. In each pair, the residuals in the upper panel and in lower panel are obtained from single ($\chi^2 > 2.5$) and bi-exponential fits ($\chi^2 \sim 1.3$), respectively. Decays for all of the mutants are best fit with a single exponential ($\chi^2 \leq 1.3$). The results are collated in Table V.2.

C153 is rigidly bound inside the heme pocket at a fixed orientation and that it is immobile within the time-scale of the experiment. On the other hand, the three mutants all provided single exponential rise times for the energy transfer. Such a result can be interpreted in at least three ways: 1) R^6/κ^2 is the same for C153 and each of the two Trps (assuming a fixed dipole moment for C153); 2) the position and orientation of C153 only favors energy transfer from a single Trp residue; 3) the mutants proteins are not correctly folded and there are multiple C153 binding sites or the C153 is mobile on the time scale of the energy transfer giving rise to a averaged time constant.

Quantitative structural details can be gleaned from the energy transfer data by computing the critical distance, R_0, between the Trps and C153:

$$k_{ET} = \frac{1}{\tau_D}\left(\frac{R_0}{R}\right)^6 \tag{V.4}$$

$$R_0^6 = \frac{9000(\ln 10)\Phi_D}{128\pi^5 n^4 N}\kappa^2 \left(\frac{\int_0^\infty F_D(\bar{\nu})\varepsilon_A \bar{\nu}^{-4} d\bar{\nu}}{\int_0^\infty F_D(\bar{\nu})d\bar{\nu}}\right) \tag{V.5}$$

where k_{ET} is the rate of energy transfer, τ_D is the average fluorescence lifetime of the donor, R is the distance between donor and acceptor, κ^2 is the orientation factor, n is the index of refraction of the medium (considered as 1.33), N is Avogadro's number, Φ_D is the

fluorescence quantum yield of the donor, F_D is the emission spectrum of the donor on a wavenumber scale, and ε_A is the molar extinction coefficient of the acceptor ($M^{-1}cm^{-1}$).

(a)

(b)
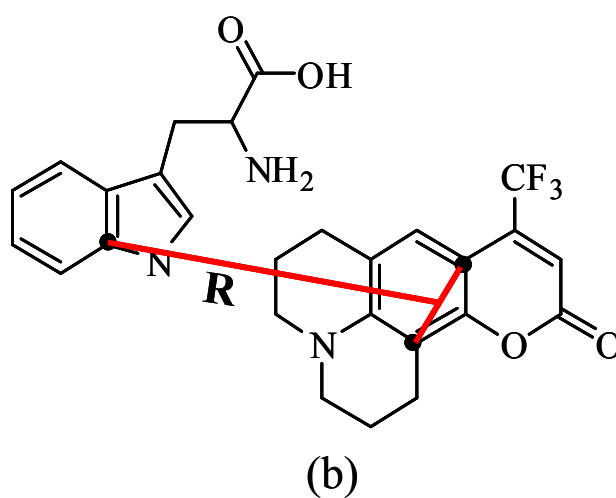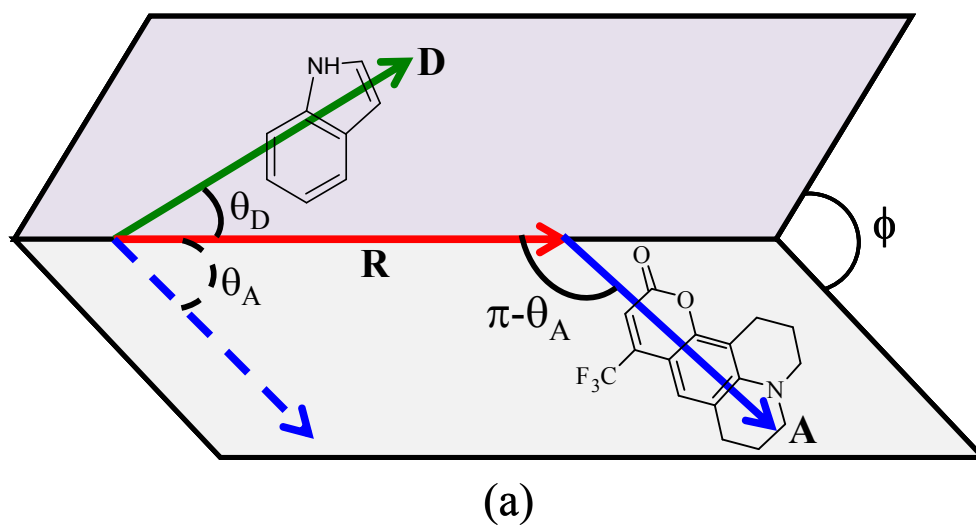
Figure V.11. (a) Geometry used to calculate κ^2 for the determination of R_0 for the energy transfer between Trp and C153 in the complexes. The figure presents the mutual orientation of the donor transition dipole of Trp, θ_D, and the acceptor transition dipole of C153, θ_A. R is the separation vector between the donor and acceptor. κ^2 is calculated using eqn 6. θ_A is fixed at 21°, along the dipole moment of C153; and the donor is assumed to be isotropically oriented. The angles θ_D and ϕ are thus integrated over the range of $0-\pi$ and $0-2\pi$, respectively. This geometry gives $\kappa^2 = 5/4$. (b) The D–A distances from the equilibrated structures from the molecular dynamics simulations are computed with respect to the atoms illustrated. Distances obtained from energy transfer results and from simulations are summarized in Table V.4.

A thorny problem in using energy transfer data to determine distances is obtaining an appropriate value for κ^2. Typically it is assumed that D and A can move freely and assume all orientations, in which case $\kappa^2 = 2/3$. This is clearly incorrect for the C153/apoMb system, where there is ample evidence suggesting that C153 is rigidly held in the heme pocket, at least for the wild type proteins. We have thus assumed that D is randomly orientated and that A is fixed at the angle θ_A with respect to the separation vector between the D and A, as shown in Figure V.11. Various orientations between donor and acceptor have been discussed in detail by Dale and Eisinger.[98] For further simplicity, we assume that C153 is oriented along its transition dipole moment vector, $\theta_A=21°$.[47] This is a reasonable and convenient assumption. The NMR data were not sufficient to permit the determination of the location of the coumarin's plane inside the heme pocket. If, however, the location of the C153 plane is undetermined to within a rotation about its transition dipole, κ^2 remains unchanged. Using the equation

$$\kappa^2 = \left[\sin\theta_D \sin\theta_A \cos\varphi - 2\cos\theta_D \cos\theta_A\right]^2 \tag{V.6}$$

we thus obtain $\kappa^2 = 5/4$. The overlap integral was calculated using the emission spectra of single Trp mutants of apoMb[99] and the absorption spectrum of C153 in WT apoMb. Finally, eqs 4 and 5 yielded R_0 as 25.5 and 27.0 Å for Trp14 and Trp7 in the HH-WT complex, using the quantum yields of Trp14 and Trp7 as 0.14 and 0.19, which were calculated from the ratio of the lifetimes of the individual Trps.[100] The distances, R, from Trp14 and Trp7 to C153 were thus determined to be 17.3 and 20.1 Å, respectively. For the SW-WT complex, the Trp-C153 distances were found to be 14.4 and 18.4 Å, which are significantly different from HH-WT complex. The distances obtained from energy transfer experiments have been

compared with those in equilibrated simulation structures in Table V.4. Unlike the case of the mutants, there is reasonably good agreement for the Trp–C153 distances determined by experiment and simulation in the wild type proteins. The differences in the location of C153 in the heme pockets of the two WT apoproteins, is also reflected in the reorganization energies and solvation correlation functions.

In concluding this section, it is well to note that other workers have studied the very efficient energy transfer from tryptophan to heme in myoglobin and place our measurements and analysis in this context. Hochstrasser and Negus [101] provided a detailed analysis of energy transfer between Trps 7 and 14 to the heme in sperm whale myoglobin. They agree with our assessment that these two Trps are close to the exterior of the protein. They also conclude that the directions of the tryptophan transition moments are probably not a critical factor for the energy transfer. This conclusion is consistent with our assumption that the Trps are randomly distributed. They do, however, invoke anisotropy data to suggest that Trp 14 is restricted enough to transfer energy to the heme with a time constant of 30 ps. More recently, Zhong and coworkers [102] have extended these studies. They conclude that for ultrafast energy transfer, it is incorrect to assume that that the donor and acceptor are randomized.

We recognize that it is a gross approximation to assume that the Trps are completely randomly distributed. But we feel that it is a useful approximation and that it is unnecessary in the present case to assume that the Trps are not randomized. *The point of our energy transfer experiments is not to assay the rigidity of the tryptophans but to verify the location of the coumarin*, which is crucial for a proper comparison with simulations. The most important results of our experiments are that for the WT systems we clearly resolve two

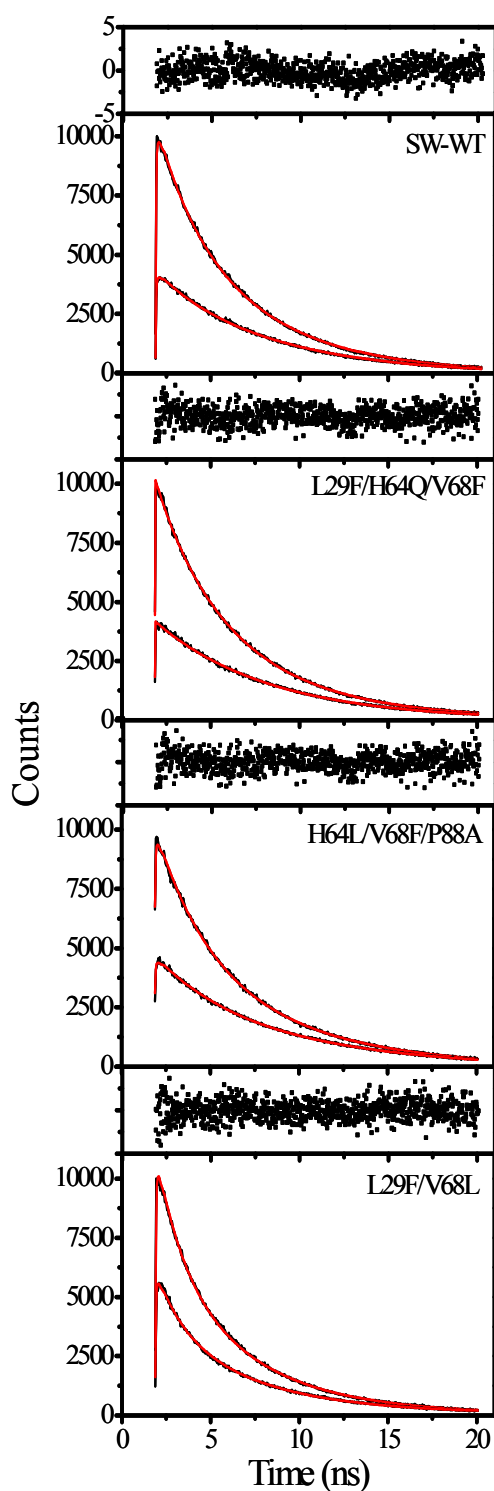**Figure V.12.** Polarized fluorescence decays of the complexes of C153 with wild type sperm whale apomyogobin and its mutants. $\lambda_{ex} = 407$nm; $\lambda_{em} \geq 500$ nm. A normalization factor was applied to the traces such that the maximum count was 10000 owing to the requirements of the analysis software. The anisotropy measurements were repeated three times. The

rotational reorientation times were obtained from simultaneous fitting[103] of parallel and perpendicular decays, and the results are summarized in Table V.2. The top panels present the residuals from the fits (χ^2 ~1.2).

different energy transfer events and that the distances computed from these time constants are consistent with distances obtained from the simulations.

Fluorescence Anisotropy. Time-resolved fluorescence anisotropy data for C153/apoMb complexes are presented in Figure V.12. The anisotropy decay of bound C153 in WT and the two triple mutants was single exponential with a rotational time of ~10 ns (Table V.2), which supports rigid binding of the probe in the heme pocket; because a single-exponential decay would not be expected for a surface bound chromophore. [61,62] The r(0) values for these systems were found to be similar (~0.3). These results are consistent with our previous reports with HH-WT apoMb, which was single exponential with a rotational time of 9.2 ns. On the other hand, the double mutant L29F/V68L showed a much higher rotational time (>20 ns), with a significantly lower r(0) of ~0.2. These two values clearly impugn the structure integrity of the double mutant. The higher rotational diffusion time could arise from aggregation or improper folding of the protein. The reduced limiting anisotropy could arise from multiple binding sites of the C153.

Comparison of the Experimental and Simulated *C*(*t*)s

As suggested earlier, the origin of this discrepancy between the experimental and simulated *C*(*t*)s for the mutants may be found from structural studies of the complexes. From a comparison of the C153-Trp distances obtained from equilibrated simulation structures and energy transfer experiments (Table V.4) and from the NMR measurements, it appears that

the structural features for the C153/WT complex obtained from simulations and experimental

measurements are in reasonable agreement. Again, this is not the case for the mutants.

TABLE V.3. Steady-State parameters for C153/apoMb Complexes

System	$\nu_{em}^{max\ a}$ cm^{-1}	$\nu("0")^{max\ a}$ cm^{-1}	$\nu_{ex}^{max\ a}$ cm^{-1}	$\lambda("0")^{b,}$ c cm^{-1}	$\lambda(\infty)^{b,}$ c cm^{-1}	$\lambda(\infty) - \lambda("0")$ c cm^{-1}	$\lambda_{simul.}$ c cm^{-1}
HH WT	22940	20260	18730	1850	2450	600	888
SW WT	18970	20322	22910	1815	2453	638	715
L29F/H64Q/ V68F	19160	20307	22840	1786	2355	569	1094
H64L/V68F/ P88A	19690	20660	23360	1847	2450	603	1252
L29F/V68L	19360	20600	23090	1743	2390	647	755

[a] Peak maxima are obtained from log-normal fits of the spectra.
[b] λ values from experiments are calculated using eq. 1 and have an error of $\pm\ 5$ cm^{-1} as determined from 3 different measurements.
[c] $\lambda(\infty)$ is the *total* Stokes shift including intramolecular and solvent contribution, whereas $\lambda("0")$ exclusively estimates the intramolecular vibrational contribution to the total Stokes shift. Their difference, $\lambda(\infty) - \lambda("0")$, is commensurate with that obtained from simulations, $\lambda_{simul.}$, calculated as $\lambda = < (\delta\Delta E)^2 > / 2k_B T$ and which *only* accounts for the dynamic Stokes shift due to solvent contribution or relaxation.

The way in which the initial structures for the simulations are determined may

provide a clue for understanding such discrepancies. For the wild type, the apo structure is

obtained directly from the protein data bank, presumably the same structure as the one used

in the experimental measurements. On the other hand, the initial structures of the mutants

are obtained from simple site mutations in the presence of the coumarin in the heme pocket.

TABLE V.4. Distances from Trp7 and Trp14 to C153 in the Complexes

System	Simulations[a]		FRET			
			R_0[b]		R[c]	
	Trp7	Trp14	Trp7	Trp14	Trp7	Trp14
HH WT	21.1	17.0	26.9	25.5	20.1	17.3
SW WT	16.7	11.6	25.3	23.9	18.4	14.4
L29F/H64Q/V68F	17.8	13.8	25.2	23.8	16.8	16.7
H64L/V68F/P88A	17.2	12.9	25.5	24.1	15.9	15.9
L29F/V68L	18.1	12.1	25.9	24.4	17.3	17.2

All distances are in Angstroms.
[a] Distances between C153 and Trp are obtained from the equilibrated structures as shown in Figure V.11b.
[b] R_0 is the so-called "critical distance" distance between donor and acceptor defined by eqs 4 and 5.
[c] R is the distance from the center of mass of donor (Trp) and acceptor (C153) as shown in Figure V.11a.

This construction of the initial complex for the wild type proteins is different from

those for the mutant complexes. More precisely, the construction of the mutant complexes

for the simulations is not analogous to the preparation of the complexes for the experimental

measurements. In the latter, the mutant protein is first expressed and the heme is removed,

C153 diffuses into the heme pocket, and the heme pocket relaxes around the coumarin. In

other words, the mutation and apoprotein formation and the subsequent introduction of the C153 correspond to two different equilibration steps in the molecular dynamics simulations. Indeed, the structures from simulations for the two wild type C153/apoMb complexes are in reasonable agreement with the experimental observations (Table V.4), but the structures for the mutants are not.

One possible way to check this argument is to equilibrate the mutant apoprotein first and then insert the coumarin into the heme pocket with the initial structure being consistent with the energy transfer and NMR measurements. From such initial structures of the mutants the reorganization energies and solvation correlation functions from simulations could be tested against the experimental ones. Another possible way to test the reliability of the mutant complex structure is annealing, namely raising the simulation temperature to 500 K for some time, and then cooling the system down to 300 K to equilibrate for 10 ns. For the HH-WT/C153 complex, an annealing was done at 500 K for 3 ns and an equilibration at 300 K for 10 ns. There was no significant change for the structure of the complex.

Conclusion

We have continued to explore the use of the complex of C153 and apoMbs to study the protein dielectric response [30-33], which has proven to be extremely successful. Comparisons between experimental and simulated $C(t)$s for wild-type heme proteins, such as horse heart myoglobin,[32,33] leghemoglobin,[32,33] and sperm whale myoglobin range from very good to excellent. Furthermore, examination of these systems demonstrates the sensitivity of C153 to its environment and permits the observation of differences in the heme pockets among these three proteins. Perhaps most impressive is that we can detect changes in $C(t)$

arising from only one change between the heme pockets of the horse heart and sperm whale myoglobins: Val67 in HH is replaced by Thr in SW (Figure V.3).

Our success with the wild-type proteins encouraged us to study mutant sperm whale myoglobins. For the three mutants we investigated, however, agreement between experiment and simulation was considerably inferior to that for the wild-type systems. Our previous work suggests no reason to attribute such disagreement to the force fields used in the simulation but rather to question the structure of the complex used as the starting point for the simulation. Thus painstaking attention must be paid to structural details when comparisons are being made between theory and experiment for different proteins and, in particular, the same proteins with slight modifications. We consequently performed an NMR study of the complex of C153 with HH-WT apoMb, along with fluorescence energy transfer and anisotropy of all of the horse heart and sperm whale complexes to complement the NMR studies.

The NMR measurements provide important confirmation of our earlier conclusions [30-33] that the C153 lies in the heme pocket of the HH-WT apoMb. For the wild-type complexes, fluorescence energy transfer measurements provide two rise times, suggesting a definite spatial relationship between the two Trp donors and the C153 acceptor. On the other hand, the three mutants all provided single exponential rise times for the energy transfer. Such a result can be interpreted in at least three ways: R^6/κ^2 is the same for C153 and each of the two Trps (assuming a fixed dipole moment for C153); or the position and orientation of C153 only favors energy transfer from a single Trp residue; or the mutants proteins are not correctly folded and there are multiple C153 binding sites or the C153 is mobile on the time

scale of the energy transfer giving rise to a averaged time constant. Fluorescence anisotropy studies suggest that the double mutant was not structurally intact.

It is important to stress that the rather poor agreement between simulation and experiment for, at least the triple mutants, is *not* a suggestion that it is not possible to identify the contribution of a single amino acid to the dielectric response. We reiterate that for HH-WT apoMb and apoLba (where the heme pockets differs significantly[88,89]), we have found excellent agreement between the $C(t)$ obtained from both experiments and simulations, and it is also significant that the only difference between the heme pockets of the two WT Mbs is that Val67 in HH is replaced by Thr in SW.[32,33] The mutant results point, rather, to the importance of the structural characterization of modified proteins used in studies of the dielectric response and suggest strategies for performing molecular dynamics simulations of modified proteins—i.e., starting perhaps with (limited) NMR data and employing more than one equilibration step. We believe that ours is the most thorough structural characterization to date of any system, whether it be based on nonnatural fluorescence probes or mutants, employed for the investigation of the dielectric response of proteins.

Acknowledgements

References

(1)   Nandi, N.; Bhattacharyya, K.; Bagchi, B. *Chem. Rev.* **2000**, *100*, 2013.

(2)   Simon, J. D. *Acc. Chem. Res.* **1988**, *21*, 128.

(3)   Fleming, G. R.; Wolynes, P. G. *Phys. Today* **1990**, *43*, 36.

(4)   Barbara, P. F.; Jarzeba, W. Ultrafast Photochemical Intramolecular Charge Transfer and Excited State Solvation. In *Advances in Photochemistry*; Volman, D. H., Hammond, G. S., Gollnick, K., Eds.; John Wiley & Sons, 1990.

(5)   Maroncelli, M. *J. Mol. Liq.* **1993**, *57*, 1.

(6)   Hynes, J. T. Charge Transfer Reactions and Solvation Dynamics. In *Ultrafast Dynamics of Chemical Systems*; Kluwer Academic: Dordrecht, 1994; Vol. 7; pp 345.

(7)   Fleming, G. R.; Cho, M. H. *Annu. Rev. Phys. Chem.* **1996**, *47*, 109.

(8)   Stratt, R. M.; Maroncelli, M. *J. Phys. Chem.* **1996**, *100*, 12981.

(9)   Castner, E. W., Jr.; Maroncelli, M. *J. Mol. Liq.* **1998**, *77*, 1.

(10)   Mukamel, S. *Principles of Nonlinear Optical Spectroscopy*, First Edition ed.; Oxford University Press: New York, 1995.

(11)   Hsu, C. P.; Song, X. Y.; Marcus, R. A. *J. Phys. Chem. B* **1997**, *101*, 2546.

(12)   Song, X.; Chandler, D. *J. Chem. Phys.* **1998**, *108*, 2594.

(13)   Marcus, R. A.; Sutin, N. *Biochim. Biophys. Acta* **1985**, *811*, 265.

(14)   King, G.; Warshel, A. *J. Chem. Phys.* **1989**, *91*, 3647.

(15)   Bader, J. S.; Kuharski, R. A.; Chandler, D. *Abstr. Paper Am. Chem. Soc.* **1990**, *199*, 65.

(16)   Halder, M.; Headley, L. S.; Mukherjee, P.; Song, X.; Petrich, J. W. *J. Phys. Chem. A* **2006**, *110*, 8623.

(17)   Lang, M. J.; Jordanides, X. J.; Song, X.; Fleming, G. R. *J. Chem. Phys.* **1999**, *110*, 5884.

(18)   Perutz, M. F. *Science* **1978**, *210*, 1187.

(19)   Moser, C. C.; Keske, J. M.; Warncke, K.; Farid, R. S.; Dutton, P. L. *Nature* **1992**, *355*, 796.

(20)   Warshel, A.; Russel, S. T. *Q. Rev. Biol.* **1984**, *17*, 283.

(21)   Sharp, K. A.; Honig, B. *Ann. Rev. Biophys. Chem.* **1990**, *19*, 301.

(22)   Nakamura, H. *Q. Rev. Biophys.* **1996**, *29*, 1.

(23)   King, G.; Lee, F. S.; Warshel, A. *J. Chem. Phys.* **1991**, *95*, 4366.

(24)   Simonson, T.; Perahia, D.; Brünger, A. T. *Biophys. J.* **1991**, *59*, 670.

(25)   Simonson, T.; Perahia, D. *Proc. Natl. Acad. Sci. U. S. A.* **1995**, *92*, 1082.

(26)   Simonson, T.; Brooks, C. L. *J. Am. Chem. Soc.* **1996**, *118*, 8452.

(27)   Simonson, T. *J. Am. Chem. Soc.* **1998**, *120*, 4875.

(28)   Simonson, T.; Archontis, G.; Karplus, M. *J. Phys. Chem. B* **1999**, *103*, 6142.

(29)   Warshel, A.; Sharma, P. K.; Kato, M.; Parson, W. W. *Biochimica et Biophysica Acta, Proteins and Proteomics* **2006**, *1764*, 1647.

(30)   Chowdhury, P. K.; Halder, M.; Sanders, L.; Arnold, R. A.; Liu, Y.; Armstrong, D. W.; Kundu, S.; Hargrove, M. S.; Song, X.; Petrich, J. W. *Photochem. Photobiol.* **2004**, *79*, 440.

(31)   Mukherjee, P.; Halder, M.; Hargrove, M.; Petrich, J. W. *Photochem. Photobiol.* **2006**, *82*, 1586.

(32)   Halder, M.; Mukherjee, P.; Bose, S.; Hargrove, M. S.; Song, X.; Petrich, J. W. *J. Chem. Phys.* **2007**, *127*, 055101/1.

(33)   Bose, S.; Adhikary, R.; Mukherjee, P.; Song, X.; Petrich, J. W. *J. Phys. Chem. B* **2009**, *113*, 11061.

(34)   Cocco, M. J.; Lecomte, J. T. J. *Protein Sci.* **1994**, *3*, 267.

(35)   Nemkovich, N. A.; Baumann, W.; Kruchenok, Y. V.; Reis, H.; Rubinov, A. N. *J. Appl. Spectrosc.* **1999**, *66*, 415.

(36)   Pal, S. K.; Peon, J.; Bagchi, B.; Zewail, A. H. *J. Phys. Chem. B* **2002**, *106*, 12376.

(37)   Pal, S. K.; Peon, J.; Zewail, A. H. *Proc. Natl. Acad. Sci. USA* **2002**, *99*, 1763.

(38)   Peon, J.; Pal, S. K.; Zewail, A. H. *Proc. Natl. Acad. Sci. USA* **2002**, *99*, 10964.

(39)   Shen, X.; Knutson, J. R. *J. Phys. Chem. B* **2001**, *105*, 6260.

(40)   Jordanides, X. J.; Lang, M. J.; Song, X.; Fleming, G. R. *J. Phys. Chem. B* **1999**, *103*, 7995.

(41)   Chowdhury, P. K.; Halder, M.; Sanders, L.; Calhoun, T.; Anderson, J. L.; Armstrong, D. W.; Song, X.; Petrich, J. W. *J. Phys. Chem. B* **2004**, *108*, 10245.

(42)   Stryer, L. *J. Mol. Biol.* **1965**, *13*, 482.

(43)   Pierce, D. W.; Boxer, S. G. *J. Phys. Chem.* **1992**, *96*, 5560.

(44)   Macgregor, R. B.; Weber, G. *Nature* **1986**, *316*, 70.

(45)   Bashkin, J. S.; Mclendon, G.; Mukamel, S.; Marohn, J. *J. Phys. Chem.* **1990**, *94*, 4757.

(46)   Adhikary, R.; Barnes, C. A.; Petrich, J. W. *J. Phys. Chem. B* **2009**, *113*, 11999.

(47)   Maroncelli, M.; Fleming, G. R. *J. Chem. Phys.* **1987**, *86*, 6221.

(48)   Horng, M. L.; Gardecki, J. A.; Papazyan, A.; Maroncelli, M. *J. Phys. Chem.* **1995**, *99*, 17311.

(49)   Lewis, J. E.; Maroncelli, M. *Chem. Phys. Lett.* **1998**, *282*, 197.

(50)   Maroncelli, M.; Fee, R. S.; Chapman, C. F.; Fleming, G. R. *J. Phys. Chem.* **1991**, *95*, 1012.

(51)   Kovalenko, S. A.; Ruthmann, J.; Ernsting, N. P. *Chem. Phys. Lett.* **1997**, *271*, 40.

(52)   Muhlpfordt, A.; Schanz, R.; Ernsting, N. P.; Farztdinov, V.; Grimme, S. *Phys. Chem. Chem. Phys.* **1999**, *1*, 3209.

(53)   Changenet-Barret, P.; Choma, C. T.; Gooding, E. F.; DeGrado, W. F.; Hochstrasser, R. M. *J. Phys. Chem. B* **2000**, *104*, 9322.

(54)   Jiang, Y.; McCarthy, P. K.; Blanchard, D. J. *Chem. Phys.* **1994**, *183*, 249.

(55)   Flory, W. C.; Blanchard, D. J. *Appl. Spectrosc.* **1998**, *52*, 82.

(56)   Palmer, P. M.; Chen, Y.; Topp, M. R. *Chem. Phys. Lett.* **2000**, *318*, 440.

(57)   Chen, Y.; Palmer, P. M.; Topp, M. R. *Int. J. Mass Spectrom* **2002**, *220*, 231.

(58)   Agmon, N. *J. Phys. Chem.* **1990**, *94*, 2959.

(59)   Chakrabarty, D.; Hazra, P.; Chakraborty, A.; Seth, D.; Sarkar, N. *Chem. Phys. Lett.* **2003**, *381*, 697.

(60)   Tcherkasskaya, O.; Ptitsyn, O. B.; Knutson, J. R. *Biochemistry* **2000**, *39*, 1879.

(61)   Petrich, J. W.; Martin, J. L.; Breton, J. *Springer Ser. Chem. Phys.* **1988**, *48*, 576.

(62)   Das, K.; Smirnov, A. V.; Wen, J.; Miskovsky, P.; Petrich, J. W. *Photochem. Photobiol.* **1999**, *69*, 633.

(63)   Song, X. *J. Chem. Phys.* **2002**, *116*, 9359.

(64)   Cocco, M. J.; Kao, Y.-H.; Phillips, A. T.; Lecomte, J. T. J. *Biochemistry* **1992**, *31*, 6481.

(65)   Alayash, A. I.; Ryan, B. A. B.; Eich, R. F.; Olson, J. S.; Cashon, R. E. *J. Biol. Chem.* **1999**, *274*, 2029.

(66)   Nguyen, B. D.; Zhao, X.; Vyas, K.; La Mar, G. N.; Lile, R. A.; Brucker, E. A.; Phillips, G. N., Jr.; Olson, J. S.; Wittenberg, J. B. *J. Biol. Chem.* **1998**, *273*, 9517.

(67)   Hargrove, M. S.; Singleton, E. W.; Quillin, M. L.; Ortiz, L. A.; Phillips, G. N.; Olson, J. S.; Mathews, A. J. *J. Biol. Chem.* **1994**, *269*, 4207.

(68)   Headley, L. S.; Mukherjee, P.; Anderson, J. L.; Ding, R.; Halder, M.; Armstrong, D. W.; Song, X.; Petrich, J. W. *J. Phys. Chem. A* **2006**, *110*, 9549.

(69)   Mukherjee, P.; Crank, J. A.; Halder, M.; Armstrong, D. W.; Petrich, J. W. *J. Phys. Chem. A* **2006**, *110*, 10725.

(70)   Fee, R. S.; Maroncelli, M. *Chem. Phys.* **1994**, *183*, 235.

(71)   Arzhantsev, S.; Ito, N.; Heitz, M.; Maroncelli, M. *Chem. Phys. Lett.* **2003**, *381*, 278.

(72)   Ito, N.; Arzhantsev, S.; Heitz, M.; Maroncelli, M. *J. Phys. Chem. B* **2004**, *108*, 5771.

(73)   Mukherjee, P.; Crank, J. A.; Sharma, P. S.; Wijeratne, A. B.; Adhikary, R.; Bose, S.; Armstrong, D. W.; Petrich, J. W. *J. Phys. Chem. B* **2008**, *112*, 3390.

(74)   Zhong, D. P.; Pal, S. K.; Zhang, D. Q.; Chan, S. I.; Zewail, A. H. *Proc. Natl. Acad. Sci. USA* **2002**, *99*, 13.

(75)   Lu, W.; Kim, J.; Qiu, W.; Zhong, D. *Chem. Phys. Lett.* **2004**, *388*, 120.

(76)   Qiu, W.; Kao, Y.-T.; Zhang, L.; Yang, Y.; Wang, L.; Stites, W. E.; Zhong, D.; Zewail, A. H. *Proc. Natl. Acad. Sci. USA* **2006**, *103*, 13979.

(77)   Qiu, W.; Zhang, L.; Okobiah, O.; Yang, Y.; Wang, L.; Zhong, D.; Zewail, A. H. *J. Phys. Chem. B*. **2006**, *110*, 10540.

(78)   Zhang, L.; Wang, L.; Kao, Y.; Qiu, W.; Yang, Y.; Okobiah, O.; Zhong, D. *Proc. Natl. Acad. Sci. USA* **2007**, *104*, 18461.

(79)   Zhang, L.; Yang, Y.; Kao, Y.-T.; Wang, L.; Zhong, D. *J. Am. Chem. Soc.* **2009**, *131*, 10677.

(80)   Marchi, M.; Procacci, P. *J. Chem. Phys*. **1998**, *109*, 5194.

(81)   Pearlman, D. A.; Case, D. A.; Caldwell, J. W.; Ross, W. S.; Cheatham, T. E., III; DeBolt, S.; Ferguson, D.; Seibel, S.; Kollman, P. *Comp. Phys. Commun.* **1995**, *91*, 1.

(82)   Maroncelli, M.; Fleming, G. R. *J. Chem. Phys*. **1988**, *89*, 5044.

(83)   Jimenez, R.; Fleming, G. R.; Kumar, P. V.; Maroncelli, M. *Nature* **1994**, *369*, 471.

(84)   Li, T.; Hassanali, A. A.; Kao, Y.-T.; Zhong, D.; Singer, S. J. *J. Am. Chem. Soc.* **2007**, *129*, 3376.

(85)   Nilsson, L.; Halle, B. *Proc. Natl. Acad. Sci. U. S. A.* **2005**, *102*, 13867.

(86)   Abbyad, P.; Shi, X.; Childs, W.; McAnaney, T. B.; Cohen, B. E.; Boxer, S. G. *J. Phys. Chem. B* **2007**, *111*, 8269.

(87)   Golosov, A. A.; Karplus, M. *J. Phys. Chem. B* **2007**, *111*, 1482.

(88)   Kundu, S.; Snyder, B.; Das, K.; Chowdhury, P.; Park, J.; Petrich, J. W.; Hargrove, M. S. *Proteins: Struct. Funct. Genet.* **2002**, *46*, 268.

(89)   Kundu, S.; Hargrove, M. S. *Proteins: Struct. Funct. Genet.* **2003**, *50*, 239.

(90)   Lecomte, J. T. J.; Cocco, M. J. *Biochemistry* **1990**, *29*, 11057.

(91)   Cocco, M. J.; Lecomte, J. T. J. *Biochemistry* **1990**, *29*, 11067.

(92)   Cocco, M. J.; Barrick, D.; Taylor, S. V.; Lecomte, J. T. J. *J. Am. Chem. Soc.* **1990**, *114*, 11000.

(93)   Kao, Y.-H.; Lecomte, J. T. J. *J. Am. Chem. Soc.* **1993**, *115*, 9754.

(94)   Lecomte, J. T. J.; Kao, Y.-H.; Cocco, M. J. *Proteins: Struct. Funct. Genet.* **1996**, *25*, 267.

(95)   Lecomte, J. T. J.; Sukits, S. F.; Bhattacharyya, S.; Falzone, C. *Protein Sci.* **1999**, *8*, 1484.

(96)   Avouris, P.; Yang, L. L.; El-Bayoumi, M. A. *Photochem. Photobiol.* **1976**, *24*, 211.

(97)   Rich, R. L.; Gai, F.; Lane, J. W.; Petrich, J. W.; Schwabacher, A. W. *J. Am. Chem. Soc.* **1995**, *117*, 733.

(98)   Dale, R. E.; Eisinger, J. *Biopolymers* **1974**, *13*, 1573.

(99)   Glandieres, J.-M.; Twist, C.; Haouz, A.; Zentz, C.; Alpert, B. *Photochem. Photobiol.* **2000**, *71*, 382.

(100)   Sirangelo, I.; Malmo, C.; Casillo, M.; Irace, G. *Photochem. Photobiol.* **2002**, *76*, 381.

(101)   Negus, D. K.; Hochstrasser, R. M. *Proc. Natl. Acad. Sci. U. S. A.* **1984**, *81*, 4399.

(102)   Stevens, J. A.; Link, J. J.; Kao, Y.-T.; Zang, C.; Wang, L.; Zhong, D. *J. Phys. Chem. B* **2010**, *114*, 1498.

(103)   Cross, A. J.; Fleming, G. R. *Biophys. J.* **1984**, *46*, 45.

CHAPTER VI. ENZYME CATALYZED HYDROLYSIS OF CELLULOSE IN IONIC LIQUIDS: A GREEN APPROACH TOWARDS THE PRODUCTION OF BIOFUELS

A paper published in the *Journal of Physical Chemistry B*

Sayantan Bose[1], Daniel W. Armstrong[2], and Jacob W. Petrich[1,*]

Abstract

We investigated the reactivity and stability of a commercial mixture of cellulases in eight ionic liquids by optical and calorimetric techniques. First, hydrolysis by cellulases from *Tricoderma reesei* in these ionic liquids was benchmarked against that in aqueous buffer. Only 1-methylimidazolium chloride (mim Cl) and tris-(2-hydroxyethyl)-methylammonium methylsulfate (HEMA) provided a medium in which hydrolysis could occur. While hydrolysis at 65˚C is initially much faster in buffer than in these two liquids, it reaches a plateau after two hours; whereas, the reaction progresses monotonically in the two ionic liquids. This difference in the rate of hydrolysis is largely attributed to two factors: 1) the higher viscosity of the ionic liquids; 2) the enzymes are irreversibly denatured at 50˚C in buffer while they are stable to temperatures as high as 115˚C in HEMA. We explore

---

[1]Departments of Chemistry, Iowa State University; Ames, Iowa 50011 USA.
[2]Department of Chemistry and Biochemistry, University of Texas, Arlington, Box 19065 Arlington, Texas 76019, USA
* Author to whom all correspondence should be addressed.

whether fluorescence quenching of aromatic amino acids of the enzymes was indeed a signature of protein denaturation, as has been suggested in the literature and concluded that quenching is not necessarily associated with denaturation. When it does occur, for example, in the presence of ionic liquids formed from imidazolium cations and chloride anions, it arises from the imidazolium rather than the chloride. Finally, we conclude that HEMA is a promising, novel, green medium for performing cellulose hydrolysis reactions to convert biomass into biofuels. Because of the thermal stability it imparts to enzymes, its ability to solubilize biomass, and the fact that it does not quench tryptophyl fluorescence (thus permitting monitoring of the enzymes by fluorescence spectroscopy), HEMA provides an ideal starting point for the design of ionic liquids, not only for the hydrolysis of biomass, but for use with a wide spectrum of enzymatic reactions.

Introduction

Converting biomass into fuel is becoming increasingly important owing to the desirability of finding substitutes for fossil fuels and to the need to address the problem of global warming. Cellulose, one of the main constituents of biomass, is the most abundant biorenewable material on the planet. Consequently, during the past two decades, considerable effort has been devoted to the hydrolysis of cellulose in order to convert it into fuel. [1-7] There are, however, limitations to this process that are imposed mainly because of the limited solubility of cellulose in water or other organic solvents. That is, cellulose is a linear polysaccharide chain (Figure VI.1a) consisting of hundreds to thousands of D-anhydroglucopyranose linked together by β (1$\rightarrow$4)–glycosidic bonds[3]; and this highly

symmetrical polymer is sparingly soluble in most solvents. Thus the traditional dissolution processes are not only cumbersome and expensive, but they also require extreme conditions,[8] which in turn may cause serious environmental problems because the solvents they require, such as LiCl/*N,N*-dimethylacetamide, *N*-methylmorpholine-*N*-oxide/water, DMSO/paraformaldehyde, etc., are not only volatile, toxic, and costly; but they also cannot be recovered and reused. [9,10]
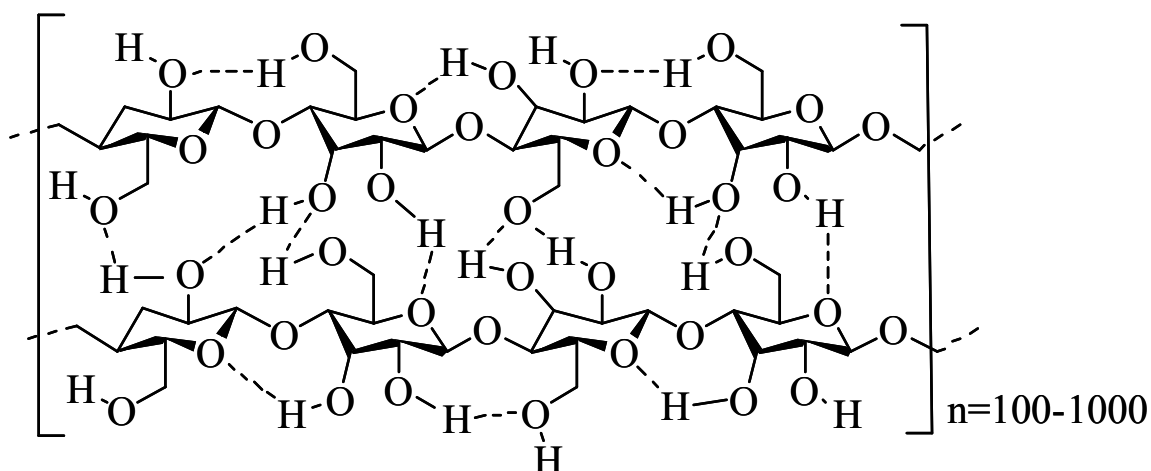
(a)
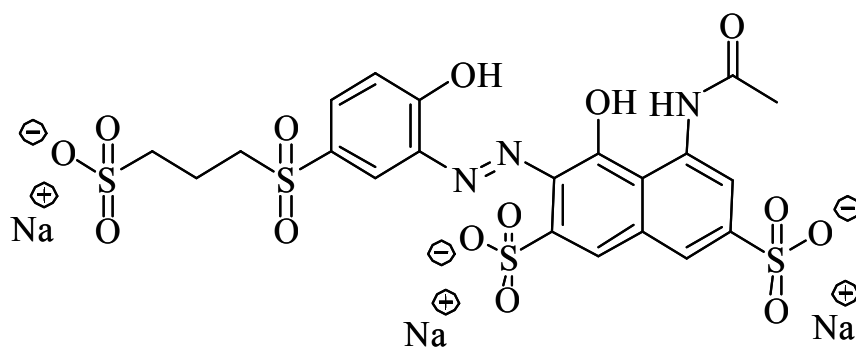
(b)

Figure VI.1.   Structure of (a) linear polymer chain of cellulose, showing inter chain hydrogen bonding interactions and (b) remazol brilliant violet dye tagged to cellulose chain in cellulose azure.

Recently, it has been reported that a special class of solvents, room temperature ionic liquids (RTILs), can dissolve cellulose. [9,11-19] Ionic liquids are green solvents, in contrast to volatile organic compounds (VOCs), owing to their high chemical and thermal stabilities, negligible vapor pressure,[20] and high recoverability and reusability.[21,22]   These properties have piqued the interest of the scientific community, and a variety of fundamental studies[23-29] have been performed on them to obtain a better understanding of their characteristics. Rogers and coworkers[9,15-17,30] have performed extensive studies on the dissolution of cellulosic materials in different ionic liquids. They have shown that ionic liquids can be used as nonderivatizing solvents for cellulose. Among the different solvents they studied, 1-butyl-3-methylimidazolium chloride (bmim Cl) was found to be most effective in dissolving cellulose, and they attributed this effect to strong hydrogen bonding interactions of the hydroxyl group with the halide anion. [9,15,30] They have also reported the dissolution of other lignocellulosic sources, such as wood [17] and banana pulp[16], in ionic liquids. Sheldon and coworkers have shown high solubility of di- and polysaccharides in ionic liquids containing dicyanamide anions.[12] More recently it has been found that *Bombyx mori* silk, fibroin [11], and hard and soft woods [18] are readily solubilized in imidazolium based ionic liquids.

Of the several steps involved in the production of ethanol from cellulose, the most crucial and difficult is the cellulolysis, which is the hydrolysis of the cellulose polymer chain into glucose units.[3,5,7] Different catalysts have been used for this reaction, such as metal chlorides,[4,6] acids, or enzymes.[1,31,32] The most common and widely used enzyme for this saccharification of cellulose is cellulase. In order to make the entire process of enzyme-catalyzed hydrolysis of cellulose green, the use of ionic liquids as solvents or co-solvents has received growing attention. The most thoroughly studied enzyme in ionic liquids is *Candida*

antarctica lipase B, used to catalyze transesterification reactions. [31,33,34] While the hydrophobic effect that increases protein stabilization is absent in organic ionic liquids, one advantage to biocatalysis in ILs as opposed to aqueous buffers is the longer activity of enzymes in ILs, which is thought to arise from the slow breaking and remaking of hydrogen bonds in the non-aqueous medium. [35] Studies of cellulase-induced catalysis in ionic liquids are, however, still limited. [5,36-39]

The physical and chemical properties of ionic liquids vary considerably depending on their cation–anion pair. Several attempts have been made to explore the activity of enzymes in ionic liquids, and there are various issues concerning the stability of these biomacromolecules in ionic liquids. Most of them are ineffective for biocatalyis. It has been suggested that ionic liquids containing the anions Cl^-, Br^-, NO_3^-, $CF_3SO_3^-$ denature enzymes owing to their higher basicity and, hence, higher affinity for hydrogen bonds.[22,40] There are diverse opinions concerning the effect of fluorinated anions, such as BF_4 and PF_6, on the enzyme's lifetime. Some reports suggest that since charge can be distributed over several fluorine atoms, the hydrogen bond affinity is minimized between the solvent and the enzyme and that, consequently, there is no interference with the internal hydrogen bonding network of the enzyme, maintaining its secondary structure. [31] On the other hand, Swatloski et al. [41] have reported that BF_4 and PF_6 have a high propensity to undergo self decomposition with the liberation of HF, which is detrimental for the enzymes.

One must also consider the tradeoff between viscosity and solubility. The inherent high viscosity of the ionic liquids is a retarding factor for the rate of enzymatic hydrolysis, since it slows the diffusion of the enzyme to its target. Viscosity increases with the length of the alkyl chain. Although the highly viscous bmim Cl (Table VI.I) slows down the rate of

cellulase induced hydrolysis of cellulose,[36] it can dissolve substantial amount of cellulose.[9] As opposed to bmim Cl, cellulose has very limited solubility in bmim PF_6 and bmim BF_4, whereas the latter keeps the enzyme active. Thus it is very challenging to find the right combination for the cation–anion pair that can form a compromise between the opposing factors of dissolving cellulose, retaining the activity of the enzymes, and having a low viscosity.

Consequently, this work delves into the activity of cellulase in eight ionic liquids and is motivated by that of Rogers and coworkers, who studied the activity of cellulase from *Tricoderma reesei* in bmim Cl and bmim BF_4. [36] They reported that the enzymatic activity ceases within an hour of reaction due the presence of high concentration of chloride ions in the bmim Cl, whereas the activity is retained in bmim BF_4. Enzymatic activity was monitored as a function of time using cellulose azure (an azo–dye tagged to the cellulose chain), [42] which upon hydrolysis releases the dye, whose absorbance is measured as a signature of the progress of reaction. In this work, we employ steady-state optical absorbance and fluorescence measurements as well as differential scanning calorimetry and thermal and microwave heating techniques to understand the stability of cellulase and its activity in different ionic liquids. We found that certain ionic liquids stabilize the cellulases at temperatures as high as 115 ˚C whereas the enzymes are irreversibly denatured at 50 ˚C in aqueous buffer. Hydrolysis in ionic liquids is slower than that in buffer, which is attributed to the higher viscosity of the ionic liquids. Furthermore, while quenching of the fluorescence of the intrinsic amino acids of cellulases has been interpreted as a signal of protein denaturation (attributed to chloride ions), we demonstrate that such quenching is not necessarily associated with denaturation. When it does occur, for example, in the presence of

ionic liquids formed from imidazolium cations and chloride anions, it arises from the imidazolium rather than the chloride.
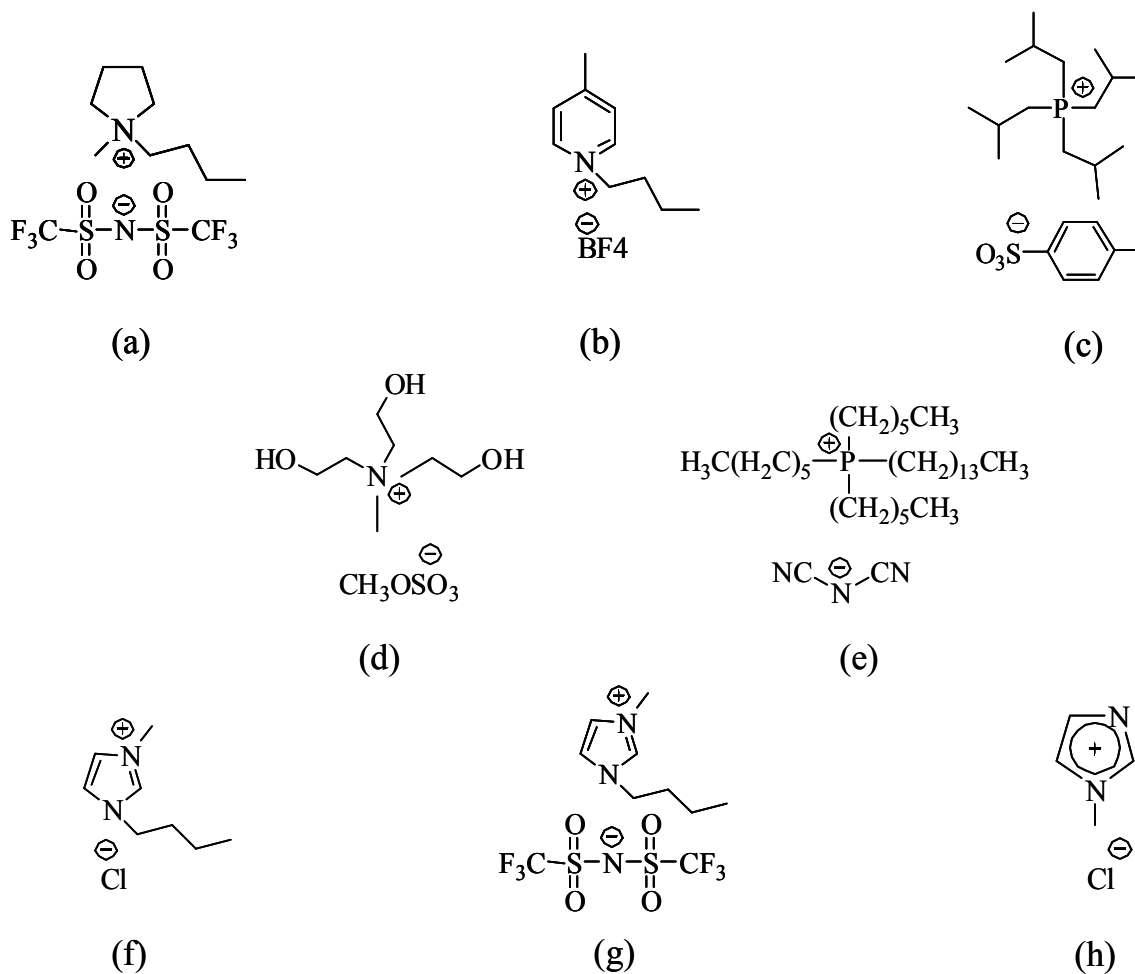
Figure VI.2. Structures of ionic liquids studied: (a) bmpyro NTf$_2$, (b) bmpy BF$_4$, (c) bmph OTs, (d) HEMA, (e) hdph dca, (f) bmim Cl, (g) bmim NTf$_2$ and (h) mim Cl. See text for abbreviations.

Experimental Section

Materials and Methods. GC 220 cellulase from *Tricoderma reesei* (1.2g/mL) was a gift from Genecor International Co. and was used without further purification. GC 220 is a heterogeneous mixture of several cellulase components, which includes endoglucanases and

cellobiohydrolases. In the subsequent discussion, whenever we refer to "cellulase" or "the enzyme," we are referring globally to the GC 220 preparation. Cellulose azure from Sigma Aldrich, which although may not be used for quantitative purposes but is appropriate for comparative activity studies,[43] was washed multiple times with deionized water to eliminate any unbound dye particles from the surface of cellulose, and was dried before using. (It is made from purified cotton linters and then covalently tagged with remazol brilliant violet dye (Figure VI.1b).) Upon hydrolysis of cellulose, the dye is solubilized and its absorbance reports on the activity of the enzyme. The ionic liquids used in this study are given in Figure VI.2, 1-butyl-1-methyl pyrrolidinium bis(trifluoromethane)-sulfonimide (bmpyro NTf_2), 1-butyl-4-methyl pyridinium tetrafluoroborate (bmpy BF_4), triisobutylmethylphosphonium tosylate (bmph OTs), tris-(2-hydroxyethyl)-methylammonium methylsulfate (HEMA), trihexyltetradecylphosphonium dicyanamide (hdph dca) and BASF grade 1-butyl-3-methylimidazolium chloride (bmim Cl) were purchased from Sigma Aldrich. 1-methylimidazolium chloride (mim Cl) and 1-butyl-3-methylimidazolium bis(trifluoromethane)-sulfonimide (bmim NTf_2), were synthesized as described elsewhere. [23] Ionic liquids were not dried before using, since aqueous enzyme solution was introduced into them before performing the experiments. Viscosity measurements were made with a ViscoLab 4000 piston style viscometer from Cambridge Applied system at desired temperatures.

Steady State Measurements. Steady-state absorption spectra were obtained on a Varian Cary 100 Bio UV-visible spectrophotometer with 1-nm resolution equipped with a Peltier temperature controller. All the activity measurements were done in a double-beam spectrometer, where both sample and reference cells were maintained at identical conditions.

The latter contained substrate without enzyme for automatic subtraction of the absorbance of the liberated dye (if any) in the absence of enzyme. The concentration of cellulose azure was 1.5mg/mL; and that of cellulase, 0.7mg/mL. Steady-state fluorescence spectra were obtained on a Spex Fluoromax-4 with a 2-nm bandpass and corrected for lamp spectral intensity and detector response. For both fluorescence and absorption measurements, a 1-cm path-length quartz cuvette was used. All cellulase samples were excited either at 284 or 295 nm and identical spectra were obtained at both wavelengths. In all the solvents, the enzyme was equilibrated for at least one hour with constant stirring at the desired temperature before the fluorescence measurements were done.

Differential Scanning Calorimetry Measurements. Differential heat flow curves were measured using a Q 10 Differential Scanning Calorimeter (TA Instruments.), attached to a liquid nitrogen cooling system (LNCS). The sample and reference pans were filled with 70 µL of the solutions. Cellulase in pH 4.8 citrate buffer and cellulase in ionic liquids were scanned from 10 to 100°C and from 10 to 150°C respectively. The enzyme concentration was maintained at 2.13-4.5 mg/mL. DSC scans were also done with pure buffer and ionic liquids without enzymes to ensure that no transitions occurred in the same temperature range.

Results and Discussion

Optical Measurements Probing Enzymatic Stability and Function

Steady-state fluorescence from cellulase (GC 220 obtained from the fermentation of the fungus *T. reesei*) was monitored in eight ionic liquids at room temperature and compared with that obtained in pH 4.8 citrate buffer (Figure VI.3). GC 220 consists of a mixture of enzymes. In each of the enzymes, there are several tryptophans, which provide intrinsic fluorescent markers. Misfolding or unfolding of the enzyme is typically accompanied by

quenching of fluorescence or a red shift [44] of the emission spectra. Baker et al. have shown that thermal denaturation of four *T. reesei* components was accompanied by quenching of fluorescence and a red shift in the emission maxima. [45] All the ionic liquids, except HEMA, quenched nearly all of the cellulase fluorescence. Interestingly, cellulase showed higher fluorescence in HEMA than in buffer, with retention of spectral shape. This is consistent with higher stability of the enzyme in the ionic liquid at ambient conditions, but it is not a necessary condition for stability as we shall see below.
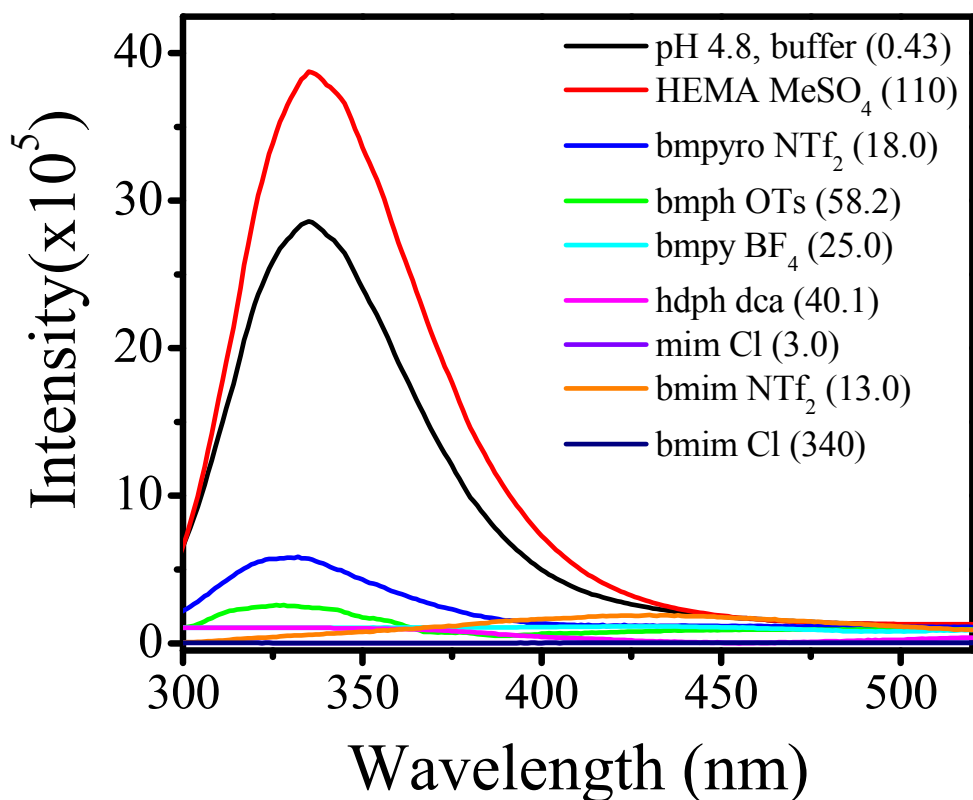

Figure VI.3. Steady-state emission spectra of cellulase (2.13 mg/mL) in pH 4.8 buffer and ionic liquids at room temperature. The samples were excited at 284 nm. Enzyme fluorescence is quenched in all the ionic liquids except in HEMA, which shows higher fluorescence than in buffer, with retention of spectral shape and peak maxima. The numbers in parenthesis are the viscosities measured in centi-poise (cP) at 65°C. The spectrum of cellulase in mim Cl is not visible due to superposition with other spectra.
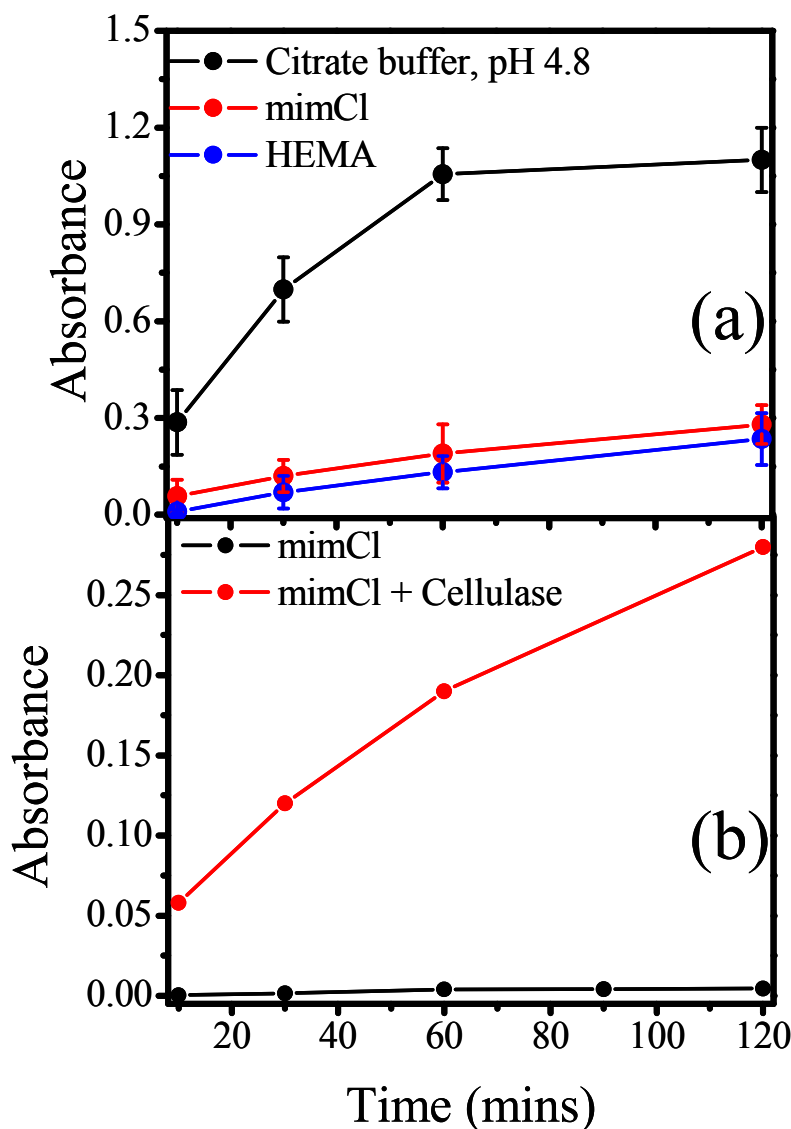
Figure VI.4. (a) Cellulase activity at 65°C as monitored via the absorbance of cellulose azure (1.5 mg/mL) at 575 nm in pH 4.8 citrate buffer, mim Cl, and HEMA. In buffer, cellulase showed maximum activity, which is represented by higher absorbance of the liberated dye, compared to those in the ionic liquids. We attribute this to the relative viscosities of the solvents. On the other hand, in buffer there is almost no hydrolysis after two hours (i.e., the absorbance reaches a plateau), whereas, the reaction progresses monotonically in the ionic liquids. (b) Hydrolysis of cellulose azure (1.5 mg/mL) monitored as a function of time, as in (a), in mim Cl with and without cellulase. The red data points correspond to the absorbance of dye liberated only due to hydrolysis by cellulase, whereas almost negligible hydrolysis (black) was observed without the enzyme.
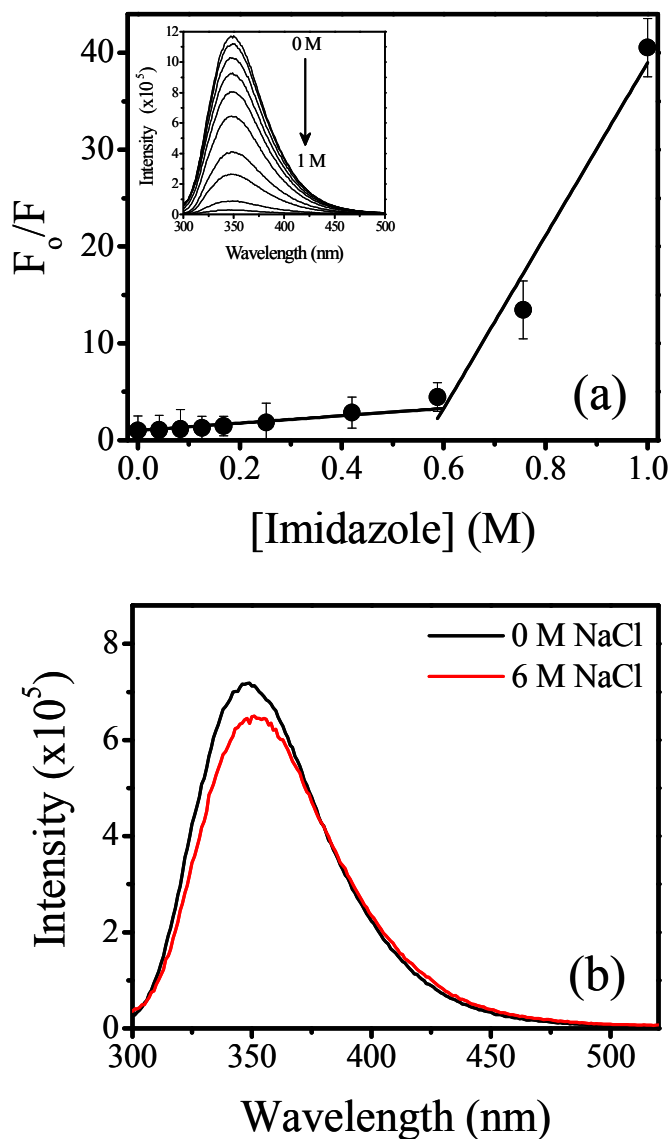
Figure VI.5. Stern–Volmer quenching plot of tryptophan in pH 7.0 buffer with 1-methylimidazole., where F and F_0 are the fluorescence intensities with and without quencher. The samples were excited at 284 nm. The inset shows a decrease of the fluorescence intensity of tryptophan with increasing quencher concentration, indicated by the downward arrow. The data points were fit to two straight lines to obtain the Stern–Volmer quenching constants (K_{sv}), which were found be 3.8 and 89 M^{-1}. (b) Representative fluorescence spectra of tryptophan (6×10^{-7} M) in pH 7.0 buffer and aqueous 6 M NaCl solution. The quenching of fluorescence due to chloride ions is negligible compared to that of 1-methylimidazole. This demonstrates that complete loss of fluorescence from cellulase in mim Cl is due to the imidazolium cation rather than to the chloride anion. For purposes of comparison, pure mim Cl is 9 M in chloride ion.

The activity of the enzyme was monitored at 65°C in pH 4.8 buffer and in all the eight ionic liquids using cellulose azure as the substrate. The absorbance of the solubilized dye increased with time in pH 4.8 buffer, mim Cl, and HEMA (Figure VI.4); but the initial rate of hydrolysis was much faster in buffer. After one hour, the absorbance due to the liberated dye became constant, whereas it increased monotonically for the two ionic liquids, mim Cl and HEMA. The plateau observed in the absorbance curve for the buffer is not due to the exhaustion of the substrate in the reaction medium, since visibly detectable amounts of unreacted solid cellulose azure remained in the reaction vessel in all of the activity experiments. Because cellulase in buffer denatures, its activity ceases; and no further hydrolysis occurred. On the other hand cellulase remains active and stable in mim Cl and HEMA, and hydrolysis can continue. Cellulase did not show any activity in the other ionic liquids.

Rogers and coworkers [36] have argued that bmim Cl deactivates the enzyme within an hour due to the presence high concentration of chloride ions and interpret the quenching of trytophan fluorescence in that ionic liquid as a signature of denaturation. We found that the tryptophan fluorescence is completely quenched in mim Cl, which is consistent with the reports of Rogers and coworkers for bmim Cl; *but the hydrolysis of cellulose continued even 1 hour after the addition of cellulase in mim Cl.* Negligible hydrolysis of cellulose was observed in the absence of enzyme in mim Cl, contrary to the observation of Vanoye and coworkers, who reported that, owing to its inherent acidity, mim Cl can act both as a catalyst and solvent in the dehydration of fructose. [46] The difference between our work and that of Vanoye and coworkers merits comment. The latter reports on the dehydration of simple sugar molecules, such as fructose and sucrose, to yield 5-hydroxymethylfurfural (HMF)

using the ionic liquid 1-methylimidazolium chloride (mim Cl), in which the latter acts both as a catalyst and solvent. Dehydration of sugars is reported to be catalyzed by acids. [6] Owing to the inherent Brønsted acidity of mim Cl, the dehydration process is facilitated as shown in their work.   Our experiments, on the other hand, deal with a much more complicated polymer, cellulose, as opposed to monomeric sugar units such as glucose, fructose, etc.   Cellulose (Figure VI.1a), as noted earlier, is a polydispersed linear homopolymer of β-(1→4)–glycosidic linked D-anhydroglucopyranose units, with intra- and inter chain hydrogen bonds. Hydrolysis of cellulosic polymer is much more complicated than dehydration of single sugar unit. This is most likely the reason for mim Cl being unable to cause substantial hydrolysis of cellulose (Figure VI.4b).

Furthermore, we monitored the fluorescence intensity of tryptophan in buffer as a function of Cl⁻ and did not observe any quenching even at 1M NaCl. At 6M NaCl (the highest concentration obtainable in water at room temperature), only slight quenching was observed (Figure VI.5). On the other hand, efficient quenching was found on the addition of the cationic moiety of the ionic liquid, 1-methylimidazole (Figure VI.5). A Stern–Volmer quenching plot was biphasic, with $K_{sv} = 3.8$ M^{-1} up to 0.4 M and with $K_{sv} = 89$ M^{-1} from 0.4 to 1 M, which is consistent with the trends reported by Engelborghs and coworkers.[47,48] The efficiency of quenching increases in the presence of positively charged imidazolium cation, due to electron transfer from tryptophan to the imidazolium ring. Thus the quenching of fluorescence from cellulase is not due to chloride ions, but to the imidazolium moiety.

Enzymatic Stability: Calorimetry and Temperature Studies

In order to characterize the behavior and stability of cellulase in the ionic liquids, temperature induced unfolding of the enzymes was studied using optical absorbance and

differential scanning calorimetry measurements.   The stability of cellulase in buffer, mim Cl and HEMA was monitored by recording the absorbance of tryptophan at 280 nm as a function of temperature (Figure VI.6).   Conformational changes have been associated with large absorbance changes as a function of temperature.[49] The buffer solution containing the enzyme turned turbid at 50°C, thus absorbance was recorded until 45°C. In both the ionic liquids, however, no turbidity was observed.   A jump in absorbance was found at temperatures greater than 100°C in HEMA, which probably is an indication of a conformational change in the cellulase; whereas in mim Cl, a monotonic increase of absorbance was observed with temperature. Reversibility of the unfolding of cellulase in the ionic liquid was observed by slow cooling, which led to a drop in the absorbance to the initial value in HEMA which was not observed in mim Cl or in buffer. The precipitated enzyme in buffer did not dissolve on cooling. Thus the cellulase is probably more stable and gains higher heat resistance in the HEMA than in buffer.

Heat flow curves from differential scanning calorimetry (DSC) measurements in Figure VI.7 show thermal unfolding of cellulase in pH 4.8 citrate buffer, mim Cl, and HEMA. The minima in the heat flow curves correspond to $T_{1/2}$, the "transition temperature" where 50% of the enzyme is unfolded. The transition peaks are very broad because of the presence of multiple enzyme components from *T. reesei*. Baker et al. [45] reported DSC studies of four major enzyme components produced *T. reesei,* which are the two endoglucanases, EG I and EG II, and the two cellobiohydrolases, CBH I and CBH II. CBH I, CBH II and EG I have nearly identical transition temperatures at ~ 64°C, whereas the EG II shows a transition temperature at ~ 75°C in pH 4.8 acetate buffer. Our results showed a broad transition peak ranging from 60–75°C in pH 4.8 citrate buffer, which is in good

agreement with those reported by Baker et al. On the other hand, the transition temperature

of cellulase in HEMA shifted to ~ 115–125°C, which suggests that the ionic liquid is

increasing its thermal stability.   Fused transition peaks were also observed in ionic liquids as

in buffer.   An additional small transition peak was observed at ~ 70°C, which is probably

due to early denaturation of a particular component of *T. reesei*. In mim Cl, cellulase showed

multiple transition peaks (75 and 94°C), which are also higher than those observed in pure
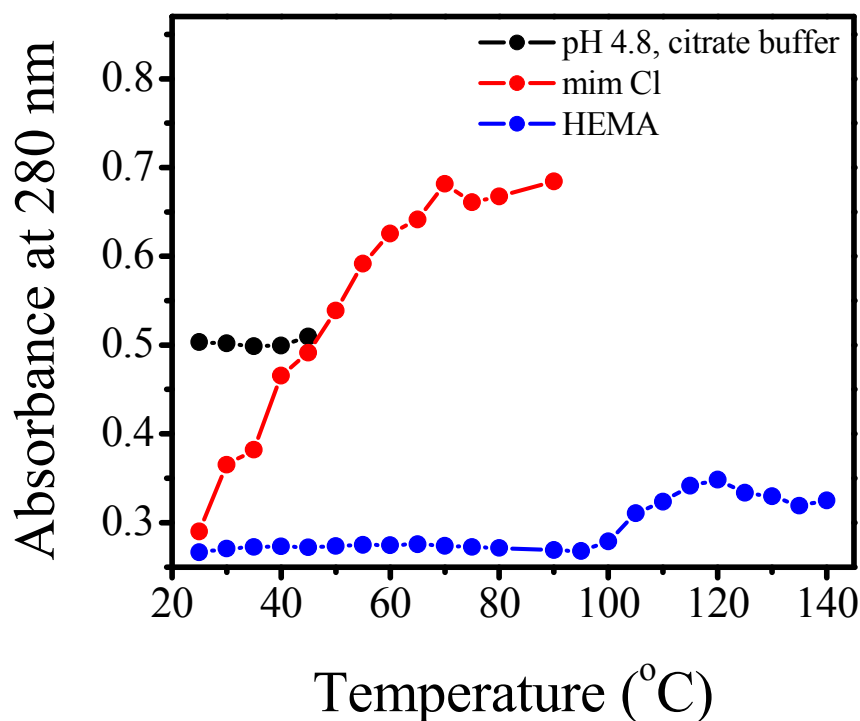
buffer solution.

Figure VI.6. Temperature dependence of absorbance of trytophan in cellulase in buffer, mim Cl, and HEMA. The cellulase precipitates at 50°C in buffer, indicating denaturation of the enzyme and limiting the temperature range for the experiment to 45°C. The transition from the native to the unfolded state was observed at ~ 110°C and is associated with a sudden increase in the absorbance of the enzyme in HEMA. No such denaturation profile was observed in mim Cl.
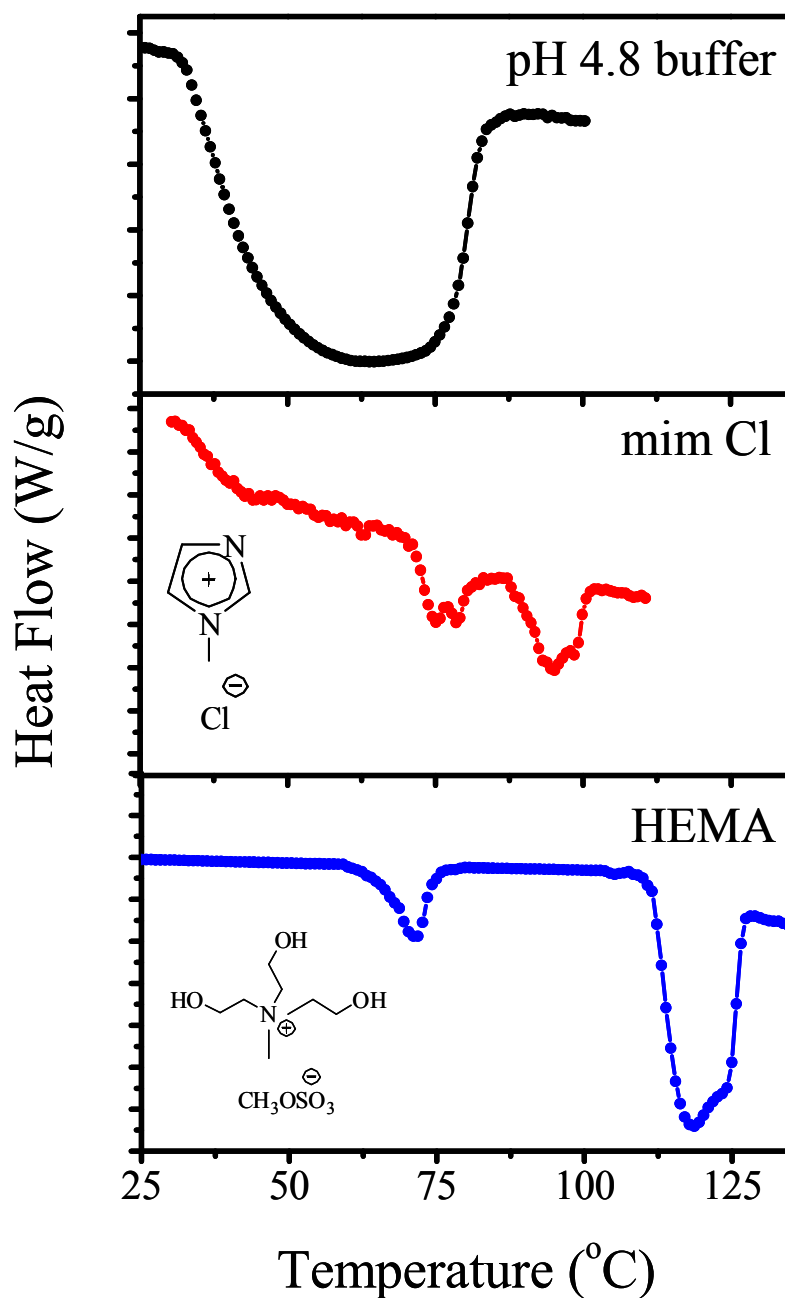
Figure VI.7. DSC heat-flow profiles of cellulase in pH 4.8 citrate buffer (black), mim Cl (red), and in HEMA (blue). Broad transition peaks were obtained due to the presence of multiple cellulase components from *T. reesei* fungus. The transition temperature ($T_{1/2}$) in buffer at ~ 60–75°C, and in ionic liquids at 74–85°C for mim Cl and 115–125°C for HEMA, shows that the ionic liquid imparts higher heat resistance to cellulase enzymes, indicating greater thermal stability.

Reversibility of the unfolding process was checked by gradual cooling of the denatured enzyme from temperatures greater than the $T_{1/2}$. Cellulase unfolding was irreversible in buffer and accompanied by precipitation of the enzyme. In HEMA, reversibility was observed until 120°C. The unfolding process was completely irreversible in mim Cl. These observations are consistent with our absorbance studies (Figure VI.6), confirming that cellulase is more stable and can withstand higher temperatures in the ionic liquids.
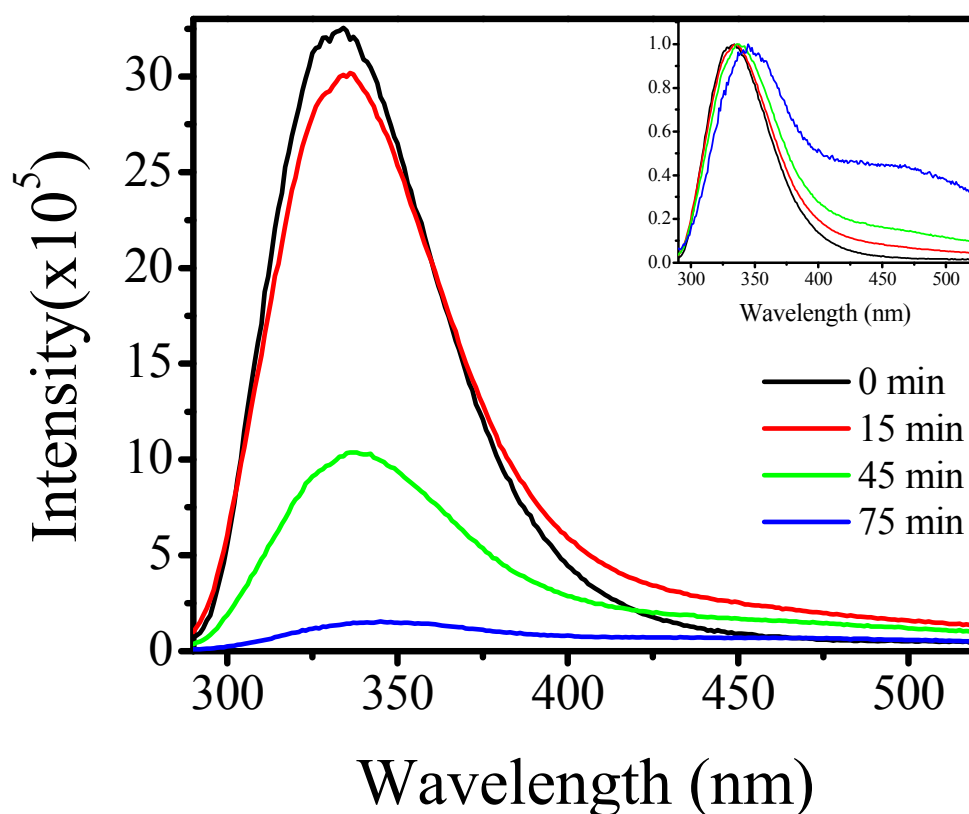
Figure VI.8. Time dependent study of steady state fluorescence intensity of cellulase in HEMA in a microwave oven at 65°C. The samples were excited at 284 nm. The significant quenching and red shift (shown in inset) in the emission suggest that the enzyme is denatured by strong internal heating from the microwave irradiation. Experiments with cellulase in buffer were not performed, since the enzyme denatures and precipitates at $\sim50^{\circ}$C.

Since microwave irradiation has been reported to assist dissolution of cellulose in ionic liquids,[9] cellulase activity in HEMA was also studied using microwave heating at 65°C, but no liberation of the dye was observed even after 2 hours. The fluorescence intensity of cellulase was monitored with time during microwave heating as shown in Figure VI.8 and was quenched drastically with time, accompanied by a red shift of the peak maxima. This is most likely due to internal heating by microwaves, producing a local temperature at the enzymes greater than 100°C, resulting in denaturation.

Enzymatic activity is strongly dependent upon the ionic liquid in which it is dissolved. There have been reports that suggest that ionic liquids can deactivate enzymes. Bmim nitrate, bmim lactate and emim ethylsulfate deactivate enzyme *Candida antarctica* lipase B. [34] Denaturation is likely due to the interaction of different charged groups in the enzyme with the cations and anions in the ionic liquid. [50] Herrmann and coworkers[51] have reported denaturation of Ribonuclease A in different imidazolium based ionic liquids with different anionic combinations and have argued that the stability of the enzyme in ionic liquids is governed by Hofmeister effects. Anions in ionic liquids have been reported to have a more dominant effect than cations for the stability of enzymes. [52] Those with lower hydrogen bond basicity and nucleophilicity are effective for the stability of the enzymes. Baker et al. [53] studied the protein monellin in bmpyro NTf$_2$ using steady-state fluorescence and have reported higher thermodynamic stability (T$_m$~105°C) compared to buffer (~40°C), which is consistent with our observation with cellulase in HEMA. They have suggested that the ionic liquid might significantly alter the hydration level and compactness of the protein structure. Strikingly, we have found that cellulase was unstable and inactive in bmpyro NTf$_2$, in which a dramatic quenching of tryptophan fluorescence was observed.

TABLE VI.1. Viscosity of Various Solvents

Solvent	Temp. (^{o}C)	η (cP) [a]
H$_2$O [55]	20	1.0
	50	0.55
	65	0.43
bmim Cl [56]	30	11000
	70	330
mim Cl	20	9.8 ± 0.2
	30	6.8 ± 0.1
	50	4.2 ± 0.1
	65	3.0 ± 0.1
	85	2.2 ± 0.1
HEMA	20	1460 ± 30
	30	640 ± 8
	50	230 ± 5
	65	110 ± 2
	85	50 ± 1

[a] Viscosity in centipoise for various solvents, including the ionic liquids: 1-butyl-3-methylimidazolium chloride (bmim Cl); 1-methylimidazolium chloride (mim Cl); and tris-(2-hydroxyethyl)-methylammonium methylsulfate (HEMA).

Viscosity plays an important role. As we have seen above, although cellulase is extremely stable and heat resistant in HEMA, its activity is still lower than in buffer. We suggest that this is because of the high viscosity of the ionic liquid (Table VI.I). Although cellulase has been reported to be inactive in chloride containing ionic liquids such as bmim Cl, [36], our studies in mim Cl reveal appreciable activity, which might also be due to its low viscosity relative to other imidazolium ionic liquids with longer alkyl chains, such as bmim Cl. A large viscosity obviously reduces the rate of diffusion, resulting in a lower observed activity of the enzyme. A similar observation by Lozano et al.[54] reveals a reduction in the α-chymotrypsin activity in highly viscous methyltrioctylammonium NTf$_2$ (574 cP) compared to 1-ethyl-3-methylimidazolium NTf$_2$ (34 cP). The viscosities of the six ionic liquids (given in Figure VI.4) in which cellulase did not show any significant activity are all higher than that of mim Cl , but lesser than HEMA. From these data, we suggest that the rate of hydrolysis may depend on the viscosity of the ionic liquid, but it cannot be directly correlated with the activity of the enzyme.

Conclusions

This work provides a detailed study of cellulase activity and stability in various ionic liquids. Among the eight ionic liquids studied here, extensive experiments have been done with mim Cl and HEMA. The former was chosen to compare with the results obtained with bmim Cl reported by Rogers and coworkers. [36] Although cellulase did not fluoresce in mim Cl (consistent with its reported behavior in bmim Cl [36]), it was active in mim Cl, and its activity was higher than that in bmim Cl. The quenching of trytophyl fluorescence in these ionic liquids is due to the high concentration of imidazolium cations and does not necessarily indicate deactivation of the enzyme, as we have observed in case of mim Cl.   The lower

viscosity of mim Cl increases enzymatic activity with respect to bmim Cl. Our studies show that in HEMA the enzyme is stable and thermally resistant even at temperatures close to 100°C; whereas in pH 4.8 buffer, it denatures at ~50°C. Activity assays and DSC studies prove to be powerful and reliable methods to determine the activity and stability of enzymes in different media. Slight differences in the transition temperatures reported are due to the different techniques used to determine its stability. Although microwave heating can dissolve large quantities of cellulose, the enzyme is denatured under these conditions.

In conclusion, of the eight solvents investigated, HEMA is in many ways the most promising. It is a novel, green medium for performing cellulose hydrolysis reactions to convert biomass into biofuels. Because of the thermal stability it imparts to enzymes, its ability to solubilize biomass, and the fact that it does not quench tryptophyl fluorescence (thus permitting monitoring of the enzymes by fluorescence spectroscopy), HEMA provides an ideal starting point for the design of ionic liquids, not only for the hydrolysis of biomass, but for use with a wide spectrum of enzymatic reactions. It is also important to investigate the behavior of the *individual* cellulase components of *T. reesei,* such as the endoglucanases, cellobiohydrolases, etc. in different ionic liquids. This is part of our ongoing studies.

References

(1)   Ladisch, M. R.; Ladisch, C. M.; Tsao, G. T. *Science* **1978**, *201*, 743.

(2)   Lynd, L. R.; Cushman, J. H.; Nichols, R. J.; Wyman, C. E. *Science* **1991**, *251*, 1318.

(3)   Zhang, Y.-H. P.; Lynd, L. R. *Biotechnol. Bioeng.* **2004**, *88*, 797.

(4)   Su, Y.; Brown, H. M.; Huang, X.; Zhou, X.-d.; Amonette, J. E.; Zhang, Z. C. *Appl. Catalysis A* **2009**, *361*, 117.

(5)   Dadi, A. P.; Varanasi, S.; Schall, C. A. *Biotechnol. Bioeng.* **2006**, *95*, 904.

(6)   Zhao, H.; Holladay, J. E.; Brown, H.; Zhang, Z. C. *Science* **2007**, *316*, 1597.

(7)   Xiang, Q.; Lee, Y. Y.; Pettersson, P. O.; Torget, R. W. *Appl. Biochem. Biotechnol.* **2003**, *107*, 505.

(8)   Suganuma, S.; Nakajima, K.; Kitano, M.; Yamaguchi, D.; Kato, H.; Hayashi, S.; Hara, M. *J. Am. Chem. Soc.* **2008**, *130*, 12787.

(9)   Swatloski, R. P.; Spear, S. K.; Holbrey, J. D.; Rogers, R. D. *J. Am. Chem. Soc.* **2002**, *124*, 4974.

(10)   Zhang, H.; Wu, J.; Zhang, J.; He, J. *Macromol.* **2005**, *38*, 8272.

(11)   Phillips, D. M.; Drummy, L. F.; Conrady, D. G.; Fox, D. M.; Naik, R. R.; Stone, M. O.; Trulove, P. C.; Long, H. C. D.; Mantz, R. A. *J. Am. Chem. Soc.* **2004**, *126*, 14350.

(12)   Liu, Q.; Janssen, M. H. A.; Rantwijk, F. v.; Sheldon, R. A. *Green Chem.* **2005**, *7*, 39.

(13)   Murugesan, S.; Linhardt, R. J. *Curr. Org. Synth.* **2005**, *2*, 437.

(14)   Zhu, S.; Wu, Y.; Chen, Q.; Yu, Z.; Wang, C.; Jin, S.; Dinga, Y.; Wu, G. *Green Chem.* **2006**, *8*, 325.

(15)   Remsing, R. C.; Swatloski, R. P.; Rogers, R. D.; Moyna, G. *Chem. Commun.* **2006**, 1271.

(16)   Fort, D. A.; Swatloski, R. P.; Moyna, P.; Rogers, R. D.; Moyna, G. *Chem. Commun.* **2006**, 714.

(17)   Fort, D. A.; Remsing, R. C.; Swatloski, R. P.; Moyna, P.; Moyna, G.; Rogers, R. D. *Green Chem.* **2007**, *9*, 63.

(18)   Kilpelainen, I.; Xie, H.; King, A.; Granstrom, M.; Heikkinen, S.; Argyropoulos, D. S. *J. Agric. Food Chem.* **2007**, *55*, 9142.

(19)   Zhao, H.; Jones, C. L.; Baker, G. A.; Xia, S.; Olubajo, O.; Person, V. N. *J. Biotechnol.* **2009**, *139*, 47.

(20)   Krossing, I.; Slattery, J. M.; Daguenet, C.; Dyson, P. J.; Oleinikova, A.; Weingartner, H. *J. Am. Chem. Soc.* **2006**, *128*, 13427.

(21)   Seddon, K. R. *Nature (Materials)* **2003**, *2*, 363.

(22)   Anderson, J. L.; Ding, J.; Welton, T.; Armstrong, D. W. *J. Am. Chem. Soc* **2002**, *124*, 14247.

(23)   Chowdhury, P. K.; Halder, M.; Sanders, L.; Calhoun, T.; Anderson, J. L.; Armstrong, D. W.; Song, X.; Petrich, J. W. *J. Phys. Chem. B* **2004**, *108*, 10245.

(24)   Headley, L. S.; Mukherjee, P.; Anderson, J. L.; Ding, R.; Halder, M.; Armstrong, D. W.; Song, X.; Petrich, J. W. *J. Phys. Chem. A* **2006**, *110*, 9549.

(25)   Adhikary, R.; Bose, S.; Mukherjee, P.; Thite, A.; Kraus, G. A.; Wijeratne, A. B.; Sharma, P.; Armstrong, D. W.; Petrich, J. W. *J. Phys. Chem. B* **2008**, *112*, 7555.

(26) Mukherjee, P.; Crank, J. A.; Sharma, P. S.; Wijeratne, A. B.; Adhikary, R.; Bose, S.; Armstrong, D. W.; Petrich, J. W. *J. Phys. Chem. B* **2008**, *112*, 3390.

(27) Bose, S.; Wijeratne, A. B.; Thite, A.; Kraus, G. A.; Armstrong, D. W.; Petrich, J., W. *J. Phys. Chem. B* **2009**, *113*, 10825.

(28) Hu, Z.; Margulis, C. J. *Acc. Chem. Res.* **2007**, *40*, 1097.

(29) Rogers, R. D.; Voth, G. A. *Acc. Chem. Res.* **2007**, *40*, 1077.

(30) Remsing, R. C.; Hernandez, G.; Swatloski, R. P.; Massefski, W. W.; Rogers, R. D.; Moyna, G. *J. Phys. Chem. B* **2008**, *112*, 11071.

(31) Park, S.; Kazlauskas, R. J. *Curr. Opin. Biotechnol.* **2003**, *14*, 432.

(32) Lu, Y.; Zhang, Y.-H. P.; Lynd, L. R. *Proc. Natl. Acad. Sci.* **2006**, *103*, 16165.

(33) Lau, R. M.; Rantwijk, F. v.; Seddon, K. R.; Sheldon, R. A. *Org. Lett.* **2000**, *2*, 4189.

(34) Sheldon, R. A.; Lau, R. M.; Sorgedrager, M. J.; Rantwijk, F. v.; Seddon, K. R. *Green Chem.* **2002**, *4*, 147.

(35) Rantwijk, F. v.; Sheldon, R. A. *Chem. Rev.* **2007**, *107*, 2757.

(36) Turner, M. B.; Spear, S. K.; Huddleston, J. G.; Holbrey, J. D.; Rogers, R. D. *Green Chem.* **2003**, *5*, 443.

(37) Kamiya, N.; Matsushita, Y.; Hanaki, M.; Nakashima, K.; Narita, M.; Goto, M.; Takahashi, H. *Biotechnol. Lett.* **2008**, *30*, 1037.

(38) Liying, L.; Hongzhang, C. *Chinese Science Bulletin* **2006**, *51*, 2432.

(39) Jones, P. O.; Vasudevan, P. T. *Biotechnol. Lett.* **2010**, *32*, 103.

(40) Kaar, J. L.; Jesionowski, A. M.; Berberich, J. A.; Moulton, R.; Russell, A. J. *J. Am. Chem. Soc.* **2003**, *125*, 4125.

(41)   Swatloski, R. P.; Holbrey, J. D.; Rogers, R. D. *Green Chem.* **2003**, *5*, 361.

(42)   Fernley, H. N. *Biochem. J.* **1963**, *87*, 90.

(43)   Lai, T. E.; Pullammanappallil, P. C.; Clarke, W. P. *Talanta* **2006**, *69*, 68.

(44)   Lakowicz, J. R. *Principles of fluorescence spectroscopy*, 3rd ed.; Springer: New York, 2004.

(45)   Baker, J. O.; Tatsumoto, K.; Grohmann, K.; Woodward, J.; Wichert, J. M.; Shoemaker, S. P.; Himmel, M. E. *Appl. Biochem. Biotechnol* **1992**, *34-35*, 217.

(46)   Moreau, C.; Finiels, A.; Vanoye, L. *J. Mol. Catal. A: Chem.* **2006**, *253*, 165.

(47)   Willaert, K.; Engelborghs, Y. *Eur. Biophys. J.* **1991**, *20*, 177.

(48)   Vos, R.; Engelborghs, Y. *Photochem. Photobiol.* **1994**, *60*, 24

(49)   Kishore, N. K.; Ranjana. *J. Chem. Thermodynamics* **2001**, *33*, 1325.

(50)   Ru, M. T.; Hirokane, S. Y.; Lo, A. S.; Dordick, J. S.; Reimer, J. A.; Clark, D. S. *J. Am. Chem. Soc.* **2000**, *122*, 1565.

(51)   Constantinescu, D.; Weingartner, H.; Herrmann, C. *Angew. Chem. Int. Ed.* **2007**, *46*, 8887.

(52)   Yang, Z.; Pan, W. *Enzyme Microbial Technol.* **2005**, *37*, 19.

(53)   Baker, S. N.; McCleskey, T. M.; Pandey, S.; Baker, G. A. *Chem. Commun.* **2004**, 940.

(54)   Lozano, P.; de Diego, T.; Guegan, J.-P.; Vaultier, M.; Iborra, J. L. *Biotechnol. Bioeng.* **2001**, *75*, 563.

(55)   Weast, R. C. Viscosity of Water $0^{o}C$ to $100^{o}C$. In *CRC Handbook of Chemistry and Physics*; 53rd ed.; Weast, R. C., Ed.; CRC Press, The Chemical Rubber Co.: Cleaveland, Ohio, 1973; pp F.

(56)   Seddon, K. R.; Stark, A.; Torres, M.-J. Viscosity and density of 1-alkyl-3-methylimidazolium ionic liquids. In *Clean Solvents: Alternative Media for Chemical Reactions and Processing.*; ACS Symposium Series, 2002; Vol. 819; pp 34.

CHAPTER VII. ENHANCED STABILITY AND ACTIVITY OF *Aspergillus niger* CELLULASE IN THE IONIC LIQUID TRIS-(2-HYDROXYETHYL)-METHYLAMMONIUM METHYLSULFATE (HEMA)

Sayantan Bose[1] and Jacob W. Petrich[1,*]

Abstract

We discuss the hydrolysis of cellulose using a pure cellulase: endo-1,4-β-D-glucanase (EG) from the fungus, *Aspergillus niger*, in buffer, the pure ionic liquid, tris-(2-hydroxyethyl)-methylammonium methylsulfate (HEMA), and various mixtures of the two at different temperatures. *A. niger* is an important commercial source of inexpensive cellulase (EG) in the food, textile, and pharmaceutical industries. We have performed steady–state fluorescence and absorbance studies to monitor the stability and activity of EG using cellulose azure as the substrate. We found that EG attains its highest activity at 45˚C in buffer and denatures at ~55˚C. On the other hand, in buffer there is almost no hydrolysis after two hours, whereas, the reaction progresses monotonically in the ionic liquid. Furthermore, HEMA imparts substantial stability to the enzyme, permitting the activity to

---

[1]Departments of Chemistry, Iowa State University; Ames, Iowa 50011 USA.
* Author to whom all correspondence should be addressed.

peak at 75˚C. We discuss the role of temperature on the rate of catalysis and on solution viscosity.

Introduction

Limited reserves of fossil fuels and global climate change have directed increasing attention to the use of renewable biomaterials for energy production. Ethanol produced by the fermentation of glucose is a promising fuel derived from biomass.[1] Its production, however, from edible agricultural feedstocks is problematic.[2] Research has thus focused on its production from cellulose, which is an abundant polymeric raw biomaterial. Consequently, during the past two decades, considerable effort has been devoted to the hydrolysis of cellulose for its ultimate conversion it into fuel. [3-9] There are, however, limitations to this process that are imposed mainly because of the limited solubility of cellulose in water or other organic solvents. Namely, cellulose is a polydispersed linear homopolymer consisting of regio- and enantioselective β-(1→4)–glycosidic linked *D*-anhydroglucopyranose units [5, 10]; and this highly symmetrical polymer is sparingly soluble in most solvents. [11] Thus the traditional dissolution processes are not only cumbersome and expensive, but they also require extreme conditions,[10, 12-15] which in turn may cause serious environmental problems[13, 15, 16] because the solvents they require, such as LiCl/*N,N*-dimethylacetamide, *N*-methylmorpholine-*N*-oxide/water, DMSO/paraformaldehyde, etc., are not only volatile, toxic, and costly; but they also cannot be recovered and reused. [13, 14]

Owing to the high chemical and thermal stability, extremely low volatility,[17] non-inflammability, and high recoverability and reusability[18, 19] of ionic liquids, they have been the focus of green and eco-friendly research over the past decade. These novel compounds have great potential for replacing conventional, volatile, environmentally harmful organic

solvents used in many catalytic and organic reactions. The physical and chemical properties of ionic liquids are highly tunable by making the appropriate modifications to their constituent cations and anions. A variety of fundamental studies[20-26] has been performed on them to obtain a better understanding of their characteristics. Notably, ionic liquids have been reported to dissolve substantial amounts of cellulose.[11, 13, 27-36] Rogers and coworkers[13, 30-32, 37, 38] have carried out comprehensive studies on cellulose dissolution and regeneration in ionic liquids. They found that 1-butyl-3-methylimidazolium chloride (bmim Cl) was the most effective in dissolving cellulose; and they attributed this effect to strong hydrogen bonding interactions of the hydroxyl groups with the halide anions, [13, 30-32, 37] consistent with the report of Zhang et al. [14] for 1-allyl-3-methylimidazolium chloride (amim Cl). Sheldon and coworkers have shown high solubility of di- and polysaccharides in ionic liquids containing dicyanamide anions. [28] More recently it has been found that *Bombyx mori* silk, fibroin, [27] and hard and soft woods [33] are readily solubilized in imidazolium based ionic liquids.
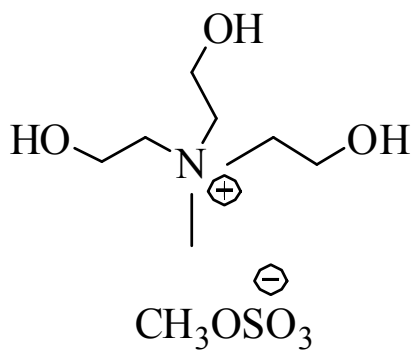

Figure VII.1. Structure of tris-(2-hydroxyethyl)-methylammonium methylsulfate (HEMA).

Employing enzymes with ionic liquids for cellulose hydrolysis is another step in making the entire process green. [7, 39-46] Enzymes have been reported to exhibit increased stability in ionic liquids, as opposed to common organic solvents.[43, 47] Furthermore, recycling and reusing enzymes in ionic liquids [45, 48-50] is an additional advantage enabling continuous processing. The most thoroughly studied enzyme in ionic liquids is *Candida antarctica* lipase B (Cal B), used to catalyze transesterification reactions.[43-45, 51] While the hydrophobic effect that increases protein stabilization is absent in organic ionic liquids, one advantage to biocatalysis in ILs as opposed to aqueous buffers is the longer activity of enzymes in ILs, which is thought to arise from the slow breaking and remaking of hydrogen bonds in the non-aqueous medium. [52] There are also some reports of enzyme activity in mixtures of water and ionic liquids. An early study of alkaline phosphatase from *E. coli* in aqueous mixtures of ethylammonium nitrate (EAN) showed maximum activity at 10% EAN. Further addition of EAN reduced activity, and none was observed at 80% EAN. [53] Chloroperoxidase (CPO) from *Caldariomyces fumago* was used to catalyze a sulfoxidation reaction in aqueous mixtures containing up to 70% of hydroxyethyltrimethylammonium (HOEtMe$_3$N) citrate ionic liquid. CPO also tolerated up to 70% of 1,3-dimethylimidazolium dimethylphosphate (mmim Me$_2$PO$_4$). There was a significant dip in activity at 30% ionic liquid and a maximum at 50%.[54] Kaftzik et al. have reported that while triethylammonium methylsulfate (Et$_3$NH MeSO$_4$) deactivated enzymes, such as formate dehydrogenase (CbFDH) from *Candida boidinii* and the β-galactosidase from *Bacillus circulans*, a similar ionic liquid, triethylmethylammnoium methylsulfate (Et$_3$MeN MeSO$_4$), was tolerated by CbFDH with 55% residual activity in 50% aqueous medium.[55] Recent reports by Sapra and coworkers showed higher tolerance of purified endoglucanase from a hyperthermophilic

bacterium, *Thermatoga maritima*, and a hyperthermophilic archaeon, *Pyrococcus horikoshii*, towards the ionic liquid, 1-ethyl-3-methylimidazolium acetate (emim OAc), compared to that of the industrial benchmark, *Trichoderma viride* cellulase, in the same ionic liquid. [56]

In our recent work,[46] we have shown that a commercial preparation (GC 220) consisting of a mixture of endoglucanases and cellobiohydrolases from *Tricoderma reesei* gained significantly enhanced stability in two ionic liquids: 1-methylimidazolium chloride (mim Cl) and tris-(2-hydroxyethyl)-methylammonium methylsulfate (HEMA). While hydrolysis at 65˚C was initially much faster in buffer than in these two liquids, it reached a plateau after two hours. On the other hand, the hydrolysis progressed monotonically in the two ionic liquids. This difference in the rate of hydrolysis was largely attributed to two factors: first, the viscosity of the ionic liquids is greater than that of the buffer; and second, the enzymes are irreversibly denatured at 50˚C in buffer, while they are stable to temperatures greater than 100˚C in HEMA. This work motivated us to initiate a study of a pure cellulase component in HEMA and to explore its activity for the saccharification of cellulose.

Here, we describe new studies made with a *pure* cellulase: endo-1,4-β-*D*-glucanase (EG) from the fungus, *Aspergillus niger,* in buffer, in neat HEMA, and in various mixtures at different temperatures. *A. niger* is an important commercial source of inexpensive cellulase[57] (EG) in the food, textile, and pharmaceutical industries. [58] Several properties of EG from *A. niger* have already been well characterized, such as substrate specificity and optimum temperature and pH for its activity.[59-62] We have performed steady–state fluorescence and absorbance studies to monitor the stability and activity of EG using cellulose azure as the substrate. We found that EG attains its highest activity at 45˚C in buffer and denatures at

~55˚C. On the other hand, HEMA imparts substantial stability, permitting the activity to peak at 75˚C. Finally, we studied the activity of EG in aqueous mixtures of the ionic liquid as a function of temperature and viscosity.

Experimental

Materials and Methods. A pure cellulase component, endo-1,4-β-*D*-glucanase (EG) (EC 3.2.1.4), from the fungus, *Aspergillus niger,* was purchased from Megazyme, Ireland, was reported to show a single band on SDS PAGE, and was used without further purification. The enzyme was equilibrated in pH 4.8 citrate buffer prior to any experiments. Cellulose azure from Sigma Aldrich, which although may not be used for quantitative purposes but is appropriate for comparative activity studies,[74] was washed multiple times with deionized water to eliminate any unbound dye particles from the surface of cellulose, and was dried before using. (It is made from purified cotton linters and then covalently tagged with remazol brilliant violet dye.) Upon hydrolysis of cellulose, the dye is solubilized and its absorbance reports on the activity of the enzyme. The room temperature ionic liquid used in this study is tris-(2-hydroxyethyl)-methylammonium methylsulfate (HEMA, Figure VII.1) obtained from Sigma Aldrich. HEMA was not dried before using, since aqueous enzyme solution was introduced before performing experiments. Coumarin 153 (C153) (Exciton Inc., Dayton, OH) was used as received. Acetonitrile (HPLC grade), methanol (HPLC grade), and acetone were purchased from Aldrich and were used as received. Viscosity measurements were made with a ViscoLab 4000 piston style viscometer from Cambridge Applied system at desired temperatures.

Steady-State Measurements. Steady-state fluorescence spectra were obtained on a Spex Fluoromax-4 with a 3-nm bandpass and corrected for lamp spectral intensity and detector

response. A temperature dependent study of fluorescence from cellulase in pH 4.8 buffer and HEMA was performed from 20°C to 105°C, with spectra obtained at 5° intervals. The cellulase concentration was maintained at 5×10^{-7} M. All cellulase samples were excited either at 284 or 295 nm and identical spectra were obtained at both wavelengths. Coumarin 153 samples were excited at 407 nm and the emission was collected in range of 430–800 nm with a 2-nm bandpass. Steady-state absorption spectra for the cellulase activity experiments were obtained on a Varian Cary 100 Bio UV-visible spectrophotometer with 1-nm resolution equipped with a Peltier temperature controller. EG activity was monitored in binary mixtures of buffer and HEMA (0%, 10%, 50%, and 100%). All the activity measurements were done in a double-beam spectrometer, where both sample and reference cells were maintained at identical conditions. The latter contained substrate without enzyme for automatic subtraction of the absorbance of the liberated dye (if any) in the absence of enzyme. Temperature dependent studies at 45, 55, 65 and 75°C were performed in all the solvent systems. The concentration of cellulose azure was maintained at 1.5 mg/mL, and the enzyme concentration was 4.8×10^{-6} M for all the activity measurements. For both fluorescence and absorption measurements, a 1-cm path-length quartz cuvette was used.

Results and Discussions

Steady-state fluorescence from endo-1,4-β-*D*-glucanase (EG) obtained from *A. niger* was monitored in pH 4.8 citrate buffer and HEMA as a function of temperature from 20°C to 105°C. EG in HEMA had a higher fluorescence quantum yield at all temperatures compared to that in buffer. Quenching of fluorescence from tryptophan residues in EG was observed in both solvents. Significant fluorescence quenching at 50°C, accompanied by precipitation of
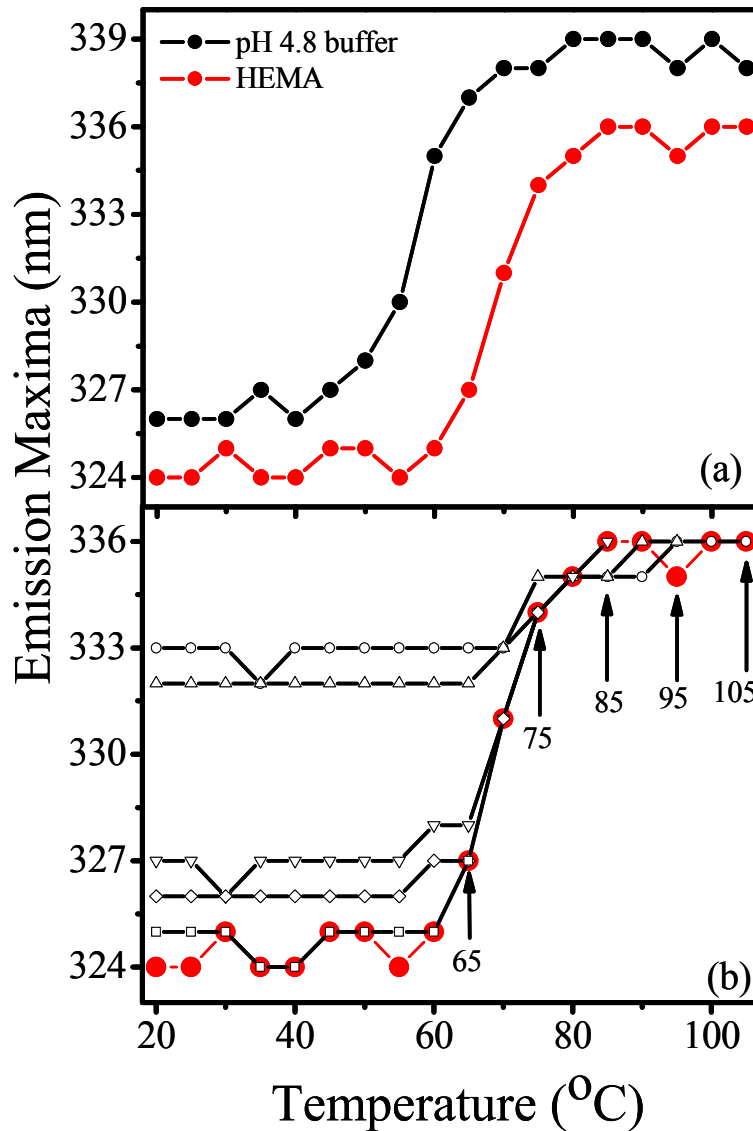
Figure VII.2. (a) Shift in the maximum of tryptophan fluorescence from *A. niger* endoglucanase (EG) with temperature in pure pH 4.8 citrate buffer and HEMA. The red shift is associated with the unfolding of the enzyme. The transition temperature of EG in HEMA is higher than that in buffer, indicating greater thermal stability of the enzyme in the ionic liquid. (b) Cooling of the enzyme in HEMA, starting from temperatures 105, 95, 85, 75 and 65˚C (indicated by arrows), produces different blue shifts. The unfolding of EG was completely reversible up to 65˚C, whereas partial reversibility was observed at temperatures greater than 75˚C.

the enzyme in buffer, indicated its denaturation. Such quenching did not occur until 75°C in

HEMA, indicating that the ionic liquid imparts a higher thermal stability to EG. Precipitation

of EG was not observed in HEMA, which speaks to the ability of the ionic liquid to

solubilize the denatured protein. (It is important to note, as we have discussed in detail, [46]

that *in itself*, fluorescence quenching is not necessarily a signature of denaturation. It is

possible that there are nonradiative processes between the aromatic amino acid residues of

the enzyme and the solvent that quench the fluorescence without perturbing the protein's
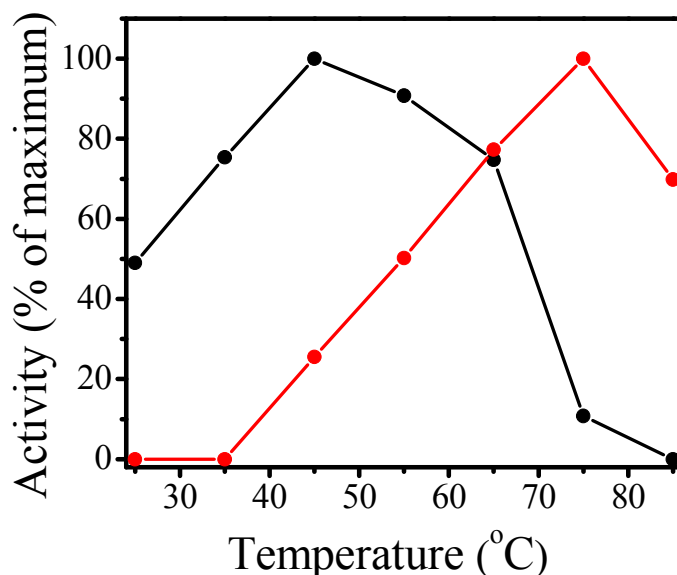
structure of function.)

Figure VII.3.   The variation of the relative percent activity of endoglucanase in pH 4.8 citrate buffer (•) and HEMA (•) as a function of temperature (25 - 85°C) measured after 2 hours using cellulose azure as the enzyme assay. The activity of endoglucanase peaked (arbitrarily taken as 100% activity) at 45°C in buffer whereas in HEMA, the maximum activity was at 75°C.

The fluorescence emission maximum of EG was monitored in buffer and HEMA

(Figure VII.2a). At room temperature, it is 326 nm in buffer and 324 nm in HEMA. In

buffer the emission maximum undergoes a large red-shift (326 to 339 nm) at ~ 55°C;
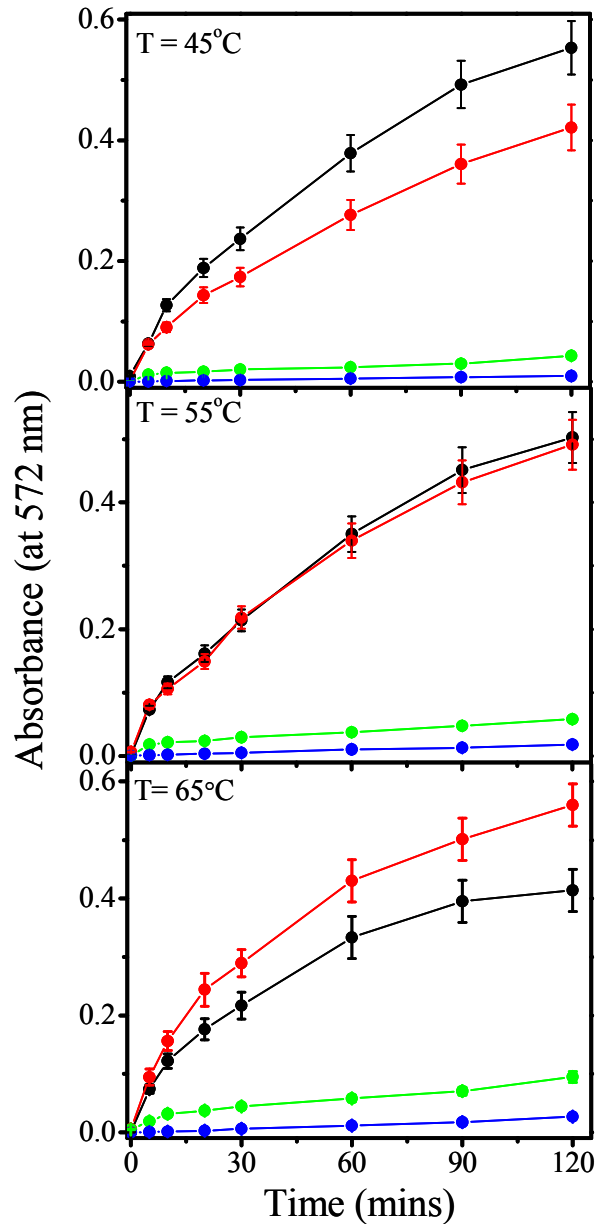
Figure VII.4. Endoglucanase activity at 45, 55, and 65˚C as monitored via the absorbance of cellulose azure (1.5 mg/mL) at 572 nm for 2 hours in pure (•-black) and mixtures of HEMA (10% •-red, 50% •-green, 100% •-blue) and buffer. In buffer, cellulase showed maximum activity at 45˚C, which is represented by higher absorbance of the liberated dye, which decreased with increasing percentages of HEMA. We attribute this to the relative viscosities of the solvents. On the other hand, in buffer there is almost no hydrolysis after two hours (i.e., the absorbance reaches a plateau) at 65˚C, whereas, the reaction progresses monotonically in pure HEMA and mixtures at all temperatures. Error bars are determined from triplicate measurements.

whereas a corresponding large red shift (324 to 336 nm) is not observed until ~75°C in HEMA. This again indicates the higher thermal stability of EG in HEMA.

Reversibility of the unfolding process of the enzyme was studied in HEMA by gradual cooling, starting from different elevated temperatures as indicated by the arrows in Figure VII.2b. On cooling, a gradual blue-shift of the emission maxima was observed. The extent of the blue shift (i.e., the extent of the return to native conditions) depended on the starting temperature. Cooling from 95 and 105°C resulted in blue shifts from 336 to 333 nm. The native conformation of the enzyme corresponds to λ_{max} = 324 nm in HEMA. Partially folded structures of the enzyme, with λ_{max} ~326 nm, were attained when cooled from 75 – 85 °C. The enzyme completely folded back to its native conformation when cooled down from 65°C. This leads us to conclude that enzyme unfolding is completely reversible until 65°C, whereas partial reversibility was obtained up to temperatures as high as 75 – 85°C. Irreversible denaturation occurred beyond 85°C. On the contrary complete recovery of fluorescence intensity was observed on cooling the enzyme in HEMA irrespective of the starting temperature. This suggests that fluorescence intensity quenching cannot be reliably considered as a signature of protein denatuation, which is consistent with our previous studies. [46]

Endoglucanase activity was studied at four different temperatures (45, 55, 65, and 75°C) using cellulose azure as a substrate in different mixtures of HEMA and pH 4.8 citrate buffer, namely, 0, 10, 50, and 100% HEMA. The progress of EG-catalyzed hydrolysis of cellulose was monitored as a function of the absorbance of the liberated dye with time. The liberated dye showed three different peaks at 250, 323 and 572 nm. For all the activity

measurements, the absorbance at 572 nm was monitored, although there was a slight shift in optical absorbance spectra in increasing proportions of the ionic liquid in buffer. The percent of maximum activity of EG in pure pH 4.8 buffer and in HEMA after 2 hours is shown in Figure VII.3. In buffer, the activity peaked at 45°C, drastically dropped to 10% at 75°C, and finally decayed to zero at 85°C. Even though the enzyme is in its native state in buffer at 25°C and 35°C, the lower activity indicates that the optimum temperature for the enzyme provides a balance between the catalytic rate and the rate of enzyme denaturation. Earlier reports by Hurst et al. showed that a cellulolytic enzyme from *A. niger* had a maximum activity at 45°C at pH 4.0, which diminished to almost zero beyond 65°C. [62] Okada reported the optimum pH and temperature to be 4.0 and 45~50°C for a pure cellulase from *A. niger*. The enzyme was completely stable over the range of pH 5.0~8.0 at 4°C for 24 hours, and retained about 50% of its original activity after heating at 70°C for 10min. [63] On the other hand in HEMA, the activity was maximal at 75°C, and then dropped to 75% of this value at 85°C. The initial lower activity at low temperatures in HEMA may be due to its high viscosity of 1460 cP at 20°C (see below).

Figure VII.4 presents a plot of the absorbance (at 572 nm) of the liberated dye for up to 2 hours in different mixtures of buffer and HEMA at different temperatures. In pure buffer, EG activity peaked at 45°C, and drastically dropped at temperatures greater than 65°C. In pure HEMA, its activity peaked at 75°C and decreased at higher temperatures. At 45°C, EG activity decreased with increasing concentration of HEMA. However, at 65 and 75°C the EG activity curve increased monotonically in aqueous HEMA mixtures, whereas in pure buffer it levels off after 1.5 hours. Comparing relative activities of the enzyme for

various HEMA/buffer mixtures, the highest activity was at 65°C for 10% and 50% HEMA.

EG activity after 2 hours decreased in the order 65 > 55 > 45 > 75°C for 10% HEMA and 65
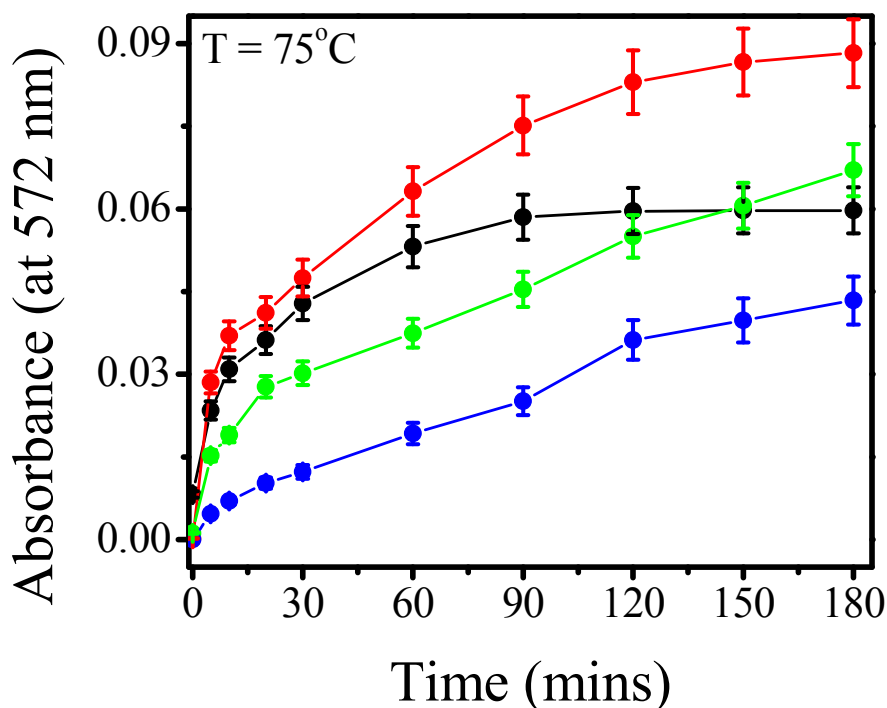
> 55 ≅ 75 > 45°C for 50% HEMA.

Figure VII.5. Endoglucanase activity at 75˚C as monitored via the absorbance of cellulose azure (1.5 mg/mL) at 572 nm in pure (●-black) and mixtures of HEMA (10% ●-red, 50% ●-green, 100% ●-blue) and buffer for 3 hours. Activity in both 10% and 50% HEMA exceeds that in pure buffer after 3 hours, whereas the hydrolysis ceases in the latter after 1.5 hours. Error bars are determined from triplicate measurements.

Studies at 75°C (Figure VII.5) indicated the highest EG activity at 10% HEMA.

While the activity plot flattens out after 1.5 hours in pure buffer, the hydrolysis continued

even after 2 hours in the presence of HEMA. After 2 hours, the activity in 50% HEMA

equalized with that in pure buffer. At longer times, hydrolysis continues in 50% HEMA but

it plateaus (i.e., ceases) in the pure buffer. These observations indicate that the ionic liquid

imparts an additional stability to the enzyme at higher temperatures. Our results are not

consistent with those obtained by Rogers and coworkers, who reported that the concentration of ionic liquid, 1-butyl-3-methylimidazolium chloride (bmim Cl), is inversely proportional to the activity of cellulase in aqueous bmim Cl mixtures.[39] Apart from studies at 45°C, we observed equal or higher activity with addition of HEMA in water. HEMA does not have a significant Brønsted acidity, unlike triethylammonium methylsulfate,[55] and thus helps to keep the enzyme active without altering the acidity of the medium.
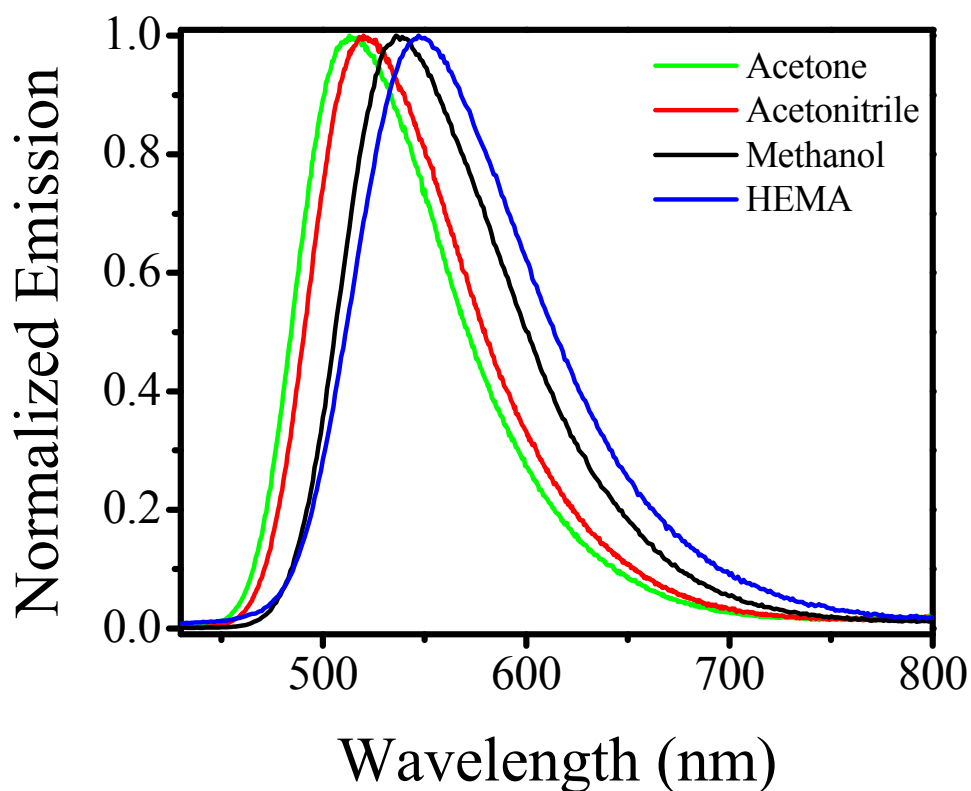

Figure VII.6. Normalized steady-state emission spectra of C153 in different solvents. The fluorescence spectra were obtained by exciting the sample at 407 nm with a 2-nm bandpass. From the peak maxima, the order of polarity of the solvents is: acetone < acetonitrile < methanol < HEMA.

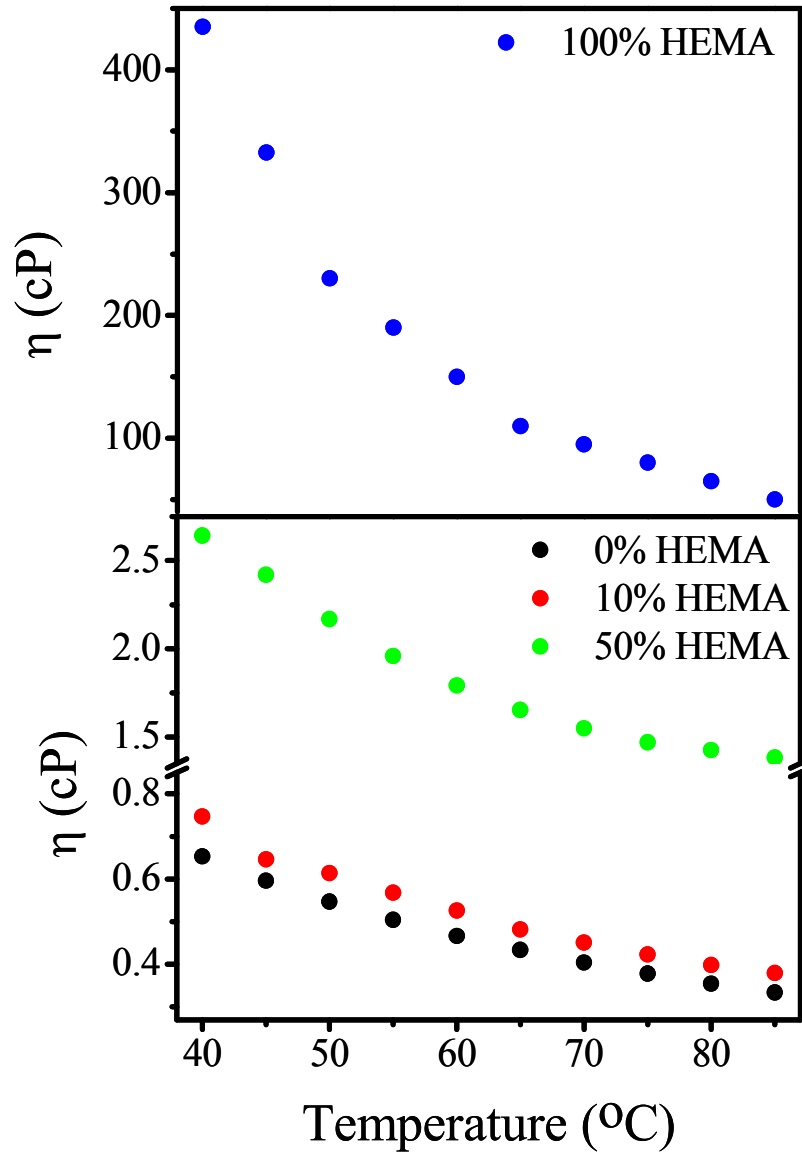**Figure VII.7.** Plot of viscosity as a function of temperature for buffer, HEMA, and buffer/HEMA mixtures. Pure HEMA is extremely viscous (~ 330 cP) compared to buffer (~ 0.6 cP) at 45˚C. The viscosity activation energies of the different solvent systems determined from the slope of the plot of $\ln(1/\eta)$ versus $1/T$ are 10.3, 4.0, 3.1 and 3.0 kcal/mol for 100%, 50%, 10% and 0% HEMA in buffer, respectively.

Unlike organic solvents, ions constituting the ionic liquids have strong interactions with water molecules. Depending on their size and charge density, they stabilize or destabilize the water structure around the enzyme,[64, 65] which in turn influences the stability and activity of the enzymes.[66] But these effects vary from one enzyme to other. For example whereas methylsulfate ($MeSO_4^-$) anion in HEMA imparted extreme stability to cellulase, [46] it proved to be detrimental for other enzymes such as penicillin G amidase, [65] Cal B, [51] and β-galactosidase. [55]

Polarity of the medium in which the enzyme is studied is also crucial for its stability and activity. [52, 65] In order to determine the relative polarity of the ionic liquids studied here, steady-state emission spectra of coumarin 153 (C153) have been obtained in a series of organic solvents and ionic liquid, as shown in Figure VII.6. C153 is an extremely well studied solvatochromic probe, whose emission is highly sensitive to solvent polarity. Polarity was found to increase in the order of acetone < acetonitrile < methanol < HEMA.

The rate of hydrolysis of cellulose is also dependent on the viscosity of the medium. [46, 67-69] A higher viscosity obviously reduces the rate of diffusion of the enzyme to the substrate, resulting in a lower observed activity. Figure VII.7 compares the viscosities of the solvent systems studied at different temperatures. That of pure HEMA is much higher than those of pure buffer and of the binary mixtures at all temperatures. In general, ionic liquids have higher viscosities than most commonly used organic solvents.[70] In addition to hydrogen bonding interactions, strong intermolecular forces between charged ions are responsible for their high viscosity.[17, 25, 70-72]

At 45°C, where EG showed its highest activity in pure buffer with decreasing activity upon addition of HEMA, this can be attributed to increasing viscosity (Figures VII.4 and

VII.7). A similar observation by Lozano et al.[73] reveals a reduction in the α-chymotrypsin activity in highly viscous methyltrioctylammonium NTf_2 (574 cP) compared to that in 1-ethyl-3-methylimidazolium NTf_2 (34 cP). It is significant that we did not observe this trend at the higher temperatures of 55, 65 and 75°C. For 10% HEMA the activity was greater than that in pure buffer at 55 and 65°C. This is because the viscosities of pure buffer and 10% HEMA solution are nearly equal at these temperatures (Figure VII.7), and thus the increase in EG activity is solely due to the enhanced stabilization provided by HEMA. The viscosity activation energy of pure HEMA and pure buffer were determined to be 10.3 and 3.0 kcal/mol respectively. Owing to the higher activation energy in HEMA, EG activity is obviously lower than that in buffer at 45°C.

The situation is different at 75°C, where not only in 10% but also in 50% HEMA solution, cellulase showed enhanced activity compared to that in pure buffer after 3 hour period. Even though the viscosity of 50% HEMA is ~ 4 times higher that of pure buffer, the stability that HEMA imparts to EG results in its higher activity, overcoming the barrier of activation due to viscosity. Thus the resultant activity of cellulase and the rate of hydrolysis of cellulosic polymers is governed by both factors: the stability of the enzyme in the solvent and the inherent viscosity of the solvent.

Conclusion

This work provides a detailed study of EG stability and activity in buffer, HEMA, and their binary mixtures at different temperatures. Motivated by our recent work, in which we have established that HEMA imparts considerable thermal stability to cellulases from *T. reesei*, we have focused on studying the behavior of a pure cellulose, EG from *A. niger,* rather than a mixture, as we did in our previous work.[46] From fluorescence studies, we

conclude that the enzyme denatures and precipitates at ~55°C in buffer, whereas the transition temperature shifts to ~75°C in HEMA, which show that the enzyme gains higher heat tolerance in the ionic liquid. We found that the activity of the enzyme was highest at 45°C in pH 4.8 buffer and then drastically decreased at temperatures greater than 65°C and that the temperature optimum for the enzyme is a balance between the effect of temperature on catalytic rate and on the rate of enzyme denaturation. Studies in aqueous HEMA mixtures showed enhanced activity of the EG in the presence of HEMA, which varied with temperature. While identical EG activity was observed at 55°C in buffer and 10% HEMA, at 65 and 75°C, the activity in 10% HEMA exceeded that in pure buffer. The viscosity of the solvent is a crucial factor determining the rate of hydrolysis, and we have shown that increasing the viscosity reduces the rate of the hydrolysis reaction and thus decreases the activity, which is borne out from the lower activity in HEMA in spite of the latter imparting higher stability to the enzyme. On the contrary, even though 50% HEMA solution is more viscous than pure buffer, the enzyme showed higher activity in the former, which we have attributed to the higher thermal stability that HEMA imparts to the enzyme. This thus reaffirms our hypothesis that the enzymatic activity is a compromise between both enzyme stability in a particular solvent and temperature and the viscosity of the medium, since a direct correlation between activity and solvent viscosity could not be established.

To our knowledge this is the first study dealing with a pure endoglucanase from commercial *A. niger,* which not only shows higher tolerance to ionic liquids such as HEMA but also whose thermostability is markedly enhanced in the presence of the ionic liquid. As a result HEMA proves to be a novel, green medium for performing cellulose hydrolysis reactions to convert biomass into biofuels. Because of the thermal stability it imparts to

enzymes, it provides an ideal starting point for the design of ionic liquids, not only for the hydrolysis of biomass, but for use with a wide spectrum of enzymatic reactions.

References

1. A. J. Ragauskas, C. K. Williams, B. H. Davison, G. Britovsek, J. Cairney, C. A. Eckert, W. J. Frederick, Jr., J. P. Hallett, D. J. Leak, C. L. Liotta, J. R. Mielenz, R. Murphy, R. Templer and T. Tschaplinski, *Science*, 2006, **311**, 484-489.

2. R. Kumar, S. Singh and O. V. Singh, *J. Ind. Microbiol. Biotechnol.*, 2008, **35**, 377-391.

3. M. R. Ladisch, C. M. Ladisch and G. T. Tsao, *Science*, 1978, **201**, 743-745.

4. L. R. Lynd, J. H. Cushman, R. J. Nichols and C. E. Wyman, *Science*, 1991, **251**, 1318-1323.

5. Y.-H. P. Zhang and L. R. Lynd, *Biotechnol. Bioeng.*, 2004, **88**, 797–824.

6. Y. Su, H. M. Brown, X. Huang, X.-d. Zhou, J. E. Amonette and Z. C. Zhang, *Appl. Catalysis A*, 2009, **361**, 117-122.

7. A. P. Dadi, S. Varanasi and C. A. Schall, *Biotechnol. Bioeng.*, 2006, **95**, 904-910.

8. H. Zhao, J. E. Holladay, H. Brown and Z. C. Zhang, *Science*, 2007, **316**, 1597-1600.

9. Q. Xiang, Y. Y. Lee, P. O. Pettersson and R. W. Torget, *Appl. Biochem. Biotechnol.*, 2003, **107**, 505-514.

10. T. Heinze and T. Liebert, *Prog. Polym. Sci.*, 2001, **26**, 1689–1762.

11. S. Zhu, Y. Wu, Q. Chen, Z. Yu, C. Wang, S. Jin, Y. Dinga and G. Wu, *Green Chem.*, 2006, **8**, 325–327.

12. S. Suganuma, K. Nakajima, M. Kitano, D. Yamaguchi, H. Kato, S. Hayashi and M. Hara, *J. Am. Chem. Soc.*, 2008, **130**, 12787–12793.

13. R. P. Swatloski, S. K. Spear, J. D. Holbrey and R. D. Rogers, *J. Am. Chem. Soc.*, 2002, **124**, 4974-4975.

14. H. Zhang, J. Wu, J. Zhang and J. He, *Macromol.*, 2005, **38**, 8272-8277.

15. J. Wu, J. Zhang, H. Zhang, J. He, Q. Ren and M. Guo, *Biomacromol.*, 2004, **5**, 266-268.

16. N. Reddy and Y. Yang, *Green Chem.*, 2005, **7**, 190-195.

17. I. Krossing, J. M. Slattery, C. Daguenet, P. J. Dyson, A. Oleinikova and H. Weingartner, *J. Am. Chem. Soc.*, 2006, **128**, 13427-13434.

18. K. R. Seddon, *Nature (Materials)*, 2003, **2**, 363-365.

19. J. L. Anderson, J. Ding, T. Welton and D. W. Armstrong, *J. Am. Chem. Soc*, 2002, **124**, 14247-14254.

20. P. K. Chowdhury, M. Halder, L. Sanders, T. Calhoun, J. L. Anderson, D. W. Armstrong, X. Song and J. W. Petrich, *J. Phys. Chem. B*, 2004, **108**, 10245-10255.

21. L. S. Headley, P. Mukherjee, J. L. Anderson, R. Ding, M. Halder, D. W. Armstrong, X. Song and J. W. Petrich, *J. Phys. Chem. A*, 2006, **110**, 9549-9554.

22. R. Adhikary, S. Bose, P. Mukherjee, A. Thite, G. A. Kraus, A. B. Wijeratne, P. Sharma, D. W. Armstrong and J. W. Petrich, *J. Phys. Chem. B*, 2008, **112**, 7555-7559.

23. P. Mukherjee, J. A. Crank, P. S. Sharma, A. B. Wijeratne, R. Adhikary, S. Bose, D. W. Armstrong and J. W. Petrich, *J. Phys. Chem. B*, 2008, **112**, 3390-3396.

24. S. Bose, A. B. Wijeratne, A. Thite, G. A. Kraus, D. W. Armstrong and J. Petrich, W., *J. Phys. Chem. B*, 2009, **113**, 10825–10829.

25. Z. Hu and C. J. Margulis, *Acc. Chem. Res.*, 2007, **40**, 1097–1105.

26. R. D. Rogers and G. A. Voth, *Acc. Chem. Res.*, 2007, **40**, 1077-1078.

27. D. M. Phillips, L. F. Drummy, D. G. Conrady, D. M. Fox, R. R. Naik, M. O. Stone, P. C. Trulove, H. C. D. Long and R. A. Mantz, *J. Am. Chem. Soc.*, 2004, **126**, 14350-14351.

28. Q. Liu, M. H. A. Janssen, F. v. Rantwijk and R. A. Sheldon, *Green Chem.*, 2005, **7**, 39-42.

29. S. Murugesan and R. J. Linhardt, *Curr. Org. Synth.*, 2005, **2**, 437-451.

30. R. C. Remsing, R. P. Swatloski, R. D. Rogers and G. Moyna, *Chem. Commun.*, 2006, 1271-1273.

31. D. A. Fort, R. P. Swatloski, P. Moyna, R. D. Rogers and G. Moyna, *Chem. Commun.*, 2006, 714-716.

32. D. A. Fort, R. C. Remsing, R. P. Swatloski, P. Moyna, G. Moyna and R. D. Rogers, *Green Chem.*, 2007, **9**, 63-69.

33. I. Kilpelainen, H. Xie, A. King, M. Granstrom, S. Heikkinen and D. S. Argyropoulos, *J. Agric. Food Chem.*, 2007, **55**, 9142–9148.

34. H. Zhao, C. L. Jones, G. A. Baker, S. Xia, O. Olubajo and V. N. Person, *J. Biotechnol.*, 2009, **139**, 47-54.

35. A. Pinkert, K. N. Marsh, S. Pang and M. P. Staiger, *Chem. Rev.*, 2009, **109**, 6712–6728.

36. C. Li, Q. Wang and Z. K. Zhao, *Green Chem.*, 2008, **10**, 177–182.

37. R. C. Remsing, G. Hernandez, R. P. Swatloski, W. W. Massefski, R. D. Rogers and G. Moyna, *J. Phys. Chem. B*, 2008, **112**, 11071–11078.

38. M. Mazza, D.-A. Catana, C. Vaca-Garcia and C. Cecutti, *Cellulose*, 2009, **16**, 207–215.

39. M. B. Turner, S. K. Spear, J. G. Huddleston, J. D. Holbrey and R. D. Rogers, *Green Chem.*, 2003, **5**, 443–447.

40. N. Kamiya, Y. Matsushita, M. Hanaki, K. Nakashima, M. Narita, M. Goto and H. Takahashi, *Biotechnol. Lett.*, 2008, **30**, 1037-1040.

41. L. Liying and C. Hongzhang, *Chinese Science Bulletin*, 2006, **51**, 2432-2436.

42. P. O. Jones and P. T. Vasudevan, *Biotechnol. Lett.*, 2010, **32**, 103-106.

43. R. M. Lau, F. v. Rantwijk, K. R. Seddon and R. A. Sheldon, *Org. Lett.*, 2000, **2**, 4189-4191.

44. R. A. Sheldon, R. M. Lau, M. J. Sorgedrager, F. v. Rantwijk and K. R. Seddon, *Green Chem.*, 2002, **4**, 147-151.

45. S. Park and R. J. Kazlauskas, *Curr. Opin. Biotechnol.*, 2003, **14**, 432-437.

46. S. Bose, D. W. Armstrong and J. W. Petrich, *J. Phys. Chem. B*, 2010, **114**, 8221-8227.

47. P. Lozano, T. d. Diego, D. Carrié, M. Vaultier and J. L. Iborra, *Chem. Commun.*, 2002, 692 - 693.

48. S. Park and R. J. Kazlauskas, *J. Org. Chem.*, 2001, **66**, 8395–8401.

49. T. Itoh, E. Akasaki, K. Kudo and S. Shirakami, *Chem. Lett.*, 2001, **30**, 262-263.

50. E. Feher, B. Major, K. Belafi-bako and L. Gubicza, *Biochem. Soc. Trans.*, 2007, **35**, 1624-1627.

51. R. M. Lau, M. J. Sorgedrager, G. Carrea, F. v. Rantwijk, F. Secundo and R. A. Sheldon, *Green Chem.*, 2004, **6**, 483-487.

52. F. v. Rantwijk and R. A. Sheldon, *Chem. Rev.*, 2007, **107**, 2757-2785.

53. D. K. Magnuson, J. W. Bodley and D. F. Evans, *J. Solution Chem.*, 1984, **13**, 583-587.

54. C. Chiappe, L. Neri and D. Pieraccini, *Tetrahedron Lett.*, 2006, **47**, 5089-5093.

55. N. Kaftzik, P. Wasserscheid and U. Kragl, *Org. Process Res. Dev.*, 2002, **6**, 553-557.

56. S. Datta, B. Holmes, J. I. Park, Z. Chen, D. C. Dibble, M. Hadi, H. W. Blanch, B. A. Simmons and R. Sapra, *Green Chem.*, 2010, **12**, 338-345.

57. B. Henrissat and A. Bairoch, *Curr. Opin. Struct. Biol.*, 1997, **7**, 637-644.

58. N. Bakalova, S. Petrova and D. Kolev, *Pharmazie*, 1996, **51**, 761-764.

59. A. E. Clarke and B. A. Stone, *Biochem. J.*, 1965, **96**, 802-807.

60. A. E. Clarke and B. A. Stone, *Biochem. J.*, 1965, **96**, 793-801.

61. P. L. Hurst, P. A. Sullivan and M. G. Shepherd, *Biochem. J.*, 1978, **169**, 389-395.

62. P. L. Hurst, J. Nielsen, P. A. Sullivan and M. G. Shepherd, *Biochem. J.*, 1977, **165**, 33-41.

63. G. Okada, *Agric. Biol. Chem.*, 1985, **49**, 1257-1265.

64. H. Zhao, *J. Chem. Technol. Biotechnol.*, 2006, **81**, 877–891.

65. S. Cantone, U. Hanefeld and A. Basso, *Green Chem.*, 2007, **9**, 954–971.

66. M. T. Ru, S. Y. Hirokane, A. S. Lo, J. S. Dordick, J. A. Reimer and D. S. Clark, *J. Am. Chem. Soc.*, 2000, **122**, 1565-1571.

67. A. E. Sitnitsky, *Quant. Biol.*, 2008, 1-25, arXiv:0804 2749v0801 [q-bio BM].

68. Y. Pocker and N. Janjic, *Biochemistry*, 1987, **26**, 2597-2606.

69. S. Hay, C. R. Pudney, M. J. Sutcliffe and N. S. Scrutton, *Angew. Chem.*, 2008, **47**, 537-540.

70. K. R. Seddon, A. Stark and M.-J. Torres, in *Clean Solvents: Alternative Media for Chemical Reactions and Processing.*, ACS Symposium Series, 2002, pp. 34-49.

71. K. R. Harris, M. Kanakubo and L. A. Woolf, *J. chem. Eng. Data*, 2007, **52**, 2425-2430.

72. H. Li, M. Ibrahim, I. Agberemi and M. N. Kobrak, *J. Chem. Phys.*, 2008, **129**, 124507/124501.

73. P. Lozano, T. de Diego, J.-P. Guegan, M. Vaultier and J. L. Iborra, *Biotechnol. Bioeng.*, 2001, **75**, 563-569.

74. T. E. Lai, P. C. Pullammanappallil and W. P. Clarke, *Talanta*, 2006, **69**, 68-72.

CHAPTER VIII. INFLUENCE OF CHIRAL IONIC LIQUIDS ON STEREOSELECTIVE FLUORESCENCE QUENCHING BY PHOTOINDUCED ELECTRON TRANSFER IN A NAPROXEN DYAD

A paper published in the *Journal of Physical Chemistry B*

Sayantan Bose [1], Aruna B. Wijeratne [2], Aniket Thite [1], George A. Kraus [1],

Daniel W. Armstrong [2] and Jacob W. Petrich [1,*]

Abstract

In a previous study of a naproxen dyad in a pair of N-methylimidazoliummethyl menthylether-NTf$_2$ chiral ionic liquids (*J. Phys. Chem. B* **2008**, *112*, 7555), we observed that though intramolecular electron transfer was impeded, a consistent small stereodifferentiation in the fluorescence lifetime of the dyad was obtained. We proposed that this discrimination was purely electronic in nature and did not arise from geometrical effects, which can influence nonradiative rate processes, such as intramolecular electron transfer. In our present work, we have studied the interaction of the same chiral naproxen dyad molecule in both the previously studied menthyl-based NTf$_2$ ionic liquids and also in Bis(tertrabutylphosphonium) *D*-, *L*-tartrate ionic liquids. Unlike in the menthyl-based IL pair, the amount of quenching is

_____

different in the bis(TBP) tartrate enantiomeric liquids; and the tartrate enantiomers have a different temperature dependence on the nonradiative rate of the dyad. This chiral discrimination most likely arises from the steric effects of the different conformations of the chiral molecules. We have shown that viscosity and polarity of the solvents can influence the rate of electron transfer. On the other hand, no such electron transfer quenching is observed in the menthyl-based NTf_2 IL-solvents. To our knowledge, this is the first example of *chiral* ionic liquids inducing a stereoselective fluorescence quenching by photoinduced, intramolecular electron transfer.

Introduction

Chiral recognition is a very important phenomenon in biochemical systems as well as in technological applications, enabling specific design of pharmaceuticals, chiral sensors and molecular devices.[1] In asymmetric organic photochemistry, chiral recognition in the excited state is vital to achieve enantio-selectivity during photosensitization and quenching processes. As a result, investigation of stereoselective photochemical processes have become an attractive area in recent years,[2,3] and chiral ionic liquids provide a fascinating medium to study stereoselective processes. Only a few examples of chiral ionic liquids have been reported so far. Howarth and coworkers described the use of chiral imidazolium cation in Diels–Alder reactions.[4] However, the syntheses of these systems required an expensive chiral alkylating agent and elaborate synthetic schemes. The synthesis of ionic liquids employing chiral anions is can be more practical owing to the ready availability of many such anions as sodium salts. For example, Seddon and coworkers investigated Diels–Alder reactions in lactate ionic liquids.[5] More recently, Wasserscheid and coworkers synthesized three different groups of chiral ionic liquids.[6] They observed a positive diasteriomeric

interaction between racemic substrates of sodium salt of chiral mosher's acid and chiral ionic liquids by NMR spectroscopy. Bao *et al.* reported the first synthesis of chiral imidazolium ionic liquids derived from natural amino acids.[7] Very recently Warner and coworkers have synthesized amino acid based chiral ionic liquids via anion metathesis reaction between commercially available *D-* and *L*-alanine *tert* butyl ester chloride using a variety of counterions by employing lithium bis(trifluoromethanesulfonimide), silver nitrate, silver lactate, and silver tetrafluoroborate. In addition to NMR, they have used steady-state fluorescence to evaluate chiral recognition and enantio-selectivity of the chiral ionic liquids on 2,2,2-trifluoroanthrylethanol, warfarin, and naproxen as chiral fluorophores.[8] Yu et al. have used chiral borate anions and immidazolium cations to synthesize varieties of ionic liquids which consist of both chiral cations and chiral anions.[9]

Armstrong and co-workers have used a variety of methods to synthesize chiral ionic liquids either from chiral starting materials or using asymmetric synthesis.[10] They have provided the first application of chiral ionic liquids as stationary phases in chromatography using chiral ionic liquids as stationary phases in gas chromatography. Several compounds have been separated using these ionic-liquid-based chiral selectors. A large number of compounds, including alcohols, amines, sulfoxides, and epoxides were injected into the chiral-ionic-liquid based columns. These experiments demonstrate the first successful application of chiral ionic liquids as stationary phases in gas chromatography.[11] Ding et al. have been the first to report the use of chiral ionic liquids inducing irreversible, unimolecular photoisomerization of dibenzobicyclo[2.2.2]octatrienes to chiral products.[12]

Chiral discrimination in excited-state processes has been studied by several groups in the past few years. The groups of Miranda[13-24] and Tolbert[25] have made considerable

advances in this domain. In our recent work on N-methylimidazoliummethyl menthylether-NTf_2 chiral ionic liquids,[26] we observed a 10% stereodifferentiation in the fluorescence lifetimes of (S,S)-NPX-PYR dyad as well as in the parent compound, (S)-naproxen (S-NPX) (Figure VIII.1). This differentiation was shown not to be due to any difference in physical properties of the ionic liquids (such as viscosity or polarity) or the presence of impurities. The choice of (S,S)-NPX-PYR as the chromophore was inspired by the work of Miranda and co-workers,[24] who have shown that its diastereomers exhibit different behavior with regard to electron transfer or exciplex formation in polar solvents. We proposed, consequently, that (S,S)-NPX-PYR would also provide a promising entrée into the study of chiral ionic liquids. But electron transfer, however, was frustrated in the N-methylimidazoliummethyl menthylether-NTf_2 chiral ionic liquids (Figure VIII.1a), which we studied at room temperature. In the present work, we perform similar studies in a different pair of optically pure, chiral, enantiomeric ionic liquids, bis(tetrabutylphosphonium) (TBP) *D-, L*-tartrates (Figure VIII.1b) to investigate further the effects of chiral ionic liquids on excited-state electron transfer. In addition, the temperature dependence of the photophysics of the dyad in both the menthyl-based NTf_2, and bis(TBP) tartrate solvents was investigated. Although photoinduced electron transfer has been studied in ionic liquids, to our knowledge, this would be the first example of *chiral* ionic liquids inducing a stereoselective fluorescence quenching by photoinduced intramolecular electron transfer.

Experimental Section

Materials. Tetrabutylphosphonium (TBP) hydroxide (40 wt. % solution in water) and *D-, L*-tartaric acid were purchased from Aldrich. All HPLC grade organic solvents were obtained from Fisher. For the decolorization of ionic liquids, decolorizing charcoal was purchased

from Acros Organics; silica gel for flash chromatography, from Fluorochem; and celite and alumina, from Aldrich. (*S*)- and (R)- (+)-6-methoxy-α-methyl-2-naphthaleneacetic acid (naproxen, NPX) were purchased from Sigma Aldrich and were used without any further purification. Coumarin 153 (C153) (Exciton Inc., Dayton, OH) was used as received. Acetonitrile (HPLC grade), methanol, acetone and 99% (R)- and (S)-2-butanol were purchased from Aldrich and were used as received.

Scheme 1
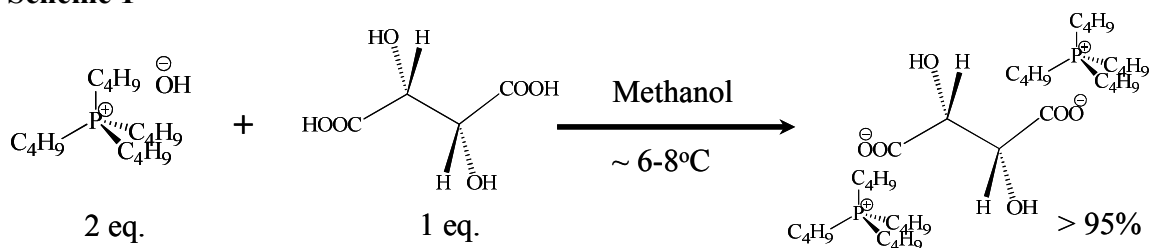
Synthesis of Chiral Di-anionic Tartrate ILs with Tetrabutylphosphonium (TBP) Counter Cations. Nonracemic, di-anionic, low-melting, colorless organic salts from *L*-tartaric acid, were prepared by reacting tetrabutylphosphonium hydroxide (2 eq.) with *L*-tartaric acid (1 eq.) in cold methanol (Scheme 1). *L*-tartaric acid (10.000 g, 6.67×10^{-2} mol) was dissolved in methanol (~ 150 ml) in a round-bottomed flask (500 ml) and kept in an ice water bath (~ 20 mins) in order to lower the solution temperature to ~ 6-8 $^{\circ}$C. Pre-cooled (~5-7° C) tetrabutylphosphonium hydroxide (40 wt. % solution in water: 46.512 ml, 3.33×10^{-2} mol) was gradually added while stirring the cold methanolic tartaric acid solution. Keeping the reaction mixture in an ice-water bath was necessary in order to obtain colorless low melting salts as final products. Otherwise a pale-yellow color results. Complete removal of the solvent was achieved by first evaporating it in a rotary-evaporator at room temperature to

obtain a dense liquid and then keeping the resulting content in a vacuum oven (-30 in. Hg) at room temperature for three days. All salts resulted in good yield (> 95%) as colorless liquids. Characterizations of the salts are provided in the supporting information. The other enantiomer was also synthesized and characterized using identical methods described above for *L*-tartrate salts.
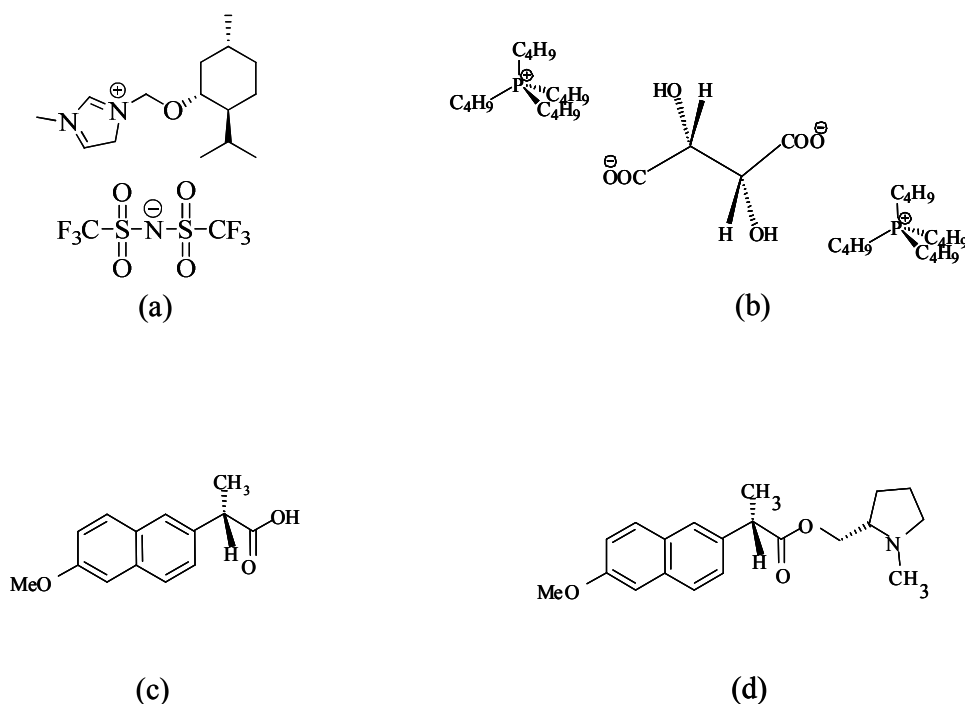

(a)

(b)

(c)

(d)

Figure VIII.1. Structures of (a) the chiral N-methylimidazoliummethyl menthylether bis(trifluoromethylsulfonyl)imide ionic liquid, (b) the *L*- di-anionic tartrate ionic liquids with TBP (tetrabutylphosphonium) counter cations, (c) (S)-(+)-6-methoxy-2-naphthylpropionic acid [S-naproxen, (S)-NPX], (d) (S)-N-methyl-2-pyrrolidinemethyl 2(S)-(6-methoxy-2-naphthyl) propionate [(S,S)-NPX-PYR].

The syntheses of (S,S)-NPX-PYR and the N-methylimidazoliummethyl menthylether-NTf$_2$ ionic liquids are described in detail elsewhere.[26] For the methylmenthyl ether based ILs our previously published (vide infra) purification method was used. For the (TBP)-titrate ILs, no decoration method was necessary as they were synthesized with no

color by a new procedure reported herein. Viscosity measurements were made with ViscoLab 4000 piston style viscometer from Cambridge Applied system at temperatures 22, 35, 45 and 55 ^{o}C.

Steady-State Measurements. Steady-state absorption spectra were obtained on a Hewlett-Packard 8453 UV-visible spectrophotometer with 1-nm resolution. The optical density was $\leq$ 0.8 at 266 nm. Steady-state fluorescence spectra were obtained on a Spex Fluoromax-2 with a 2-nm bandpass and corrected for lamp spectral intensity and detector response. For both fluorescence and absorption measurements, a 3-mm path-length quartz cuvette was used. Naproxen and dyad samples were excited at 266 nm; and coumarin 153, at 420nm.

Fluorescence Lifetime Measurements. Lifetime measurements were acquired using the time-correlated single-photon counting (TCSPC) apparatus described elsewhere.[27,28] The data were acquired in 1024 channels. Usually the time window was chosen to be $\geq$ 4 times that of the fluorescence lifetime measured. The instrument response function had a full width at half-maximum (FWHM) of ~50 ps. A 3-mm path length quartz cuvette was used for all the time-resolved measurements. Fluorescence decays were collected at the magic angle (polarization of 54.7^o) with respect to the vertical excitation light at 266 nm, with ~ 30,000 counts in the peak channel.

Results and Discussions

Our chiral ionic liquids are transparent from 380 nm to 800 nm. Contrary to the report by Samanta and co-workers,[29] who proposed that ionic liquids can be intrinsically colored, we find that their preparation can produce small amounts of strongly absorbing and emitting species, which can present problems in performing and analyzing spectroscopic studies[30] and that, in fact, these impurities can alter physical properties such as the viscosity.

We have used either the protocol cited above to purify these solvents or have taken precautions to make them in colorless form. All the measurements were performed at low temperatures (< 70°). To ensure that the ionic liquids did not deteriorate on heating, absorbance and fluorescence spectra at all temperatures were monitored and found to be unperturbed.
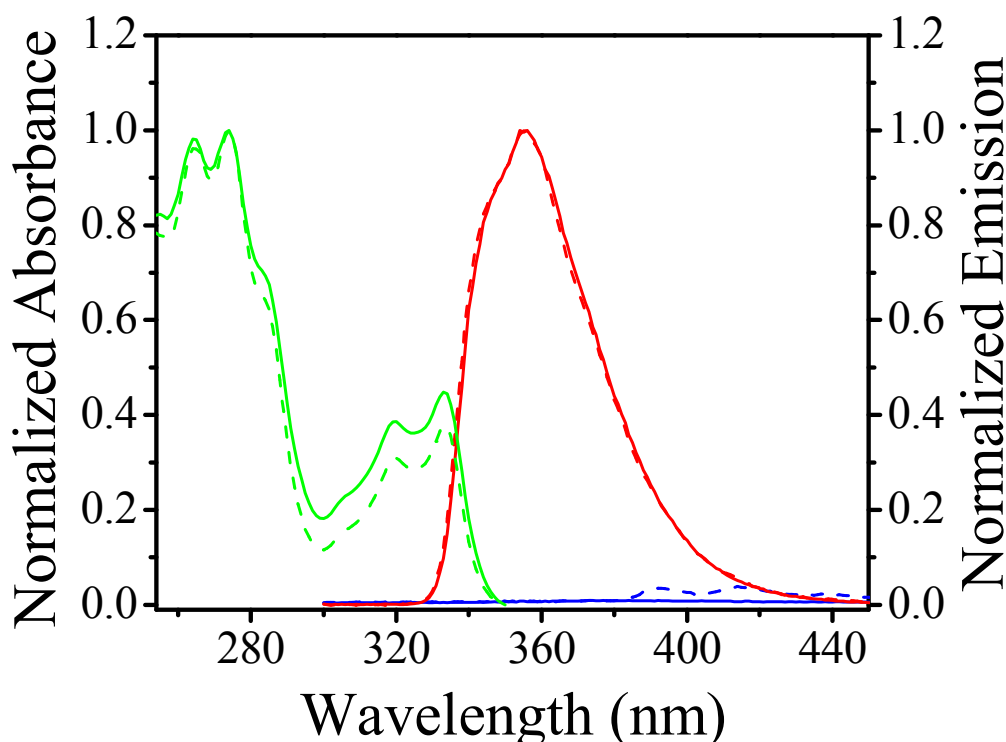

Figure VIII.2. Normalized absorption (green) and emission spectra (red) of the (S,S)-NPX-PYR dyad in the *D*- (━━━) and *L*-tartrate ionic liquid (┅┅). The fluorescence maximum of the dyad in both of the ILs is ~ 355 nm. The fluorescence spectra of the ILs (blue) are plotted on the same scale, but their intensity is negligible compared to that of the naproxen derivatives. The fluorescence spectra were obtained by exciting the sample at 266 nm with a 2-nm bandpass.

Representative steady-state absorption and emission spectra of the (S,S)-NPX-PYR dyad in the two enantiomeric bis(TBP) tartrate ionic liquids, along with the intrinsic fluorescence of the ionic liquids excited at 266 nm, are given in Figure VIII.2. The

fluorescence intensity of the ionic liquids is negligible in comparison to that of the solute, verifying the solvents' high level of purity. The chiral dyad molecule showed identical emission spectrum in the bis(TBP) *D*- and *L*- tartrate solvents, with peak maxima at 355 nm. In the menthyl-based NTf$_2$ ionic liquids, the peak maxima are identical, but slightly blue shifted to 352 nm.
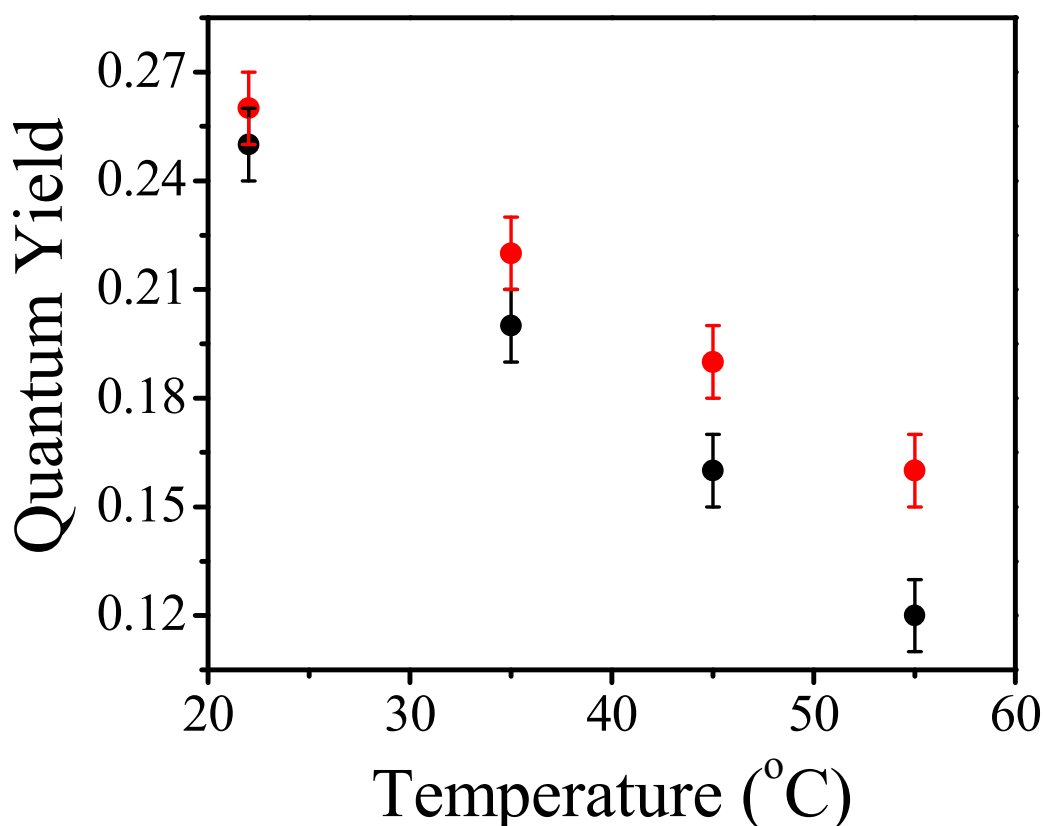

Figure VIII.3. Plot of singlet quantum yields against temperature of the (S,S)-NPX-PYR dyad in *D*- (black dots) and *L*- (red dots) tartrate ionic liquids, obtained from the steady-state emission spectra, taking tryptophan in buffer (pH 7.0) as the standard (Φ_{trp} =0.18) [34-36]. The error bars are based on the average of three measurements. The fluorescence quantum yields are almost same at 22°C, but they increasingly differ with temperature.

Steady-state spectra were also obtained as a function of temperature.   The fluorescence intensity decreased differently for the two tartrate liquids, without any shift in the peak maxima. Steady-state quenching was observed to be higher in the case of the *D*-isomer. The fluorescence quantum yield (Φ) was calculated using tryptophan in buffer (pH 7.0) as a standard. A clear difference in the extent of quenching of the dyad was observed in the bis(TBP) *D*- and *L*- tartrate solvents (Figure VIII.3).
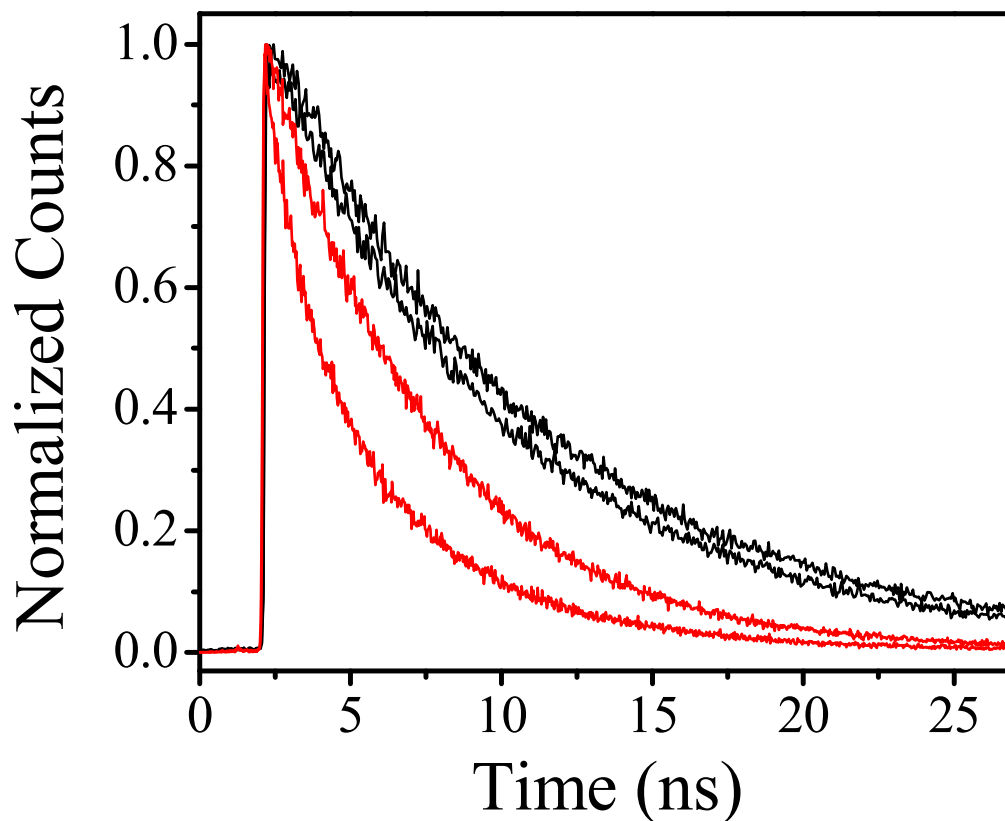
Figure VIII.4. Fluorescence decay traces (λ_{ex} = 266 nm, $\lambda_{em} \geq$ 300 nm) of (S,S)-NPX-PYR in *D*- and *L*- tartrate ionic liquids at room temperature (black) and at 55°C (red)   Traces for all the temperatures are not shown for clarity of presentation. There is an ~ 10% decrease in lifetime of (S,S)-NPX-PYR in *D*- compared to that of in *L*- at room temperature, whereas the difference of lifetime increased with temperature. The lifetimes of (S,S)-NPX-PYR in the chiral ILs are given in Table VIII.I.

TABLE VIII.1. Fluorescence Lifetimes and Steady-State Quantum Yields of (S,S)-NPX-PYR and (S)-NPX in Different Solvents

Solute	Solvent [a]	Temp. (^{o}C)	Lifetime [b, c] (ns)	Φ [b]
(S,S)-NPX-PYR	*D*- IL	22	8.1 ± 0.2	0.25 ± 0.01
	L- IL		8.9 ± 0.2	0.26 ± 0.01
	D- IL	35	6.1 ± 0.2	0.20 ± 0.01
	L- IL		7.1 ± 0.2	0.22 ± 0.01
	D- IL	45	4.3 ± 0.2	0.16 ± 0.01
	L- IL		6.1 ± 0.2	0.19 ± 0.01
	D- IL	55	3.3 ± 0.2	0.12 ± 0.01
	L- IL		5.3 ± 0.2	0.16 ± 0.01
	(R)-2-butanol		8.6 ± 0.3	
	(S)-2-butanol	22	7.5 ± 0.3	
	Acetonitrile		3.2 ± 0.3	
(S)-NPX	*D*- IL	22	5.0 ± 0.2	
	L- IL		4.2 ± 0.2	
	D- IL	55	2.0 ± 0.1	
	L- IL		1.6 ± 0.1	
	Acetonitrile		7.2 ± 0.2	
(R)-NPX	*D*- IL	22	4.5 ± 0.2	
	L- IL		3.6 ± 0.2	

[a] IL: Bis(tetrabutylphophonium) (TBP) tartrate ionic liquids.
[b] Error bars are based on the average of three measurements.
[c] All of the fluorescence lifetimes reported are single exponential, except for that of the *D* tartrate at 45 and 55°C, where they are fit to a sum of two exponentials and an average lifetime is reported.

Time-resolved experiments were also performed on the (S,S)-NPX-PYR dyad in the *D*- and *L*- tartrate ionic liquids. A 10% difference in lifetime (~8.9 and ~8.1 ns) is observed in the two chiral solvents at room temperature (Figure VIII.4), which is consistent with our previous results in the menthyl-based ionic liquids.[26] As a control, similar experiments were also done with (S)-naproxen, which is the parent compound of the dyad, and the stereodifferentiation in the lifetimes, is also observed at room temperature (Figure VIII.5).

To ensure that this discrimination is not due to impurities in the ionic liquids, (S)- and (R)-naproxen were also studied in the same ionic liquids, and a ~ 10% difference in fluorescence lifetimes was observed for the two naproxen isomers (Table VIII.1). As a further control, lifetimes of the dyad molecule were also determined in (R)- and (S)-2-butanol. In all cases, the chiral differentiation of lifetimes is consistent (Table VIII.1). This unambiguously indicates that the observed difference in lifetimes is not due to fortuitous impurity quenching, but to solute-solvent interactions.
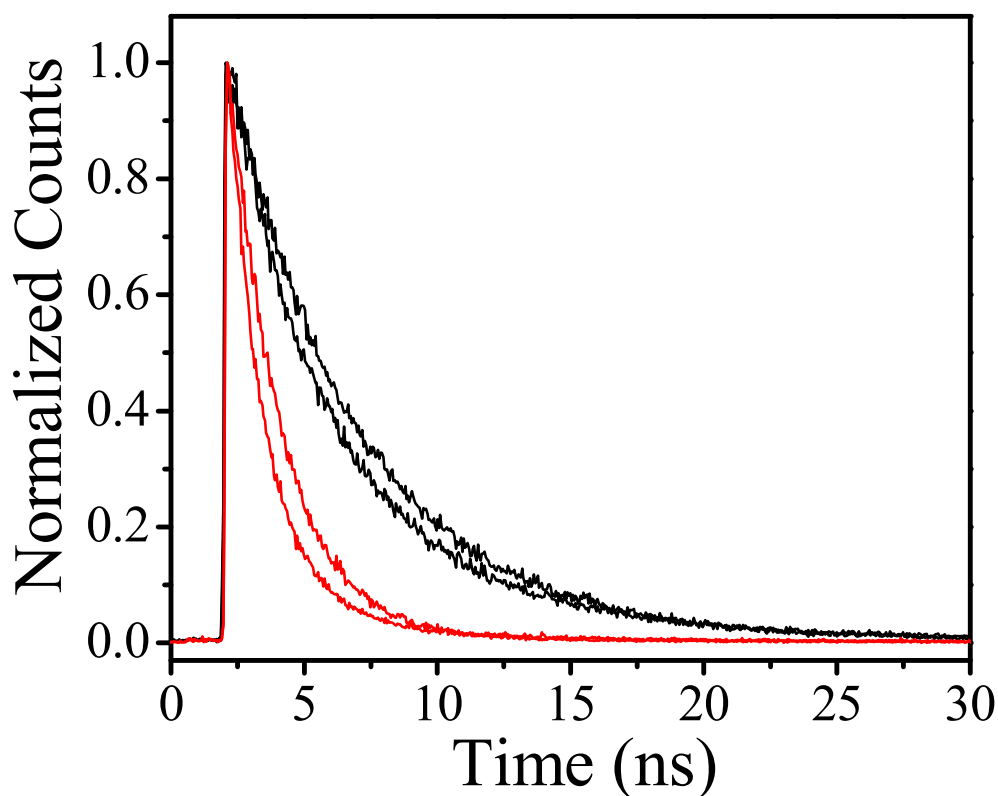
Figure VIII.5. Fluorescence decay traces (λ_{ex} = 266 nm, λ_{em} ≥ 300 nm) of (S)-NPX in *D*-, *L*-tartrate ionic liquids at room temperature (black) and at 55°C (red). There is a consistent ~ 10% decrease in lifetime of (S)-NPX in *L*- compared to that of in D- at room temperature, and this difference of lifetime is conserved with increasing temperature.
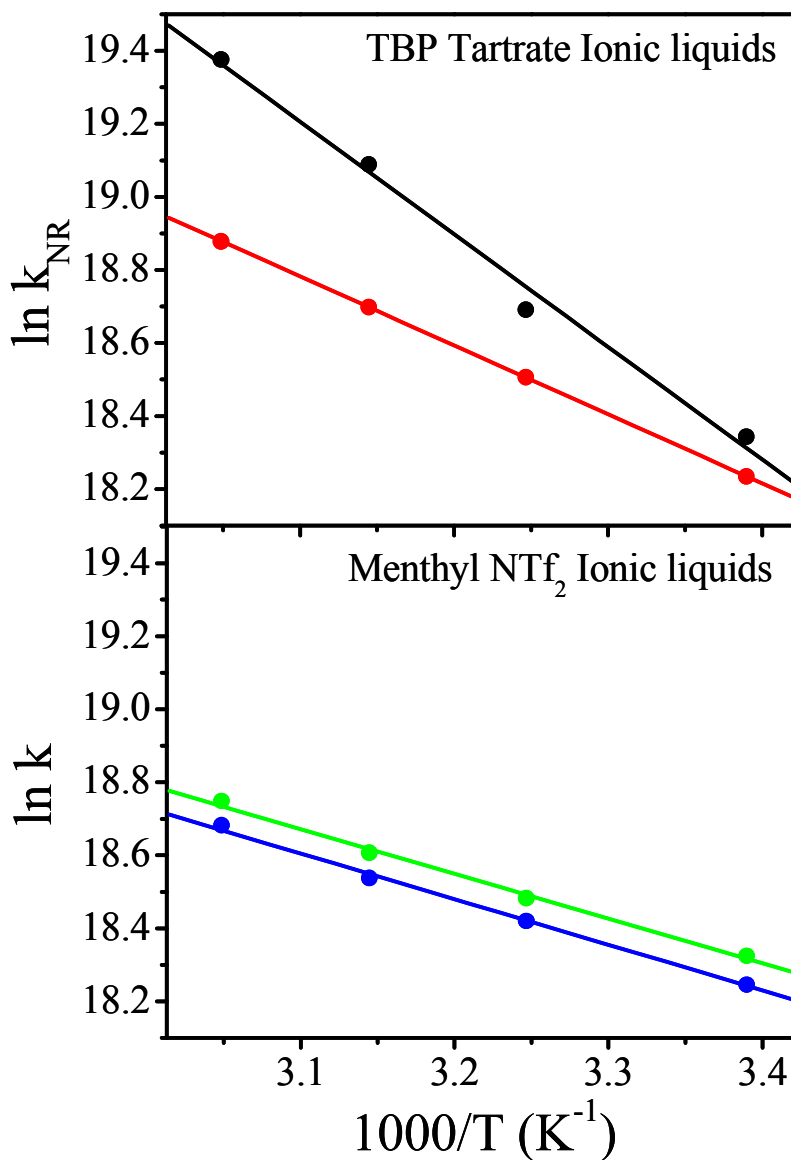
Figure VIII.6. Arrhenius plots obtained from fluorescence lifetimes of (*S,S*)-NPX-PYR dyad in the *D*- (black dot) and *L*- (red dots), tartrate ionic liquids (upper panel), and in (+) – (green dots) and (−) – (blue dots) menthyl-based ionic liquids (lower panel). The activation energy, E_a, for the menthyl-based IL pair is almost the same, 2.48 and 2.43 kcal mol^{-1}, but for the tartrates it is 6.2 and 3.7 kcal mol^{-1}, for the *D*- and *L*- isomers, respectively, suggesting that electron transfer quenching is occurring in the tartrate ionic liquids, but not in the menthyl-based pair. The frequency factors, A, are 3.0 x 10^{12} and 4.9 x 10^{10} s^{-1} for the *D*- and *L*- tartrates and 5.8 x 10^{9} and 5.7 x 10^{9} s^{-1} for the (+)- and (−)− menthyls, respectively.

Lifetime quenching was monitored as a function of temperature, and Arrhenius plots were constructed from the nonradiative rates (assumed to be from intramolecular electron transfer) extracted from the lifetime data. The activation energies are different for the tartrates: 6.2 and 3.7 kcal/mol for the *D*- and *L*- forms, respectively. In the case of the menthyl-based pair, they are equal within experimental error: 2.45 kcal/mol (Figure VIII.6). This suggests that the chiral donor-acceptor dyad interacts differently in the two chiral tartrate ionic liquids.

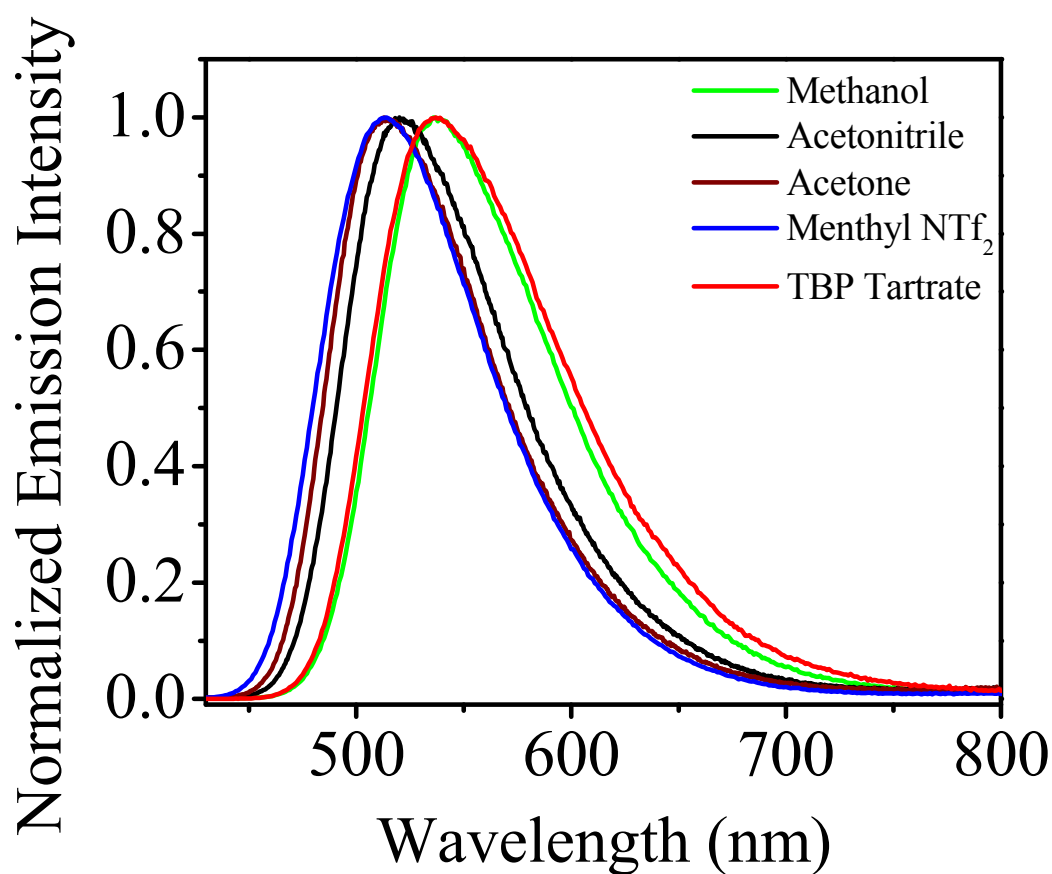**Figure VIII.7**. Normalized steady-state emission spectra of C153 in different solvents. The fluorescence spectra were obtained by exciting the sample at 420 nm with a 2-nm bandpass. From the peak maxima, the order of polarity of the solvents is: menthyl ILs < acetone < acetonitrile < tartrate ILs ≈ methanol. The $E_T(30)$ values of the menthyl ionic liquids are 41.1 and 41.3 and those of tartrate ionic liquids are 53.3 and 53.5.

TABLE VIII.2. Viscosity, η (cP), Data for Chiral Ionic Liquids

Temp. (^{o}C)	η, TBP Tartrate		η, Menthyl NTf$_2$	
	D	L	(+)	(-)
22	123 ± 3	125 ± 3	940 ± 10	930 ± 10
35	46 ± 2	46 ± 2	265 ± 5	270 ± 5
45	30 ± 2	31 ± 2	120 ± 3	118 ± 3
55	24 ± 2	23 ± 2	60 ± 2	61 ± 2

The viscosity activation energy ($E_{a,\eta}$) was calculated from the slope of the plot of $\ln(1/\eta)$ versus $1/T$. $E_{a,\eta}$ was larger in the menthyl-based pair than in the tartrate pair: 15.8 and 9.2 kcal/mol, respectively.

The pyrrolidine moiety in the dyad is a potential electron donor and the naphthalene ring acts as an acceptor. The interaction of the donor-acceptor moiety (in the excited state) with the two chiral solvents must be sufficiently different to produce different excited-state kinetics. The viscosity and solvent motion play an important role by influencing twisting motion of single bond and chain conformation linking the donor and acceptor moieties. The dependence of viscosity of the ionic liquids on temperature is shown in Table VIII.2. The bis(TBP) tartrate ionic liquids are less viscous than the menthyl-based ionic liquids and most likely favor the attainment of preferred geometries for electron transfer to occur, which is also consistent with the lower viscosity activation energy of the former (Table VIII.2). In our case, the less viscous tartrate ionic liquids, probably allows the pyrrole nitrogen to come into closer proximity with the naphthyl ring by undergoing a conformational change of the donor-

acceptor linking chain at higher temperatures, resulting in the electron transfer, which is not seen in highly viscous menthyl-based ionic liquids.

Viscosity is not the sole criterion determining the possibility of electron transfer. The dielectric constant of the solvent or, more appropriately, the micropolarity is equally important because it also influences the radiative and nonradiative rate constants.[31] A detailed study of electron transfer from N,N-dimethyl aniline (DMA) to pyrene in ionic liquids was undertaken by Paul and Samanta,[32] who made several observations. First, the rate of electron transfer in the ionic liquid is smaller than that in conventional organic solvents, which was attributed to the higher bulk viscosity of the ionic liquids. Second, the rate constant for electron transfer in the ionic liquids is in general 2-4 times larger than the diffusion controlled values. This was attributed to the difference between microviscosity and bulk viscosity in ionic liquids, which was originally suggested by Skrzypczak and Neta.[33] Third, as in our case, no exciplex emission was observed in any of the ionic liquids studied, which is striking given that the DMA-pyrene system is well known for exciplex formation in conventional bulk solvents. The lack of exciplex formation led the authors to conclude that it is the microscopic and not the bulk polarity that could be related to the $E_T(30)$ scale that determines the formation of exciplex in ionic liquids.

In order to determine the relative polarity of the ionic liquids studied here, steady-state emission spectra of coumarin 153 have been obtained in a series of solvents. Coumarin 153 (C153) is an extremely well studied solvatochromic probe, whose emission is highly sensitive to solvent polarity. From Figure VIII.7, it can be seen that the emission of C153 in the bis(TBP) tartrate ionic liquids is red-shifted compared to that in the menthyl-based NTf_2 ionic liquids. Thus the former being more polar, solvates the charge transferred polar excited

state of the dyad, imparting more stability and in turn facilitates electron transfer, which is absent in the menthyl-based ionic liquids.

Conclusion

In our previous work,[26] we observed that though electron transfer was frustrated in the menthyl-based NTf$_2$ ionic liquids, still a consistent small stereodifferentiation in the fluorescence lifetime of (S,S)-NPX-PYR and (S)-naproxen was obtained. We proposed that this discrimination was purely electronic in nature and did not arise from geometrical effects, which can influence nonradiative rate processes, such as intramolecular electron transfer. In our present work, we have studied the interaction of the same chiral naproxen dyad molecule in both the previously studied menthyl-based NTf$_2$ ionic liquids and also in bis(tertrabutylphosphonium) tartrate ionic liquids. Unlike in the menthyl pair, the amount of quenching is different in the bis(TBP) tartrate isomeric liquids; and the tartrate enantiomers have a different temperature dependence on the nonradiative rate of the dyad. This chiral discrimination most likely arises from the steric effects of the different conformations of the chiral molecules. We have shown that viscosity and polarity of the solvents can influence the rate of electron transfer. On the other hand, no such electron transfer quenching is observed in the menthyl-based NTf$_2$ solvents. To our knowledge, this is the first example of *chiral* ionic liquids inducing a stereoselective fluorescence quenching by photoinduced, intramolecular electron transfer. It is noteworthy that we have observed chiral discrimination by ionic liquids on both radiative and nonradiative processes.

Acknowledgments

References

(1)   Beddell, C. R. *The Design of Drugs to Macaromolecular Targets*; Wiley, Chichester, 1992.

(2)   Inoue. *Chem. Rev.* 1992, *92*, 741.

(3)   Griesbeck, A. G.; Meierhenrich, U. J. *Angew. Chem.* 2002, *41*, 3147.

(4)   Howarth, J.; Hanlon, K.; Fayne, D.; McCormac, P. B. *Tetrahedon Lett.* 1997, *38*, 3097.

(5)   Earle, M. J.; McCormac, P. B.; Seddon, K. R. *Green Chem.* 1999, *1*, 23.

(6)   Wasserscheid, P.; Bösmann, A.; Bolm, C. *Chem. Commun.* 2002, *2002*, 200.

(7)   Bao, W.; Wang, Z.; Li, Y. H. *J. Org. Chem.* 2003, *68*, 591.

(8)   Bwambok, D. K.; Marwani, H. M.; Fernand, V. E.; Fakayode, S. O.; Lowry, M.; Negulescu, I.; Strongin, R. M.; Warner, I. M. *Chirality* 2008, *20*, 151.

(9)   Yu, S.; Lindeman, S.; Tran, C. D. *J. Org. Chem.* 2008, *73*, 2576.

(10)   Ding, J.; Armstrong, D. W. *Chirality* 2005, *17*, 281.

(11)   Ding, J.; Welton, T.; Armstrong, D. W. *Anal. Chem.* 2004, *76*, 6819.

(12)   Ding, J.; Desikan, V.; Han, X.; Xiao, T. L.; Ding, R.; Jenks, W. S.; Armstrong, D. W. *Org. Lett.* 2005, *7*, 335.

(13)   Abad, S.; Pischel, U.; Miranda, M. A. *J. Phys. Chem. A* 2005, *109*, 2711.

(14)   Pischel, U.; Abad, S.; Miranda, M. A. *Chem. Commun.* 2003, 1088.

(15)   Boscá, F.; Andreu, I.; Morera, I. M.; Samadi, A.; Miranda, M. A. *Chem. Commun.* 2003, 1592.

(16)   Miranda, M. A.; Lahoz, A.; Martinez-Mañez, R.; Boscá, F.; Castell, J. V.; Pérez-Prieto, J. *J. Am. Chem. Soc* 1999, *121*, 11569.

(17)   Pischel, U.; Abad, S.; Domingo, L. R.; Boscá, F.; Miranda, M. A. *Angew. Chem. Int. Ed.* 2003, *42*, 2531.

(18)   Miranda, M. A.; Lahoz, A.; Boscá, F.; Metni, M. R.; Abdelouahab, F. B.; Castell, J. V.; Pérez-Prieto, J. *Chem. Commun.* 2000, 2257.

(19)   Boscá, F.; Marin, M. L.; Miranda, M. A. *Photochem. Photobiol.* 2001, *74*, 6 37.

(20)   Boscá, F.; Canudas, N.; Marin, M. L.; Miranda, M. A. *Photochem. Photobiol.* 2000, *71*, 173.

(21)   Vayá, I.; Jiménez, M. C.; Miranda, M. A. *Tetrahedron: Asymm.* 2005, *16*, 2167.

(22)   Jiménez, M. C.; Stiriba, S.-E.; Tormos, R.; Pérez-Prieto, J.; Miranda, M. A. *Photochem. Photobiol. Sci.* 2004, *3*,

36.

(23)   Encinas, S.; Climent, M. J.; Belmadoui, N.; Miranda, M. A. *Chem. Commun.* 2005, 2572.

(24)   Abad, S.; Pischel, U.; Miranda, M. A. *Photochem. Photobiol. Sci.* 2005, *4*, 69.

(25)   Solntsev, K. M.; Tolbert, L. M.; Cohen, B.; Huppert, D.; Hayashi, Y.; Feldman, Y. *J. Am. Chem. Soc.* 2002, *124*, 9046.

(26)   Adhikary, R.; Bose, S.; Mukherjee, P.; Thite, A.; Kraus, G. A.; Wijeratne, A. B.; Sharma, P.; Armstrong, D. W.; Petrich, J. W. *J. Phys. Chem. B* 2008, *112*, 7555.

(27)   Chowdhury, P. K.; Halder, M.; Sanders, L.; Calhoun, T.; Anderson, J. L.; Armstrong, D. W.; Song, X.; Petrich, J. W. *J. Phys. Chem. B* 2004, *108*, 10245.

(28)   Bose, S.; Adhikary, R.; Mukherjee, P.; Song, X.; Petrich, J. W. *J. Phys. Chem. B* **2009**, *113*, 11061.

(29)   Paul, A.; Mandal, P. K.; Samanta, A. *Chem. Phys. Lett.* 2005, *402*, 375.

(30)   Mukherjee, P.; Crank, J. A.; Sharma, P. S.; Wijeratne, A. B.; Adhikary, R.; Bose, S.; Armstrong, D. W.; Petrich, J. W. *J. Phys. Chem. B* 2008, *112*, 3390.

(31)   Sarkar, M.; Kanaparthi, R. K.; Bhattacharya, B.; Samanta, A. *J. Phys. Chem. A* 2008, *112*, 3302.

(32)   Paul, A.; Samanta, A. *J. Phys. Chem. B* 2007, *111*, 1957.

(33)   Skrzypczak, A.; Neta, P. *J. Phys. Chem. A* 2003, *107*, 7800.

(34)   Avouris, P.; Yang, L. L.; El-Bayoumi, M. A. *Photochem. Photobiol.* 1976, *24*, 211.

(35)   Rich, R. L.; Gai, F.; Lane, J. W.; Petrich, J. W.; Schwabacher, A. W. *Journal of the American Chemical Society* 1995, *117*, 733.

(36)   Das, K.; Smirnov, A. V.; Wen, J.; Miskovsky, P.; Petrich, J. W. *Photochem. Photobiol.* 1999, *69*, 633.

Supporting Information

Structural characterization of the bis(TBP) tartrate ionic liquids.   This information is available free of charge via the Internet at http://pubs.acs.org.   The text is included below.

Characteriation   of   Chiral   Di-anionic   Tartrate   Ionic   Liquids   with Tetrabutylphosphonium (TBP) Counter Cations by NMR.

Bis(tetrabutylphosphonium) *L*-tartrate (Figure VIII.1b): ^{1}H-NMR (300 MHz, D4-MeOH): δppm = 0.98 (24H, t, *J* = 6.8 Hz), 1.48-1.59 (32H, m), 2.20-2.29 (16H, m), 4.21

(2H, s); ^{13}C-NMR (75 MHz, D4-MeOH): δppm = 12.81, 17.51, 18.14, 23.19, 23.25, 23.62, 23.83, 73.80, 177.46. Structural confirmations were carried out by comparing chemical shifts of ^{1}H/^{13}C-NMR signals of the product with that of *L*-tartratic acid. *L*-tartaric acid: ^{1}H-NMR (300 MHz, D4-MeOH): δppm = 4.61 (2H, s); ^{13}C-NMR (75 MHz, D4-MeOH): δppm = 72.65, 174.17. The proton signal corresponding to *L*-tartaric acid: (δppm = 4.61, s, 2H) is observed shifted up-field in the *L*- isomer of the bis(TBP) tartrate (δppm = 4.21, s, 2H) due to electron enrichment of the *L*-tartrate dicarboxylate anions. The carbonyl carbon ^{13}C-NMR signal corresponding to *L*-tartaric acid (δppm = 174.17) is also observed to be considerably shifted up-field in the bis(TBP) *L*-tartrate ionic liquid (δppm = 177.46), which is also attributed to the electron enrichment *L*-tartrate dicarboxylate anions. This type of ^{1}H-NMR-signal variation has been previously reported for di-anionic tartrate-based, low melting salts with tetrabutylammonium counter cations, which is consistent with our observations.[1]

Reference

(1)   Allen, C. R.; Richard, P. L.; Ward, A. J.; van de Water, L. G. A.; Masters, A. F.; Maschmeyer, T. *Tetrahedron Lett.* **2006**, *47*, 7367.

CHAPTER IX. GENERAL CONCLUSIONS

This thesis focuses on different steady-state and time-resolved spectroscopic techniques to explore the excited state photophysics of different biologically and environmentally relevant systems.

The work presented here is mainly based on solvation dynamics in protein environments. Studies of the solvation dynamics in proteins offer an excellent direct means of investigating proteins' dielectric response. Although a lot of studies are undertaken to understand the solvation response of proteins, their outcomes are disparate. We attribute these discrepancies due to lack of a robust model system which can be exploited to unambiguously study the solvation response in protein environments. In our previous work we have thoroughly characterized coumarin 153 (C153) – apomyoglobin complex as a model system to study solvation dynamics both experimentally and theoretically. We have experimentally studied solvation of C153, inside the heme pockets of wild type (WT) horse-heart (HH) myoglobin (Mb) and leghemoglobin (Lba), using fluorescence upconversion technique and comparison of the experimental results with those obtained from molecular dynamic simulations are presented in chapter III. We found that there is an excellent agreement between the experimental results and those obtained from molecular dynamics simulations. In both cases initial faster solvation is followed by a slower response, which is slower in apoLba than in apoMb. Solvation of the C153 inside the heme pockets is very rapid with approximately 60% occurring within ~300 fs and we have attributed this to interactions with water and possibly the protein. The differences in the response in the two proteins are probably due to the differences in the hemepockets, the region probed by C153.

Our results are in odds with those of Zhong, Zewail and coworkers where they have reported that aqueous solvation in proteins (using the intrinsic tryptophan as a probe), is much slower than that in bulk water and the slow solvation was attributed to "biological water." The nonexponential fluorescence decay of tryptophan has stimulated the generation of an alternative method of constructing $C(t)$, which Zewail, Zhong, and coworkers use to calculate the solvation correlation functions, $C(t)$. We provided an analysis of various methods of constructing $C(t)$ and reviewed selected examples from the literature in chapter IV. We have demonstrated that it is possible to exaggerate the amplitudes of slower solvation phenomenon that may be attributed to "biological water", water-protein interactions, or the protein itself. We concluded that $C(t)$ is a normalized function whose form and interpretation depend critically upon the terms in its denominator, namely the positions of the "zero-time" and "steady-state" spectra, the former of which we argue is most accurately provided by the method of Fee and Maroncelli.

We extended our studies of solvation dynamics inside the heme pockets, using wild-type sperm whale myoglobin and its mutants as described in chapter V. The results we found are interesting. Consistent with our previous studies, we found a remarkable agreement between the solvation correlation functions, ($C(t)$s), from fluorescence upconversion experiments and those obtained from molecular dynamics simulations in wild-type apoprotein, but deviations were observed in the mutants. A close comparison of the $C(t)$s for these two wild-type systems, namely horse-heart and sperm-whale indicates small but significant differences that must arise from this single amino acid substitution in the heme pocket. The agreement between experiment and theory suggests no reason to attribute the disagreement observed in case of mutants, to the force fields used in the simulation but rather

to question the structure of the complex used as the starting point for the simulation. We consequently performed exhaustive characterization of the mutant complexes by NMR study of the complex of C153 with equine apoMb, along with fluorescence energy transfer and anisotropy of all of the equine and sperm-whale complexes to complement the NMR studies. All our experiments collectively provide solid evidence that molecular dynamics simulations can be used to interpret solvation dynamics measurements successfully, provided the initial structures of the system under study are well characterized.

Besides studying protein solvation, we also focused on study of utilizing room temperature ionic liquids (RTILs) as green medium for hydrolysis of cellulose (a major biomass constituent) to produce biofuels in chapter VI and VII. Using optical and calorimetric techniques, we investigated the reactivity and stability of a *T. reesei* cellulases in eight ionic liquids, out of which only 1-methylimidazolium chloride (mim Cl) and tris-(2-hydroxyethyl)-methylammonium methylsulfate (HEMA) provided a medium in which hydrolysis could occur. While hydrolysis at 65°C was initially much faster in buffer than in these two liquids, it ceased after two hours; whereas, the reaction continued monotonically in the two ionic liquids. This difference in the rate of hydrolysis is largely attributed to two factors: 1) the higher viscosity of the ionic liquids; 2) the enzymes are irreversibly denatured at 50°C in buffer while they are stable to temperatures as high as 115°C in HEMA. We also found that fluorescence quenching of aromatic amino acids of the enzymes is not necessarily a signature of the enzyme denaturation. Contrary to the literature reports, we further explored that this quenching mechanism in the presence of ionic liquids formed from imidazolium cations and chloride anions, arises from the imidazolium rather than the chloride. Having established that *T. reesei* cellulases are more stable in HEMA than in

buffer, we extended our work to pure enzyme component endo-1,4-β-*D*-glucanase (EG) from *A. niger* to understand how HEMA can influence its activity and impart temperature stability as well as how it can contribute to the hydrolysis of cellulose. Studies in aqueous HEMA mixtures showed enhanced activity of the EG in the presence of HEMA, which varied with temperature. This thus reaffirmed our hypothesis that the enzymatic activity is a compromise between both enzyme stability in a particular solvent and temperature and the viscosity of the medium, since a direct correlation between activity and solvent viscosity could not be established. Because of the thermal stability that HEMA imparts to enzymes, it proves to be a novel, green medium for performing cellulose hydrolysis reactions to convert biomass into biofuels and provides an ideal starting point for the design of ionic liquids, not only for the hydrolysis of biomass, but for use with a wide spectrum of enzymatic reactions.

Chapter VIII demonstrates an extension of our previous study on a chiral naproxen dyad in a chiral pair of menthyl-based NTf$_2$ ionic liquids where we observed that though intramolecular electron transfer was frustrated, a consistent small stereodifferentiation in the fluorescence lifetime of the dyad was obtained. We studied the interaction of the same chiral naproxen dyad molecule in both the previously studied menthyl-based NTf$_2$ and also in bis(tertrabutylphosphonium) tartrate ionic liquids. Unlike in the menthyl pair, the amount of quenching is different in the bis(TBP) tartrate isomeric liquids. This chiral discrimination most likely arises from the steric effects of the different conformations of the chiral molecules. We observed that viscosity and polarity of the solvents can influence the rate of electron transfer. It is noteworthy that we have observed chiral discrimination by ionic liquids on both radiative and nonradiative processes.

VITA

NAME OF AUTHOR: Sayantan Bose

DATE AND PLACE OF BIRTH: January 21st, 1982, Kolkata, India.

DEGREES AWARDED: B.S. Chemistry (Hons.), Calcutta University, India, 2003.
M.S. Physical Chemistry (Major), IIT Bombay, India, 2005.

HONORS AND AWARDS:
- ISU Teaching Excellence Award, 2007.
- ISU Research Excellence Award, 2010.
- ACS Conveyance Award, Physical Chemistry Symposium Division, 2008.
- ACS Travel Award, Chemistry Dept, Iowa State University, for Oral presentation and merit of the work presented, 2008.

PROFESSIONAL EXPERIENCE:
- Research Assistant, Iowa State University and Ames Laboratory, Ames, IA, USA (Fall '07, '09, Spring '09, '10, Summer '06, '07, '08, '09, '10)
- Teaching Assistant, Iowa State University, Ames, IA, USA: Chem 155, 177, 177L, 178, 178L, 201, 322L, 321L (Fall '05, '06, '08, Spring '06, '07, '08)

PROFESSIONAL PUBLICATIONS:

1. Halder, M., Mukherjee, P., **Bose, S.**, Hargrove, M.S., Song, X., Petrich, J.W. (2007) Solvation dynamics in protein environments: Comparison of fluorescence upconversion measurements of coumarin 153 in monomeric hemeproteins with molecular dynamics simulations *J. Chem. Phys.* **127**, 055101/1-055101/6.
2. Mukherjee, P., Crank, J.A., Sharma, P.S., Wijeratne, A.B., Adhikary, R., **Bose, S.**, Armstrong, D.W., Petrich, J.W. (2008) Dynamic Solvation in Phosphonium Ionic Liquids: Comparison of Bulk and Micellar Systems and Considerations for the Construction of the Solvation Correlation Function, C(t). *J. Phys. Chem. B* **112**, 3390-3396.
3. Adhikary, R., **Bose, S**., Mukherjee, P., Thite, A., Kraus, G.A., Wijeratne, A.B., Sharma, P., Armstrong, D.W., Petrich, J.W. (2008) Influence of Chiral Ionic Liquids on the Excited-State Properties of Naproxen Analogs. *J. Phys. Chem. B* **112**, 7555-7559.
4. Mukherjee, P., **Bose, S**., Hurd, A.A., Adhikary, R., Schönenbrücher, H., Hamir, A.N., Richt, J.A., Casey, T.A., Rasmussen, M.A., Petrich, J.W. (2009) Monitoring the Accumulation of Lipofuscin in Aging Murine Eyes by Fluorescence Spectroscopy. *Photochem. Photobiol.* **85**, 234-238.
5. **Bose, S.**, Adhikary, R., Mukherjee, P., Song, X., Petrich, J.W. (2009) Considerations for the Construction of the Solvation Correlation Function and Implications for the

Interpretation of Dielectric Relaxation in Proteins. *J. Phys. Chem. B* **113**, 11061–11068.

6. **Bose, S.**, Wijeratne, A.B., Thite, A., Kraus, G.A., Armstrong, D.W., Petrich, J., W. (2009) Influence of Chiral Ionic Liquids on Stereoselective Fluorescence Quenching by Photoinduced Electron Transfer in a Naproxen Dyad. *J. Phys. Chem. B* **113**, 10825–10829.

7. **Bose, S**., Armstrong, D.W., Petrich, J.W. (2010) Enzyme Catalyzed Hydrolysis of Cellulose in Ionic Liquids: A Green Approach Towards the Production of Biofuels. *J. Phys. Chem. B* **114**, 8221-8227.

8. **Bose, S.**, Adhikary, R., Barnes, C.A., Fulton, D.B., Hargrove, M.S., Song, X., Petrich, J.W. (2010) Comparison of the Dielectric Response Obtained from Fluorescence Upconversion Measurements and Molecular Dynamics Simulations for Coumarin 153- Apomyoglobin Complexes and Structural Analysis of the Complexes by NMR and Fluorescence Methods. *J. Phys. Chem. A*, in press.

9. Adhikary, R., **Bose, S**., Casey, T.A., Gapsch, A., Rasmussen, M.A., Petrich Jacob, W. (2010) Applications of fluorescence spectroscopy to problems of food safety: detection of fecal contamination and of the presence of central nervous system tissue and diagnosis of neurological disease. *Proceedings of SPIE (Review)*, in press.

10. **Bose, S.**, Petrich, J.W. (2010) Enhanced Stability and Activity of Aspergillus niger Cellulase in the Ionic Liquid Tris-(2-hydroxyethyl)-methylammonium methylsulfate (HEMA). *Green. Chem.*, submitted.

11. Intemann, J.J., Mike, J.F., Min, C., **Bose, S.**, Xiao, T., Mauldin, T., Shinar, J., Shinar, R., Jeffries-EL, M. (2010) Synthesis and Characterization of Poly (9,9-dialkylfluorenevinylene benzobisoxazoles): New Solution Processable Electron-Accepting Conjugated Polymers. *Chem. Matter*, submitted.

12. Nalwa, K.S., Mahadevapuram, R., **Bose, S.**, Petrich, J.W., Chaudhary, S. (2010) Effect of spin-coating conditions on impedance and photophysics of polythiophene:fullerene thin films. In preparation.

13. Chakraborty, J., **Bose, S.**, halder, U. (2010) Studies of Reversibility of Thermal Unfolding of bovine β-Lactoglobulin. *Biochemistry*, submitted.